60

INTRA-SEASONAL OSCILLATIONS OF CONVECTION OVER SOUTHERN AFRICA

by

Kevin M Levey

Oceanography Department, University of Cape Town

University of Cape Town

A thesis submitted to the University of Cape Town in fulfilment of the requirements for the degree of Master of Science

September 1993

The University of Cape Town has ... the right to reproduce this ... or in part. Copyright is held by ...

The copyright of this thesis vests in the author. No quotation from it or information derived from it is to be published without full acknowledgement of the source. The thesis is to be used for private study or non-commercial research purposes only.

Published by the University of Cape Town (UCT) in terms of the non-exclusive license granted to UCT by the author.

University of Cape Town

ABSTRACT

This work examines intra-seasonal rainfall variability over the summer rainfall region of South Africa. Spectral analysis of a precipitation minus evaporation index (P-E) compiled from 16 rainfall stations in the western Transvaal region of South Africa has shown that two dominant spectral peaks occur in the water budget or convection as identified by an outgoing longwave radiation (OLR) index and P-E index. A longer 40-60 day oscillation or Madden Julian Oscillation (MJO) and a shorter 20-30 day ISO are identified. The interaction between the Rossby waves of the mid-latitudes and the MJO of tropics appears to be the main cause of the 20-30 day ISO operating over southern Africa. Hövmoller analysis at 10° S and 40° S has shown that four modes exist in the propagation and oscillatory characteristics of various anomalies. Eastward and westward propagation is noted as well as standing wave patterns and "flip-flop" modes where anomalies alternate between positive and negative across the latitude band with time. The composite analysis revealed a tropically initiated signal of the 20-30 day ISO in the water vapour flux (WVF) anomaly field where strong easterly WVF vectors are noted between the equator and 10°S and between 40° E and 80° E. Strong convergence of water vapour occurs during the wet phase of the 20-30 day ISO over the south-western Indian Ocean and together with strong ridging of the South Atlantic Anticyclone (SAA) causes the south-easterly advection of moisture from the southern Mozambique Channel and over the warm Agulhas Current into South Africa. Post-wet phase anomaly composites do not show much similarity with pre-cursor anomaly composites. This implies that the 20-30 day ISO may be a half cycle of 40-60 days which is consistent with the MJO. However, it is felt that 20-30 day ISO's affecting the southern African region alternate in intensity within the period of the MJO.

University of Cape Town

CONTENTS

University of Cape Town

University of Cape Town

University of Cape Town

CHAPTER 5 : COMPOSITE ANALYSES

5.1 MEAN COMPOSITE ANALYSIS

5.1.1 KINEMATIC RESULTS

Geopotential height
Horizontal winds
Kinetic energy
Vertical winds
Velocity potential
Streamfunction

5.1.2 MOISTURE AND THERMODYNAMIC RESULTS

Temperature
Water vapour flux
Precipitable water
Divergent water vapour flux
Non-divergent water vapour flux

5.2 MEAN COMPOSITE ANALYSIS

5.2.1 KINEMATIC RESULTS

Geopotential height
Horizontal winds
Kinetic energy
Vertical winds
Velocity potential
Streamfunction

5.2.2 MOISTURE AND THERMODYNAMIC RESULTS

Temperature
Water vapour flux
Precipitable water
Divergent water vapour flux
Non-divergent water vapour flux

University of Cape Town

University of Cape Town

PREFACE

Rain-fed agricultural production plays an important role in the daily existence of millions of people in southern Africa. Rainfall is a very real issue of concern for the majority of southern African inhabitants. Rainfall is variable, especially in the western interior of South Africa, and droughts and floods are common to the African sub-continent (Tyson, 1986). It is of critical importance to know when prolonged dry and wet spells will occur, their duration and their intensity as agricultural production of the region is greatly influenced by them.

It is now increasingly important for farmers of southern Africa to have more than just a seasonal forecast, i.e. they need to know when it will be wet and dry during the rainfall season. It is obvious that a wet summer will have dry spells and dry summers will have wet spells. What is most desirable for farmers is the ability for meteorologists to forecast the most probable onset, duration and intensity of flood/drought events within a season, i.e. on an intra-seasonal scale. This is one step down from seasonal forecasting.

Owing to its geographical location the southern African region lies beneath the southern hemisphere sub- tropical high pressure belt that is characterised by subsidence and dry spells. South Africa is, by virtue of its position, generally dry. The rainfall is highly variable, especially over the interior of the country, and is influenced by the presence of the Hadley and Ferrel cells. The topography of the southern African region also plays its role in modifying rainfall.

Droughts and flood events occur regularly over this region with varying strengths and duration. Various studies at different time scales have been undertaken to

University of Cape Town

investigate the meteorological mechanisms causing these flood and drought events. Most have been on the short-term scale, or event scale, looking mainly at the event itself. Long-term studies using monthly data have focused on the cyclical nature of various meteorological variables so as to ascertain factors underlying wet and dry years. However, long-term studies tend to concentrate more on the climatological aspect and shorter time scales may be more desirable when meteorologists are looking at improving medium-term forecasts. At medium-term time scales, periods from 5 to 60 days are analysed, hence weather fluctuations are of more importance than climatological mean aspects, although the underlying climatological processes cannot be ignored.

It is the intention of this dissertation to contribute to, firstly, a better understanding of the meteorological processes operating at the medium-term time scale of between 20 and 60 days. Secondly, to discover forcing mechanisms such as kinematic and thermodynamic processes that are responsible for generating wet and dry events associated with the 40-60 day and 20-30 day convective cycles (intra-seasonal scale).

As this is a relatively new field of study in the southern African context, this work will hopefully form a basis for future studies, specifically aimed at issuing 10-30 day forecasts.

University of Cape Town

The major themes of the thesis are to :

1] establish the existence of intra-seasonal oscillations;

2] establish differences in the mean and anomalous synoptic fields of various meteorological variables such as temperature, geopotential height, zonal, meridional and vertical winds, kinetic energy, velocity potential, streamfunction, water vapour flux, precipitable water, divergent water vapour flux and non-divergent water vapour flux in the context of 20-30 day wet and dry cycles;

3] establish the role and relative importance of mid-latitude forcing on intra-seasonal oscillations.

Chapter 1 aims at informing the reader about preceding studies that have been undertaken in the field of medium-term oscillations, namely, intra-seasonal oscillations (20-60 days). A background to the various studies is given with references to the most useful analyses being discussed in brief. The hypothesis to be tested is also put forward at the end of the chapter.

Chapter 2 discusses the data used, methodology and the various meteorological variables (observed and derived) utilised in this dissertation.

Chapter 3 deals with the statistical and spectral-analysis results from analysis of OLR time-series and the precipitation minus evaporation (P-E) index. The results of the analyses are discussed.

University of Cape Town

Chapter 4 shows the results of the Hövmoller analyses of the various meteorological parameters at 10° S and 40° S. A discussion of the results is also given.

Chapter 5 discusses the results of the composite analyses in terms of dynamic/kinematic, moisture and thermodynamic processes. Composite analyses are the mean, anomaly and trend fields of the various grouped case studies.

An interpretation of the results obtained in chapter 5 is found in chapter 6 together with the conceptual models inferred from the results. All conclusions derived are also found in this chapter.

University of Cape Town

CHAPTER 1

BACKGROUND

1.1 Southern African Rainfall Variability

1.1.1 Introduction

Much attention has been given to rainfall variability over southern Africa. Temporal and spatial aspects of rainfall variability have been focused on (Tyson and Dyer 1975, Gillooly and Dyer 1979, Tyson 1980 and Lindesay 1984). Earlier studies to relate rainfall variability to atmospheric circulations were initially confined to areas within South Africa (Tyson 1981, Miron and Lindesay 1983, Tyson 1984, Taljaard 1986a, 1986b). However, looking further afield, Dyer (1979), Harrison (1986) and Lindesay (1988) have sought to explain the rainfall variability in terms of synoptic weather and climatic teleconnections and have stressed the importance of the Southern Hemisphere circulation on southern African rainfall.

Most studies of rainfall variability over southern Africa have concentrated on the long-term scale, i.e. inter-annual or year to year variability (Miron and Tyson 1984, Jury and Lyons 1992), and there have been a few studies detailing circulations associated with specific rainfall events over multi-day periods (Taljaard 1985, Lindesay and Jury 1991, Barclay 1992) or multi-week periods (Taljaard 1981, Harrison 1986, Lindesay 1988, Matarira and Jury 1990, Lyons 1991).

University of Cape Town

1.2 Intra-seasonal Oscillations

Just as the weather changes on a daily scale or short term scale, it also changes on an inter annual scale or long term scale. It is important to ascertain whether or not medium term scale fluctuations, i.e. weather patterns operating on a scale of say 20 to 60 days, occur. Recent studies have shown that intra-seasonal Oscillations (ISO's) in the different meteorological variables do take place.

As far back as 22 years ago Madden and Julian (1971) detected a spectral ISO in the zonal wind in the tropics which today is generally known as the Madden-Julian 40-60 day oscillation (MJO). According to Weickman et al (1985), Lau and Chan (1986) certain properties of this 40-60 ISO have been established and have been associated with the eastward moving equatorially-trapped Kelvin wave. However, some observations have contradicted this as Yasunari (1980) and Anyamba (1992) have reported meridional propagation in the Indian Ocean region. At times the oscillation is observed to be stationary and at other times even to propagate westwards. Another unclear issue is the apparent variability of the ISO's period in both space and time. Hayashi and Golder (1992) have shown that two distinct spectral peaks centered around 25-30 and 40-50 days have been identified in the First GARP Global Experiment (FGGE) data set.

University of Cape Town

Vincent et al (1990) concentrated their study on the tropical Southern Hemispheric region between 0°-15° S using ECMWF analyses. Having found that the MJO is all but absent during the austral winter, they focused on the austral summer months of November - April. Vincent et al (1990) also found that velocity potential at 200 hPa (χ_{200}) and OLR were the best indicators of the oscillatory convective activity. Spectral peaks of between 33 and 50-67 days were observed

from the data. The ISO propagated eastward and its convective activity was more intense over the eastern Indian Ocean-western Pacific region than elsewhere. The χ_{200}-wave could be followed continuously around the globe, but the convection (OLR) associated with the ISO was weak and difficult to track over much of the Western Hemisphere.

Knutson and Weickmann (1986) described various characteristics of the MJO, i.e. the 40-60 intra-seasonal oscillation. They found that during the entire seasonal cycle :

- large-scale (wavenumber one) tropical divergent wind features propagate eastward around the globe;
- good agreement exists between areas of upper-air divergence and areas of convection;
- convection anomalies are smaller over tropical Africa and South America than over the Pacific and Indian Ocean areas;
- anomalies of OLR are very small over cooler tropical sea surfaces, i.e. the Atlantic;
- analysis of the non-divergent (streamfunction) circulation at 250 hPa (ψ_{250}) revealed cyclonic areas to the east of convective areas and anticyclonic areas alongside or west of convective areas;
- convection anomalies are most pronounced in the summer hemisphere tropics, but the ψ_{250} features are most pronounced in the winter hemisphere;
- The East Asian jet retracts toward Asia when positive 40-60 day convection anomalies occur over the tropical Indian region. The eastward shift of convection into the western and central tropical Pacific is accompanied by a

University of Cape Town

series of circulation features over northern Asia and an eastward extension of the East Asian jet during the boreal winter.

The dominant 200 hPa zonal-wind fluctuation over the tropical Atlantic is related to global-scale circulation anomalies with their origins in the Pacific. Park and Schubert (1992) have found that OLR anomalies associated with the zonal-wind fluctuations are characterised by eastward propagation of ISO's over the Indian Ocean and the western Pacific and a standing oscillation over the tropical Atlantic. The standing oscillation over the tropical Atlantic extends from Northeast Brazil to West Africa and is the dominant component of the Atlantic OLR variability. From analysis of velocity potential and moisture convergence fields it emerged that the fluctuations in convection are coupled between the western Pacific and Atlantic via large-scale (zonal wavenumber 1), equatorially trapped, eastward propagating waves associated with the Madden-Julian 40-60 day oscillation. Also of interest is the fact that the zonal-wind fluctuation is also related to extratropical waves propagating into the tropics from both hemispheres. Of greater interest is the Southern Hemisphere wave train that makes up the dominant contribution to the zonal-wind fluctuation pattern. It appears to emanate from the western Pacific and amplifies near the west coast of South America. From these results, Park and Schubert (1992) have suggested that a major component of the 20-70 day variability over the Atlantic region is remotely forced. This forcing occurs via the MJO, which is strongly coupled with eastward propagating heating anomalies in the western Pacific and Rossby wave trains, which appear to have their origins in the middle latitudes of the Pacific.

Schubert and Park (1990) examined low-frequency (20-70 day) variability during the austral summer based on seven years (1981-1987) of European Centre for

University of Cape Town

Medium Range Weather Forecasts (ECMWF) initialised analyses. The dominant 200 hPa zonal wind fluctuations in the Pacific sector, determined from an empirical orthogonal function (EOF) analysis, provided the baseline modes of atmospheric variability, which in turn are related to fluctuations in other circulation variables and OLR. EOF component Z1, or the dominant upper level zonal wind fluctuation, is associated with an expanded/contracted region of easterlies in the tropical western Pacific and changes in the shape and intensity of the subtropical jets. The anomalous eddy streamfunction at 200 hPa showed an enhanced pair of anticyclones (cyclones) straddling the equator which are strongly coupled with eastward propagating tropical convection in the western Pacific with a time scale of about 40 days. In the Northern Hemisphere there are marked differences in the propagation of wave activity at 200 hPa as inferred from composite circulations. During the low phase (reduced easterlies) strong propagation occurs from the dominant source region over East Asia into the tropical western Pacific in conjunction with what appears to be significant reflection from the equatorward flank of the subtropical jet. During the high phase (enhanced easterlies) there is much weaker equatorward propagation together with reduced vertical propagation over East Asia and the western Pacific.

EOF component Z2 showed a more asymmetrical structure with respect to the equator. There is a simultaneous decrease (increase) in the easterly extent of the East Asian jet and increase (decrease) in the strength of the jet over the southern Australian region. The anomalous eddy streamfunction at 200 hPa showed wave trains apparently emerging from the tropical central Pacific extending into both hemispheres.

University of Cape Town

Shubert and Park (1990) suggest that the tropical convection in the western Pacific has a strong modifying influence on (extratropically forced) mid-latitude low-frequency variability. However, this influence is basically indirect via zonal wind changes that influence the propagation of waves originating in the mid-latitudes. The zonal wind changes include those associated with the strength and extent of the tropical easterlies.

Rui and Wang (1990) have explained the temporal evolution of ISO's in the equatorial region. From composite OLR anomalies for 36 cases for the period 1975-1987 they found a four-stage development process :

1] initiation over equatorial east Africa (possibly related to a surge of the monsoon);
2] rapid intensification when passing eastward through the Indian Ocean;
3] mature evolution characterised by a weakening in the maritime continent and redevelopment over the western Pacific;
4] dissipation near the date line in moderate events or emergence from the equator toward North America and the south-eastern Pacific in strong events.

University of Cape Town

Rui and Wang (1990) also found a noticeable feature in the vertical structure in that the 850 hPa convergence leads convection and midtropospheric upward motion by about 30 degrees longitude in both developing and mature phases. Equatorial convection anomalies are coupled with equatorial upper- (lower-) level easterly (westerly) anomalies and associated twin anomalous anticyclonic (cyclonic) circulation anomalies. In the development and early mature phases the wind anomalies generally lag the convection anomalies, but nearly overlap in the late mature phase and slightly lead the convection anomalies in the dissipation

phase. Rui and Wang (1990) also found that the upper level twin cyclonic anomalies associated with the westerly anomalies in front of the convection travel across the eastern Pacific after the convection ceases in the central Pacific, while the low-level wind anomalies die out east of the date line.

Chen and Yen (1990) investigated the ISO of the tropical easterly jet during the boreal summer of 1979 based on data generated by the FGGE III-b analysis of the ECMWF data set. They found that the easterly jet possesses a distinctive ISO south of its core. It was previously suggested that the temporal fluctuations of the easterly jet may be related through cumulus convection to that of the low-level Indian monsoon circulation. However, Chen and Yen (1990) have demonstrated, using a streamfunction budget analysis, that the ISO of the tropical easterly jet south of its core is primarily caused by the eastward propagating ISO of the planetary-scale divergent circulation.

Using analysed winds, OLR and satellite low-level moisture data from the National Meteorological Centre (NMC), Weickmann and Khalsa (1989) studied the propagation of a strong MJO from the tropical Indian Ocean to the western Pacific Ocean during the austral summer of 1981. They found consistent features such as a slow (5.0 m s-1) propagation of convective energy over the Indian-western Pacific Ocean and a fast (15.0 m s-1) propagation of 150 hPa tropical velocity potential (χ_{150}) in regions remote from the oceanic warm pool. Preceding the eastward shift by 12 days was an intense cold surge and accompanying convective increase near 110° E. Responding to the increased convection, an intensified anticyclone over southeast China and a downstream upper level trough were evident in the 150 hPa circulation .

University of Cape Town

At lower levels, the 850 hPa subtropical anticyclone over the North Pacific intensifies and amplifies as a wave train emerges from the region of the downstream upper level trough. Accompanying these events is a surge in the trades in the central Pacific Ocean region. In the equatorial regions a component of convection moves east accompanied by low-level westerly winds to near 170° E. Occurring between the trade surge and the westerly winds is an area of strong convergence at the 850 hPa level that favours low-level moisture increases over the western Pacific Ocean. The convection then intensifies near 150° E and weakens near 110° E, thereby causing a 150 hPa cyclone over the southeast China and anticyclone over the western Pacific Ocean.

Wang and Rui (1990) used pentad mean anomaly maps to study the climatology of tropical intra-seasonal convective anomaly (TICA) as a dynamic system. Of the one hundred and twenty-two events studied, seventy-seven were found to be eastward propagating, twenty-seven were northward propagating and eighteen displayed westward propagation. It is therefore important to note that not all ISO's are eastward propagating, although most of the literature shows that they are. Of interest is the fact that the eastward propagation is more active in austral summer and the northward propagation occurs in the boreal summer from May to October.

University of Cape Town

Wang and Rui (1990) found that the eastward moving TICA exhibits three major paths :

1] eastward along the equator from Africa to the mid-Pacific;
2] first eastward along the equator, then either turning northeast or southeast at the maritime continent;

3] the main anomaly moves eastward along the equator with split centres moving northward over the India Ocean and/or western Pacific Oceans.

The equatorial Indian Ocean and the western Pacific ITCZ are preferred locations for their development, while the maritime continent and central Pacific are regions of dissipation. Northward propagation of the ISO is confined to the Indian and western Pacific monsoon regions and its existence suggests that the mechanism responsible for meridional propagation may differ from that for eastward propagation. Wang and Rui (1990) finally concluded that the dynamic effect of the equator and the thermodynamic effect of the underlying warm ocean water are basic factors in trapping TICA in the deep tropics, while the annual march of maximum SST and the monsoon circulation have profound influences on the annual variation and meridional movement of TICA.

Many studies in terms of OLR and velocity potential (χ) have shown that energy is input into the ISO through cumulus convection, especially over the Indian-western Pacific region. Chen and Yen (1991) speculated upon a hemispheric interaction between cumulus convection and extratropical circulation in terms of an intra-seasonal time scale from previous studies that they had undertaken (Chen and Yen 1990). On the basis of their study during 1979 (boreal summer), Chen and Yen (1991) demonstrated that a coherent ISO existed between cumulus convection and divergent circulation over the equatorial western Pacific and mid-Pacific troughs. The ISO's of streamfunction (ψ) associated with these troughs, the tropical OLR, and the tropical ψ-fields exhibit coherent eastward propagations. Through a diagnostic scheme using a χ-maintenance equation and a ψ-budget equation it is shown that a tropical-midlatitude interaction exists through the eastward propagation of the intra-seasonal χ-oscillation.

University of Cape Town

Zhu and Wang (1992) have shown that two prominent areas of the tropical 40-60 day convective variability exist, one in the tropical Indian region and the other in the western Pacific. When the tropical western Pacific experiences an abnormal dry condition, the equatorial Indian Ocean experiences enhanced convection and vice versa and this convection seesaw is seen to be a fundamental characteristic of the tropical 40-60 day ISO.

This see-saw is associated with the activity of propagating low-frequency convective systems (LFCSs). The system important to the austral summer originates in the equatorial Indian Ocean and propagates eastwards and/or north-eastwards. The seesaw is caused by the longitudinal dependence of the evolution of eastward-moving LFCSs that strongly amplify in the equatorial Indian Ocean, weaken over the maritime continent and then re intensify in the South Pacific convergence zone (SPCZ).

University of Cape Town

Chen and Tzeng (1989) examined global-scale intra-seasonal and annual variations of divergent water-vapour transport (flux) and water vapour itself. They found that regarding ISO's, positive (negative) precipitable water (PW) anomalies and negative (positive) OLR anomalies couple with the convergent (divergent) centre of the potential function of water vapour transport (χ_Q) anomalies and the divergent (convergent) centre of upper level divergent circulation anomalies.

Chen and Tzeng (1989) inferred that the eastward propagating divergent circulation of the ISO converges water vapour to maintain cumulus convection, which releases latent heat, possibly to support this low-frequency ISO. Compared to the tropical areas of the Americas and Africa, the fluctuations of PW and cumulus convection associated with this ISO are large over the Indian Ocean and

the western Pacific. Identified in both boreal summer and winter is a regular southward propagation of PW anomaly bands to the south of the equator.

Chen and Tzeng (1989) have also shown that landmass cooling in the winter hemisphere and landmass warming in the summer hemisphere establish a pair of upper level convergent-divergent centres over each tropical continent. Water vapour is converged (diverged) by the divergent circulation, in order to maintain maximum (minimum) centres of PW and cumulus anomalies over each tropical continent.

Hartman, Michelsen and Klein (1991) have investigated the seasonal dependence of the frequency and intensity of tropical oscillations with intra-seasonal time scales. They have shown that the MJO in the Indian Ocean region varies in its preferred period of 50 days in the austral summer to about 35 days during the austral winter, although the evidence is weak. However, during the period September-December, there is a pronounced spectral peak of between 20-25 days in the western tropical Pacific. This spectral peak reveals that this ISO is distinct from the MJO, but may also result from coupling between large-scale motion and latent heat release on much smaller scales.

University of Cape Town

Anyamba (1992) has identified a 20-30 day oscillation in the tropical outgoing long wave (OLR) spectra in the western Indian Ocean and found that while the 40-50 day ISO is characterised by an eastward propagating wave in the Indian and West Pacific Oceans, the 20-30 day ISO has a much weaker zonal propagation. There are times when the spatial structure and phase propagation of the two ISO's are nearly identical. There have been attempts to link the extratropics with the tropics.

Ghil and Mo (1990) studied 12 years of 500 hPa geopotential heights in the Southern Hemisphere and found, using the technique of singular spectrum analysis, a dominant spectral peak between 21 and 26 days peaking at 23 days. It has a wavenumber 4 structure. The 40 day mode is the second major spectral peak, and is dominated by wavenumbers 3 and 4. A third very weak mode of 16 days is noted, but is too weak to separate its spatial behaviour from the first two modes.

Magaña and Yanai (1990) studied the interrelationship between the MJO in the tropics and the intensity of the planetary-scale upper-tropospheric (200 hPa) systems in the subtropics during the boreal summer using data obtained from the FGGE data set. They found that mid-Pacific trough and the South Asian (Tibetan) and Mexican anticyclones undergo cycles of amplification and decay with the 40-60 day fluctuation of convective activities in the Indonesia-western Pacific region and in the intertropical convergence zone (ITCZ) over Central America. Magaña and Yanai (1990) also discovered that low-frequency transients in the upper troposphere around the mid-Pacific trough (SPCZ) play a dominant role in the northward transport of westerly momentum. At the same time, the westerlies that develop southeast of the trough form an equatorial westerly "duct" , through which wave energy can propagate into the tropics from the mid-latitudes. The mid-Pacific trough, therefore, acts as a two-way link between the tropics and the mid-latitudes. A similar link may exist in South Africa.

Of interest to the present study are the findings of Tsai et al (1992). They found a 26-day oscillation in sea surface temperature (SST) data in the western Indian Ocean from 52° to 60° E and in the vicinity of the equator. The fluctuation of SST at a period of 26 days is found to be asymmetrical about the equator, trapped within the equatorial waveguide (within ±6° of the equator). Maximum variance is

University of Cape Town

found at around 3° latitude and decreases towards the equator at a faster rate than towards the poles. These characteristics are consistent with the mixed Rossby-gravity (or Yanai) waves as predicted from linear wave theory. During the period July-September (boreal summer) the temporal variation of this 26-day ISO is most energetic, with maximum values of 0.4° C and 0.8° C found during August of 1987 and 1988 respectively. Tsai et al (1992) maintain that this observation agrees with the temporal variation of Yanai waves inferred from the drifting buoy observations and numerical studies of the Indian Ocean and concluded that the Yanai wave is responsible for the 26-day ISO observed in the SST data in this area.

Kawamura (1991) studied the dependence of the MJO on SST and on large-scale air-sea coupling in the warm pool region of the western Pacific. He concluded that once the SST in this region is beyond the "upper threshold" temperature of 29.5° C, the MJO is damped in this region, even though large-scale tropical convection is still rather active. Furthermore, in contrast, high-frequency fluctuations (2-15 day periods) become relatively dominant under high SST conditions. The oceanic 40-60 day oscillation fluctuation is significant when the SST in the warm pool region of the western Pacific is in the range between 29° and 29.5° C, with the SST and large-scale convection fluctuating coherently on the intra-seasonal time scale, with a phase difference of 10-20 days. Finally, Kawamura (1991) states that the MJO is presumably modified over the warm pool area of the western Pacific by the strong air-sea interaction on the intra-seasonal time scale. Rui and Wang (1990) identified the western Pacific region as being an area where the ISO re-intensifies after a weakening over the maritime continent having propagated eastwards from the tropical Indian Ocean. It can therefore be seen that the warm pool region of the western Pacific plays an important role in

University of Cape Town

modifying the spatial and temporal characteristics of the MJO and higher-frequency oscillations.

Hayashi and Golder (1992) used space-time spectrum and filter analyses to clarify the differences between the tropical 40-50- and 25-30-day oscillations. They used a 40-level model to examine the effect of increased vertical resolution in an ocean-surface perpetual January R30 model to examine the effects of the absence of geographical and seasonal variations.

The R30 model results show that :

- the relative amplitude of the wavenumber-one component of the 40-50- and 25-30-day oscillations varies greatly from year to year;
- although the 40-50- and 25-30-day oscillations have similar structures, the 25-30-day oscillations exhibit a greater increase with height of tropospheric amplitudes than the 40-50-day oscillations, resulting in different magnitudes at different levels;
- the time variance of the two oscillations has similar longitudinal distributions, implying that the two periods are not due to differences in local phase speeds;
- the two oscillations appear to grow and decay independently without and coherent phase relationship, implying that the two periods are not a result of the seasonal modulation of an intrinsic 40-50-day period.

They concluded their research by revealing that sea surface temperature geographically modulates the intrinsically eastward-moving wavenumber-one precipitation oscillations, resulting in the major Pacific and minor Atlantic local amplitudes. This in turn causes planetary-scale eastward-moving zonal-velocity oscillations and standing geopotential oscillations.

University of Cape Town

The model results show that the dominant ISO operating on the global-scale is the Madden-Julian Oscillation (40-60 day). It is an easterly propagating ISO, originating in the Indian Ocean and propagating eastwards in the western Pacific and dissipating in the majority of cases in the central Pacific although there is evidence that the ISO occurring in the Atlantic is remotely forced (Park and Schubert, 1992).

Temporal studies show that, although the MJO is the dominant ISO in the tropics, shorter-term ISO's do occur. There has been evidence that ISO's of about 26 days occur, and not only in the atmospheric circulation (Anyamba 1992), but also in the ocean in the tropical regions of the Indian and western Pacific oceanic regions (Tsai et al, 1992).

Various methods and meteorological variables have been employed in the analysis of ISO's. Chen and Tzeng (1989) and Chen and Yen (1990, 1991, 1991a), in particular, have shown that the use of potential vorticity maintenance equations, streamfunction budgets, water vapour flux divergence, precipitable water and OLR anomalies are of great value in analysing the dynamic structures of the eastward propagating ISO's, in an effort to explain tropical convective anomalies and their subsequent eastward propagation.

However, little research has been undertaken in the subtropical areas as the effects of the ISO's are less pronounced in these regions. The major convective regions of the globe are naturally situated within the tropics, but many areas of the subtropics, such as the southern African subcontinent, derive their summer rainfall from convective processes. It is not clear whether extratropical processes could

University of Cape Town

influence the subtropical intra-seasonal oscillation to a greater degree than tropical influences such as the MJO.

Lyons (1991) examined OLR fluctuations over southern Africa during the summers of 1982/1983, 1983/1984 and 1984/1985. He found a large OLR minimum area centred at 10° S 25° E which is consistent with the climatological rainy area and persistent convective area. He proposed a possible temperate-tropical interaction responsible for the fluctuation in OLR over the southern African region. He found that the midlatitude upper level trough *does not* penetrate directly into tropical Africa. Rather, there is a merging of the midlatitude upper level trough with the Tropical Upper Tropospheric Trough (TUTT), which is a persistent feature at 300-200 hPa over the south-west Indian Ocean. The TUTT is then instrumental in modifying circulation over equatorial southern Africa. Midlatitude wave kinetic energy moves north-eastward along the TUTT into tropical southern Africa. Midlatitude wave interaction with the TUTT is important in : strengthening the TUTT, developing an upper-level cyclone within the TUTT, enhancing divergence aloft, cooling the midtroposphere, and decreasing OLR over tropical southern Africa

D'Abreton (1992) examined tropical-temperate troughs over southern Africa. To examine the interaction of tropical and temperate troughs over southern Africa he examined the water vapour content and transport. Source regions of water vapour were identified in the early summer over the south-east Atlantic Ocean, whilst during the later summer period, the south-west Indian Ocean was revealed as a source area of water vapour for the southern African region. D'Abreton (1992) used divergence of water vapour flux to establish large-scale areas of water vapour.

University of Cape Town

1.2.1 Hypothesis to be tested

It is hypothesised that

1] a subtropical ISO is evident over the southern African region during the austral summer and that the temporal and spatial characteristics of this 20-30 day subtropical ISO differ from that of the Madden-Julian Oscillation of 40-60 days;

2] the temporal scale will be shorter than that of the MJO as a result of the geographical location of the southern African region in relation to the mid-latitudes and the greater influence that the extra-tropical circulation could possibly exert on the subtropical ISO over this region;

1.2.2 Motivation

What is evident from the studies dealing with wet and dry periods over southern Africa is the apparent lack of any in-depth study of medium-term or intra-seasonal oscillations. This dissertation aims at filling this gap between event and seasonal scale rainfall variability.

Intra-seasonal studies are a recently recognised phenomenon, judging from the literature available on the subject, almost 90% of recent studies into intra-seasonal oscillations have been undertaken since 1988, with a few exceptions, for example that being of Madden and Julian (1971). Most of the available literature deals with tropical ISO's. There have been very few attempts to explain the spatial and temporal characteristics of ISO's in the sub-tropics and the role the extra-tropical forcing plays in modulating these subtropical ISO's.

University of Cape Town

Many *global* studies have illuminated various aspects of ISO's like their presence, structure and evolution. However this study is regionally based, concentrating on various aspects of ISO's that affect the southern African region in particular. Since South Africa is surrounded by two oceans which are of importance to the climate of the region, the domain includes the south-east Atlantic Ocean and most of the Indian Ocean. The domain also includes tropical Africa as far north as 20° N .

Figure 1-1 shows the regional domain used in this study.

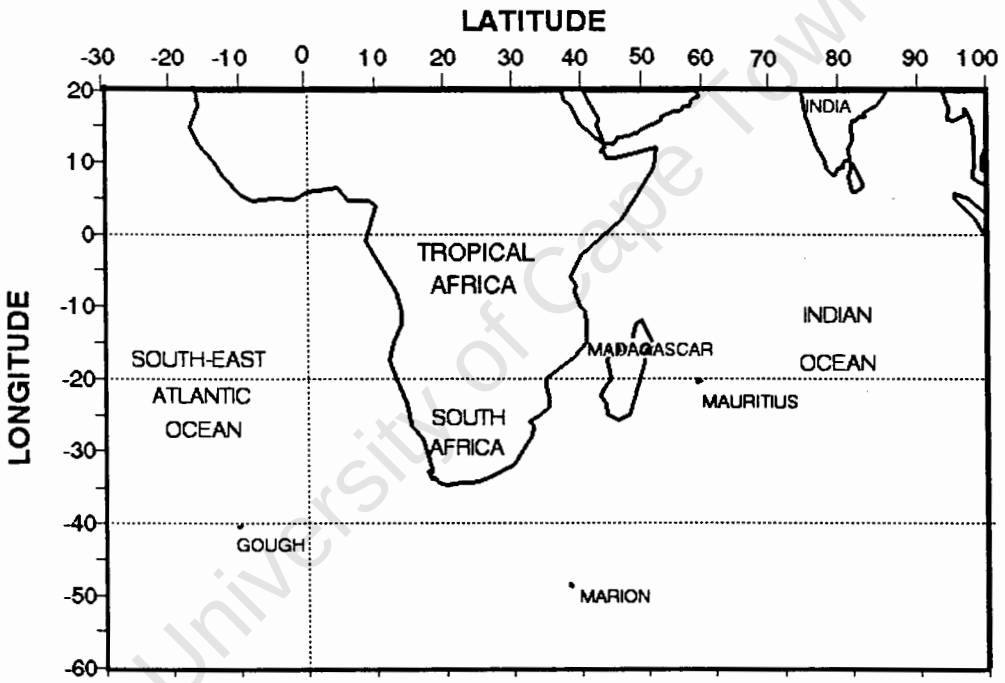

University of Cape Town

Figure 1-1 : Location map : Domain has northern boundary at latitude 20°N, western boundary 30°W , southern boundary at 60°S and eastern boundary 100°E.

CHAPTER 2

DATA AND METHODOLOGY

2.1 DATA

2.1.1 INTRODUCTION

Many studies have been undertaken to assess the currently available model-based global data sets of atmospheric circulation. These data sets have been useful for studying dynamical and physical processes and for describing the nature of the general circulation of the atmosphere. Recent studies (Bengtsson and Shukla, 1988) have shown that not all the available model-based global data sets are suitable for studying global climatic change. They state reasons such as limitations in the early data assimilation systems and inconsistencies caused by numerous model changes. With this in mind a closer inspection of the European Centre for Medium Range Forecasts (ECMWF) data set is needed, since almost 90% of the results obtained in this thesis were attained using data from the ECMWF data set.

The ECMWF data assimilation system has undergone significant improvements over the last ten years. Hoskins et al (1989) undertook a diagnostic study of the global atmospheric circulation based on ECMWF analyses 1979-1989 and discussed various changes in the data set during that period. The ECMWF analysis system undergoes continual revision and development in order to provide better forecasts and data reliability.

University of Cape Town

Several changes have been instituted at ECMWF over the past ten years. These include, in the more recent past, :

- 03/1986 : improved humidity analysis, including the use of satellite precipitable water content data;
- 09/1986 : introduction of new analysis, including analysis at new model levels and further refined structure functions;
- 01/1988 : improved analysis of divergent wind;
- 07/1988 : modifications were made to the analysis to increase effective resolution of analysis.

Resolution of the data has also increased since the mid 1980's where now basic or advanced data sets are available depending on the resolution required.

After 1982, the introduction of diabatic initialisation, strengthened and improved the tropical divergent flow and created a more realistic and intense Hadley and Walker circulation. With the introduction of a better boundary layer formulation, the new analyses have been more realistic with respect to the upward transport of moisture in the boundary layer, which has now given rise to a larger heat flux from the ocean than the older model formulation.

The use of satellite measurement of precipitable water and other changes in March 1986 appear to have made ECMWF humidity analyses more realistic (Illari, 1986, 1989). Considerable effort in the quality control of observations through frequent correspondence with the data producers to improve the quality of observation has been undertaken by ECMWF. Of concern to ECMWF has been the quality and

University of Cape Town

availability of satellite observations, especially in areas where few conventional observations are available (i.e. tropical Africa).

The ECMWF data are obtained from observations made from rawinsondes, satellite temperature and moisture soundings, pilot balloons and cloud tracked winds, surface observations from ships, oceanic buoys and land stations, aircraft reports, and (Australian) bogus observations. Based on the FGGE year, a "main" analysis of ECMWF data was produced, but with subsequent improvement and additions to the model, re analysis was undertaken and is known as "final" analyses. Studies have shown that the "final" analyses of ECMWF data agreed better with observed data. It was also found that the ECMWF "final" analyses showed a 36% more intense time-averaged 200 hPa velocity potential than the ECMWF "main" analyses. ECMWF "final" analyses also generally fit the data better. These results imply that more recent ECMWF analyses give a more intense and realistic tropical divergent circulation than earlier analyses and that they fit the data even better than before.

University of Cape Town

Studies of the large-scale divergent flow have revealed large increases in magnitude in September 1982 and May 1985 after various changes to the model were instituted. The more recent stronger divergent circulations appear to be more realistic.

Comparisons of ECMWF FGGE analyses with analyses by other centres has shown that the ECMWF data :

- gave more intense and more realistic circulation features in the Southern Hemisphere;

- more closely fit the data;
- had more balanced mass and wind fields;
- had less random error than analyses by the other centres, such as the National Meteorological Centre (NMC).

2.1.2 Climate Analysis Centre (CAC) data

Outgoing longwave radiation (OLR) has been used extensively as a proxy for cumulus convection (Wang and Rui 1989, Chen and Tzeng 1989). Low (high) values of OLR indicate greater (less) cloudiness and hence increased (decreased) depth of cumulus convection. OLR, unlike cumulus convection, can be quantitatively analysed. The OLR data used in this dissertation were obtained by Duane Waliser of SUNY (State University of New York) from the Climate Analysis Centre in Washington, D.C.. The OLR data used were for a 2.5° radius area centred on 25°S and 25°E (see fig 2.1) which encompasses most of the western Transvaal region of South Africa and the south eastern region of Botswana. The data-set extended from 1975-1987. The data was in the form of pentads (5-day means) starting at pentad 1 for each year (1-5 January) and ending at pentad 73 (27-31 December). Leap years within the data set include one 6-day mean "pentad" at the end of February, namely 25 February - 1 March, including 29 February. The reason for having a 6-day mean in a leap year is for data continuity from year to year. This means for example that pentad 56 for *each* year is the same period, namely, 3 October - 7 October.

University of Cape Town

2.1.3 European Centre for Medium Range Weather Forecasts (ECMWF) data

In light of the earlier discussion on the recent developments in the improvement of ECMWF model analyses, in particular the moisture fields, data after 1985 were used. Six years, 1986-1992, were analysed. The data window encompasses an area stretching from 20° N to 60° S and 30° W to 100° E. The data are at a resolution of 2.5° x 2.5°. The basic observed variables in this data set are (units in parentheses) :

- geopotential height (gpm)
- temperature (°C)
- zonal wind (u-component in m s^{-1})
- meridional wind (v-component in m s^{-1})
- vertical wind (w-wind component in Pa s^{-1})
- humidity (%)

The data were available for the 1000, 850, 700, 500, 300, 200 and 100 hecto Pascal (hPa) surfaces.

However, the ECMWF data set has its limitations. Some observations are interpolated and this is a real problem in data-sparse regions of the globe, especially over the oceans. An example of this is the lack of reliable SATWINDS from 60-90° E. Data density is therefore one apparent problem of the ECMWF (and most other) data set. Interpolation algorithms have overcome this problem to a certain degree, but it must be remembered that large areas within the ECMWF data set are not observed data.

University of Cape Town

2.1.4 Rainfall and evaporation data :

Daily rainfall data were collected for 16 stations in a 2.5° radius surrounding 25° S and 25° E to co-incide with outgoing longwave radiation data at this point (Figure 2-1). The rainfall and class A pan potential evaporation data were obtained from the CCWR data base in Pietermaritzburg, South Africa. Data from 1970 to 1991 were retrieved. All data were checked for missing values, and only stations with complete records were chosen. Only 16 stations from over 800 were thus selected based on this criterion.

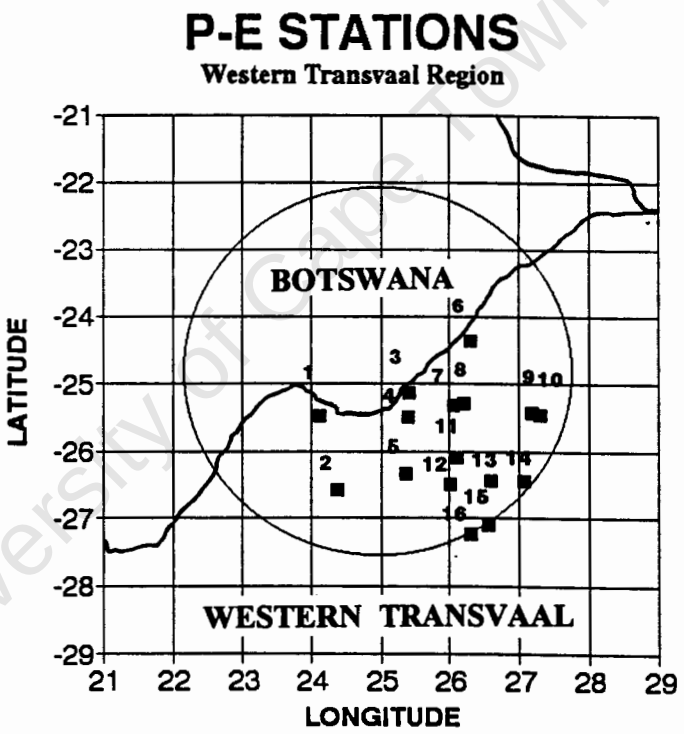

Figure 2-1 : Location of P-E stations within 5° radius of 25°S 25°E.
1° latitude at 25°S = 100 kilometers.

Station list :

1 - Vergelegen	2 - Vryburg	3 - Lobatse	4 - Mafeking
5 - Barberspan	6 - Doornlaagte	7 - Koster	8 - Koster
9 - Kroondal	10 - Buffelspoort	11 - Lichtenburg	12 - Ottosdal
13 - Brakspruit	14 - Potchefstroom	15 - Viljoenskroon	16 - Palmietfontein

University of Cape Town

Figure 2-1 shows a predominance of stations in the south-eastern sector of the encircled area. The reason for this is the lack of suitable rainfall stations in Botswana.

As mentioned Class A pan evaporation data was used. However, Class A pan evaporation data may not be the best source of evaporation data as there are a few problems associated with such measurements of evaporation as explained by Sutton (1953), Geiger (1965) and Wiesner (1970). Factors affecting accurate measurement from a Class A pan include sensible heat received through the sides and bottom of the pan resulting in higher evaporation. Also the effect of diameter, rim height, colour and depth of pans affect the evaporation rate considerably. Other factors which also affect accurate reading include natural phenomena such as animals drinking out of pans, and human error in calculating accurate readings when rainfall has occurred and filled the pan. There are non-empirical methods to establish more accurate evaporation estimates. These include different mathematical approaches, such as the Penman Equation (Wiesner, 1970) which include other meteorological parameters such as temperature and wind.

However, most of the rainfall stations used in this study only measure rainfall and evaporation as many are agricultural stations and not meteorological stations measuring other parameters such temperature and wind. Therefore it was necessary to use Class A pan evaporation data, knowing that it is not the best estimator of evaporation. It was felt that since evaporation is less variable than precipitation over large areas and since an areal index was used, that the Class A pan evaporation data was suitable. The indices used are more for purposes of identifying and gauging the relative intensities of wet and dry events, rather than their absolute quantitative attributes.

University of Cape Town

2.2 METHODOLOGY

Different techniques may be employed to analyse geophysical data. Various methods are used depending on temporal and spatial resolutions of the data to be analysed. Since medium-term (20-60 day) temporal resolution is desired in this study, a method of combining daily data into pentad (5-day mean) data was applied. Different analysis techniques have been utilised to understand the cyclic nature of the intra-seasonal oscillation. A detailed account of each technique is discussed.

2.2.1 Analysis techniques

Various techniques were employed in this study. Statistical and spectral analyses were performed on the *raw* OLR data and precipitation minus evaporation time-series data (P-E). Composites of individual case studies were also used. Longitudinal time-series (Hovmöller plots) of various anomalies along specific lines of latitudes have also been used to identify the direction of propagating systems.

University of Cape Town

2.2.2 Statistical and spectral analyses

In this study all summers are labelled according to the year in which the month of January occurs, e.g., OLR for 1987 indicates the period from October 1986 to March 1987. A P-E index was established for 16 rainfall and evaporation stations in a 2.5° radius surrounding 25°S and 25°E. 16 rainfall stations were purposefully chosen to create an area-averaged rainfall index. This effectively eliminates high-

frequency spatial convective noise from the data and improves data quality through averaging.

The reason for calculating a combined rainfall/evaporation index is that a combined index eliminates the rainfall "zero" in a time series. If only a rainfall index is used, then there is only a measure of "wet" events when standardising the data and no measure of the intensity of a dry event, since the zero value is a limiting factor. By establishing a precipitation minus evaporation index, a measure of the intensity of both wet and dry events can be analysed.

The evaporation data were subtracted from the precipitation data and means and standard deviations were calculated. A method of pentads (5-day means) has been used in this study. There are numerous references to the usage of pentads in data analysis (Wang and Rui 1989, Chen and Tzeng 1989, Hsu et al 1990). As this is an intra-seasonal study, the usage of pentads is thus justified. Daily data are temporally too short a time-scale, while monthly data are too long a time-scale. The former shows a very high frequency variability, and the latter shows a low frequency bordering on inter-annual scale. The usage of pentads has been found to be most useful in representing ISO's.

The OLR and P-E indices were calculated for a series of 36 pentads, commencing on 3 October until 31 March the following year. The summer is split into two equal halves, 18 pentads occurring from 3 October to 31 December, and 18 pentads occurring from 1 January until 31 March. The period 3 October until 31 March falls in the austral summer, and since almost all the rain in the southern African region falls during this time, the austral winter period was not analysed.

University of Cape Town

The data was then normalised, employing the following statistical technique (Norcliffe, 1985) :

$$z = (Xi - x) / \delta$$

where : z = normalised standard deviation value
Xi = individual data point
x = historical mean of data points
δ = historical standard deviation of data points

Various statistics were calculated for the raw OLR, precipitation, evaporation and P-E data. Spectral analysis, using a method of periodograms and Fast Fourier Transform (FFT), was performed on the raw OLR data, individual precipitation and evaporation and the raw and filtered P-E data series. Correlations were also done between the OLR index and individual rainfall, evaporation and P-E indices. The reason for doing these correlations was to ascertain whether the P-E index is better correlated with the OLR index than a rainfall index.

University of Cape Town

2.2.3 Composite analyses

Tyson (1981), Rasmusson and Carpenter (1982), Hirst and Hastenrath (1983), Lindesay (1988), Wang and Rui (1989) and Chen and Tzeng (1989) have used the composite analysis technique extensively in the field of climatology. Composites are better at indicating common features, trends and patterns in the various variables than individual cases. This method reduces the total number of maps and figures associated with each case study. However, first the individual case studies had to be chosen.

Results from the spectral analysis of the OLR and P-E pentad indices indicated that a period of twenty-five days (5 pentads) should constitute the time frame surrounding an individual ISO event. Since this is a study of rainfall variability, the central pentad is the wet event, while the 10 days on either side of the wet event are transitions to the dry events. Hence, there is a period 10 days prior to the wet event, 5 days prior to the wet event, the wet event of 5 days, then a period of 5 days after the wet event and then a period of 10 days after the wet event. The pentad 10 days prior to the wet event has been labelled P-2 (pentad-2), the pentad prior to the wet event is labelled P-1, the wet event pentad, P-0, the pentad just following the wet event, P+1 and the last pentad in the series is P+2. Hence, the various meteorological parameters have been studied from a dry phase leading up to a wet phase and then returning to a dry phase.

Diagramatically this scheme looks like the following :

Table 2-1 : Pentad scheme

PENTAD	**P - 2**	**P - 1**	**P - 0**	**P + 1**	**P + 2**
STATE	dry	dry ⇨ wet	wet	wet ⇨ dry	dry
Cumulative DAYS	5	10	15	20	25

Although the calculated P-E index spans the period 1970-1990, the ECMWF data was only considered from October 1986 until March 1991. ECMWF data prior to 1986 could have been used, but the moisture flux variables would have been

University of Cape Town

inaccurate. The case studies were chosen from 1986 to 1991 which is the period of data overlap. Unfortunately, the OLR data does not overlap and was not used to select case studies.

The P-E normalised index was used to establish individual case studies. Twelve ISO event case studies in total were chosen based on the following criterion :

The P-0 had to be the wet event, preceded by 2 dry pentads and followed by two dry pentads. The normalised deviation of P-0 had to be positive, indicating a pentad rainfall event.

The following cases studies were chosen :

case 1 : 27 Nov 1986 - 21 Dec 1986
case 2 : 17 Dec 1986 - 10 Jan 1987
case 3 : 10 Feb 1987 - 06 Mar 1987
case 4 : 18 Oct 1987 - 11 Nov 1987
case 5 : 17 Nov 1987 - 11 Dec 1987
case 6 : 12 Dec 1987 - 05 Jan 1988
case 7 : 02 Nov 1988 - 26 Nov 1988
case 8 : 27 Nov 1988 - 21 Dec 1988
case 9 : 27 Dec 1988 - 20 Jan 1989
case 10 : 31 Jan 1990 - 24 Feb 1990
case 11 : 02 Mar 1990 - 26 Mar 1990
case 12 : 02 Mar 1991 - 26 Mar 1991

University of Cape Town

As can be seen, these case studies have been chosen across the entire summer period, that is, from early summer in October until late summer in March. As a result of the ECMWF data only being considered after 1986, all the case studies are between 1986 and 1991.

Listed in table 2-2 are the normalised deviations of P-E for each of the 5 pentads of each case study :

Table 2-2 : Pentad P-E normalised deviations.

CASE #	P - 2	P - 1	P - 0	P + 1	P + 2
1	- 0.63 *	0.11	1.04 *	- 1.13 *	- 0.50 *
2	- 0.50 *	- 0.60 *	0.39	- 0.50 *	- 1.22 *
3	- 0.64 *	- 0.88 *	0.12	0.04	- 0.90 *
4	- 0.60 *	- 1.00 *	0.54	- 0.22	0.06
5	- 0.75 *	- 0.77 *	0.32	0.25	- 0.90 *
6	- 0.16	0.35	0.58	- 0.69 *	- 0.95 *
7	- 0.20	0.17	0.69	0.88	- 0.46
8	0.16	- 0.30 *	1.39 *	0.75	0.37
9	0.75	1.46	2.21 *	- 0.09	- 0.51 *
10	0.11	0.35	1.47 *	- 0.50 *	- 0.72 *
11	0.76	- 0.19	1.47 *	- 0.08	- 0.72 *
12	0.45	0.03	1.82 *	0.66	- 0.32

* denotes cases chosen for pentad composites.

When determining the composites, the following criteria were used :

University of Cape Town

- P-2 : deviations < - 0.50
- P-1 : deviations < - 0.25
- P-0 : deviations > +1.00 and < +2.25
- P+1 : deviations < - 0.25
- P+2 : deviations < - 0.50

Cases for P-0 which showed positive deviations greater than 2.25 were rejected as they are extreme cases and one or two extreme cases can greatly influence the mean result.

Hence, for P-2, cases 1-5 were used; for P-1, cases 2-5 and 8; for P-0, case 1 and 8-12 , for P+1, cases 1-2, 4, 6 and 10; and for P+2, cases 1-3, 4 and 5, 9-11 (the * in Table 2-2 denotes the case studies chosen). Each pentad composite (P-2 to P+2) therefore has at least 5 case studies. All the pentad data were added together to obtain a 25-day mean (all pentad mean) and then deviations from this mean were calculated for each composite pentad. Therefore, from a series of individual case studies, a series of composite pentads and composite deviations were established for spatial synoptic analyses of the various meteorological parameters, both observed and derived.

University of Cape Town

2.2.4 Meteorological parameters used

As mentioned above, the observed parameters used for spatial synoptic analyses include geopotential height, temperature, zonal, meridional and vertical winds and relative humidity. However, these are very basic meteorological parameters. It has long been acknowledged that precipitable water is a better indicator of atmospheric moisture than relative humidity, hence precipitable water is one of many derived

variables used in this study. A description of all the other derived meteorological parameters used in this study will be discussed. Owing to the vast size of the individual processed data files and the time involved in processing them, only two atmospheric levels were analysed, namely data at 850 and 200 hPa. This decision is in line with many previous studies were the 850 and 200 hPa levels have been used to represent the lower and upper tropospheric levels, respectively. The 850 hPa also co-incides with the South African Plateau (1500 m above mean sea-level). The 500 hPa surface is used for representing vertical winds as this is the level of non-divergence and maximum vertical winds.

University of Cape Town

2.3 KINEMATIC COMPUTATIONS

2.3.1 Velocity potential and Streamfunction

Chen and Yen (1991) have shown that the velocity potential at 200 hPa (χ_{200}) is a useful meteorological parameter in studying ISO's. Streamfunction budget analysis is also an invaluable analytical tool and together with velocity potential, is very useful in analyses of circulatory patterns. Going one step further than looking only at divergence and vorticity of the total horizontal wind, velocity potential and streamfunction are more useful since they are components of the horizontal circulation wind vector and give useful representations in the tropics where mean winds are light.

The total two-dimensional horizontal wind vector (**V**) can be written in the form :

$$\mathbf{V} = \mathbf{V}\psi + \mathbf{V}\chi \qquad \text{Eq. 2.1}$$

where $\mathbf{V}\psi$ is the non-divergent or streamfunction (rotational) component and $\mathbf{V}\chi$ is the divergent or velocity potential (irrotational) component of the total wind (Krishnamurti et al., 1973). The total two-dimensional velocity field components, written in Cartesian co-ordinates are as follows :

$$u = - \partial\psi / \partial y + \partial\chi / \partial x \qquad \text{Eq. 2.2}$$

$$v = + \partial\psi / \partial x + \partial\chi / \partial y \qquad \text{Eq. 2.3}$$

$$\begin{aligned} \text{Vorticity } (\nabla \times \mathbf{V}) &= \partial v / \partial x - \partial u / \partial y \\ &= \partial^2\psi / \partial x^2 + \partial^2\psi / \partial y^2 \\ &= \nabla^2\psi \end{aligned} \qquad \text{Eq. 2.4}$$

$$\begin{aligned} \text{Divergence } (\nabla \bullet \mathbf{V}) &= \partial u / \partial x + \partial v / \partial y \\ &= \partial^2\chi / \partial x^2 + \partial^2\chi / \partial y^2 \\ &= \nabla^2\chi \end{aligned} \qquad \text{Eq. 2.5}$$

where χ is the velocity potential and ψ is the streamfunction.

From the Laplace equation, $\nabla^2\chi = \nabla \bullet \mathbf{V}$, χ can be calculated if the wind components are known over a grid domain. Strict boundary conditions need to be adhered to when solving this equation through relaxation processes. Since this study is based on the entire data set available, there are four zero-boundaries, where χ is set to zero, that is 20° N, 60° S, 30° W and 100° E. Here these fields

University of Cape Town

are analysed at 200 hPa and 850 hPa. Note that positive (+) velocity potential is convergence and positive (+) streamfunction is anticyclonic in the Southern Hemisphere, but streamfunction *anomalies* show the opposite convention in the in the Southern Hemisphere, i.e. positive (+) *anomalies* are cyclonic and negative (-) *anomalies* are anticyclonic (Weickmann and Khalsa, 1989).

It must be remembered that velocity potential spatial features do not directly represent those of the divergence field. Divergence is the Laplacian of velocity potential. Velocity potential patterns are generally characterised by larger spatial scales.

2.3.2 Horizontal Kinetic energy

Kinetic energy is the energy of motion and can be calculated relatively easily, if the wind components are known, from the following relationship :

$$KE = \tfrac{1}{2} (u^2 + v^2) \quad \text{per unit mass} \qquad \text{Eq. 2.6}$$

where : u = the zonal wind component

v = the meridional wind component

University of Cape Town

2.4 THERMODYNAMIC AND MOISTURE COMPUTATIONS

2.4.1 Precipitable Water

Precipitable water (PW) is a measure of the atmospheric vertically integrated water content, either measured in g kg^{-1} or millimetres (mm). Defining PW of a column of air theoretically, it is the depth of water that would be obtained if all the water

in the column were condensed onto a horizontal plane of unit area. Mathematically, PW is defined between two specified atmospheric levels as :

$$PW = \frac{1}{g} \int_{p_2}^{p_1} x \ \delta p \qquad \text{Eq. 2.7}$$

where : x (see Appendix A) is the mean mixing ratio between pressure set levels p_1 and p_2, (p_1 = 1000-850 hPa, p_2 = 300 hPa);

$g = 9.80665 \text{ m s}^{-2}$

Normally, precipitable water is integrated between 850 hPa and 300 hPa (Chen and Tzeng, 1989), but for purposes of this study to more truly represent the moisture parameters, it was decided to integrate from the 1000 hPa level if the altitude of the data grid point was below 1000 meters above sea level, or to integrate from the 850 hPa surface if the data grid point was above 1000 meters. It was felt that by including the layer between 1000 hPa and 850 hPa, where possible, a fuller picture is obtained of how much maritime moisture is actually available. For purposes of this study, PW is in mm.

University of Cape Town

2.4.2 Water Vapour Flux

Water vapour flux (transport) ($\mathbb{Q}$) is defined as the advection of precipitable water by the horizontal wind. The total horizontal mean flux of water vapour, $\mathbb{Q}$, ($\text{g cm}^{-1} \text{ sec}^{-1}$) is obtained through vertical integration :

$$\mathbb{Q} = \frac{1}{g} \int_{p_2}^{p_1} q\mathbb{V} \ \delta p \qquad \text{Eq. 2.8}$$

where :

q = specific humidity (g kg^{-1}) (see derivation of q in Appendix A)

g = gravitation constant (m s^{-2})

$\mathbb{V}$ = horizontal wind vector in the layer (δp : m s^{-1})

p_1 = 1000-850 hPa, p_2 = 500 hPa.

The individual qu and qv components of the total two-dimensional horizontal wind are combined to give a water vapour flux vector $\mathbb{QV}$, which has both direction and magnitude.

Magnitude of the vector is calculated from :

$$\sqrt{(qu)^2+(qv)^2} \qquad \text{Eq. 2.9}$$

and direction from :

$$\arctan\left(\frac{qu}{qv}\right) \qquad \text{Eq. 2.10}$$

Since moisture in the atmosphere is concentrated in the lowest levels of the troposphere, the weighted vector average often reflects flow below 500 hPa, and is very similar to the 700 hPa level. It was felt that flow above 500 hPa may distort the results, thus integration is from the surface, as with precipitable water, to the 500 hPa level.

2.4.3 Divergent water vapour flux

The water vapour flux divergence is the velocity potential of water vapour flux. The velocity potential function is solved once the water vapour flux components

University of Cape Town

have been calculated using equation 2.8. Water vapour flux divergence is therefore a vertically integrated resultant meteorological variable and gives valuable insight into the spatial synoptic patterns of the divergent (non-rotational) nature of moisture in the integrated atmosphere. It is a more useful forecasting tool than velocity potential alone, since water vapour is included.

2.4.4 Non-divergent water vapour flux

As the name suggests, this variable is the rotational component (streamfunction) of the total two-dimensional horizontal water vapour flux circulation. It is also a vertically integrated resultant meteorological variable and may be useful in analysing the spatial features of the rotational component of the water vapour flux vector. This variable is calculated once the water vapour flux components have been calculated using equation 2.8.

The methodology described to study wet and dry composite pentads over southern Africa, and the results obtained from these analyses forms the focus for the remainder of this study.

2.5 COMPOSITE COMPUTATIONS

The asterisk (*) in Table 2-2 denotes all the case studies chosen for the various pentad composites. Since not all precursor events are dry, and not all post wet-events are dry only those cases where standard deviations were sufficiently negative were chosen for the composites. All P-2 to P+2 data as referenced at each grid point were added together for the individual composites to create a mean composite.

University of Cape Town

The anomaly fields were calculated by subtracting the mean for all the pentad cases from P-2 to P+2 from the individual P-2 to P+2 mean composites.

A temporal trend pentad composite was also established by subtracting the mean pentad composite for P-2 from P-1. This was done for forecasting purposes.

Only mean pentad composites are shown for P-1 and P-0 to illustrate maximum contrast between composites. All pentad anomaly composites are shown.

2.6 HOVMÖLLER PLOT ANALYSIS

Longitude-time diagrams or Hovmöller plots are useful in identifying propagating features in the atmosphere. Various parameters have been plotted at 10° S and at 40° S between 30° W and 100° E (or 25° W and 95° E depending on which parameter). 10° S was chosen to highlight the MJO oscillations, while 40° S was chosen because of its location in the mid-latitide wind belt and to see whether there is an ISO signal at 40° S in the various parameters. Another reason for choosing these two latitudes is to examine possible tropical-temperate linkages as proposed by Chen and Yen (1991) and D' Abreton (1992). Pentad data for the entire summer are plotted, therefore all the Hovmöller plots are of the entire summer from the beginning of October to the end of March for all the available ECMWF data, i.e., the summers of 1987 to 1992.

Anomaly data are plotted and shown. This anomaly data has been calculated by subtracting the longitude-time mean value at each grid point as shown in Appendix B. This has the effect of removing variations across the longitude imparted by the

University of Cape Town

underlying surface, and of removing the seasonal signal. Chapter 4 presents and discusses the results.

The wet phase (P-0) of each study is shown by a cross on each of the plots at both 10° S and 40 ° S. The wet phase occurring at 25° S, 25° E can then be compared to meteorological process occurring in the tropics and the midlatitudes.

Looking back at chapter 2 a methodology has been put forward to analyse the geophysical data available for this research of ISO's. It may not be a perfect methodology, but it is a sound approach to this work. Weaker points of this methodology include the use of A-class pan evaporation data instead of a derived evaporation index, but its use has been justified under the circumstances.

University of Cape Town

CHAPTER 3

OUTGOING LONGWAVE RADIATION AND

PRECIPITATION -EVAPORATION ANALYSIS

INTRODUCTION

To establish the presence of an ISO in South Africa OLR data and P-E data have been analysed. Since OLR is a good proxy for convection any ISO detected in this data should imply an oscillatory nature of the convection over southern Africa. P-E data showing an ISO will confirm this result.

University of Cape Town

3.1 OUTGOING LONGWAVE RADIATION

3.1.1 Inter annual OLR variability

RESULTS

The unfiltered pentad OLR data set at 25° S, 25° E for the October to March period was statistically analysed first. Both inter annual and intra-seasonal statistics were calculated, prior to performing spectral analysis. All statistics relate to the period 1975 to 1987 (excluding 1978 and 1979 where satellite data was missing). Table 3-1 shows the inter annual statistics.

Table 3-1 : OLR statistics (W m^{-2}) for 1975-1977, 1980-1987.

MAX	307.4
MIN	174.8
MEAN	253.5
STD. DEV	20.9
YEARS	11

DISCUSSION

Figure 3-1 shows inter annual variability in the period 1975 - 1987. A distinct change is noticeable in the different OLR variables between 1981 and 1982. This marks the change from the wetter 1970's to the drier 1980's. A distinct feature is the higher mean OLR values during the drier 1980's, that is, higher OLR values indicating less cumulus convection and hence less rain. Figure 3-2 shows the mean pentad OLR as snormalised deviations of the mean, and the transition from wet to dry (1981 to 1982) is obvious.

Maximum and minimum pentad OLR values are lower during the wetter 70's and this is to be expected with enhanced cumulus convection. As cumulus convection decreases in the 80's the maximum and minimum values increase and this is evident from Figure 3-1.

Normalised deviations of pentad OLR show increased variance during the wetter 70's as compared to the drier 80's (Figure 3-2). This can be attributed to fewer convective events during the 80's, hence the range between wet and dry events is minimised.

University of Cape Town

3.1.2 OLR intra-seasonal oscillation Calendar and statistics

Figure 3-3 shows a subjective count of the number of pentads per oscillation. The length of each oscillation was calculated by counting the number of pentads in each oscillation where the lowest pentad standard deviation was less than -0.5. It can be seen that the average length of the ISO operating in the unfiltered OLR is between 20 and 35 days, i.e. 4 to 7 pentads. Almost 80% of all OLR ISO's operating during the summer in the southern African region are between 20-30 days which is significant.

The results of the OLR analysis is shown for individual years as a calendar in Figure 3-4. Filterered OLR values are plotted for each year. The various case studies used in the composite analysis are highlighted by a "C" and the case study number mentioned in Chapter 2. The arrow points at the wet phase/pentad of the chosen case study, i.e P-0.

It is clear from the various years in Figure 3-4 that intra-seasonal variability exists in the OLR data centered on 25° S, 25° E over southern Africa. The ISO length varies from year to year. During 1986 a longer ISO operates, whereas 1977 shows a much shorter ISO operating during the summer. A few low OLR values (indicating wet events) occur during some of the summers. This is seen during 1975 during pentad 22; in 1976 during pentad 21 and in 1977 during pentad 25. Few very high values exist during the wetter 1970's, however, high values are evident during the drier 1980's. 1982 shows a very high OLR value during pentad 5 and 6 during the early summer. 1986 exhibits three high maximum peaks during the summer. Also of note is the regularity with which low OLR values occur

University of Cape Town

during late January, i.e pentads 20-26. This indicates the possiblity that the ISO as seen in the OLR is phase-locked or seasonally dependent.

3.1.3 Intra-seasonal OLR mean variability and spectra

RESULTS

The intra-seasonal oscillation is very apparent in the pentad OLR data. It should be noted that the OLR data has been de-seasonalised by removing the seasonal signal. Figure 3-5 shows the unfiltered deviations. The unfiltered OLR data shows the 20-30-day oscillation. Positive (negative) deviations indicate above (below) normal OLR or below (above) normal rainfall. Even with the seasonal siganal removed, a time series is left and is shown by Figures 3-5 and 3-6 which infer that the ISO is seasonally phase locked indicating a seasonal dependence. From Figure 3-6 it can be seen that the first seasonally dependent ISO starts at the beginning of October and lasts 40 days (8 pentads), the second ISO lasts 25 days, the third lasts 25 days, the fourth lasts 50 days and the last ISO lasts 30 days.

On average the first minor wet-spell of the summer occurs towards the end of October, from pentad four to pentad seven. The first major wet-event occurs towards the end of November (pentad 11) to early December (pentad 13). The other major wet-event period lasts from the middle of January (pentad 20) to the middle of February (pentad 26). A final wet-event occurs during the middle of March (pentad 33).

There are three distinctive dry-spells during the South African summer. The middle of November shows a large positive OLR deviation. Another large positive deviation in OLR occurs towards the end of December and into the first 10 days of

University of Cape Town

January. The middle of February also shows positive deviations. Figure 3-7 shows the negative (positive) deviations more clearly.

ISO MEAN SPECTRUM

RESULTS

A method of periodograms and Fast Fourier Transform (FFT) spectral analysis was performed on the raw and 3-point binomial filtered pentad OLR data. Both methods described above showed two peaks (raw data results are shown in Figure3-7).

DISCUSSION

From the spectral analysis (Figure 3-7), the two spectral peaks show cycles operating at 45-60 days and 20-30 days. However, in chapter 5, emphasis will be placed on the 20-30 day ISO, while chapter 4 will look at the 40-60 day MJO. Since the mean OLR spectrum exhibits a typical "red-noise" spectral distribution, the peak at 25.7 days is significant. However, the FFT frequencies are fixed, hence the peak at 25.7 days, but the subjective count of the mean pentad length per oscillation in the OLR data (Figure 3-4) showed that the mean ISO length was between 20-30 days. Hence, the OLR data for a 2.5° radius centred on 25° S and 25° E shows a dominant ISO operating at 20-30 days. This is shorter than the MJO which is 40-60 days.

University of Cape Town

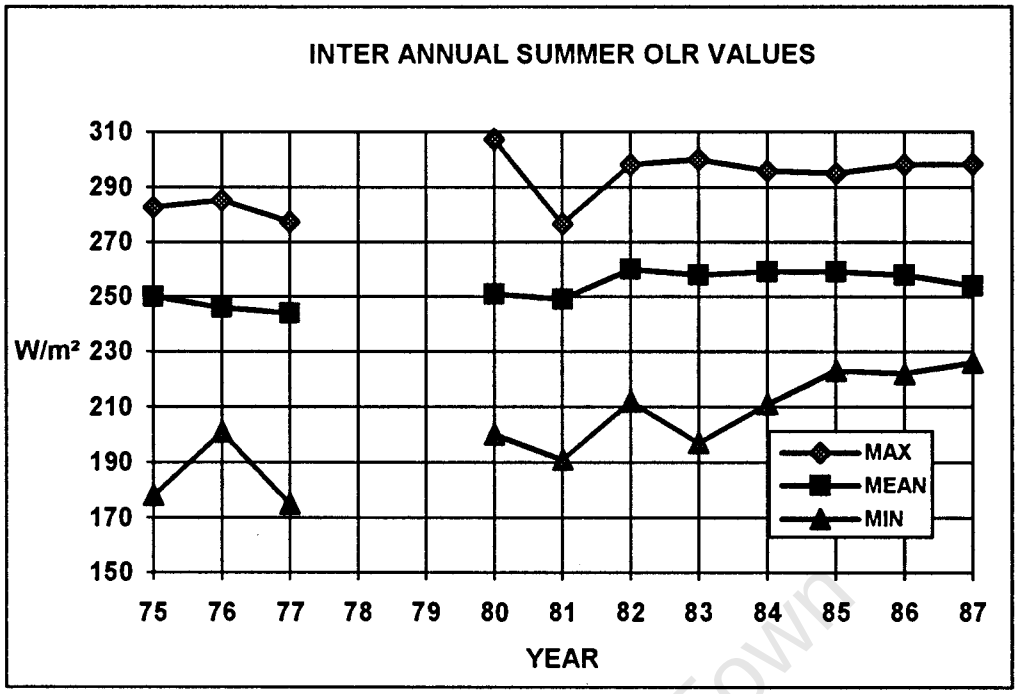

Figure 3-1 : Maximum, minimum and mean summer OLR values (W m^{-2}).

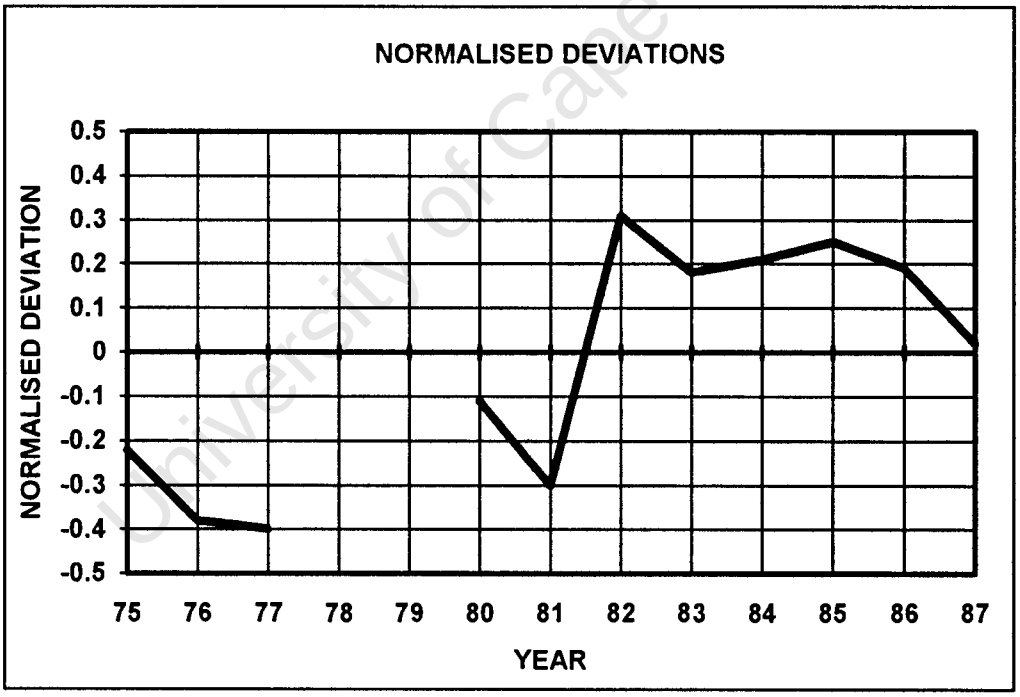

Figure 3-2 : Mean summer OLR normalised deviations.

University of Cape Town

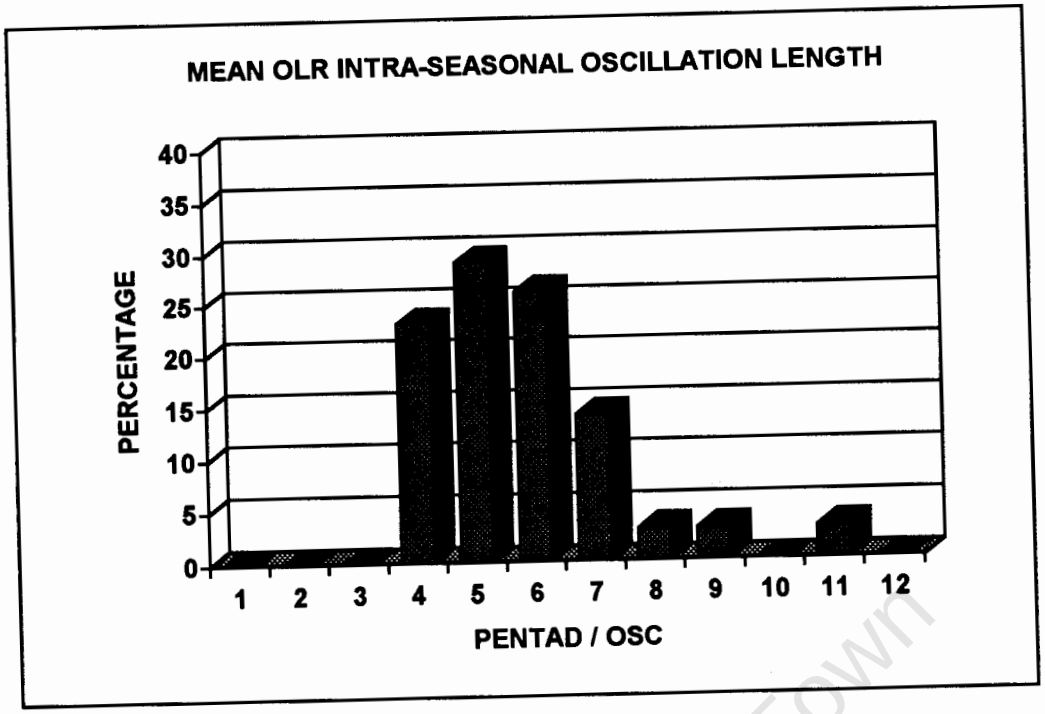

Figure 3-3 : Mean OLR ISO length shown as pentads per oscillation.

University of Cape Town

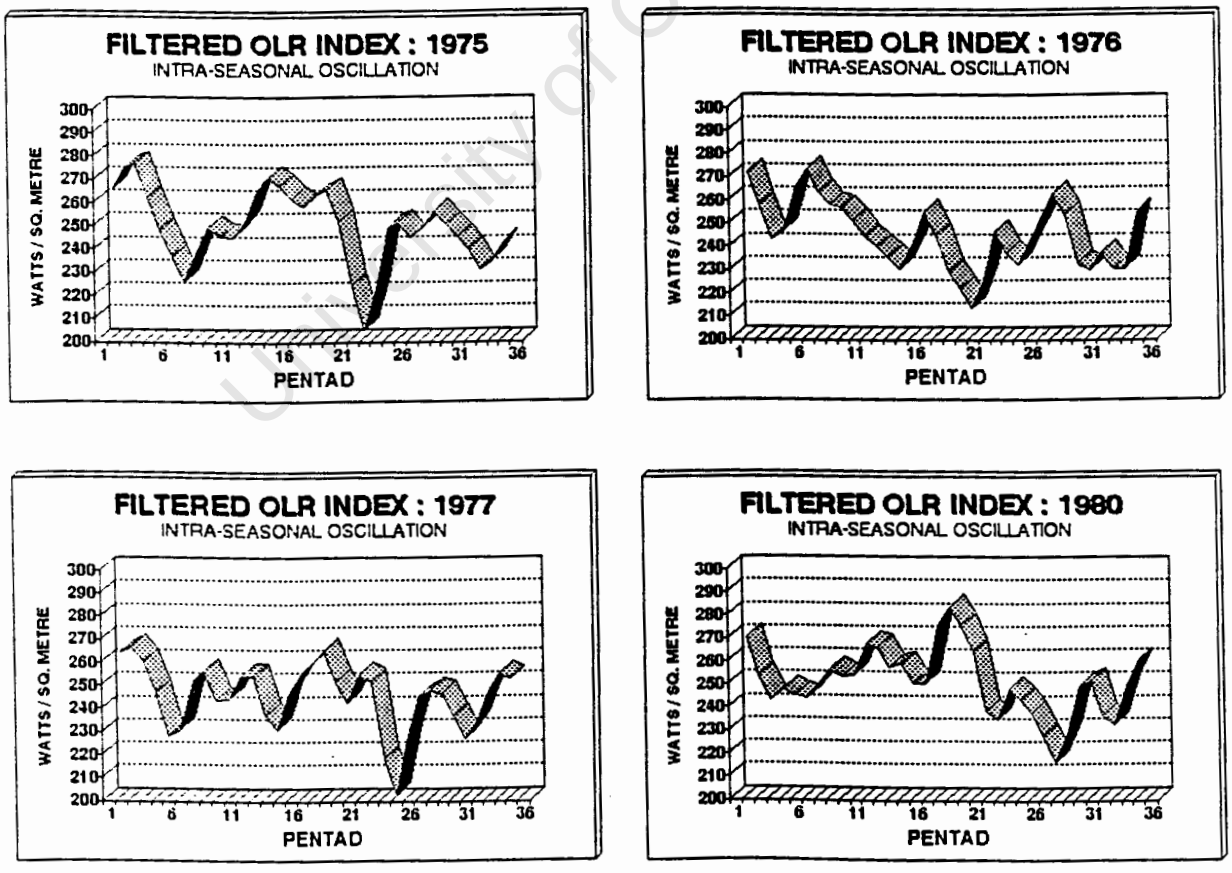

Figure 3-4 : Filtered OLR indices for individual years, 1975-1977, 1980-1987, showing intra-seasonal oscillations.

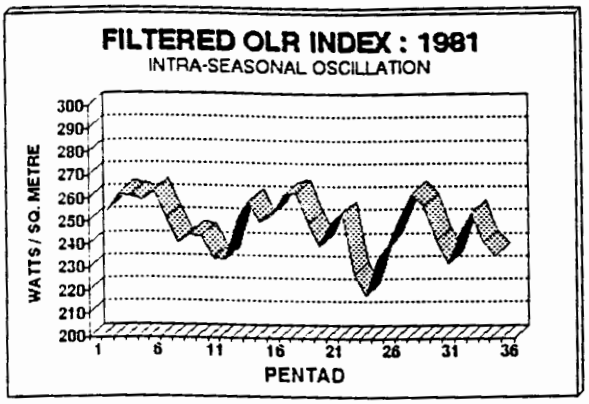

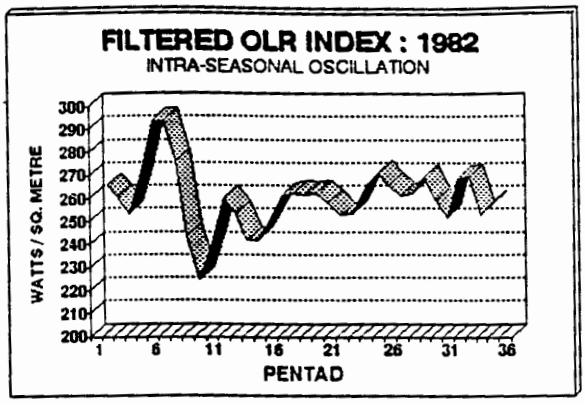

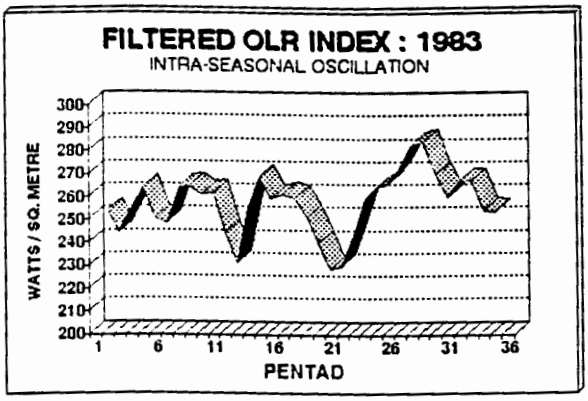

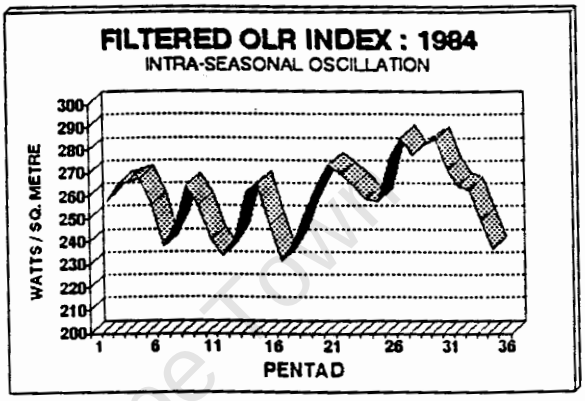

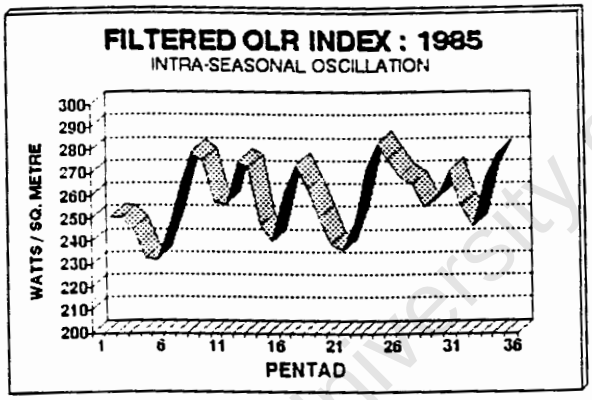

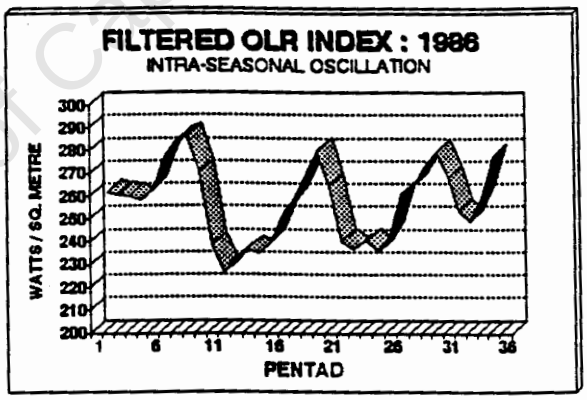

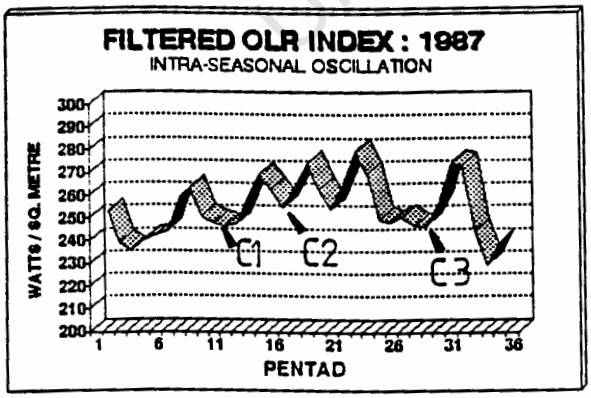

Figure 3-4 (continued)

University of Cape Town

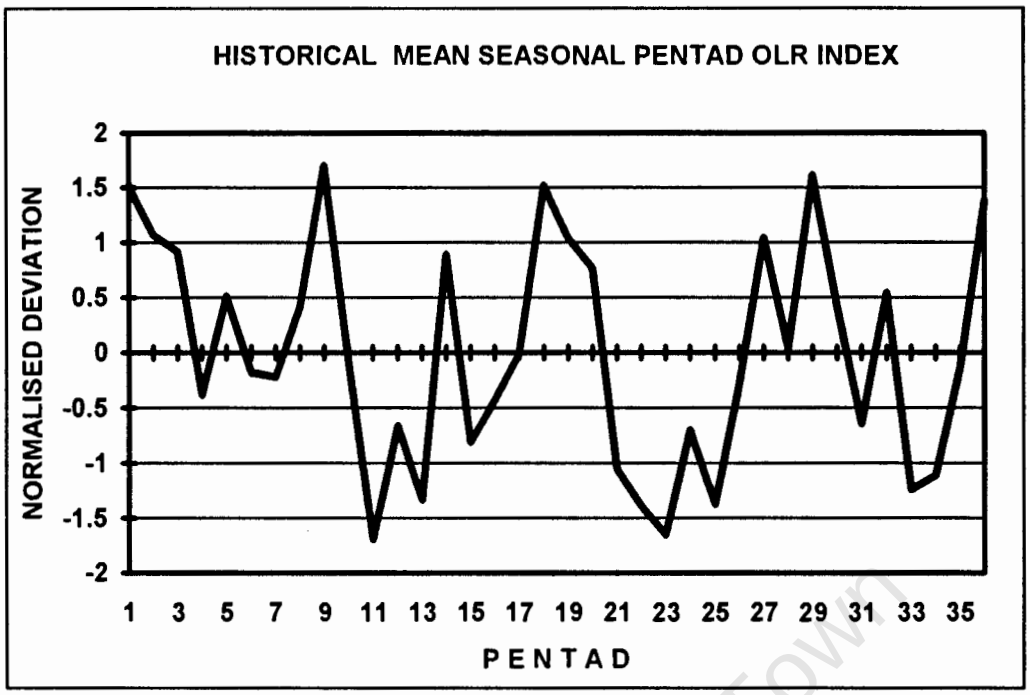

Figure 3-5 : Unfiltered mean intra-seasonal OLR pentad normalised departures for 1975 to 1987.

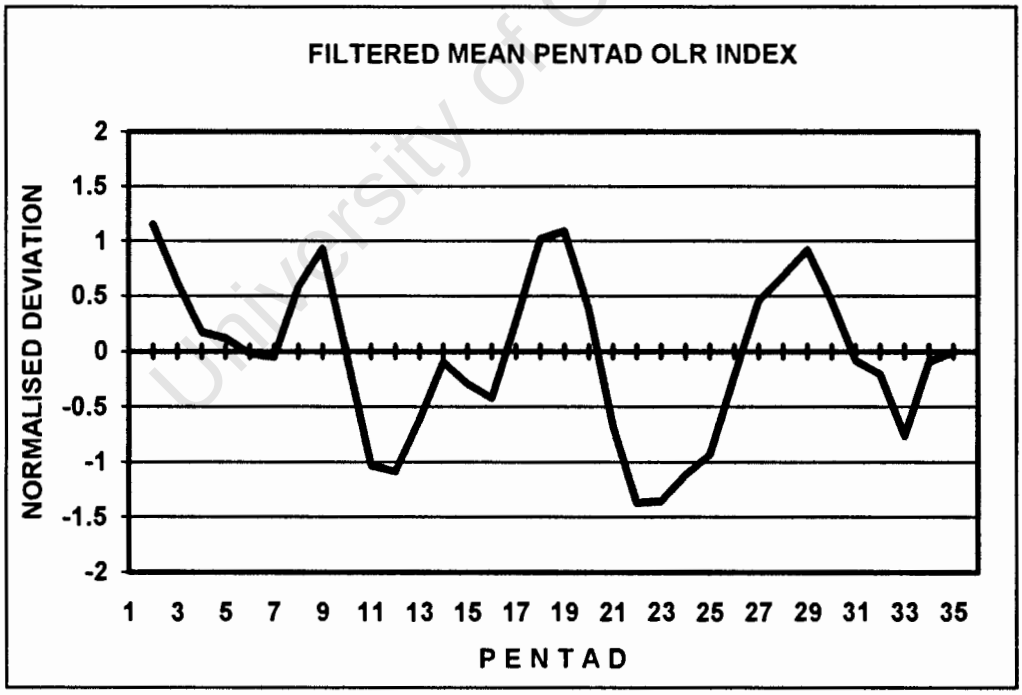

Figure 3-6 : Filtered mean intra-seasonal OLR pentad normalised departures (1975-1987).

University of Cape Town

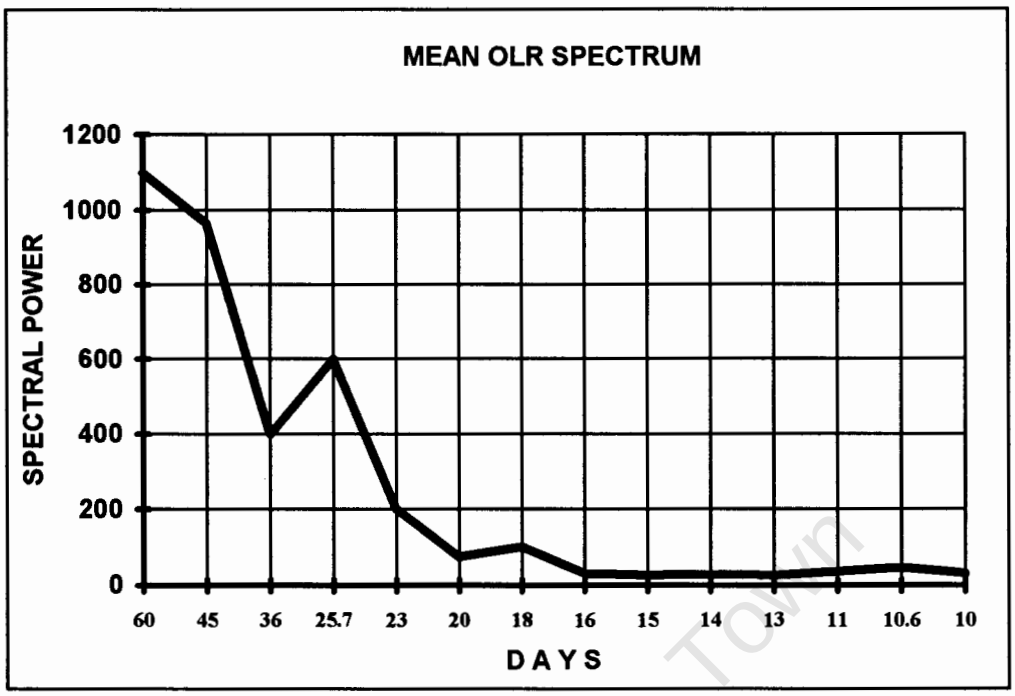

Figure 3-7 : Mean summer spectrum of OLR pentad values.

3.2 PRECIPITATION - EVAPORATION DATA

Since an index of precipitation minus evaporation (P-E) was created and analysed, separate statistical results of precipitation and evaporation will not be discussed. As mentioned in chapter 2, the reason for combining the precipitation and evaporation indices was to obtain a measure for drought events. The P-E index therefore shows a better match to the OLR index, although it is opposite in sign(when comparing standardised deviations). This is a result of negative OLR values being synonymous with high P-E values, i.e. wet events.

The results of the inter annual and intra-seasonal, the P-E calendar as well as the mean P-E spectrum will be discussed to highlight any similarities or differences found in the OLR index analysis. The P-E index is a more complete record too !

University of Cape Town

3.2.1 Inter annual P-E variability

RESULTS

The statistical results of P-E are listed below in Table 3-2.

Table 3-2 : P-E statistics (mm) for 1970-1992)

MAX	78.0
MIN	-64.0
MEAN	-24.7
STD. DEV	8.9
YEARS	21

University of Cape Town

These results are based on 36 pentad values for each year. Hence the mean pentad value of P-E is for all the pentads for all the summers.

DISCUSSION

From Figure 3-8 it can be seen that the mean P-E index is negative. This means that for the Western Transvaal region of South Africa, evaporation far exceeds precipitation. During the wetter 70's the P-E index is far less negative, indicating increased precipitation and decreased evaporation. However, this situation is reversed during the drier 1980's. This can be seen by the lower P-E values from 1979 to 1988. It is important, therefore, to realise that a longer-term inter annual oscillation is also affecting the climate. How the inter annual oscillation affects the intraseasonal signal will be discussed at the end of this chapter. Figure 3-8 shows the annual maximum, mean and minimum P-E values. It is clear that during the

wetter (drier) 1970's (1980's) maximum values are higher (lower). Minimum values do not show such a contrast between wet and dry periods. It is interesting to note that the magnitude of the deviations is greater in the wetter 1970's than the drier 1980's as seen in Figure 3-9.

3.2.2 P-E Intra-seasonal Calendar and Statistics

Figure 3-10 shows a subjective count of the number of pentads per oscillation. The length of each oscillation was calculated by counting the number of pentads in each oscillation where the lowest pentad standard deviation was greater than +0.5. It can be seen that the average length of the ISO operating in the raw P-E is between 20 and 30 days, i.e. 4 to 6 pentads. Almost 70 % of all ISO's operating during the summer in the southern African region are between 20-30 days which is significant.

The calendar for the P-E index for individual years is shown in Figure 3-11. Case studies are marked on certain years and are indicated by a "C" and the case number. It can be seen that minor rainfall events are interspersed between more major rainfall events.

Looking at individual years, the ISO varies from year to year, but there is no conclusive evidence that the ISO is longer (shorter) in the dry (wet) years. However, during the drier years the longer-term ISO (40-60 days) seems to be more dominant in modulating the seasonal P-E index, whereas during the wetter years the 20-30 cycle is very much more important.

University of Cape Town

What is evident from the yearly P-E indices is the difference in amplitude of the wet and dry events from year to year. The wetter years are generally dominated by many more very positive and negative peaks (Figure 3-11, 1978), while the drier years tend to have fewer dramatic peaks (Figure 3-11, 1985) and the ISO's amplitude is not very great. It therefore appears that the underlying inter annual oscillation is affecting the ISO. The consequence of this also seems to have an effect on the frequency of the ISO. This is significant, since, if the ISO is able to be forecast ahead temporally, the underlying inter annual signal is useful in determining the intensity and duration and number of occurrences of forecasted wet or dry events.

STATISTICS

Figure 3-11 shows that the amplitudes of the short-term ISO varies greatly from year to year. The length of the ISO also is seen to vary from year to year. This raises the question as to whether any relationship exists between the length of the ISO and the mean amplitude of the ISO operating during any one season.

Figures 3-12, 3-13 and 3-14 show the relationships between mean amplitude of the ISO against the mean spectral strength and length of the ISO operating during any particular year.

Figure 3-12 shows the mean ISO amplitude against the mean spectral power of the shorter frequencies of the MJO, i.e., 15-36 days. Figure 3-13 shows the mean ISO amplitude against the mean spectral power of the longer frequencies of the MJO, i.e., 36-60 days. Figure 3-14 shows the mean ISO amplitude against the mean ISO lengths. All three graphs show that the drier years have annual mean negative amplitudes. However, most of the drier years (1980's) show lower spectral power

University of Cape Town

(Figure 3-12 vs Figure 3-13), indicating that during the drier years, there is a tendency for longer ISO's to operate, but this is not confirmed beyond doubt, as in Figure 3-14, the drier 1980's are scattered between 20 and 45 day length ISO's. The picture is a little clearer when observing the wetter 1970's which show that the mean annual amplitude of the ISO is positive. Spectral power for the 1970's are lower in Figure 3-13 indicating that wetter years tend to have shorter ISO's operating. Figure 3-14 confirms this, as most of the wettest years of the 1970's are clustered in the lower right hand side of Figure 3-14.

As to whether any relationship exists between the ISO amplitude and ISO length, Figure 3-14 shows that during dry years, there is a tendency for years with *longer* ISO lengths to have greater *negative* amplitudes, implying more intense and longer droughts, whereas for wet years, there is a tendency for years with *short* ISO lengths to have greater positive ISO amplitudes.

University of Cape Town

3.2.3 Intra-seasonal P-E mean variability and spectrum

RESULTS AND DISCUSSION

Figure 3-15 shows that for all pentads during the summer season (3 October - 31 March) there is a water deficit, which ranges from -40 mm in early summer to -8 mm just after mid-summer to -20 mm at the end of summer. Hence, there is a trend for P-E values to increase from early to late summer. (Evaporation decreases from early to late summer, hence the P-E index increases as it is a negative index)

Separate analyses of the precipitaion and evaporatation indices show that evaporation, reduces significantly during the latter half of summer, from about pentad twenty (P20) which is from 11 January. The deficit is at a minumum at

pentad 23 (P23), which co-incides with 21-25 January, indicating that this is the time of year when cumulus convection occurs most often and is most intense. Rainfall peaks during this pentad and evaporation is at a minimum. The lower P-E values in the latter half of summer indicate the presence of more moisture in the atmosphere over southern Africa. This can be substantiated from dewpoint or precipitable water values during the latter half of summer. It may also indicate different circulation patterns operating during the early summer as compared to the later summer period. The lowest intraseasonal P-E values occur from P8-P10 (7-21 November), where rainfall values are low and evaporation values are high.

ISO MEAN P-E SPECTRUM

RESULTS AND DISCUSSION

Once again a method of periodograms and FFT were used in establishing any periodicity within the P-E index. Spectra were calculated for each year and then averaged to form a mean spectrum as shown in Figure 3-16.

More spectral peaks occur in the P-E index as compared to the OLR index. Separate spectral analysis of the rainfall and evaporation indices show similar results as shown in Figure 3-16. Once again the dominant peaks occur at 45-60 and 20-30 days respectively. The dominant shorter-term periodicity occurs at 20-30 days, and it can therefore be concluded that an ISO does occur in the sub-tropical region of southern Africa and operates at this frequency, although it may be imbedded in the MJO (40-60 day ISO). Hayashi and Golder (1992) have shown that the 20-30 day ISO is independent of the 40-60 MJO and not a half-harmonic of it.

University of Cape Town

Minor periodicities also occur at 13 days, which is near half of the dominant periodicity, and probably a function thereof. The 20-30 day cycle has a greater relative spectral power in the P-E data than the OLR data, when compared to the 60 day spectral peak. This may imply that more intensive, well-organised convective events occur on a longer-term oscillation. This raises the question of rainfall intensities. The shorter-term ISO found in the P-E index may be the result of limited areal sporadic intense rainfall than more widespread general rains associated with convection over a larger area at longer time scales. The more effective rainfall events (longer lasting) may therefore occur at longer frequencies, i.e. 40-60 days, but the 20-30 day ISO indicates that rainfall events oscillate at shorter time interval too ! Looking at the P-E index of individual years (Figure 3-12), this seems to be the case. The following figures show the P-E results graphically. Evaporation is dominant and higher (less negative) P-E values indicate wet conditions.

University of Cape Town

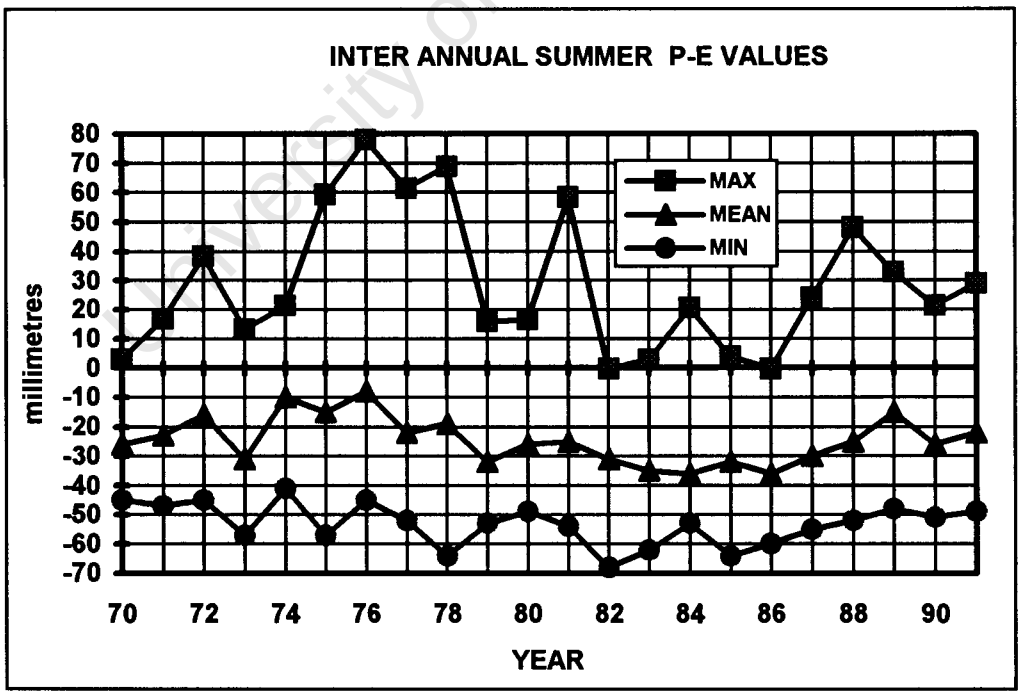

Figure 3-8 : Maximum, minimum ans mean summer P-E pentad values (mm).

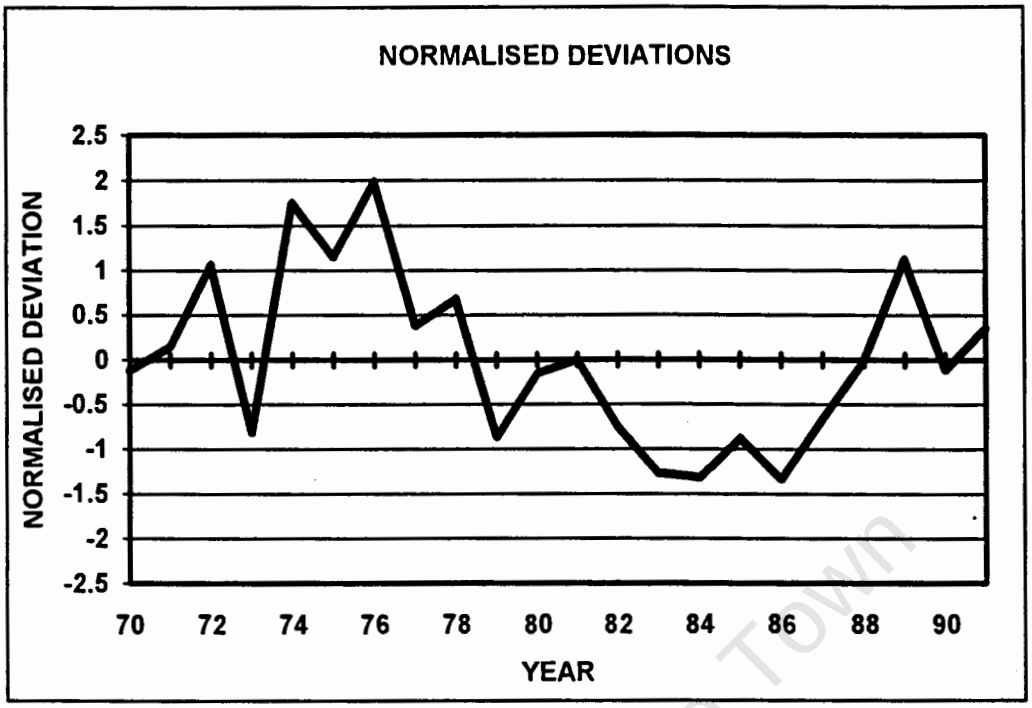

Figure 3-9 : Mean summer P-E pentad normalised deviations.

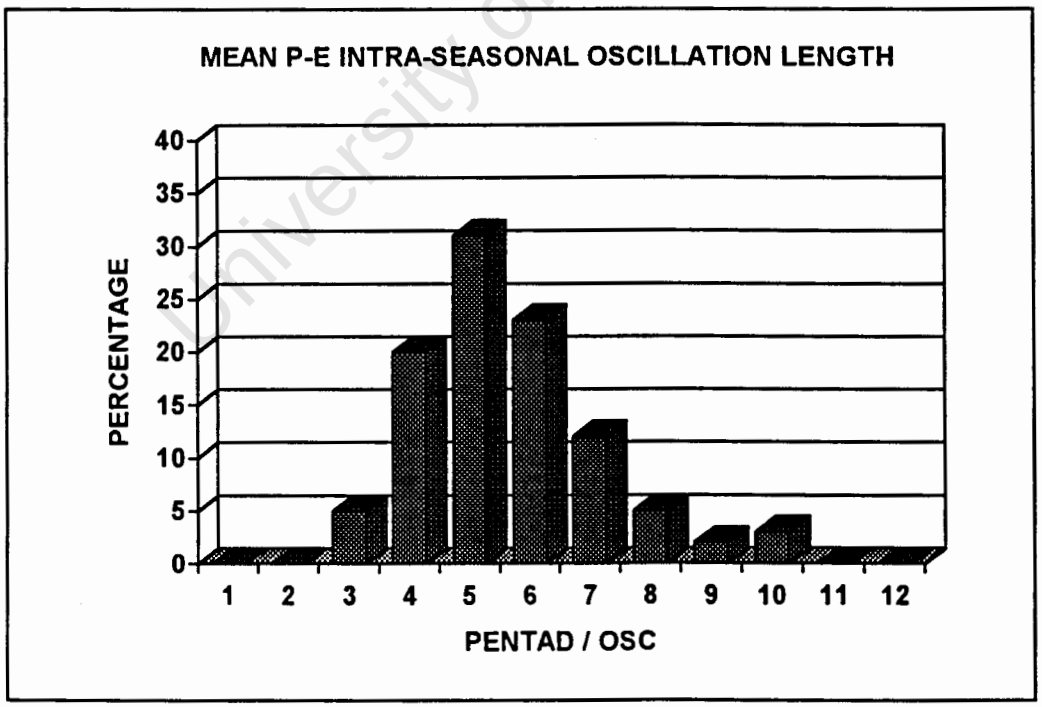

Figure 3-10 : Mean P-E ISO length shown as pentads per oscillation.

University of Cape Town

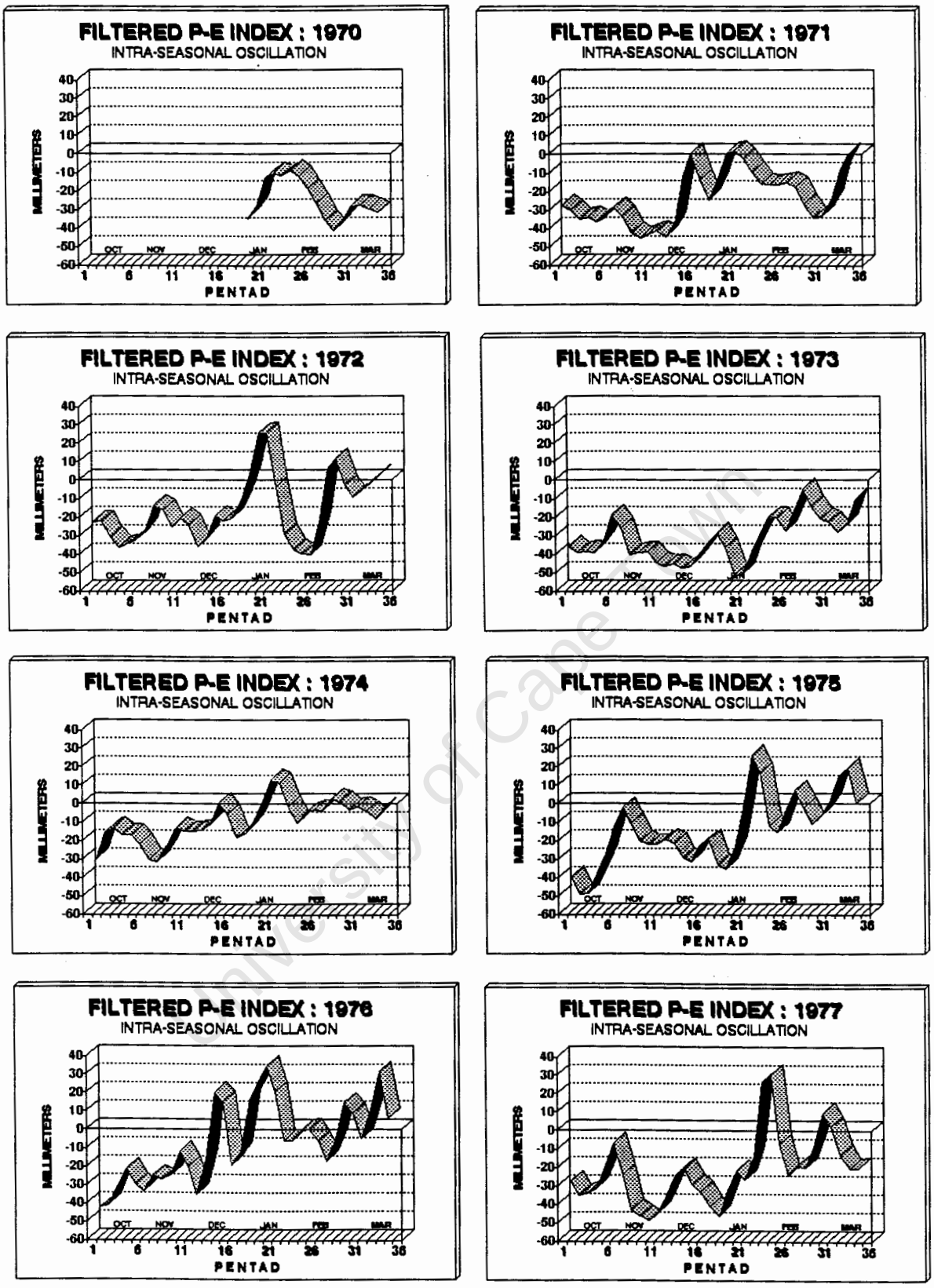

Figure 3-11: Filtered P-E indices for individual years, 1970-1991, showing intra-seasonal oscillations.

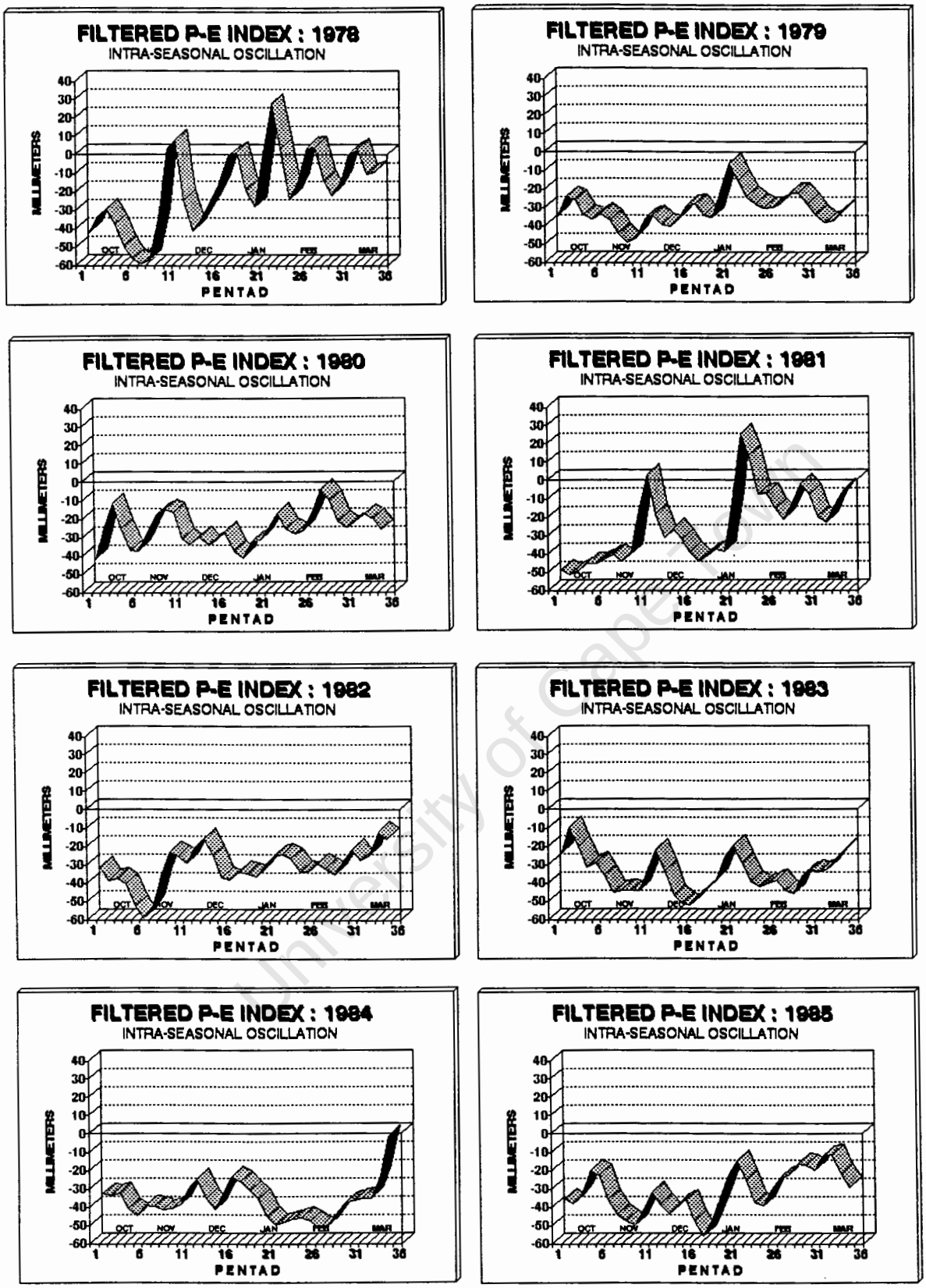

University of Cape Town

Figure 3-11 (continued)

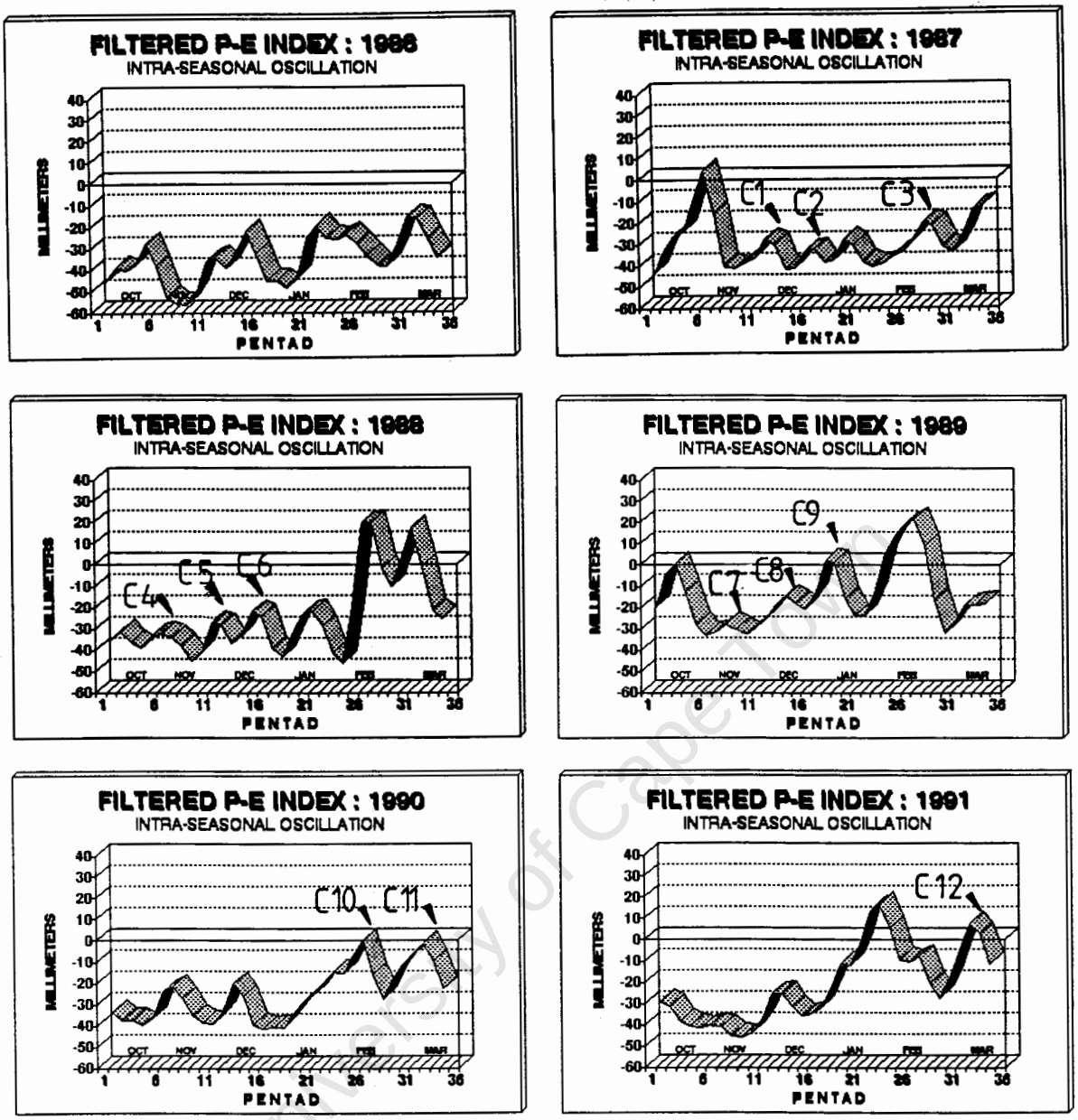

Figure 3-11 (continued)

University of Cape Town

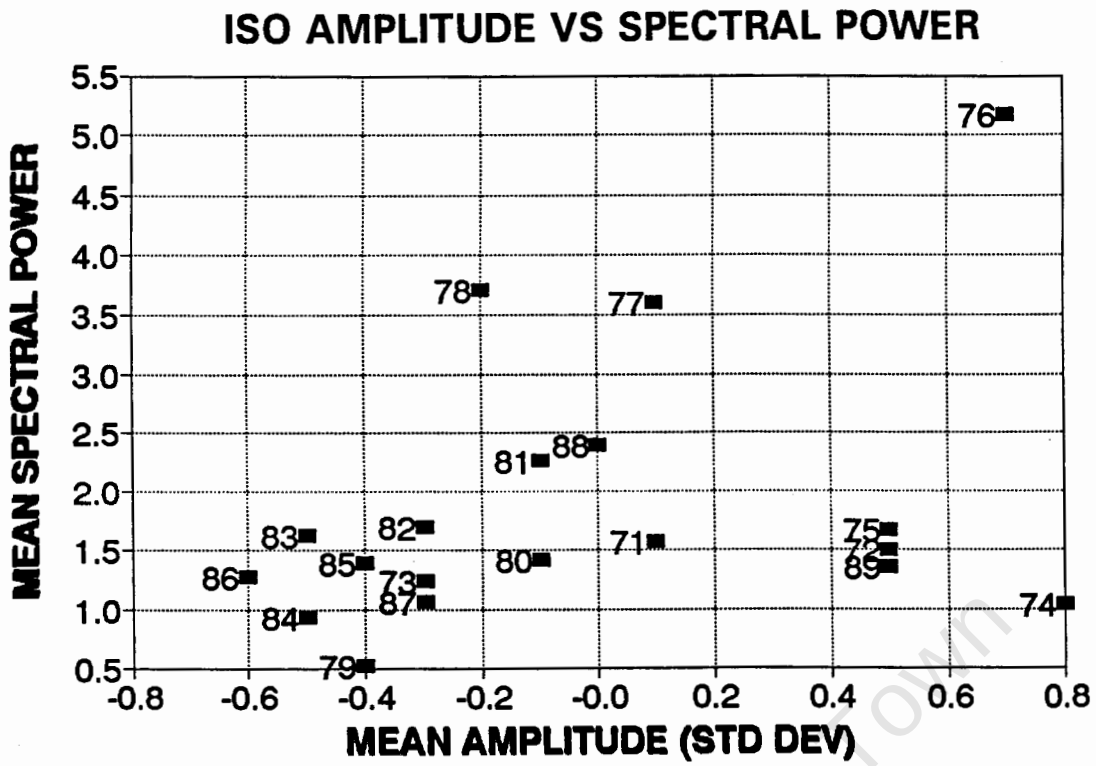

Figure 3-12 : P-E ISO amplitude versus ISO spectral power of individual years for shorter (15-36 day) ISO's.

University of Cape Town

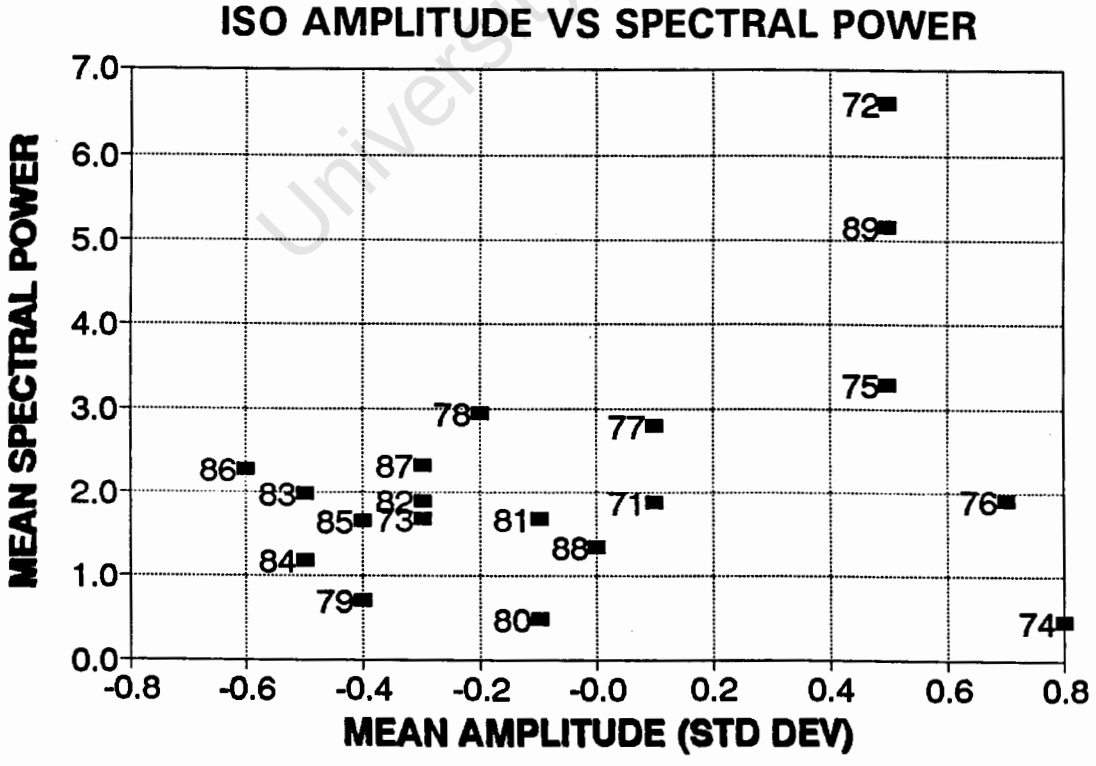

Figure 3-13 : P-E ISO amplitude versus ISO spectral power of individual years for longer (36-60 day) ISO's.

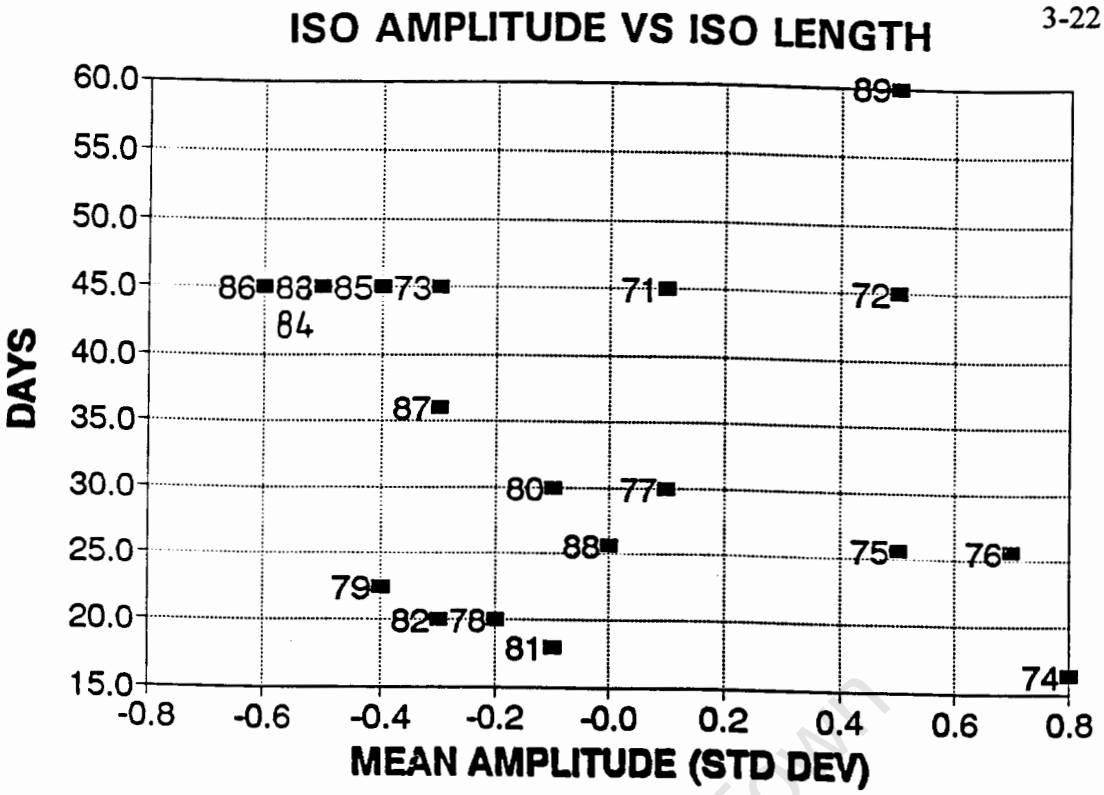

Figure 3-14 : P-E ISO amplitude versus ISO length of individual years.

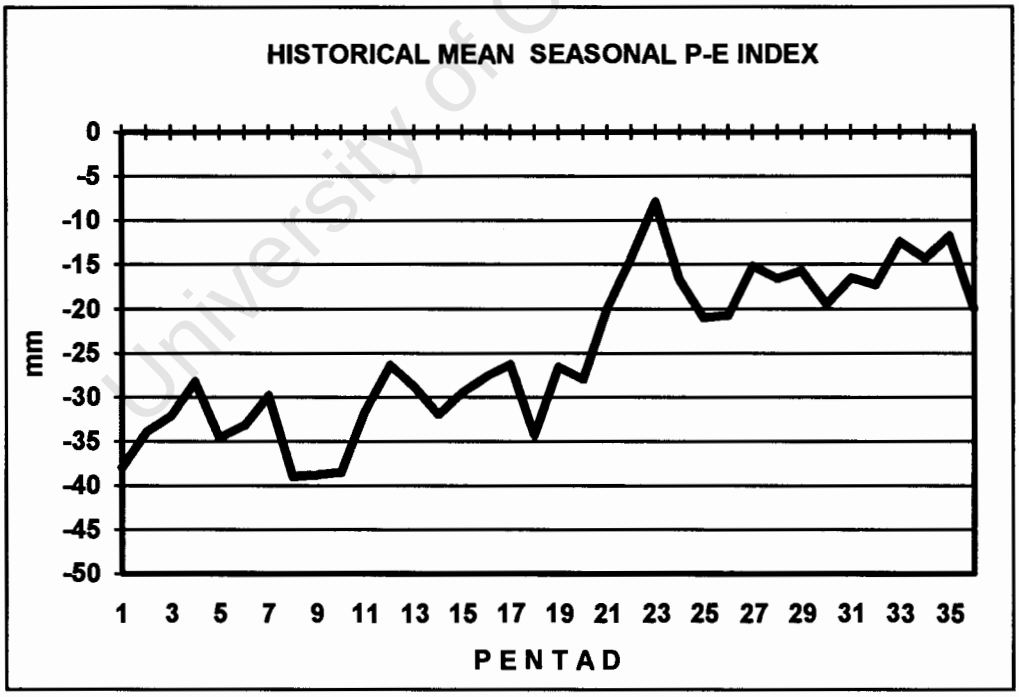

Figure 3-15 : Unfiltered mean intra-seasonal P-E pentad values (mm).

University of Cape Town

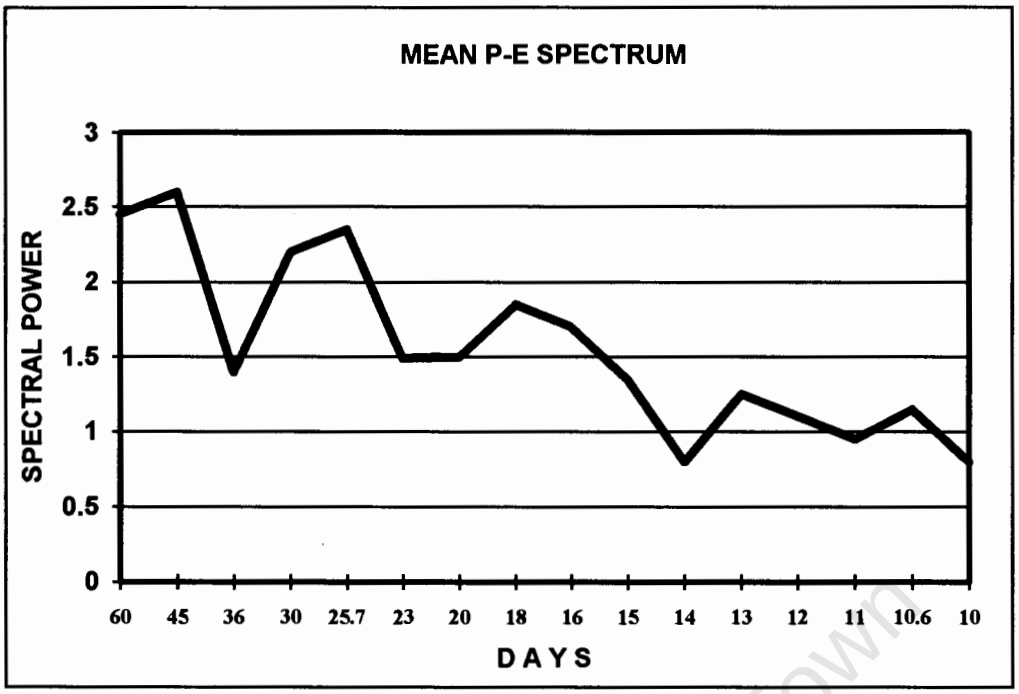

Figure 3-16 : Mean spectrum of summer P-E values.

From the different analyses of the OLR and P-E index, it has been shown that a long-term or inter annual oscillation exists. A short-term (intra-seasonal) oscillation has also been detected. Results of both indices are consistent with each other showing that OLR is a good proxy for convection. The OLR index correlated better with the P-E index ($r = 0.65$, $DF = 34$) than with the rainfall index ($r = 0.56$, $DF = 34$).

This chapter has demonstrated that an intra-seasonal oscillation modulates the weather over southern Africa at a mean frequency of between 20-30 days.

University of Cape Town

CHAPTER 4

HOVMÖLLER ANALYSIS

INTRODUCTION

Longitude-time or Hovmöller plots are most useful for identifying zonally propagating systems and climatic oscillations thereby induced. Longitude-time plots have been plotted for various variables at 10°S and 40°S to investigate the propagating nature of ISO's operating between 20-60 days. Latitude band 40° S was chosen to ascertain whether or not ISO's operating further south in the mid-latitudes are of shorter duration than those found at 10° S. Wang and Rui (1990), Chen and Tzeng (1989) have used Hovmöller plots to identify the propagating characteristics of the MJO. Chen and Tzeng (1989) trace eastward propagating divergent water vapour flux anomalies and precipitable water anomalies using longitude-category plots. This chapter aims at identifying the propagating characteristics of intra-seasonal oscillations found in various meteorological parameters at 10° S and 40° S.

University of Cape Town

Appendix B shows the mean results for the various variables such as geopotential, u- and v-wind components (m s^{-1}) at 200 and 850 hPa, vertical wind (Pa s^{-1}, + indicates sinking motion) at 500 hPa, velocity potential (10^6 m^2 s^{-1}) and streamfunction (10^6 m^2 s^{-1}) at 200 hPa, precipitable water (mm) between the surface and 300 hPa and divergent and non-divergent water vapour flux (10^9 kg s^{-1}) between the surface and 500 hPa. The six summers chosen are between 1987 and 1992. Anomaly results of the 10° S and the 40° S analyses will be discussed. Africa lies between 10° E and 40° E at 10° S on the longitude-time plots.

4.1 RESULTS

4.1.1 LATITUDE 10° S

Only the most interesting features highlighting the propagating nature of ISO's will be discussed.

geopotential height

Figure 4-1a shows the results of the geopotential height longitude-time plots at 200 hPa (P_{200}). Glancing at the years between 1987 and 1992, it can be seen that eastward propagation of troughs (negative anomalies) and ridges (positive anomalies) are rare at 10° S and abrupt changes from a positive to a negative bias across the latitude are more the norm. These last for periods of about one month and may be associated with Hadley Cell anomalies in the northern Indian Monsoon, hereafter referred to as a "flip-flop" phenomenon.

Although almost the entire summer of 1987/1988 shows positive anomalies, an eastward progression of lower positive anomalies does occur from 30° W at the end of November to the middle of January at 30 °E, lasting about 60 days.

A negative anomaly can be seen from 20°E to 90°E in 1989 from the end of October to the end of November. This is followed by a discontinuous positive anomaly during December. A large positive anomaly exists for most of the last two months of summer during 1989, with little propagation evident

1990 displays the alternating nature of the MJO distinctly with two major negative and one major positive anomaly affecting all the longitudes 10° S. Again this may

University of Cape Town

be associated with Hadley Cell anomalies as mentioned earlier. 1991 shows a tendency for a standing wave pattern over Africa at 10° S. The positive anomaly moving eastwards during January intensifies over Africa at about 25° E and then weakens as it moves over the Indian Ocean.

Whereas much of 1988 showed positive anomalies, 1992 shows mainly negative anomalies with two alternating negative anomaly core areas lasting between 20-60 days. The major eastward moving negative anomaly originates over the tropical east Atlantic in early December and then extends eastward rapidly.

The crosses denote the wet event (P-0) of the composite analysis. As mentioned in chapter 2, not all twelve P-0 cases were used. It must be noted here that case 9 (third cross in 1989) is the strongest P-0 case. The first cross in 1987 (case 1), and then all cases as denoted by the crosses from the second one in 1989 were used. It can be seen that during the wet phase over South Africa, the geopotential height at P-0 at 10° S is predominantly *negative,* although cases 1 and 8 show positive anomalies.

Figure 4-1b illustrates that at P_{850} some propagation of geopotential anomalies is evident. Standing waves seem to dominate the geopotential fields of many years, especially 1987, 1989 (La Niña, positive anomaly between 15° E to 30° E), 1991 and 1992 (El Niño, negative anomaly between 15° E to 30° E). An interesting feature to note is that many positive and negative anomalies originate near 45° E and move eastwards. This is particularly noticeable during December and January 1988, a 5 wave train pattern emerges throughout the summer of 1990 and in 1991. In January to March of 1992 alternating anomalies are found in the Indian Ocean at 10° S.

University of Cape Town

Looking at the various case studies it can be seen that the majority of wet events at 25° S, 25° E are associated with positive anomalies at 10° S. Case 9 in 1989 and cases 12 in 1991 are exceptions.

horizontal u-wind component

The u-wind anomaly plots (Figure 4-2a) at P_{200} shows some propagation of anomalies, although not always very distinctly. 1988 shows three positive anomalies moving eastwards across African longitudes during the summer lasting less than 45 days. The negative anomalies propagate eastwards for longer time periods

1992 shows some short anomalies transiting eastwards during the early summer and a retrograding positive anomaly from December to February over the east Atlantic.

There is a tendency for the P-0 events to be associated with negative anomalies at 10° S, i.e. stronger easterlies, although 1990 is an exception where weaker easterlies are evident. An interesting feature is that case 8 (middle cross in 1989) occurs at the onset of the easterlies at the beginning of December at 25° E as seen in the mean u-wind component (Figure B-1). In 1989 westerlies make way for stronger easterlies at the same time as case 8 occurs.

An interesting feature of the mean u-wind component field at P_{850} (Appendix B, Figure B-1) is the zone of westerly winds located over the Indian Ocean and much of Africa at 10° S during the late summer. Easterly winds exist over these areas prior to the end of December. Figure 4-2b gives evidence for both eastward

University of Cape Town

propagating anomalies and standing wave anomalies. Eastward propagation is prevalent over the Indian Ocean in December to January 1987, January to Feb 1988, November to February 1989, the whole summer of 1990, while standing wave patterns emerge in 1991 and 1992.

The strong negative anomalies in 1988 show that the late summer westerly winds over the Indian are replaced by easterlies which tend to propagate eastwards over a period of about 20-60 days. This is again evident in 1990 when a large negative anomaly area moves eastwards from the middle of January from 30°E over the Indian Ocean. 1990 also shows that this negative eastward moving anomaly was preceded and followed by two very strong positive eastward moving anomalies also originating between 30° and 45°E and intensifying east of 60° E. Wang and Rui (1990) have shown that this region (east Africa and western Indian Ocean) is where ISO's are initiated which then propagate eastwards towards the maritime continent.

1992 shows an almost opposite anomaly field to that found in 1988. A large very positive anomaly exists over the Indian Ocean during the early summer, indicating enhanced westerlies at 10° S where an extremely strong positive anomaly exists.

The cases show that most of the wet events at 25°S occur when the easterlies at 850 hPa are stronger at 10° S, except case 9 (last cross in 1989) exhibits stronger westerlies at 10° S. An interesting feature of cases 1, 2, 4, 5, 7, 9, and 11 is that strong low level westerly anomalies originate at about the same time between 30° E and 90° E as the occurrences of wet-events over South Africa.

University of Cape Town

horizontal v-wind component

Both Figures 4-3a and 4-3b show the horizontal v-wind component anomalies. The dominant direction of propagation at both the upper and lower levels is eastward, although at the lower levels, standing wave patterns seem to dominate

Almost all the cases shows that negative (northerly) anomalies in the upper level v-wind component occur at 10° S while the wet event occurs over South Africa. The patterns at the lower levels is less clear. For the P-0 events used in the composites, negative (northerly) anomalies are dominant. Figure B-1 shows that northerlies are dominant over Africa during most of the summer in the lower levels. This indicates that during the wet-event over South Africa, v-component at the lower level have a greater northerly component consistent with a poleward flux of momentum.

vertical wind component at 500 hPa

Although eastward propagation of anomalies is evident, most years exhibit standing wave patterns. This is particularly evident in 1990 and 1992. During 1990 a strong negative anomaly exists during the entire summer over Africa at 10° S. During January 1988, December 1989 and December 1990, eastward propagating negative anomalies can be seen over the Indian Ocean originating from over east Africa. This is consistent with Wang and Rui (1989) findings. In 1991 positive (sinking motion) anomalies were quasi-stationary over Africa. During 1992 a strong positive anomaly exists over Africa during the entire summer. This is of particular interest since the summer of 1991/1992 was dry over the summer rainfall region of southern Africa owing to a strong El Niño event. Over much of the Indian Ocean strong negative anomalies exist consistent with rising motions there.

University of Cape Town

velocity potential at 200 hPa

Appendix B (Figure B-2) shows that south-east Africa and the south-western Indian Ocean exhibit a mean upper level divergent field (negative values), conducive to convection, whereas the South Atlantic Ocean is predominantly convergent. The Hovmöller plots for 1987 to 1992 (Figure 4-5) show that during some years there is an eastward propagation of convergent and divergent (positive and negative) anomalies. 1988 shows a convergent (positive) anomaly originating between 35° E and 50° E transiting the Indian Ocean eastwards from the middle of December to the end of February at 95° E. Again, this is consistent with Wang and Rui's findings. A divergent anomaly precedes, from early December to March. The vertical wind field at P_{500} is similar in structure to the χ anomaly field at P_{200}. For example in 1992 where strong upper level convergent anomalies exist during most of the summer over Africa. Strong upper level divergent anomalies occur over much of the Indian Ocean at the same time.

The case studies show that convergence aloft occurs at 10°S, 25° E during most wet events over South Africa.

streamfunction at 200 hPa

Appendix B (Figure B-2) shows that mean field is predominantly cyclonic (positive values), except for mid-late summer over the Atlantic Ocean at 10° S.

All the summers exhibit eastward propagating anticyclonic or cyclonic (negative or positive in the Southern Hemisphere) anomalies (Figure 4-6). Unlike the χ anomaly field at P_{200}, the ψ anomaly field at P_{200} does not show frequent standing wave patterns. In 1987 over the Indian Ocean there is a positive standing wave.

University of Cape Town

1988 does show a dominant positive anomaly existing throughout most of the summer over the Indian Ocean with some eastward tendency.

Eastward propagating ψ ISO's are seen between December to January in 1989; November to December in 1990 and November 1991. In 1992 there is little propagation, but rather a "flip-flop" of alternating anomalies with a period of about 30 days.

divergent water vapour flux

An interesting feature of the mean integrated divergent water vapour flux field (between the surface and 500 hPa) as shown by figure B-2 in Appendix B is the dominant convergent area of water vapour over south-east Africa and in the south-west Indian Ocean east of 60°E. The velocity potential field at P_{200} shows a strongly divergent field over these same areas, hence facilitating good uplift. The mean vertical wind field confirms this.

The results of the divergent water vapour flux longitude-time plots (Figure 4-7) show that mainly standing wave anomalies are observed and are generally of long duration. 1987 shows a standing wave pattern and convergent (positive) anomalies exist over most of Africa at 10° S. However, many of the other years exhibit some eastward propagating systems. A strong convergent anomaly moves slowly eastwards during the early summer of 1990 from 20° E to 50° E. This is preceded by a divergent (negative) anomaly. 1991 shows a convergent anomaly developing at 50° E during early November moving slowly eastwards. Another convergent anomaly develops in the same region during January. 1992 shows that the water vapour flux field over the Indian Ocean is strongly convergent for most of the

University of Cape Town

summer and is quasi-stationary near 65° E. Jury and Lutjeharms (1993) show increased convection in that zone.

Most of the case studies show that the wet event in South Africa occurs together with a predominantly convergent water vapour flux field at 10°S, 25°E, although many cases are borderline.

non-divergent water vapour flux

Figure 4-8 shows the ψ_Q field. It is clear that both eastward and westward propagation of anomalies is evident. There is some eastward propagation in 1987. 1988 shows a broad anti-cyclonic (negative) band propagating westwards from the Indian Ocean to the east Atlantic. 1989 shows a cyclonic (positive) anomaly propagating westwards from the beginning of January over the Indian Ocean to late March over the east Atlantic Ocean. 1990 shows a stationary positive anomaly in the Indian Ocean from October to December, and from February to March a negative anomaly exists over Africa. 1991 shows a dominant standing wave pattern where most of the Indian Ocean is anomalously anti-cyclonic during the latter half of summer, whereas west Africa and the south-east Atlantic is predominantly cyclonic throughout most of the summer.

University of Cape Town

Eastward propagating cyclonic and anticyclonic anomalies are visible in 1987, 1989 and 1992, mainly in the early summer.

The majority of cases show that the non-divergent water vapour flux field is negative (anticyclonic) during the wet event in South Africa, although 1991 is an exception.

precipitable water

The precipitable water (PW) anomaly field shown in Figure 4-9 for 1987 to 1992 shows that both eastward and westward propagation of precipitable water anomalies take place. Generally, positive PW anomalies occur where convergent (positive) anomalies exist in the divergent water vapour field. There are similarities between the PW anomaly fields and the divergent water vapour fields. The PW anomaly plots show better propagation, however, than divergent water vapour anomalies.

1988 shows a clear eastward moving positive PW anomaly originating in the east Atlantic Ocean in November and gradually moving eastwards to 45° E in late January. During 1989 there are eastward moving PW anomalies over the Indian Ocean. Standing wave patterns also dominate particular years. During 1990, positive PW values exist over Africa from November until February when eastward propagation of precipitable water anomalies is observed. A positive PW anomaly is visible during 1991 from the end of December propagating westwards from 90° E to 45° E during February. Also observed in 1991 is a standing wave over the east Atlantic, where sharp negative anomalies exist everywhere at the end of November. In 1992, a positive anomaly exists over the east Atlantic as well as east of Africa, however, during most of the 1992 summer Africa experiences below average PW anomalies.

During the wet event over South Africa there are positive PW anomalies at 10°S at the same time during most cases. Case 12 at the end of 1991 is an exception

University of Cape Town

STATISTICS

Propagating systems were identified where continuous anomalies cover at least 60° of longitude in space or where anomalies last longer than 20 days in time. Counting the total number of clearly identifiable propagating systems in all the anomalies, stationary wave and "flip-flop" patterns, the following statistics emerge :

1 - eastward propagating systems : 87 (50% of total)
2 - westward propagating systems : 21 (12%)
3 - stationary wave patterns : 36 (21%)
4 - "flip-flop" patterns : 31 (18%)
: 175 total

Wang and Rui (1989) showed that, of 122 TICA events studied, 77 were eastward propagating, 27 northward and 15 westward. Their percentage of identified eastward propagating systems is about 63%, for northward propagating systems the percentage is 22% and for westward propagating systems the percentage is 12%. These results are similar to those shown above. There is roughly a 4:1 eastward versus westward propagation ratio in the tropics. However the importance of stationary waves and ""flip-flop"" patterns cannot be ignored since together they constitute almost 40% of identified oscillatory systems.

It is obvious that eastward propagation is the dominant direction of movement of the various meteorological parameters. Geopotential height at 850 hPa, u-wind component at 850 hPa and v-wind component at 200 hPa show eastward propagating systems most distinctly and most frequently. The average phase speed

University of Cape Town

of the eastward propagating systems is between 0.3 m s^{-1} and 2.0 m s^{-1}. The eastward propagating systems generally have life spans in excess of 90 days, although some originate over Africa or the western Indian Ocean and then propagate eastwards out of the domain being considered, hence an accurate life span is hard to calculate. Most eastward propagating systems last between 40-60 days on average which is consistent with the MJO observed in various meteorological parameters. Unlike Chen and Tzeng (1989) who found clear eastward propagation in the divergent water vapour flux field, the results of this analysis were not as distinct. However, Chen and Tzeng (1989) used composites which covered a wider latitude band, i.e. 0° S to 10° S and this may have lead to better results being obtained. The westward propagating systems show similar average life spans and phase speeds as those found in the eastward propagating systems. Westward propagating systems were most frequently observed in the v-wind component at 200 hPa.

The standing wave patterns last from between 90 to 180 days (from half a summer to the entire summer). What is interesting to note is that embedded within the standing wave is an oscillation which show cycle lengths lasting from between 30 and 60 days, averaging about 45 days. Standing wave patterns were most frequently observed in the PW anomaly fields and the v-wind component at 850 hPa. The "flip-flop" i.e. bands of alternating positive and negative anomalies across the latitude occur most frequently in the geopotential height fields, especially at 200 hPa where 17 such events were observed between 1987 and 1992. The most likely explanation for these "flip-flops" are changes in the Hadley Cell circulation occurring on either side of the ITCZ from 10° N to 30° S.

University of Cape Town

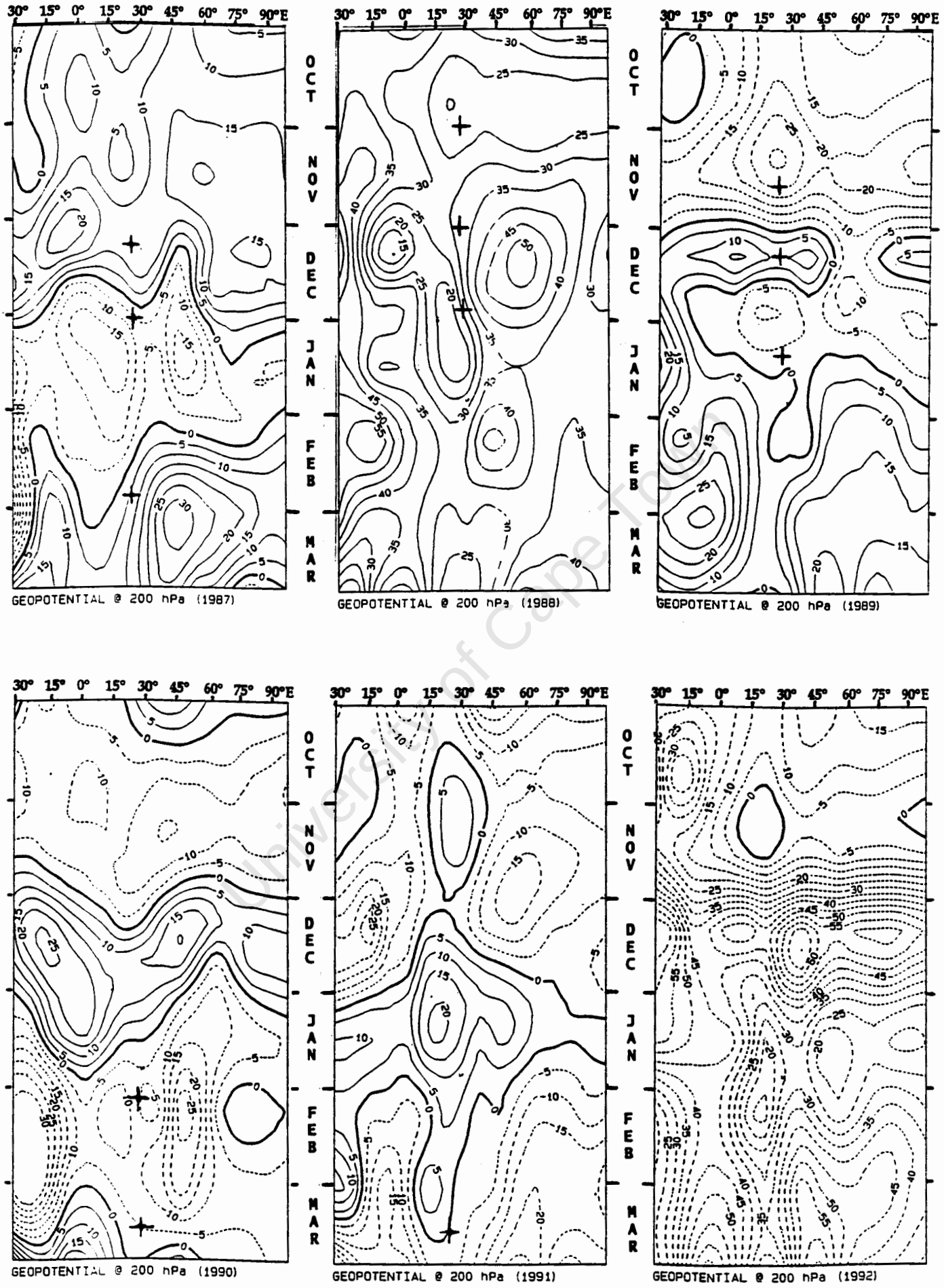

Figure 4-1a : Hovmöller plots of geopotential height anomalies @ 200 hPa along 10° S for 1987 to 1992. Contour interval is 5 gpm.

University of Cape Town

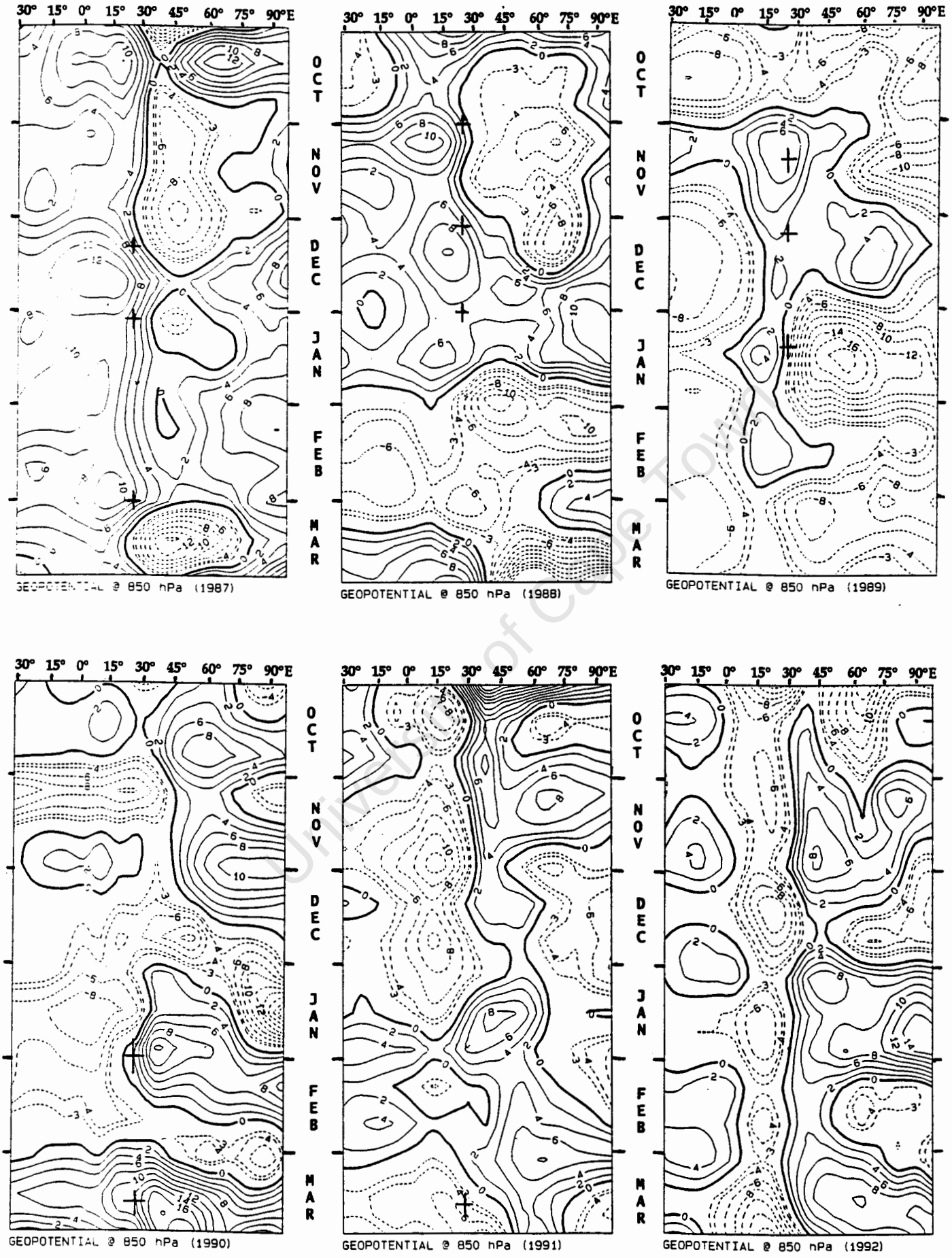

Figure 4-1b : Hovmöller plots of geopotential height anomalies @ 850 hPa along 10° S for 1987 to 1992. Contour interval is 2 gpm.

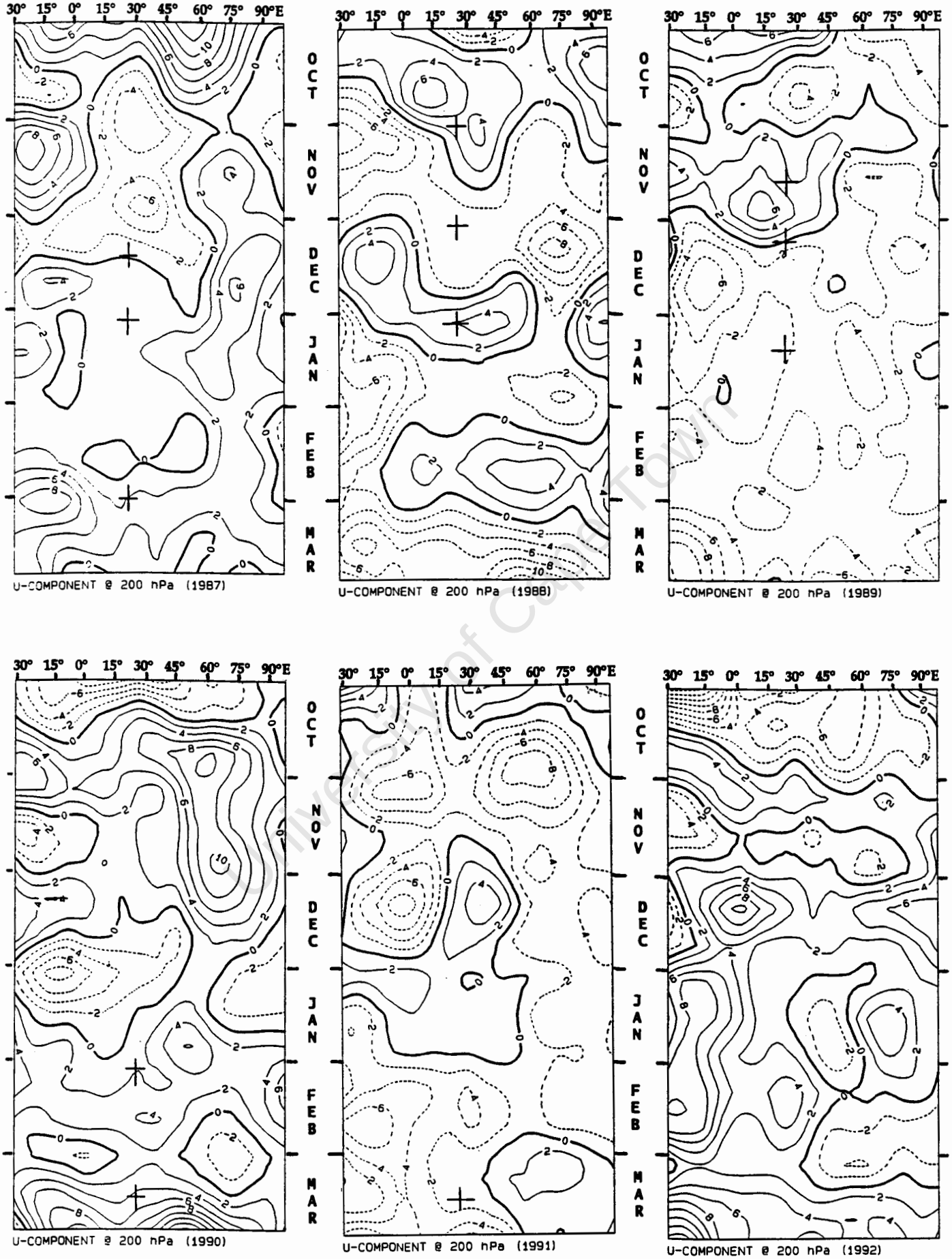

Figure 4-2a : Hovmöller plots of u-wind component anomalies @ 200 hPa along 10° S for 1987 to 1992. Contour interval is 2 m s^{-1}.

University of Cape Town

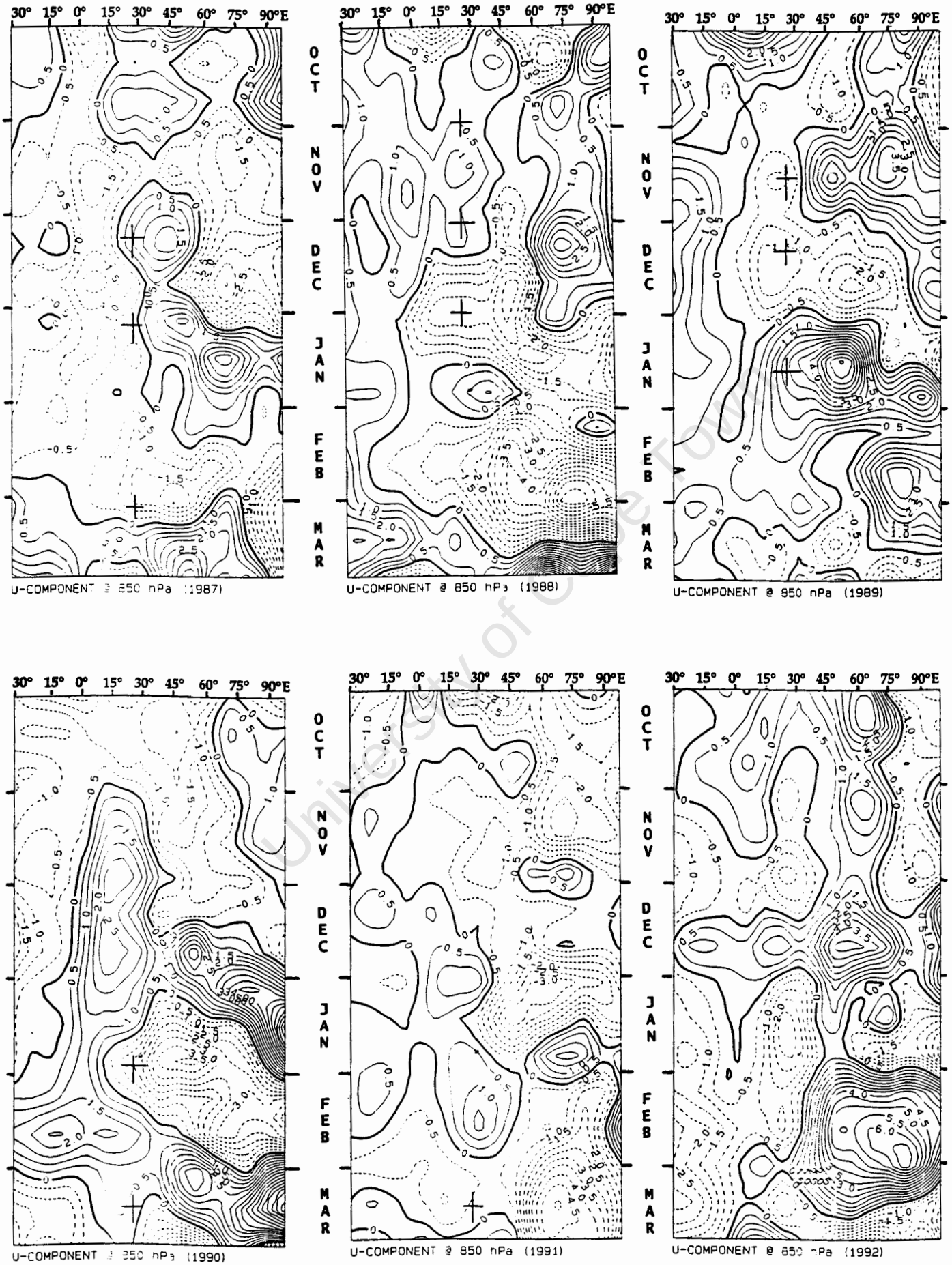

Figure 4-2b : Hövmoller plots of u-wind component anomalies @ 850 hPa along 10° S for 1987 to 1992. Contour interval = 0.5 m s^{-1}.

University of Cape Town

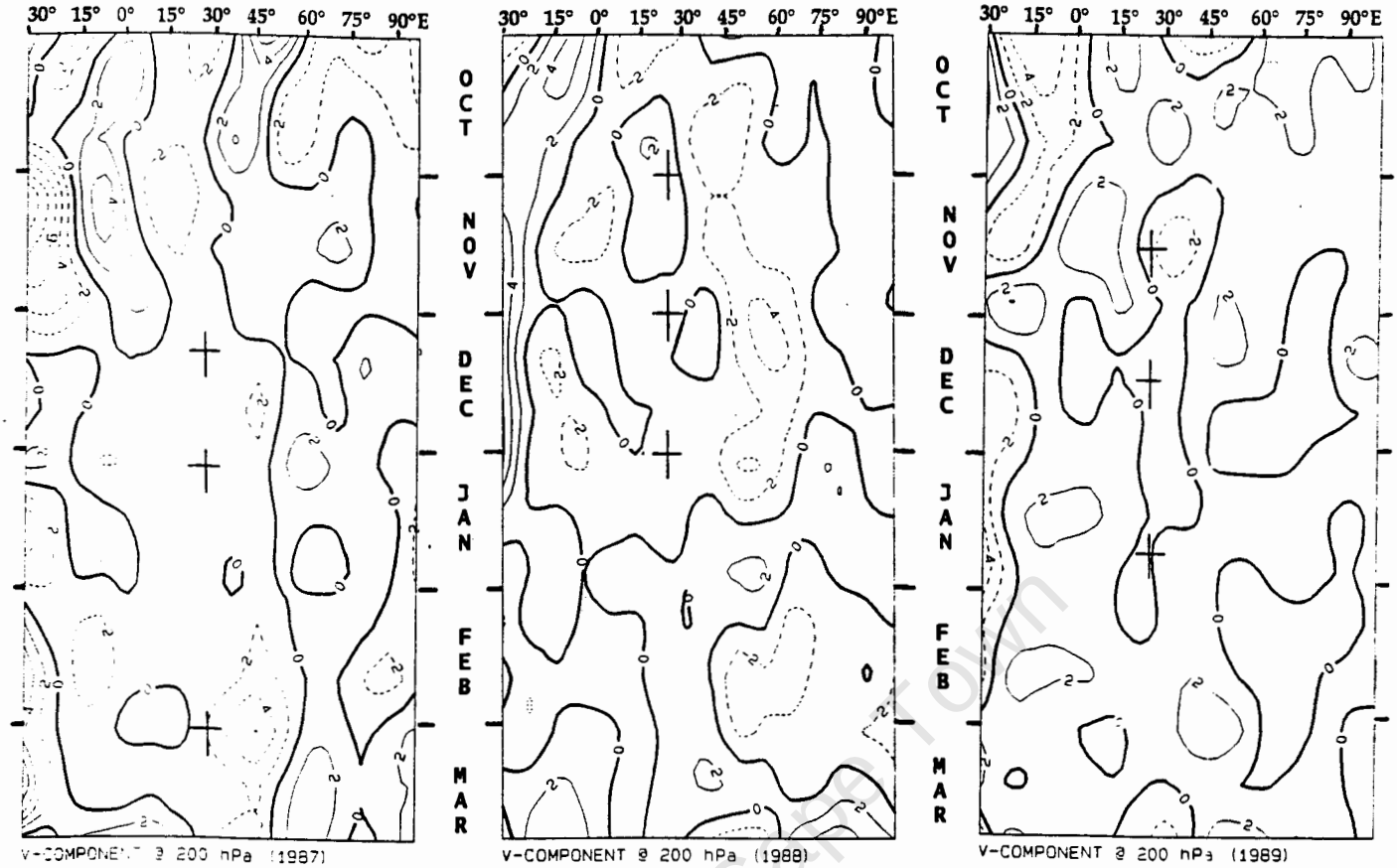

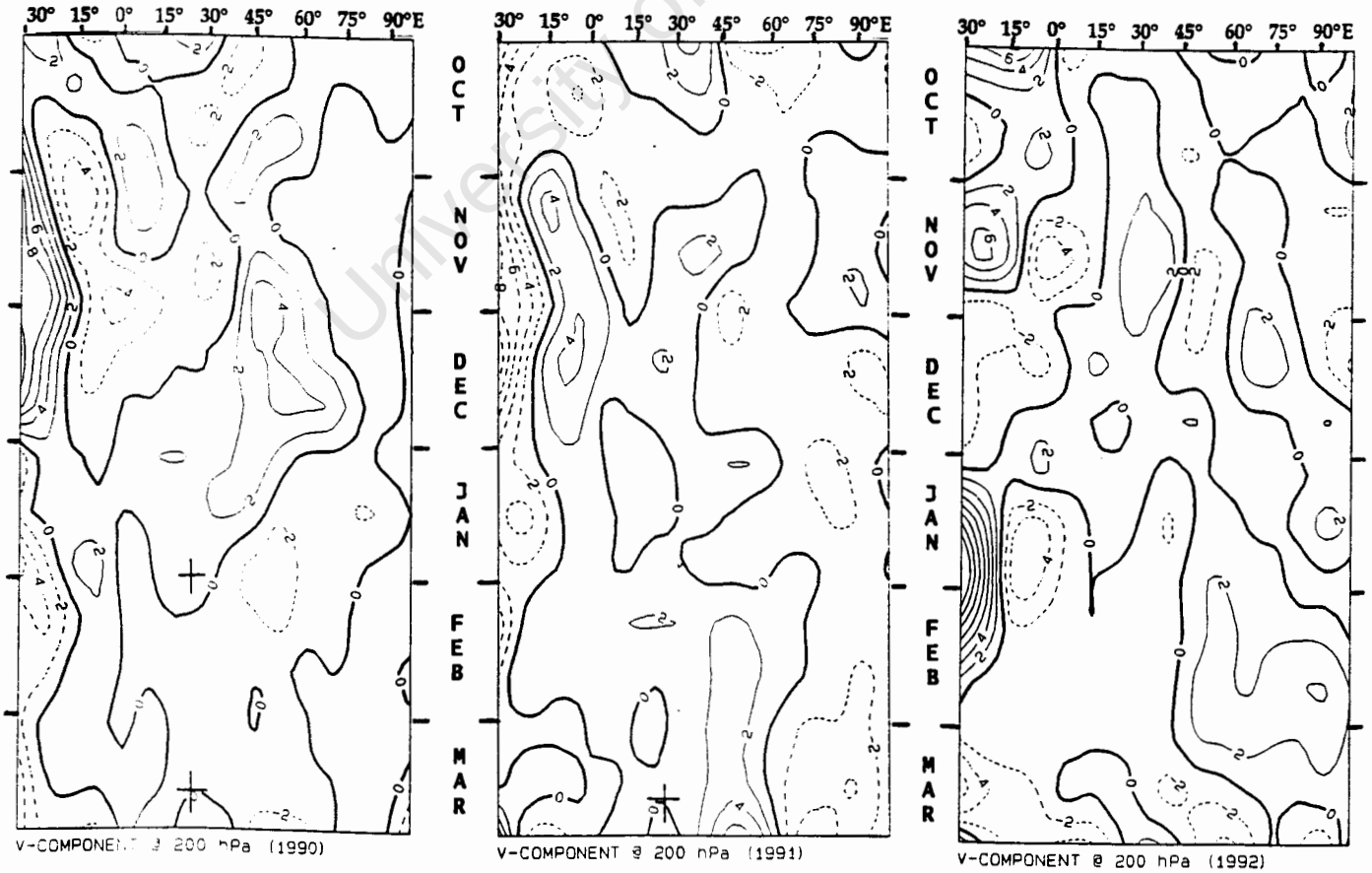

Figure 4-3a : Hovmöller plots of v-wind component anomalies @ 200 hPa along 10° S for 1987 to 1992. Contour interval is 2 m s^{-1}.

University of Cape Town

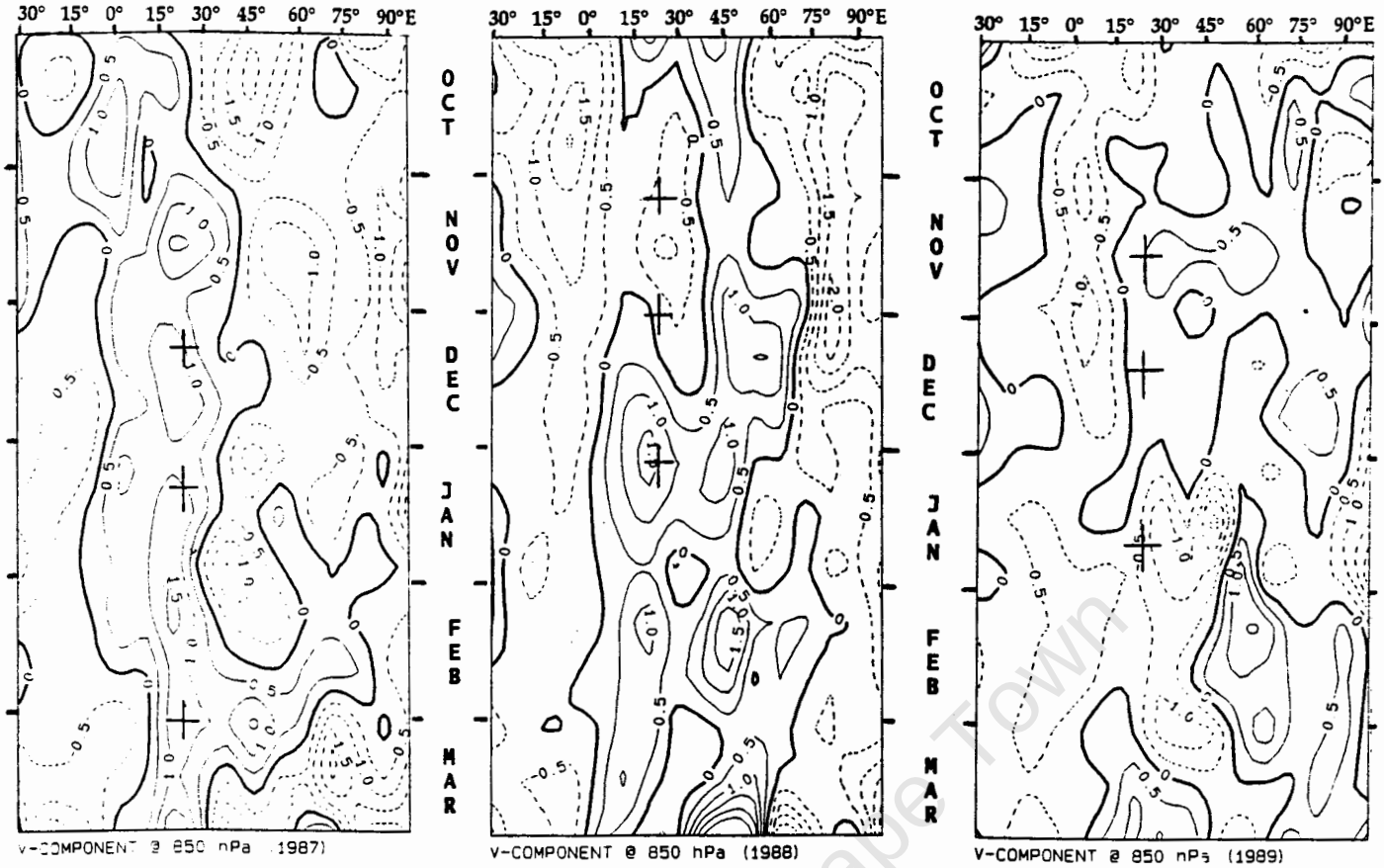

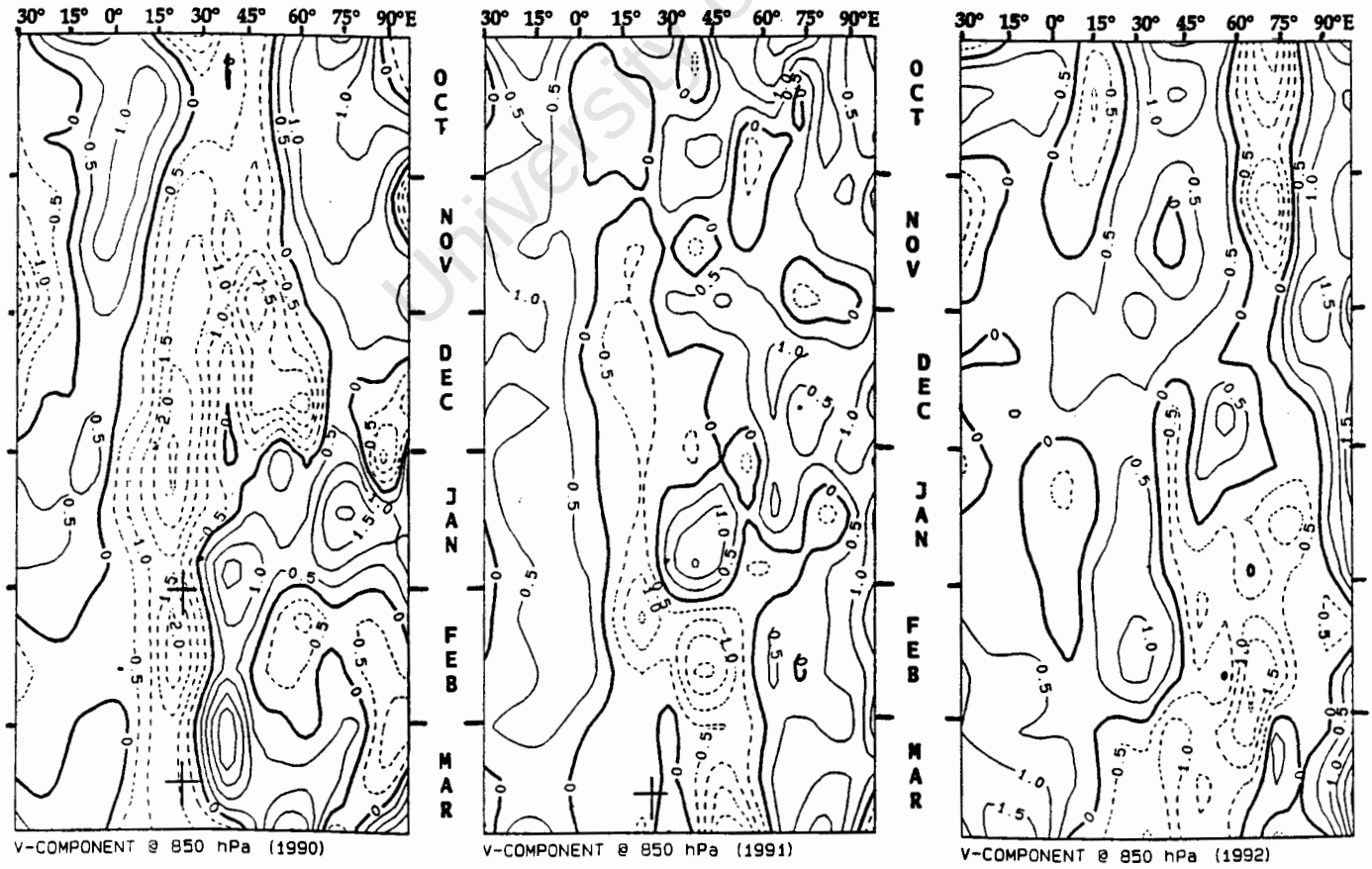

Figure 4-3b : Hovmöller plots of v-wind component anomalies @ 850 hPa along 10° S for 1987 to 1992. Contour interval is 0.5 m s^{-1}.

University of Cape Town

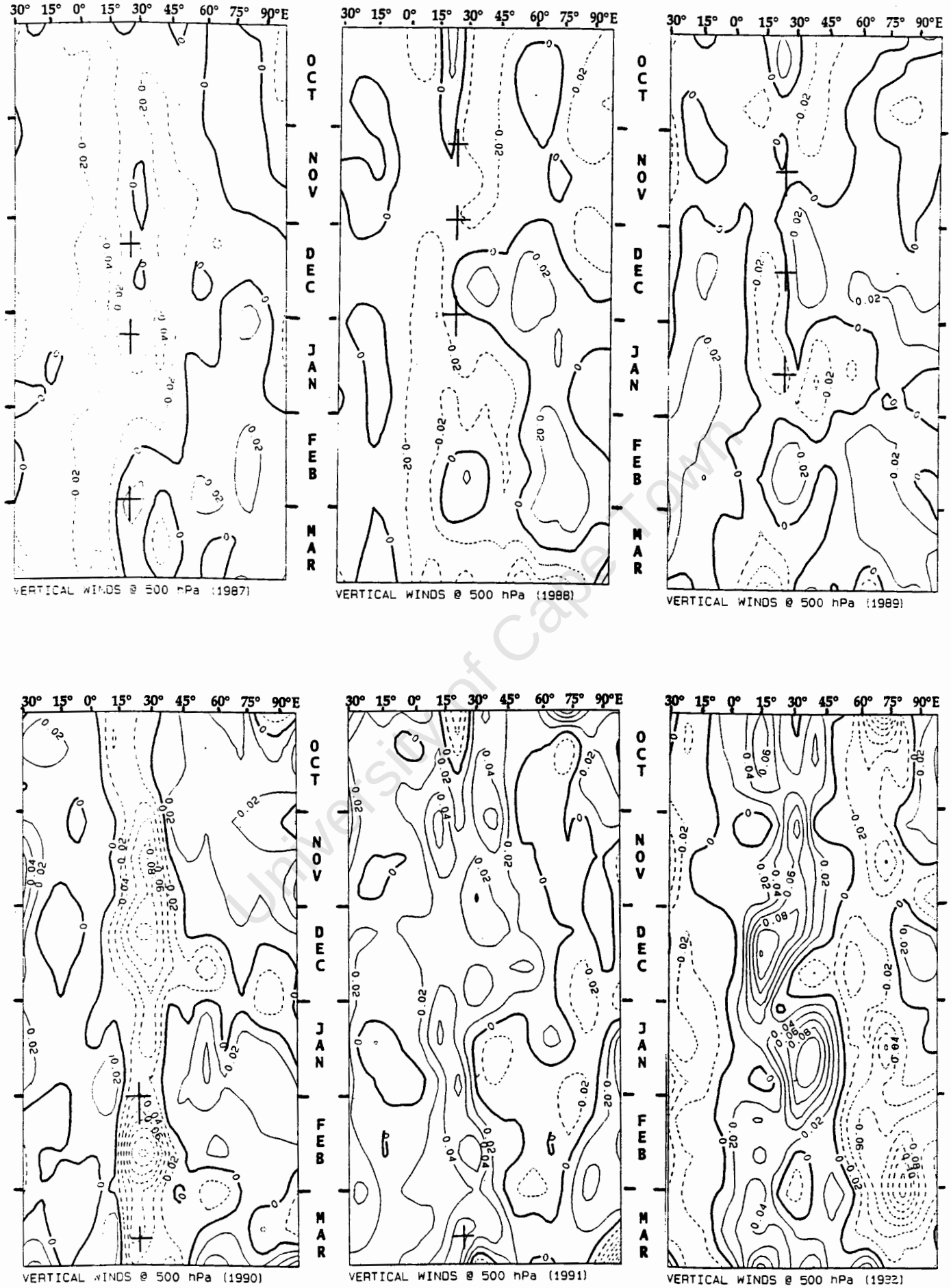

Figure 4-4 : Hovmöller plots of vertical wind anomalies @ 500 hPa along 10° S for 1987 to 1992. Contour interval = 0.02 Pa s^{-1}.

University of Cape Town

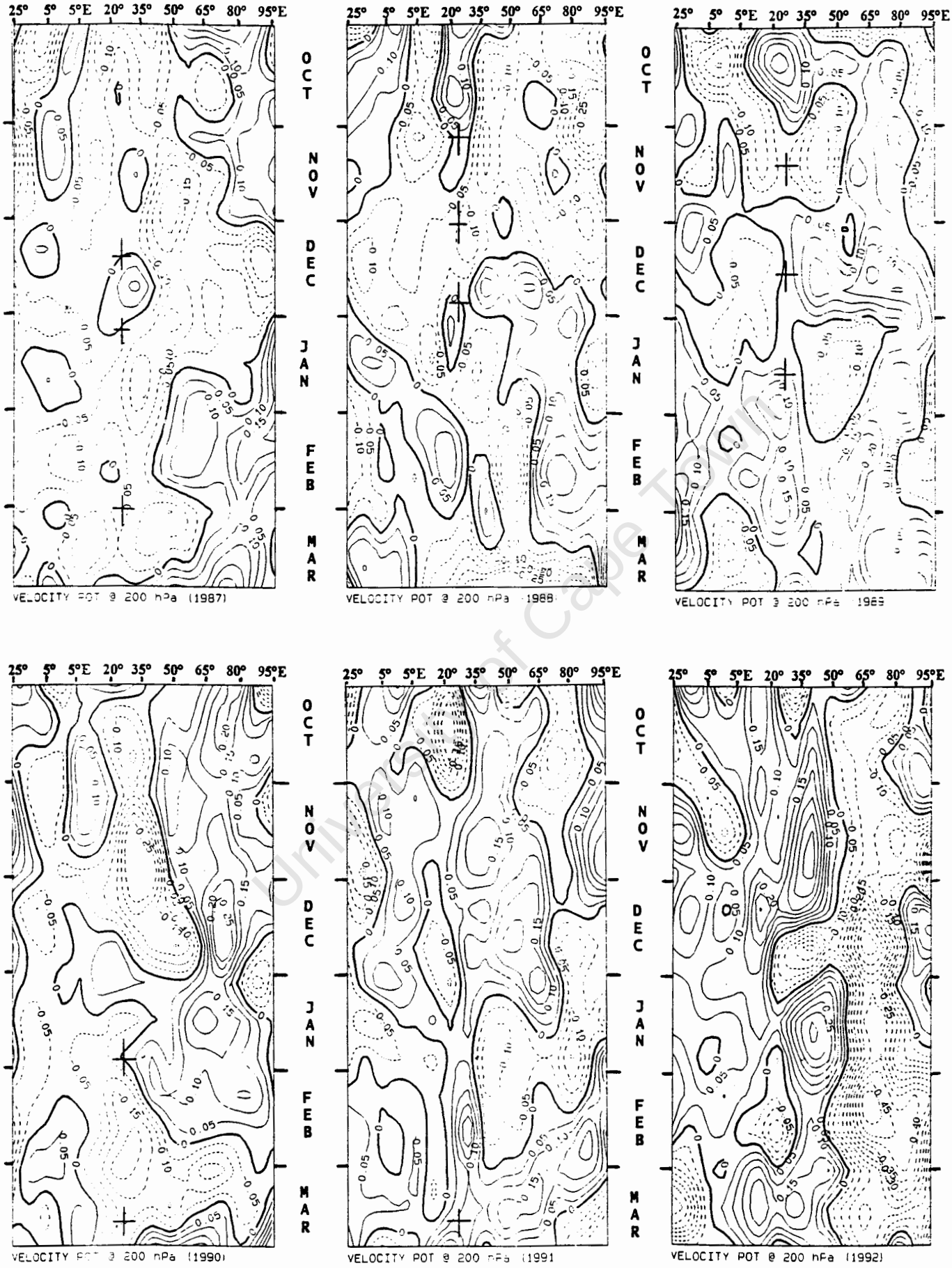

Figure 4-3 : Hovmöller plots of velocity potential (χ) anomalies @ 200 hPa along 10° S for 1987 to 1992. Contour interval is 0.1 x 10^6 m^2 s^{-1}.

University of Cape Town

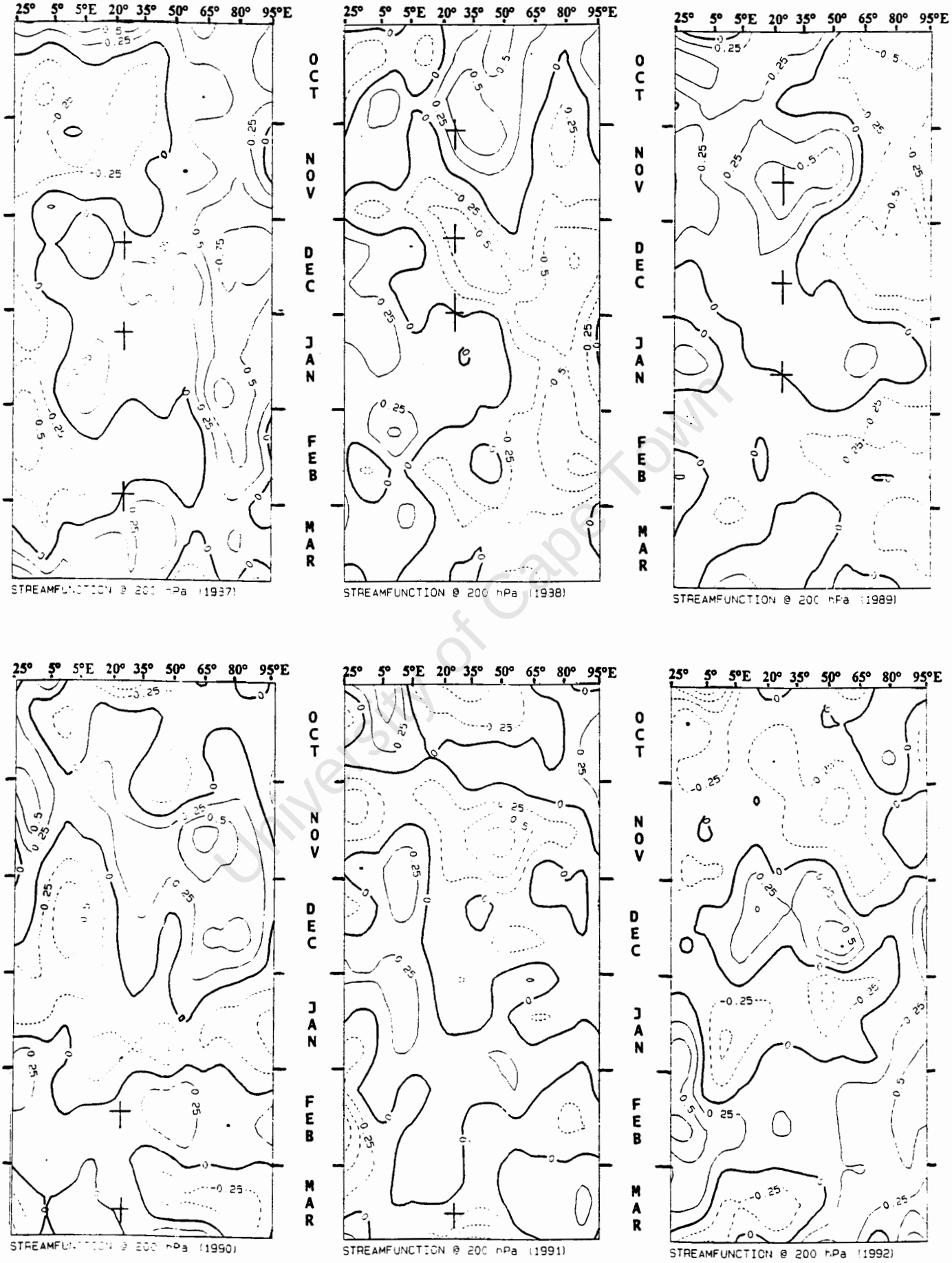

Figure 4-6 : Hovmöller plots of streamfunction (ψ) anomalies @ 200 hPa along 10° S for 1987 to 1992. Contour interval is 0.25 x 10^6 m^2 s^{-1}.

University of Cape Town

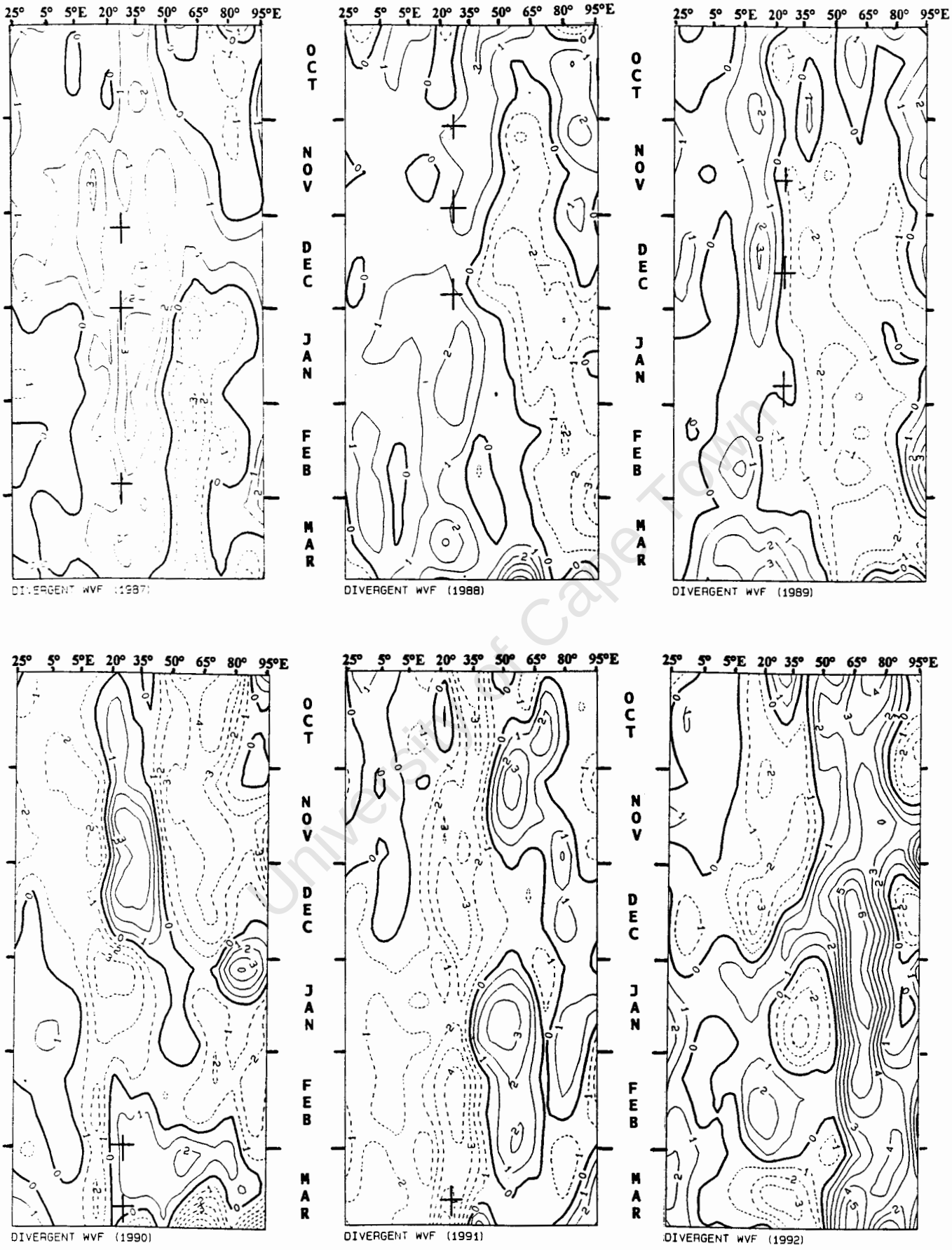

University of Cape Town

Figure 4-7 : Hovmöller plots of divergent water vapour flux (χ_Q) anomalies between the surface and 500 hPa along 10° S for 1987 to 1992. Contour interval is 1 x 10^8 kg s^{-1}.

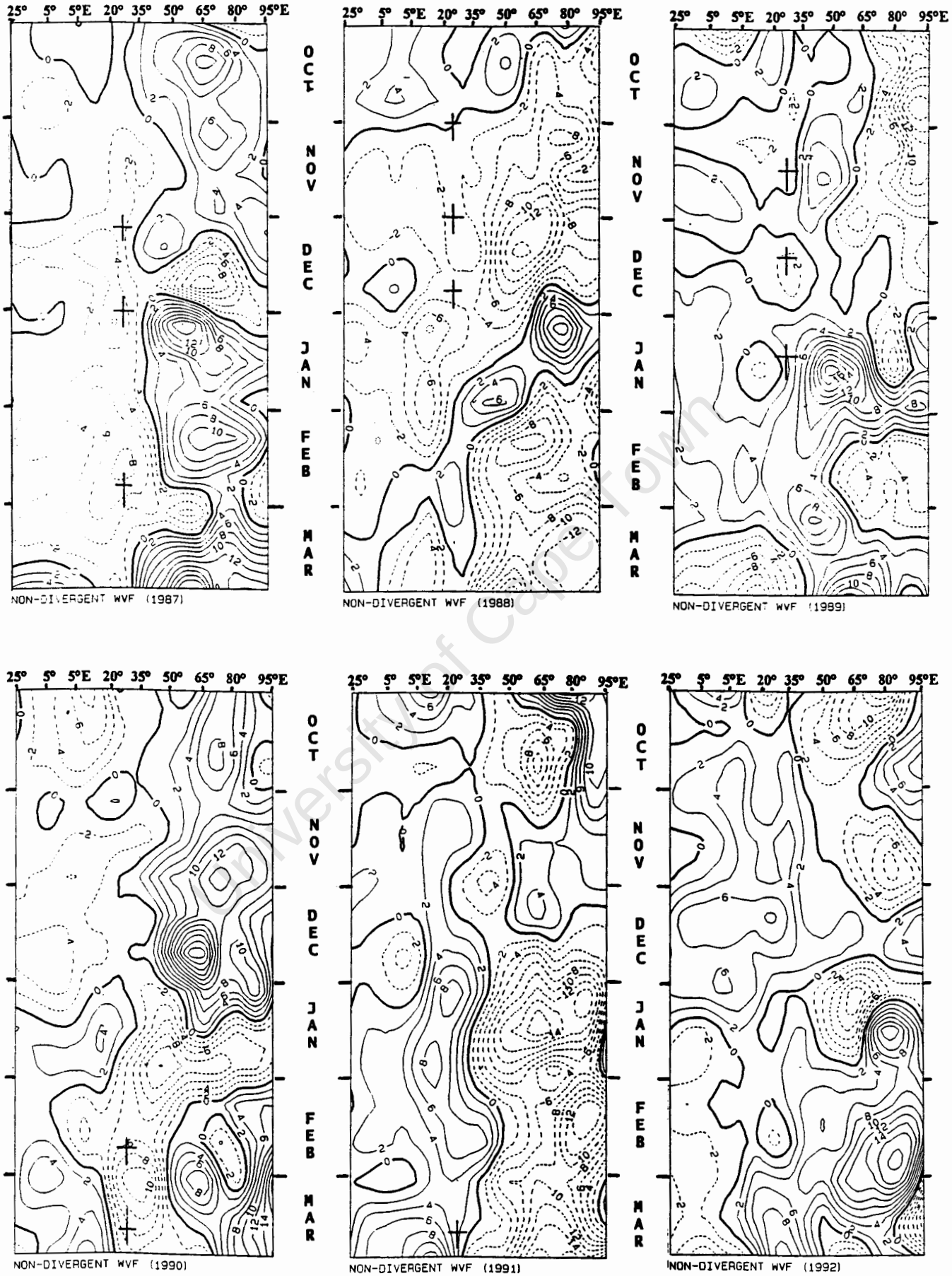

Figure 4-8 : Hovmöller plots of non-divergent water vapour flux (ψ_Q) anomalies between the surface and 500 hPa along 10° S for 1987 to 1992. Contour interval is 2 x 10^8 kg s^{-1}.

University of Cape Town

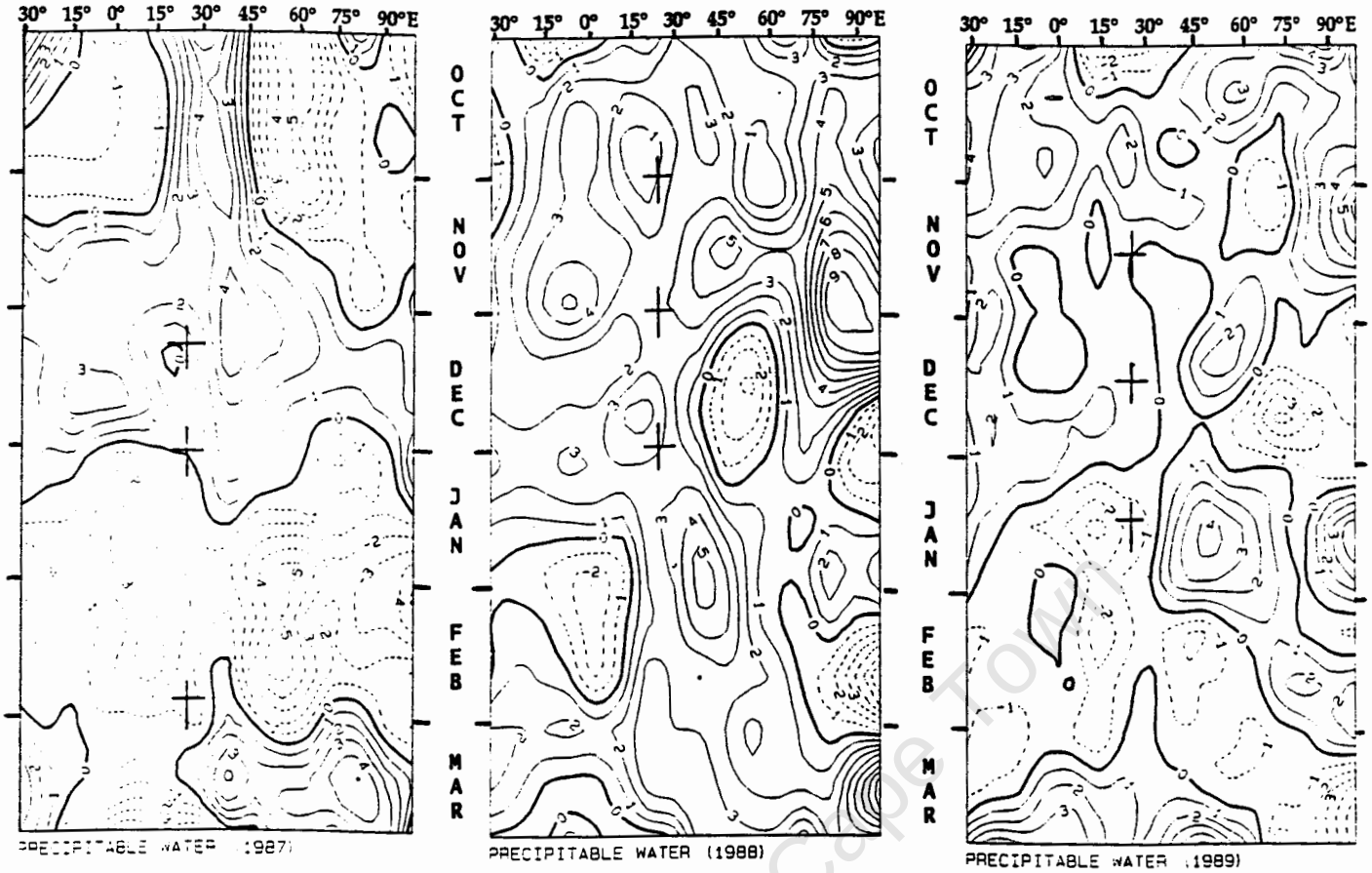

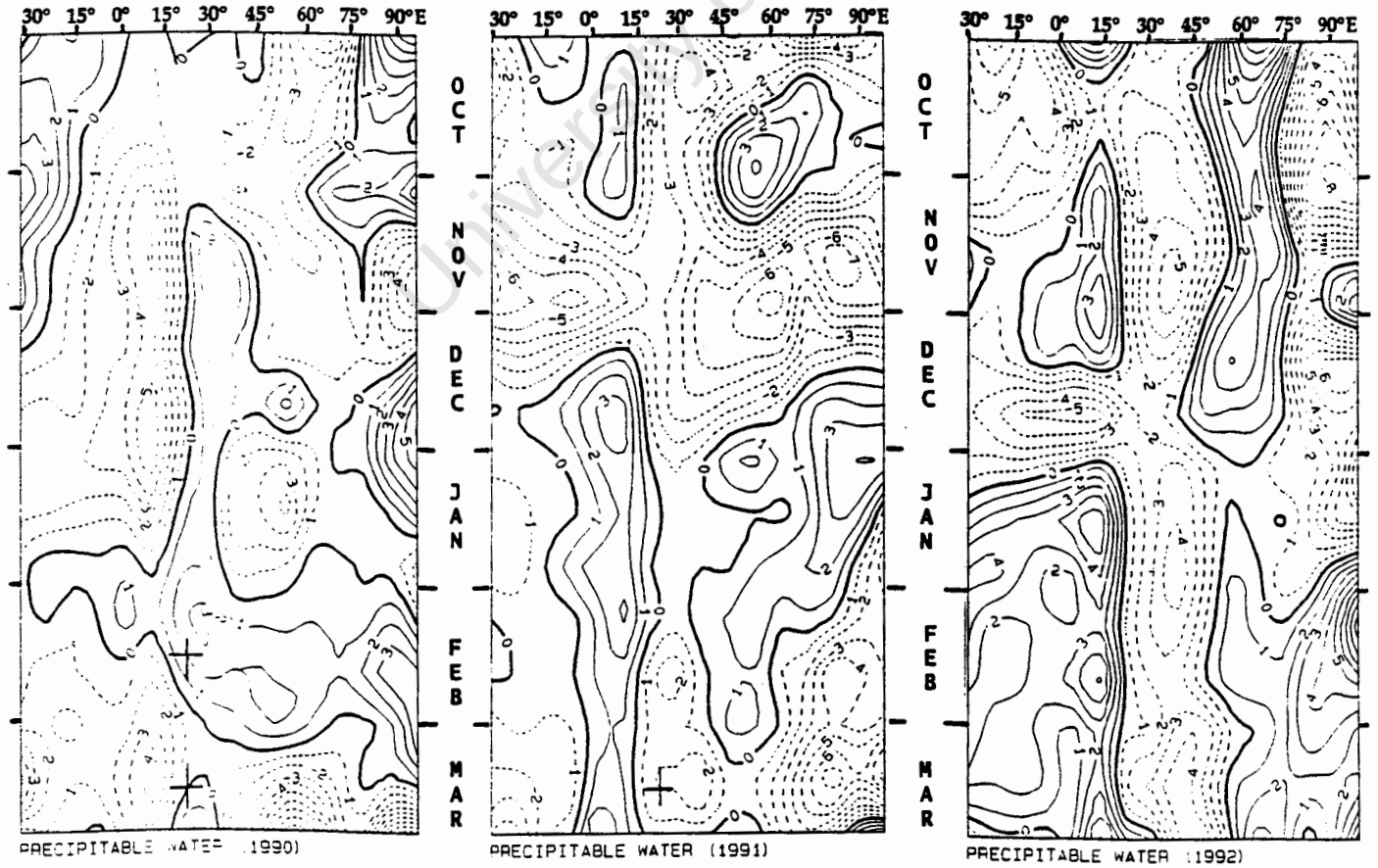

Figure 4-9 : Hovmöller plots of precipitable water anomalies between the surface and 300 hPa along 10° S for 1987 to 1992. Contour interval is 1 mm.

University of Cape Town

RESULTS AT LATITUDE 40° S :

geopotential height

From Figure 4-10a, it can be seen from the geopotential height anomalies from 1987 to 1992 at P_{200} that short-lived eastward propagating negative and positive anomalies are a regular feature. These systems have life spans of less than 30 days, although there are summers where longer ISO's or possible longwaves in the circumpolar jet are observed.

1987 shows many rapidly eastward propagating anomalies of short duration, especially during November and December. 1988 and 1989 show regular alternating negative and positive eastward propagating anomalies throughout the entire summer. The duration of most systems are less than 30 days. 1990 shows a long-lived Rossby wave operating. A positive anomaly develops during early November at 5° E which then propagates eastwards until late December when it then retrogrades through late January. There are eastward propagating systems during 1991, the most clearly defined one occurring from late October in the east Atlantic until late December in the Indian Ocean. 1992 shows a predominantly negative bias throughout most of the summer. Negative anomalies are seen moving rapidly eastwards to 75° E where their eastward movement slows.

University of Cape Town

Most cases at P-0 are associated with positive anomalies at 40° S, although cases 5, 8, 11 and 12 in 1991 show negative anomalies.

Eastward propagating systems at P_{850} are clearly visible in Figure 4-10b. Except for 1990, most of the other summers exhibit Rossby waves modulating the geopotential structure over cycle periods of less than 30 days. A long-term positive

anomaly is also seen during 1990 at the lower level of P_{850} which moves westwards from late December until February.

All P-0 cases chosen for the composite are associated with positive geopotential anomalies. Most of these anomalies are situated between 30° W and 20° E indicating the presence of South Atlantic Anticylonic ridging to the south of South Africa during the wet phase.

horizontal u-wind component

Figures 4-11a and 4-11b show that at both levels, P_{200} and P_{850}, eastward propagating systems exist although not as regularly as those seen in the geopotential height analysis. During most years alternating bands of negative and positive anomalies can be seen at P_{200}. Most of the eastward propagating anomalies last between 30 and 60 days. During some summers the eastward moving anomalies are not always continuous and negative and positive areas flip-flop across the entire domain from month to month, i.e. January to March 1987.

1988 shows that the westerlies were on average stronger (especially during December over the Indian Ocean) than normal during most of the summer. Eastward propagation of positive anomaly core areas is evident from January over the east Atlantic until late February over the east Indian Ocean. 1989 shows similar eastward moving anomalies, i.e. February to March, except, negative anomalies are seen during most of the summer, indicating weaker westerlies at 40° S. 1990 reveals negative areas in the south-west Indian Ocean with little propagation. 1991 shows that eastward propagating systems don't always persist across the band of latitude. The negative anomaly that occurs over the east Atlantic Ocean during late November only re-occurs during late December over the east

University of Cape Town

Indian Ocean, whereas the preceding positive anomaly persists in time across the latitude band. 1992 shows a number of westward retrograding u-wind component anomalies.

P-0 events chosen for the composites all show negative anomalies (reduced westerlies) at 40° S. In most cases these negative anomalies occur across the latitude band. This is consistent with higher geopotential heights at 40° S at the upper levels.

Eastward propagating anomalies between 20-60 days can be seen in the u-wind component at P_{850}. However, in December 1987 and October and November 1989 a westward positive anomaly can be seen. A few stationary anomalies are also observed, especially during the latter half 1987 and 1990.

Like the upper-level during 1989, most of the summer shows weaker westerlies (negative anomalies). However, eastward propagating negative core areas can be seen moving eastwards.

1992 shows a combination of eastward propagating (February to March over the Indian Ocean), westward propagating (late December to mid February) and "flip-flop" systems operating during the summer.

All the main wet event cases show negative anomalies (weaker westerlies). This implies that SAA ridging is occurring south of the subcontinent during the wet event over South Africa, and hence reduced westerlies in this region. This result is also consistent with higher geopotential anomalies in this region during the wet phase.

University of Cape Town

horizontal v-wind component

Eastward propagating systems are clearly visible at both levels (Figure 4-12a and 4-12b). These propagating anomalies occur with great regularity, unlike the u-wind component at the same levels. An interesting feature of the horizontal v-wind component anomaly plots at both levels is the occasional occurrence at 40° S of *westward* propagating systems. This can be seen at P_{200} during the middle of the summers of 1990 and 1992. All three summers shows a sudden change in direction of propagation from eastwards to westwards for about 20 days and then the propagation reverts back to eastwards. The other summers all show eastward propagation of negative and positive anomalies, especially during the summer of 1988. The lower-level, P_{850}, shows similar westward and eastward propagating systems with eastward propagation dominant, except in mid-1992.

Most of the P-0 events over South Africa are associated with positive (southerly) anomalies at the upper levels. This is also the case in the lower atmosphere.

vertical wind at 500 hPa

A common feature of all the summers from 1987 to 1992 as seen in Figure 4-13 is the very short duration of eastward moving negative and positive anomalies. Eastwards propagating anomalies can be seen and occur with fair regularity during all summers.

Another feature of the vertical wind anomaly field is the apparent standing wave nature of the anomalies. These standing waves are evident at 45° E in December to March 1987, at 5° W in November to March 1991 and at 25° E in January to February 1992.

University of Cape Town

The majority of the wet event cases are associated with positive (subsidence) anomalies and could act as a "sink" zone for tropical uplift.

velocity potential at 200 hPa

Figure 4-14 shows that mainly shorter duration (less than 30 days) eastward propagation of convergent (positive) and divergent (negative) anomalies occurs in the velocity potential anomaly plots during most of the summers.

Some summers show that not all eastward propagating systems are continuous in time. 1990 and 1992 are good examples of this phenomenon, i.e. "dipole" events as seen in December and February in 1992 whereby contrasting signs are evident in south-east Africa and the Indian Ocean.

The mean velocity potential field at 200 hPa as seen in appendix B, Figure B-4, shows that the circulation over most of the east Atlantic between 10° W and 30° E and the Indian Ocean between 55° E and 95° E is convergent. However, the mean circulation from November onwards over the west Indian Ocean between 30° E and 55° E is divergent.

The cases studies do not show a very distinct picture as was the case with the previous parameters. Although some cases exhibit negative (divergence) anomalies, the majority of the chosen wet events exhibit positive (convergence) anomalies at 40° S during the wet phase over South Africa. This result is more consistent with SAA ridging, although the results are not that convincing.

University of Cape Town

streamfunction at 200 hPa

Unlike velocity potential at 200 hPa, streamfunction at 200 hPa (Figure 4-15) exhibits easily identifiable eastward moving alternating negative and positive anomalies (anticyclonic and cyclonic anomalies). These anomalies are mostly continuous, although some summers exhibit non-continuous eastward propagating anomalies. One such case is 1992 where a negative anomaly originating at 10° E during January over the east Atlantic is interrupted at 40° E, but re-intensifies eastwards of 65° E. Most anomalies show duration times of about 20-60 days.

Figure B-4 in appendix B shows that the circulation over the entire area is predominantly anticyclonic, except during late October at 35° E and in October over the east Atlantic Ocean.

The P-0 cases show mixed results, with the majority of the chosen cases associated with negative (anticyclonic) anomalies indicating a stronger anticyclonic component to the upper level wind field.

divergent water vapour flux

Figure 4-16 shows that divergent water vapour (χ_Q) anomalies also propagate eastwards, but are not always continuous in time and are generally of short duration. The eastward propagation is not always clearly visible (as was the case of χ_Q at 10° S). This is the result of very slow moving anomalies, which appear to be motionless at times and can be seen during 1989 where an almost stationary negative anomaly exists during most of the summer between 35° and 50°E. During 1992 a strong convergent (positive) anomaly exists during February at 35° E. This has implications for the weather of South Africa. This convergence of water

University of Cape Town

vapour exists over the warm Agulhas Current retro-flection area and may be a source of moisture for the interior of South Africa.

Figure B-4 in appendix B shows that at 40° S most of the area is divergent, except for the south-east Atlantic from October to early February. An interesting feature of the mean χ_Q field at 40° S is that the strongest divergence occurs at 20° E which is south of South Africa.

Most wet events over South Africa are associated with divergence (negative anomalies) of the divergent water vapour flux field at 40° S. Except for cases 5,6 (1988) and 10 (1990) all the other cases show negative (divergent) anomalies.

non-divergent water vapour flux

Figure 4-17 shows non-divergent water vapour flux (ψ_Q) anomalies are more continuous (in space, not in time) in their eastward progression and occur with greater regularity than divergent water vapour flux anomalies as seen in Figure 4-16. This can be best seen in 1991 where alternating bands of anticyclonic (negative) and cyclonic (positive) anomalies can be seen propagating eastwards during the entire summer.

University of Cape Town

The "flip-flop" nature of anomalies is seen again during 1989 where wide zonal changes are seen. Most of December until late January show negative anomalies, but they become positive rapidly at the end of January but are short lived.

The mean ψ_Q field as seen in appendix B, Figure B-4, shows that the ψ_Q field is most anticyclonic over the Indian Ocean during the late summer in February. The ψ_Q field in the east Atlantic Ocean is least anticyclonic during mid-summer in late

December and early January. Half of the P-0 cases show positive (cyclonic) anomalies, and the other half negative (anticyclonic) anomalies. Only case 12 of the chosen composite P-0 events shows a positive anomaly.

precipitable water

Figure 4-18 shows positive precipitable water anomalies propagating eastwards from the east Atlantic Ocean to the Indian Ocean. However, these eastward propagations are not continuous and are of short duration, i.e. less than 30 days in most cases. An eastward negative anomaly is seen in 1987 during November and December and during February and March 1988. November and December 1990 shows a positive eastward moving anomaly. A negative eastward propagating anomaly can be seen during November to December in 1991.

An interesting feature of the mean PW field as seen in appendix B, Figure B-4, is that the highest concentration of PW occurs in the Indian Ocean between 30° and 45° E , which is south-east of South Africa, during late summer (February). 1990, 1991 and 1992 all show high positive PW anomalies originating in this region, which co-incides with the warm Agulhas Current retro-flection area.

Except for case 10 in February 1990, all the other P-0 cases are associated with negative or very weak positive anomalies at 40° S. This is consistent with SAA south of the sub-continent. An interesting feature is that although most P-0 wet events over South Africa are associated with negative anomalies at 25° E, positive anomalies do occur further east over the south-west Indian Ocean. This is seen in 1988, 1989, 1990 and 1991. The implication of this is that the ridging over the western half of the 40° S latitude band (predominantly negative anomalies) may advect water vapour from areas over the Indian Ocean (where positive anomalies

University of Cape Town

of PW occur) eastwards into South Africa , possibly at higher latitudes. However, it could be the result of a downstream (of South Africa) wave pattern.

STATISTICS

Counting the total number of clearly identifiable propagating systems, stationary wave and "flip-flop" patterns, the following statistics at 40° S emerge :

1 - eastward propagating systems	: 75 (65%)	[87 - 50%]
2 - westward propagating systems	: 14 (12%)	[21 - 12%]
3 - stationary wave patterns	: 9 (8%)	[36 - 21%]
4 - "flip-flop" patterns	: 17 (15%)	[31 - 18%]
	: 115 total	[175 total]

10° S results shown in square parentheses.

The period of the oscillations taking place at 40° S in the various propagating anomalies is typically between 20-30 days, which is shorter than the MJO observed in the tropics. Longer periods of between 30-60 days occur in the "flip-flop" mode, but this mode is less dominant than the propagating modes occurring more often. Hence the main length of the oscillations is between 20-30 days. This is consistent with the findings of Ghil and Mo (1990) where a dominant 23 day peak was found in the spectra of the 500 hPa geopotential heights in the southern midlatitudes. This infers a wavenumber 4 pattern in the Rossby wave pattern at this level. This is consistent with Jury et al (1991) who identified a 23 day cycle in the sea-surface temperature near Cape Town (south-western South Africa).

University of Cape Town

As expected the dominant direction of propagation at 40° S is eastward. 65% of propagating systems identified in the Hövmoller plot analysis are eastward propagating. The average life span of these systems is typically 60-90 days, and their phase speeds vary between 2.0 - 5.0 m s^{-1} for geopotential height and u-wind component anomalies at both levels. Phase speeds are slower for the other variables, and average between 1.5 and 3.0 m s^{-1} for variables such as v-wind components at both levels. The divergent and non-divergent WVF anomalies propagate more slowly, typically at speeds less than 2 m s-1. The meteorological variables that exhibit eastward progressing systems clearly include geopotential height at both levels, v-wind component at 200 hPa and vertical wind component at 500 hPa. Westward propagating systems are scarce (12% of the total) at 40° S, but they do occur. Westward moving systems are best observed in the u-and v-wind component at the 850 hPa level. Phase speeds are similar to those found in the eastwards progressing systems. Life spans of are typically between 60 and 90 days.

Fewer standing wave patterns are observed at 40° S than at 10° S, i.e. 4 times fewer. Standing wave patterns last between 90 and 120 days and they too have oscillations embedded in them, which vary between 20 and 50 days. Standing wave patterns are observed twice in the vertical wind component between 1987 and 1992. "Flip-flop" patterns are also observed less at 40° S than at 10°S. There are 17 occasions when this pattern is observed. "Flip-flop" patterns are most often seen in the streamfunction anomalies at 200 hPa as well as non-divergent WVF anomalies.

Figures relating to the 40° S results follow.

University of Cape Town

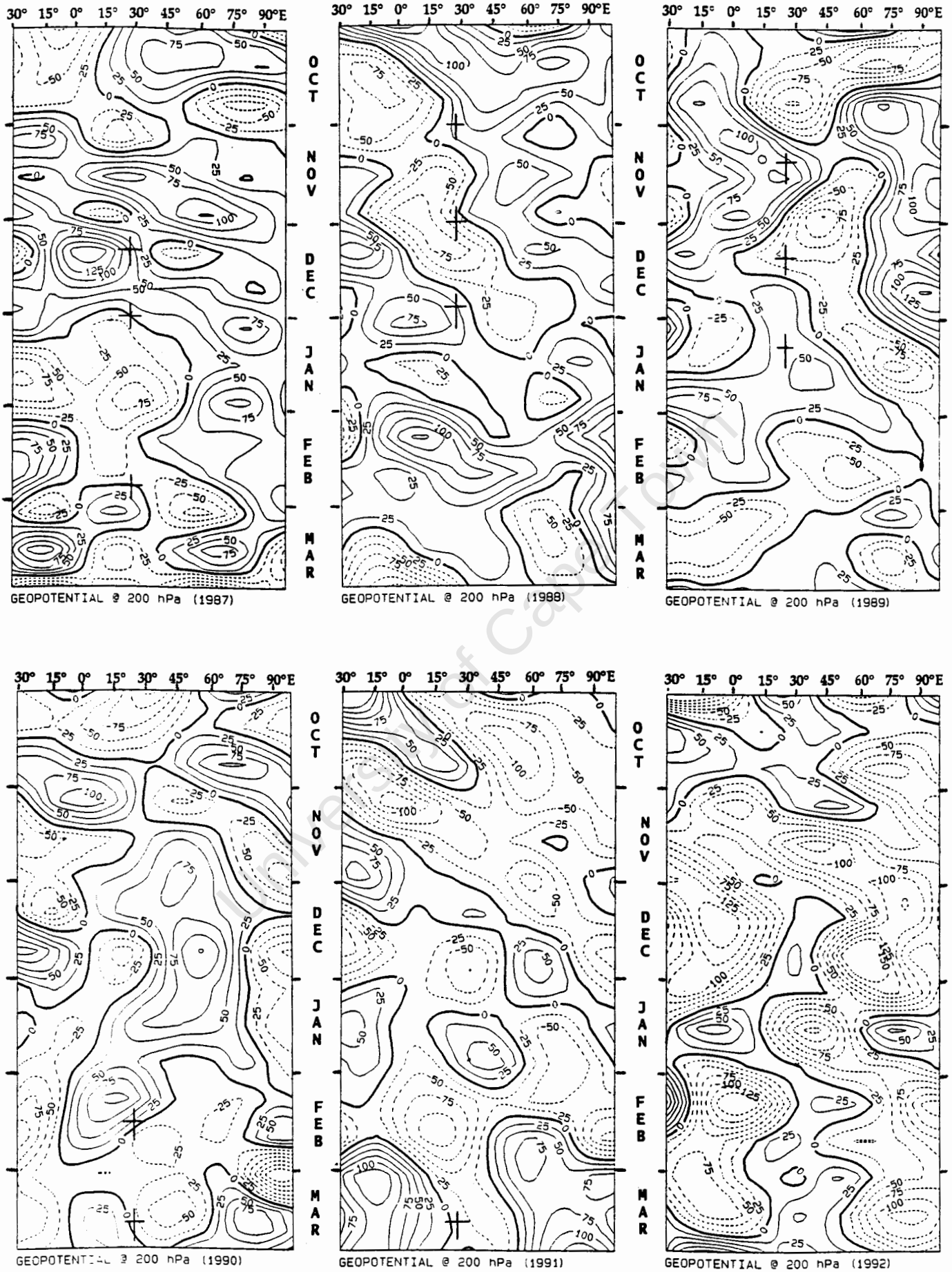

Figure 4-10a : Hovmöller plots of geopotential height anomalies @ 200 hPa along 40° S for 1987 to 1992. Contour interval is 25 gpm.

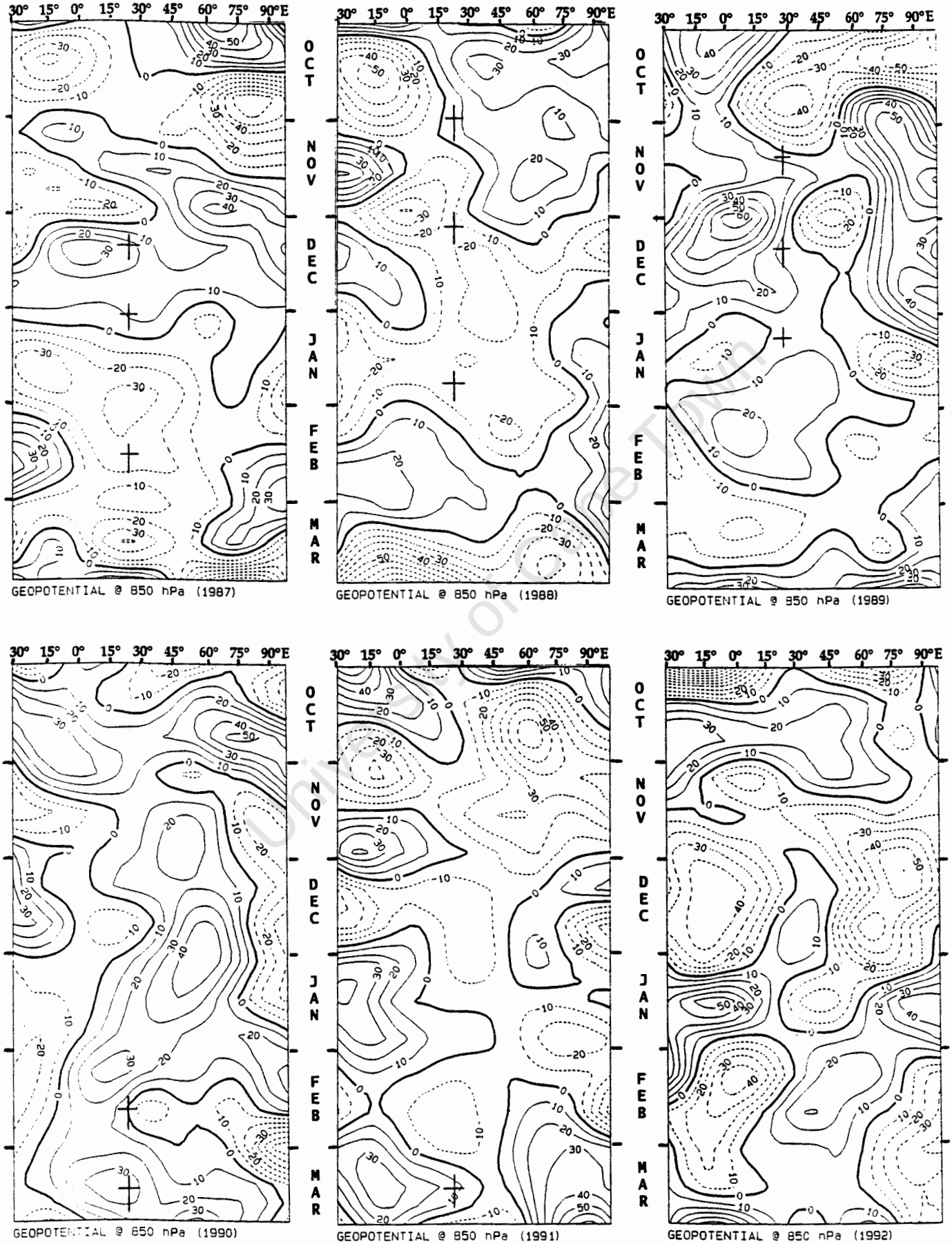

Figure 4-10b : Hovmöller plots of geopotential height anomalies @ 850 hPa along 40° S for 1987 to 1992. Contour interval is 10 gpm.

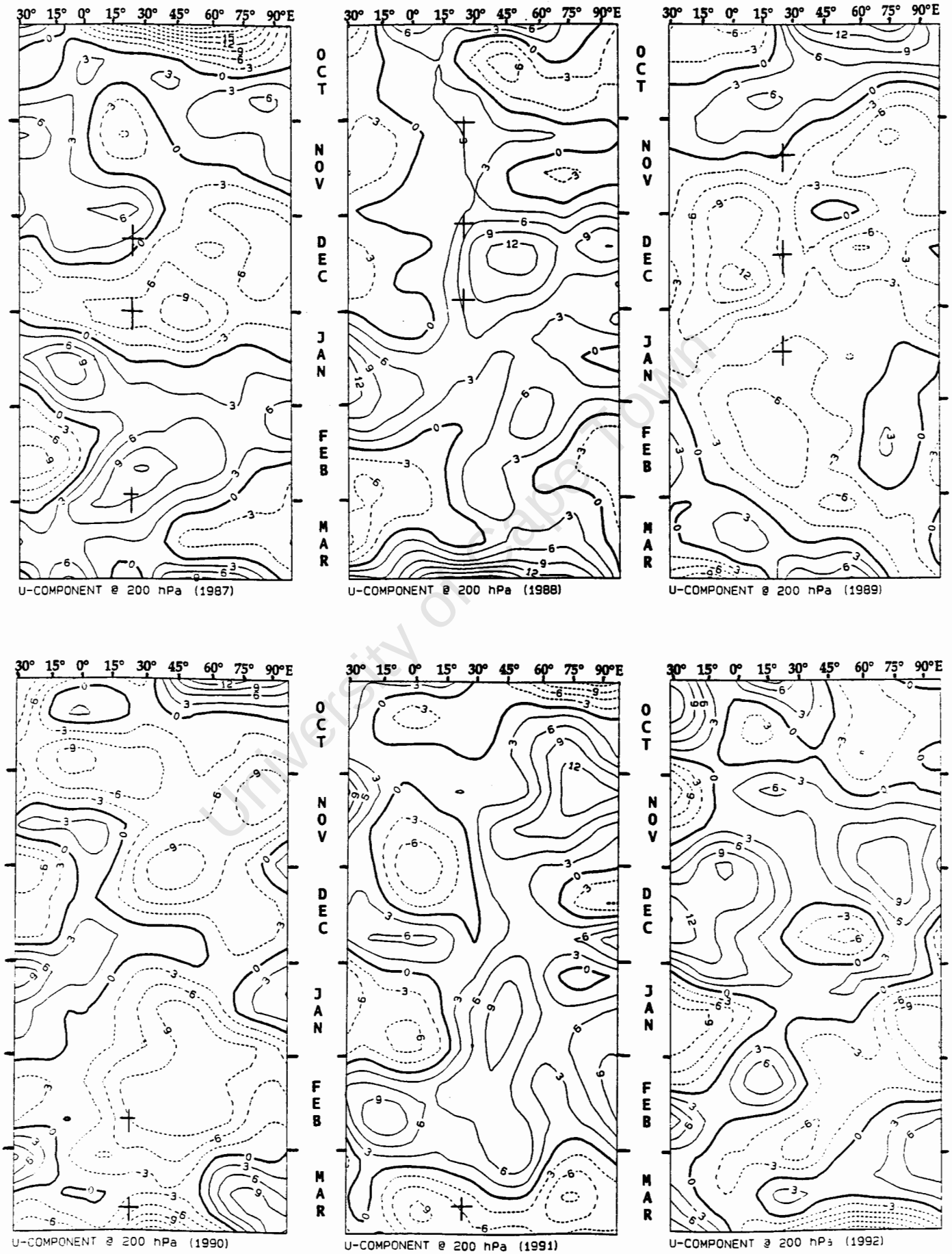

Figure 4-11a : Hovmöller plots of u-wind component anomalies @ 200 hPa along 40°S for 1987 to 1992. Contour interval is 3 m s^{-1}.

University of Cape Town

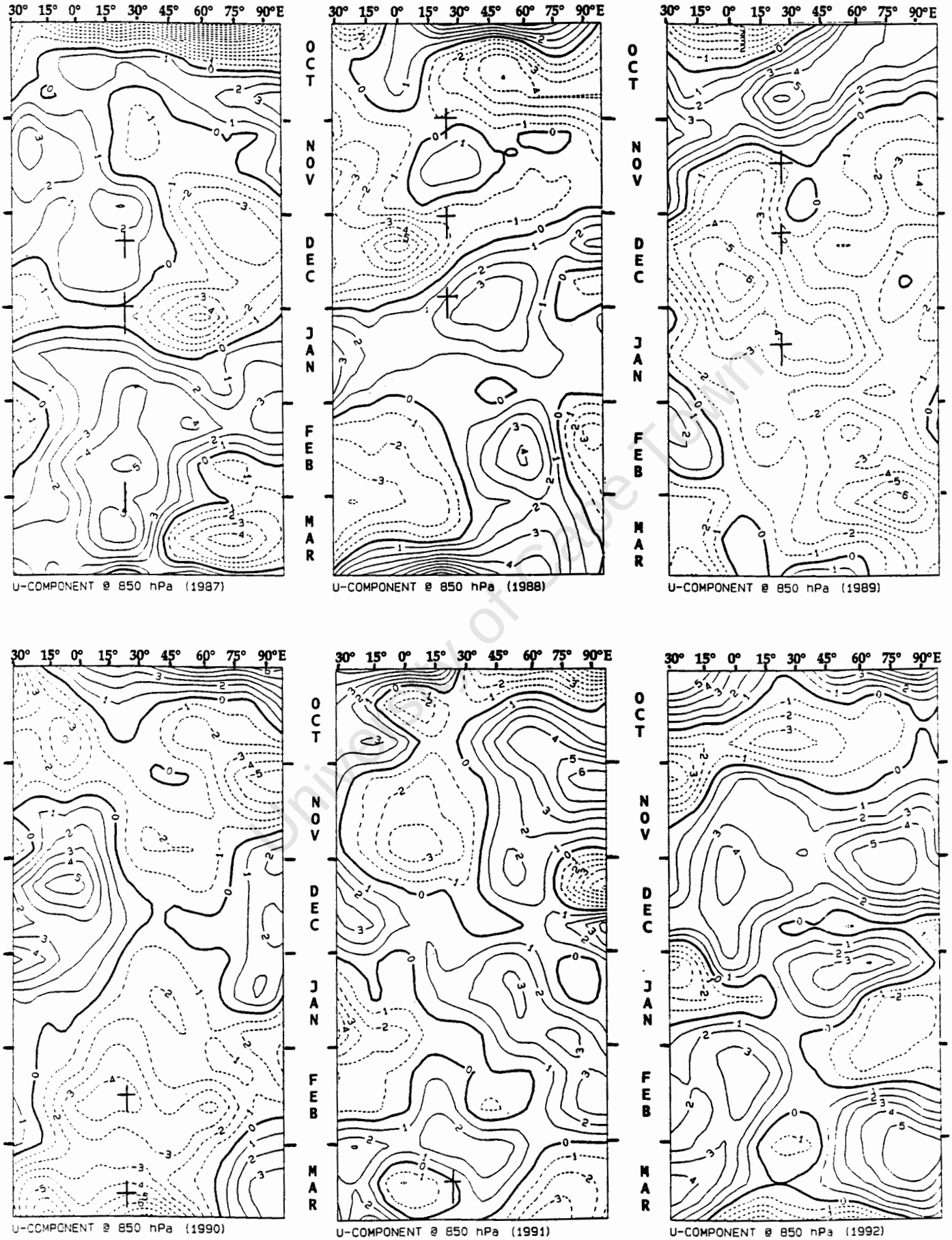

Figure 4-11b : Hovmöller plots of u-wind component anomalies @ 850 hPa along 40° S for 1987 to 1992. Contour interval is 1 m s^{-1}.

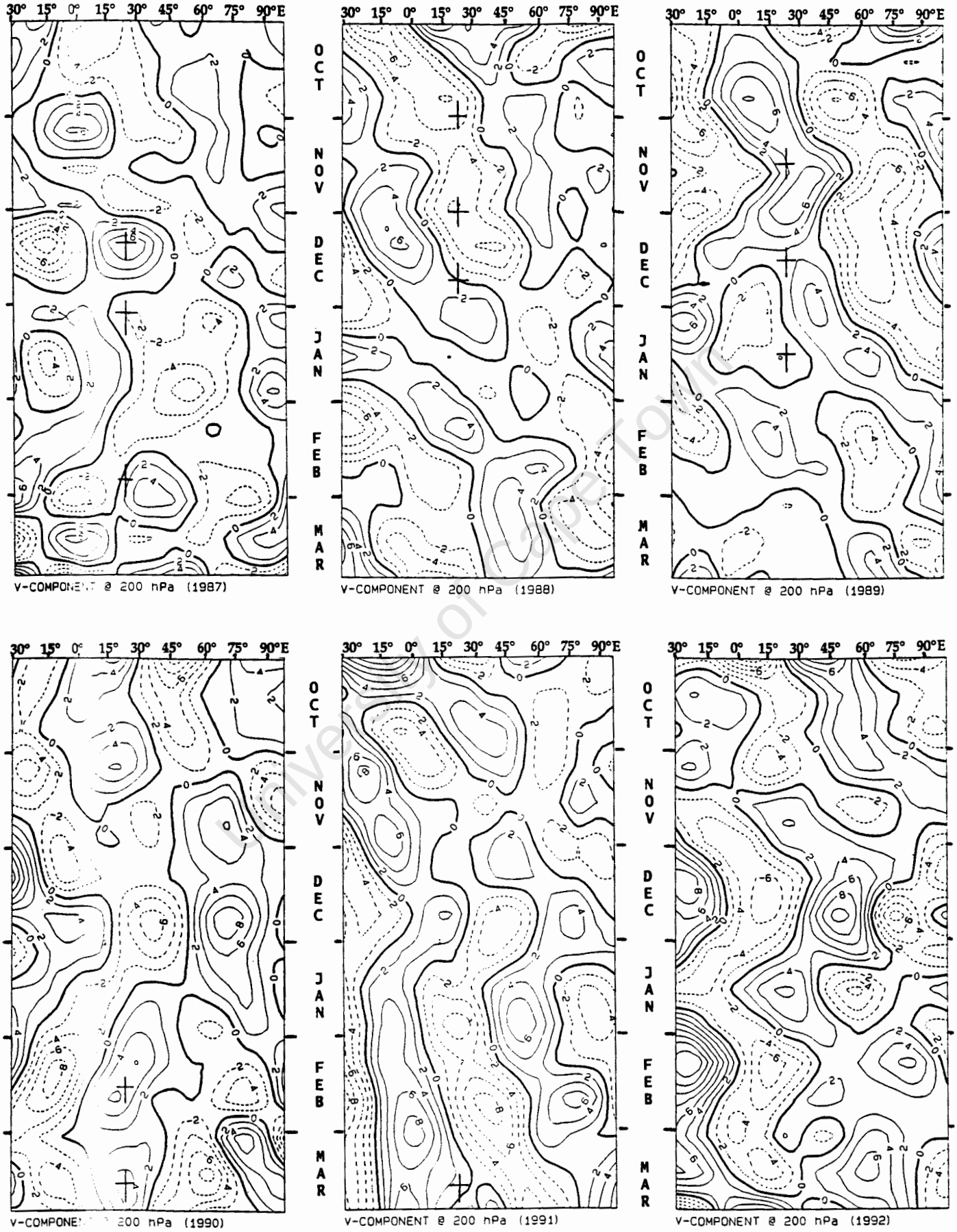

Figure 4-12 : Hovmöller plots of v-wind conponent anomalies @ 200 hPa along 40° S for 1987 to 1992. Contour interval is 2 m s^{-1}.

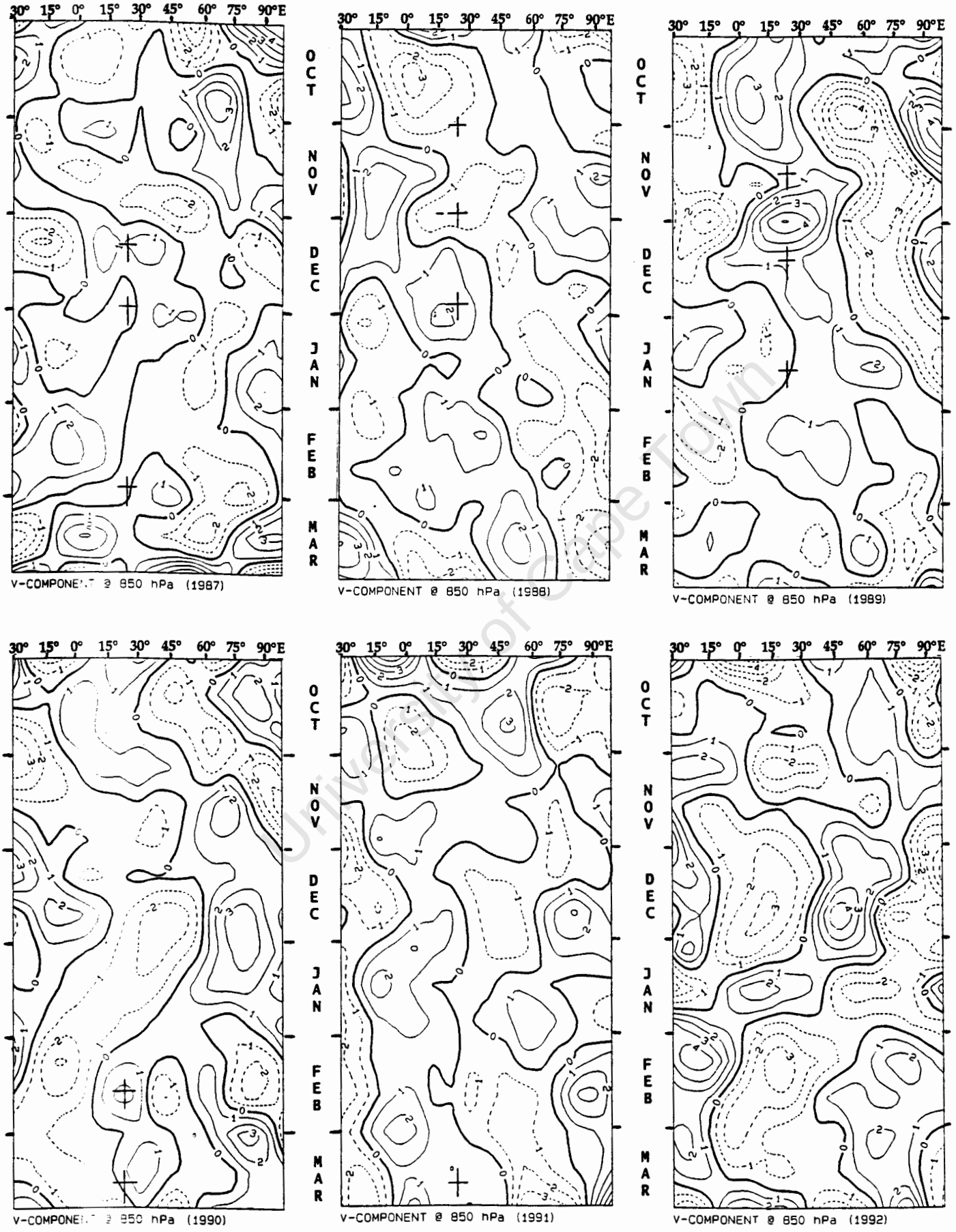

Figure 4-12b : Hovmöller plots of v-wind component anomalies @ 850 hPa along 40° S for 1987 to 1992. Contour interval is 1 m s^{-1}.

University of Cape Town

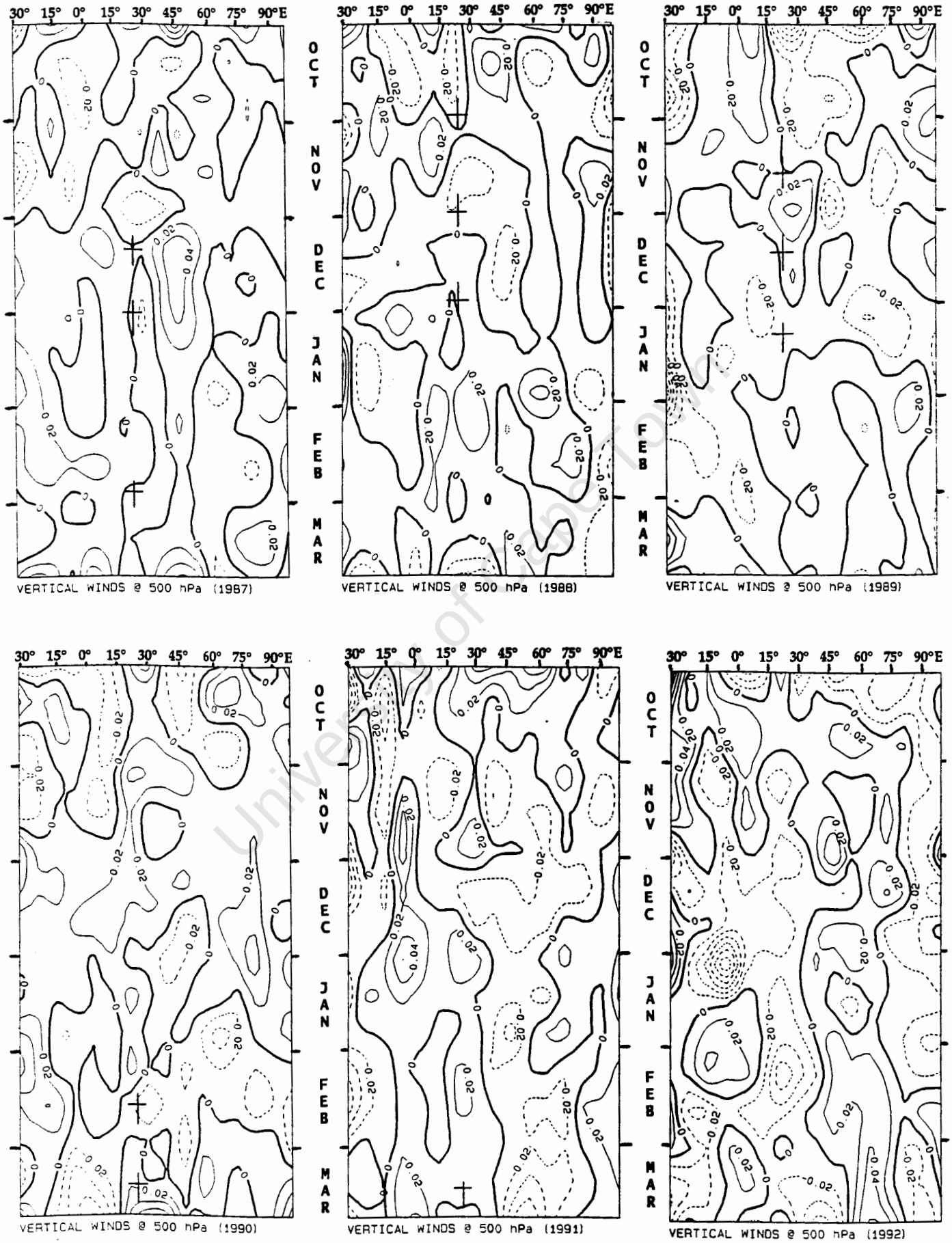

Figure 4-13 : Hovmöller plots of vertical wind anomalies @ 500 hPa along 40° S for 1987 to 1992. Contour interval = 0.02 Pa s^{-1}.

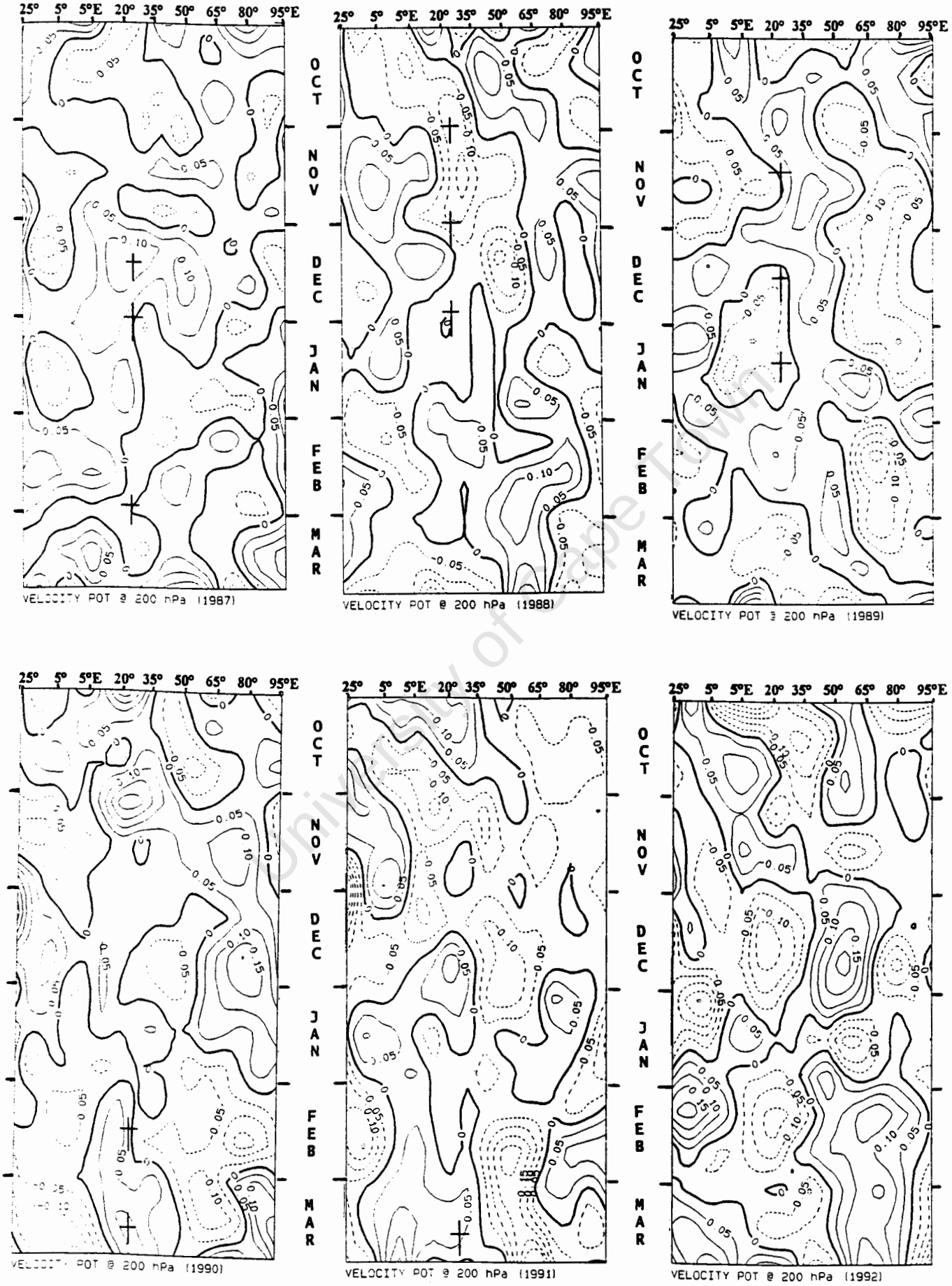

Figure 4-14 : Hovmöller plots of velocity potential (χ) anomalies @ 200 hPa along 40° S for 1987 to 1992. Contour interval is 0.05 x 10^6 m^2 s^{-1}.

University of Cape Town

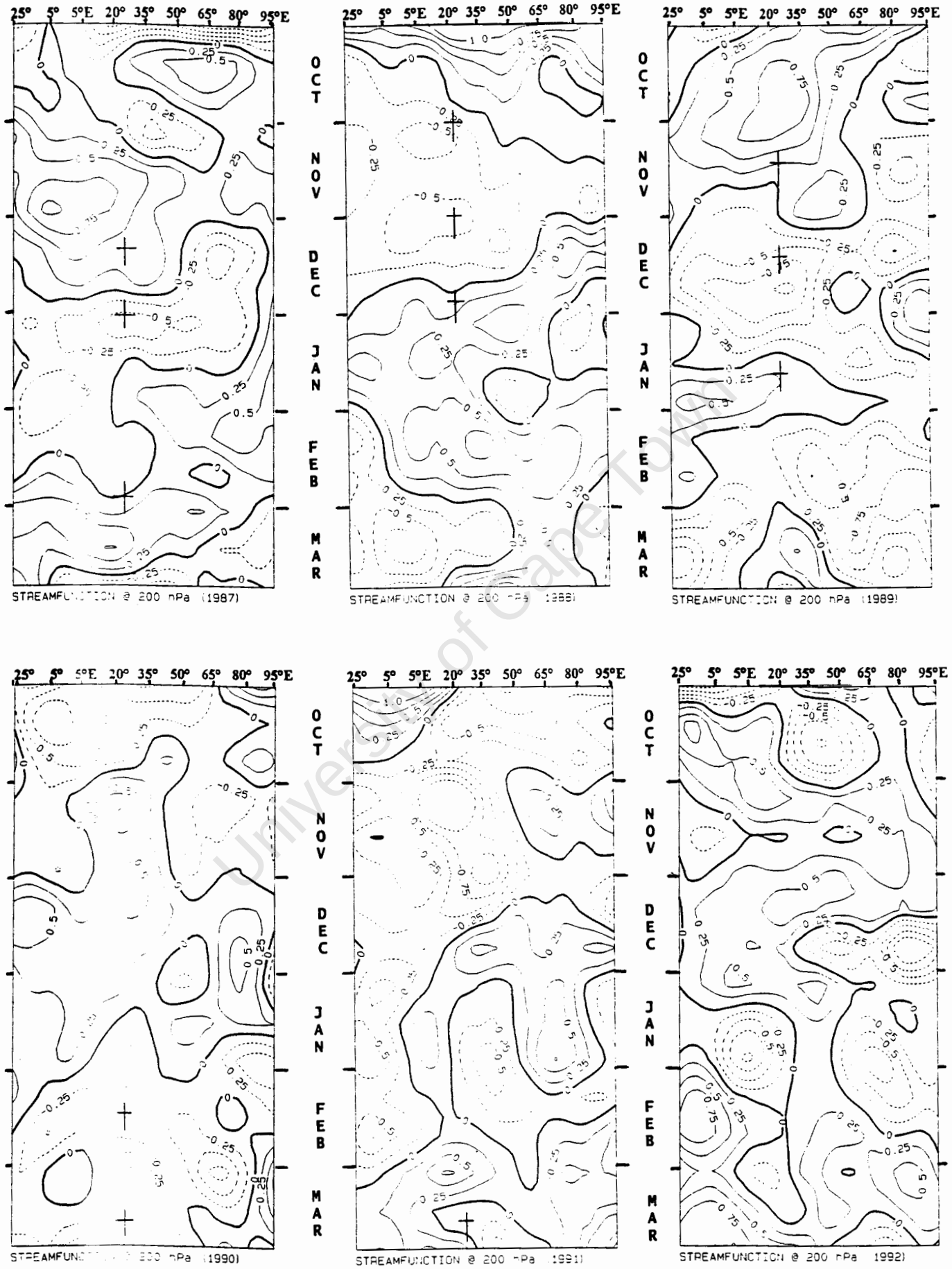

Figure 4-13 : Hovmöller plots of streamfunction (ψ) anomalies @ 200 hPa along 40° S for 1987 to 1992. Contour interval is 0.25 x 10^6 m^2 s^{-1}.

University of Cape Town

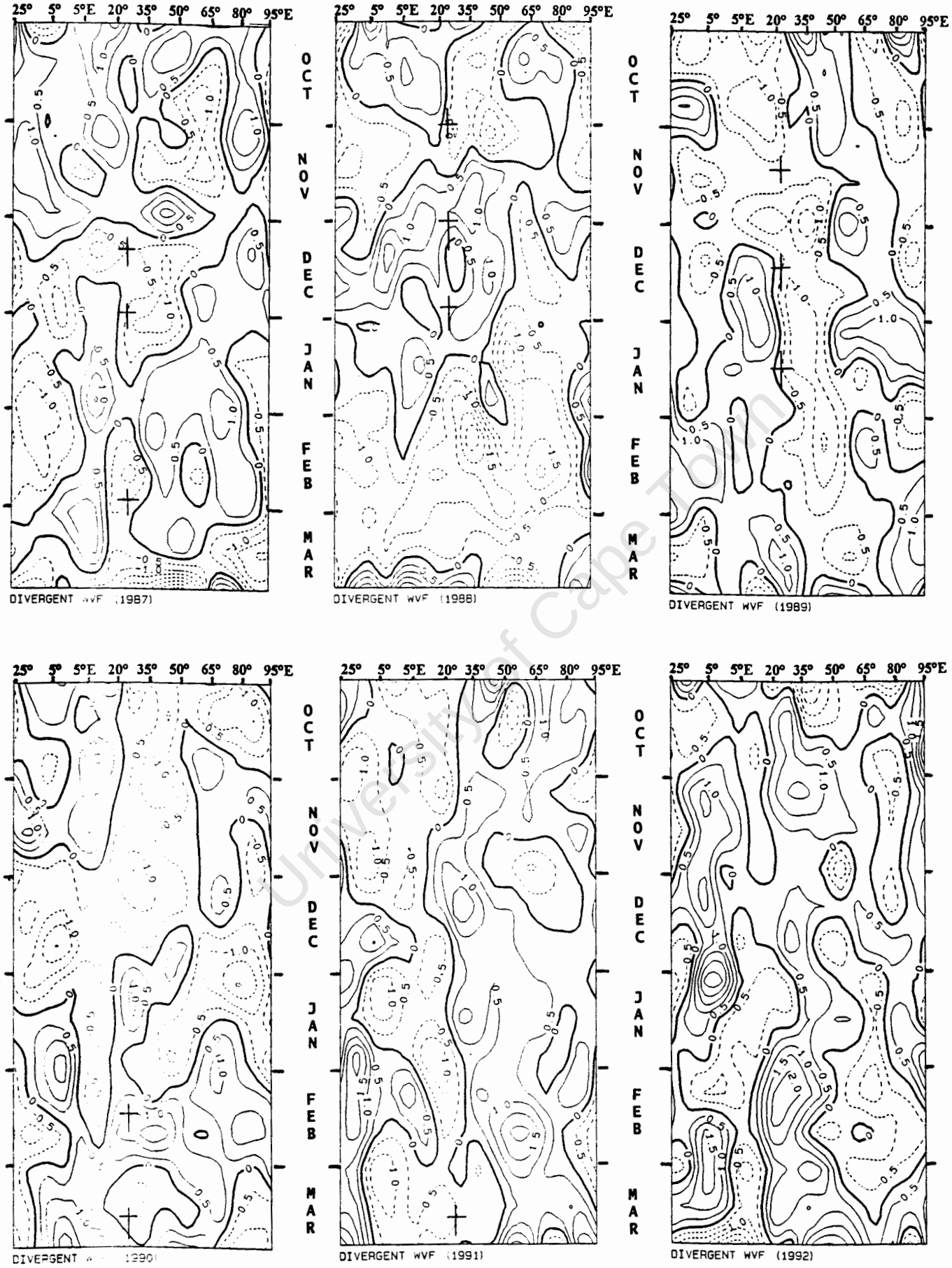

Figure 4-16 : Hovmöller plots of divergent water vapour flux (χ_Q) anomalies between the surface and 500 hPa along 40° S for 1987 to 1992. Contour interval is 0.5 x 10^8 kg s^{-1}.

University of Cape Town

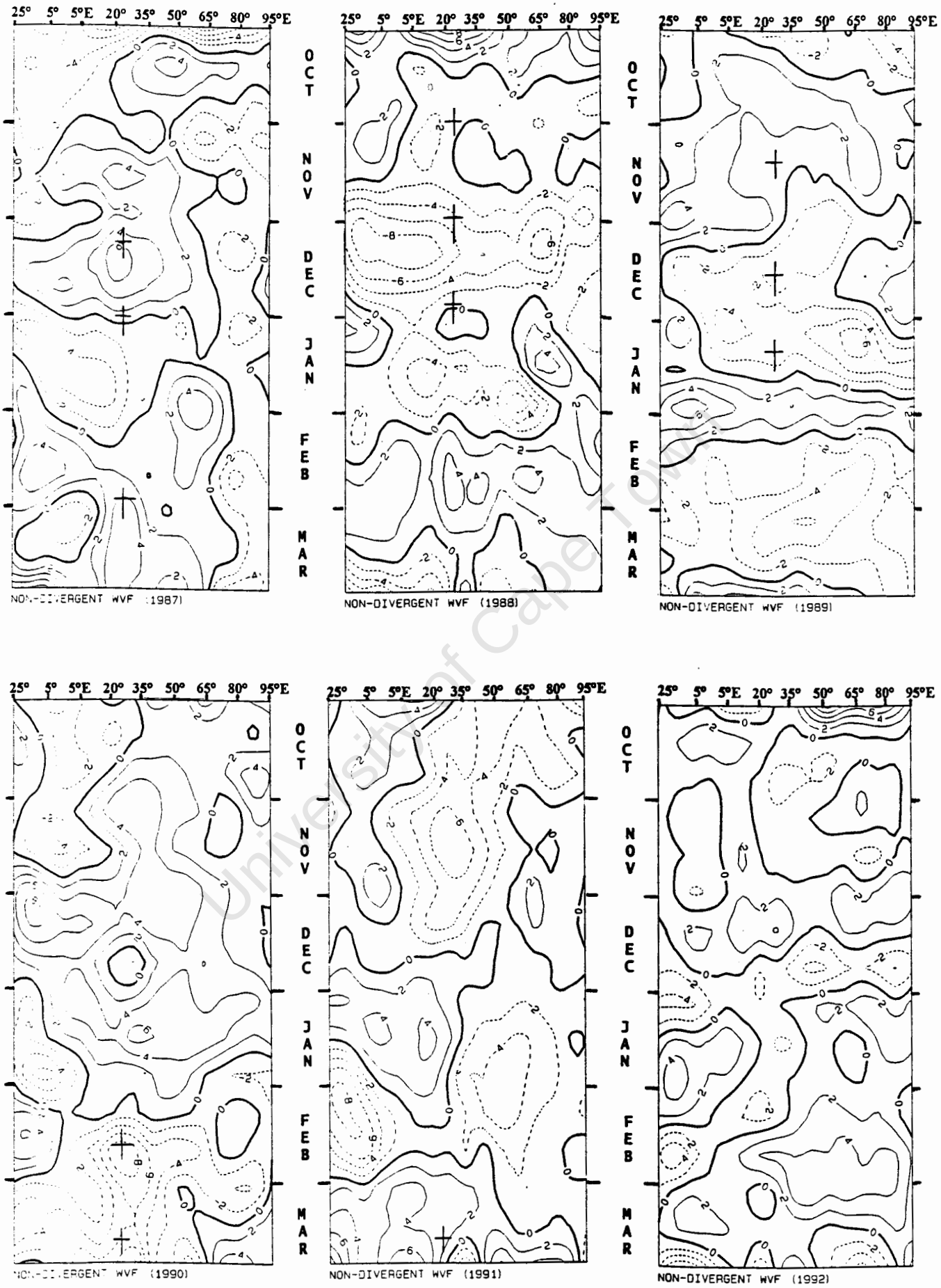

Figure 4-17 : Hovmöller plots of non-divergent water vapour flux (ψ_Q) anomalies between the surface and 500 hPa along 40° S for 1987 to 1992. Contour interval is 2 x 10^8 kg s^{-1}.

University of Cape Town

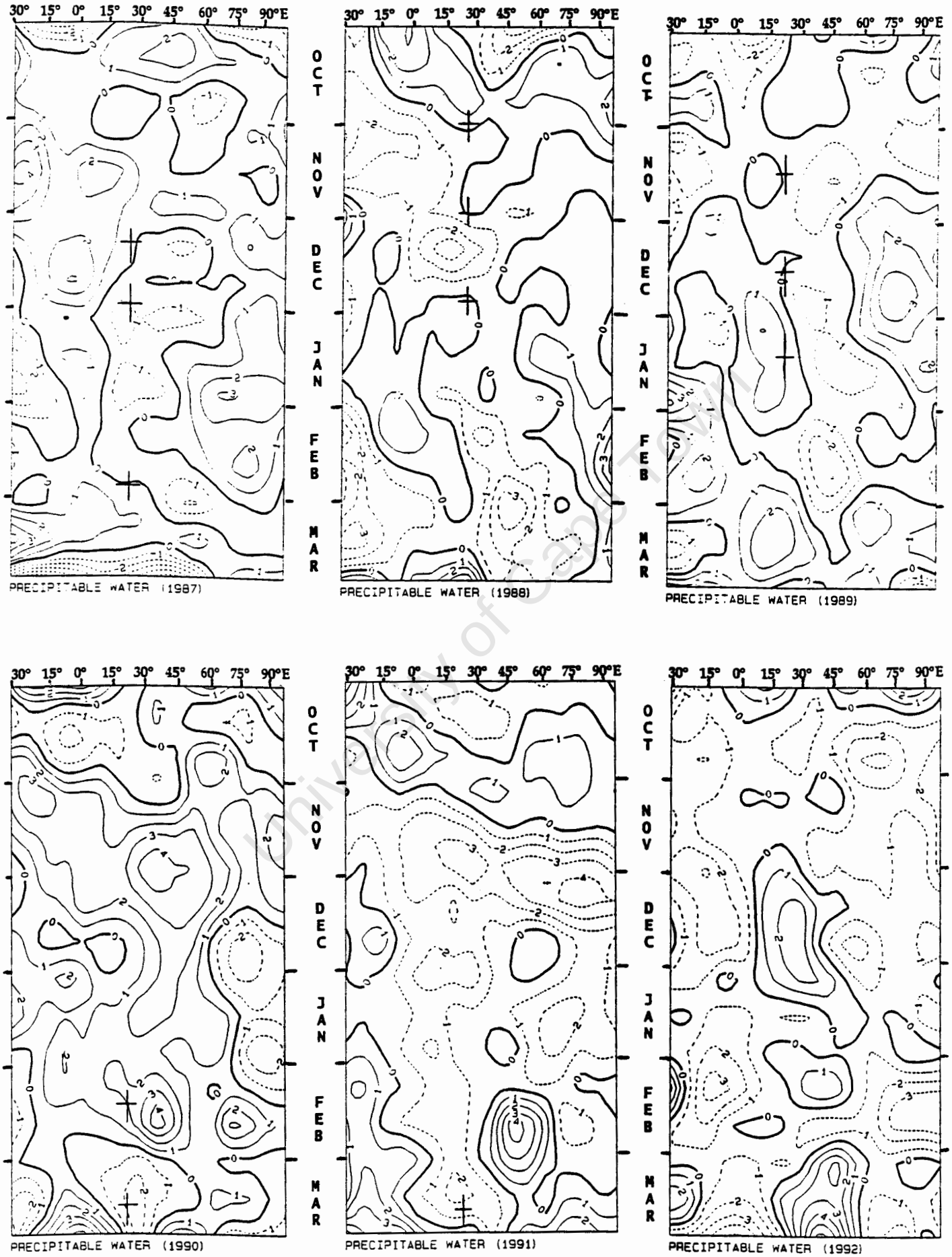

Figure 4-18 : Hovmöller plots of precipitable water anomalies between the surface and 300 hPa along 40° S for 1987 to 1992.
Contour interval is 1 mm.

University of Cape Town

4.2 DISCUSSION

What is clear from the results of the Hovmöller plot analyses is that propagation of anomalies of various variables does occur. The dominant direction of propagation is eastwards, although westward propagation, stationary waves of various variables and "flip-flop" patterns are noted in some years. The kinematic variables shows more consistent eastward propagation of anomalies, especially at 40° S. However, this is expected in the mid-latitudes where the upper-level Rossby waves are modulating the climate.

The results of the moisture variables are less well defined. Eastward propagation is not that clearly identifiable as is the case with Chen and Tzeng's work (1989), although eastward propagation is observed during most summers. There are few occurrences at 10° S where PW anomalies tend to propagate *from* the Indian Ocean *westwards* over Africa.

The eastward propagating anomalies observed at 40° S are of much shorter duration than those observed at 10° S. This can be attributed mainly to the growth and decay of the upper-level Rossby wavetrains propagating eastwards over this region. The duration of anomalies is generally less than 30 days, whereas at 10° S the duration of anomalies, which are also more continuous, range between 30-60 days, which is consistent with the MJO signal.

However, an important result that has emerged is that even when anomalies are quasi-stationary, the intensity of the anomaly still fluctuates with time. This fluctuation of intensities ranges between 20-30 days on average at both latitudes.

University of Cape Town

Another interesting feature is the "flip-flop" of anomalies seen in many years. Anomalies across the latitude change from one sign to the other, but show no propagation characteristics, nor standing wave patterns. These "flip-flop" patterns may be related to changes in the Hadley Cell.

Hence, 4 modes have been identified at 10° S and 40° S. They are :

- eastward propagation;
- westward propagation;
- standing wave patterns;
- "flip-flop" patterns.

teleconnections

The purpose of choosing a tropical (10° S) and an extra-tropical (40° S) latitude band was to establish the characteristics of propagating systems and possible differences between tropical and extra-tropical ISO's.

However, it is interesting to see whether any teleconnections exist between the tropics (10°S) and the midlatitudes (40°S). Table 4-1 is a summary of the anomalies found in the various variables at the lower and upper levels where applicable :

University of Cape Town

Table 4-1 : Sign of anomalies of various variables at 10° S and 40° S at P-0.

VARIABLE	10° S, 25°E	40° S,25°E
GPM_{200}	-	+
GPM_{850}	+	+
U_{200}	-	-
U_{850}	-	-
V_{200}	-	+
V_{850}	-	+
χ_{200}	+	+
ψ_{200}	+	-
$Vert.Wind_{500}$	-	+
χ_Q	+	-
ψ_Q	-	-
PW	+	-

University of Cape Town

The following can be deduced from the summarised results that when the summer rainfall region of South Africa is experiencing a wet event, then :

- negative geopotential heights occur at the upper levels over the tropics, whereas geopotential heights are higher in the midlatitudes at the upper levels;
- the easterlies are stronger over the tropics at both levels and the westerlies are weaker at both levels in the midlatitudes;
- the v-wind component is northerly over the tropics at both levels, whereas it is southerly at both levels in the midlatitides. This shows convergence of the wind field over the southern African region between 10° S and 40° S.
- precipitable water values are anomalously higher over the tropics and lower over the midlatitudes;

- vertical winds are anomalously negative (enhanced uplift) over tropical Africa, while they are anomalously subsident over the midlatitudes.

These suggest distinct tropical-temperate links which will be further explored in Chapter 5.

University of Cape Town

CHAPTER 5

COMPOSITE ANALYSES

This chapter will be divided into sections comparing composite results of the various ECMWF observed and derived parameters. The sections will be divided into mean, anomaly and tendency/temporal trend composite field analyses, each with their individual results.

5.1 MEAN COMPOSITE ANALYSIS

The mean composite fields do not change very dramatically in the temporal progression from P-2 to P+2. Only the P-1 (pre-cursor pentad) and P-0 (wet pentad) show interesting features and for brevity only these two stages will be discussed. However, all anomaly composite pentad stages will be discussed later.

University of Cape Town

5.1.1 KINEMATIC RESULTS

geopotential height

The mean pentad composite fields for P-1 and P-0 in Figure 5-1a,b,c and d show relatively minor differences between the various composites. The geopotential fields at 200 hPa (P_{200}) and at 850 hPa (P_{850}) indicate some subtle circulatory differences between P-1 and P-0.

At P_{200} a trough exists at P-0 where a ridge existed before at P-1 to the east of South Africa. This implies that during the wet period over southern Africa the upper-level temperate trough is located to the *east* and not to the west as is normally the case during wet events over South Africa (Figures 5-1a, 5-1b).

However, Lyons (1991) has shown that during periods of minimum OLR (convective maximum) over southern Africa, a trough exists to the south-east of South Africa at the upper levels.

At P_{850} there are two main features that change from P-1 to P-0. Firstly, a trough exists over the southern sub-continent at P-1, but is replaced by a ridge at P-0. The South Atlantic Anticyclone (SAA) migrates further polewards from P-1 to P-0. At P-1 the centre of the SAA is located at 22.5° S and 20°W and at P-0 it is located at 27.5° S and 7.5° W, which is a shift of 5° polewards and 12.5° eastwards. The South Indian Anticyclone (SIA) also shifts westwards from P-1 to P-0 and also increases in size. The SIA also exhibits a poleward shift of 5° from P-1 to P-0 (Figures 5-1c, 5-1d).

horizontal winds

A feature to note at P_{200} is the flow over the eastern Atlantic Ocean. There is a definite strong north westerly jet flowing from the equator at about 15° W to the southern sub-continent. However, this flow decreases from P-1 to P-0, but then re-intensifies at P+2 (not shown). The direction of the westerly winds over southern Africa also become more westerly at P-0 (Figure 5-2b). This north-westerly jet is most pronounced at P-1 over the eastern Atlantic Ocean, with north-westerly winds of between 10 and 20 m s^{-1} (Figure 5-2a). Easterly flow (7.5 m s^{-1}) at 10° S over the African region is at its maximum at P-0.

Associated with the geopotential field at P_{850}, the winds at this level how similar displacements (Figures 5-2c and 5-2d). The most distinctive features are the strengthening of the SAA from P-1 to P-0. The westerlies are located further polewards at P-0 and are restricted to latitudes greater than 40° S, while during P-1 the westerlies are evident as far north as 30° S. The SIA is better developed at P-0 than at P-1, but appears weaker than at P-2 (not

University of Cape Town

shown). This is observed with regard to the stronger anticyclonic winds at P-0 (± 10 m s^{-1}), than at P-1 (5 m s^{-1}). The northerly flow at 25° S and 25° E is also greater at P-0 than at P-1 (7.5 m s^{-1} as compared to 2.5 m s^{-1}).

kinetic energy

Since kinetic energy (KE) is a function of both components of the total two-dimensional horizontal circulation, it can be concluded that lower (higher) values indicate decreased (increased) wind speeds. At P_{200} KE decreases from a maximum centre of 700 m^2 s^{-2} located at between 40° and 50° S south east of Africa at P-1 (Figure 5-3a) to about 500 m^2 s^{-2} at P-0 south-west of the sub-continent (Figure 5-3b). Noteworthy features of the KE field at P_{200} are found at P-1 and P-0. At P-1, a tight gradient exists over South Africa in the shape of a trough over the western half of the sub-continent. At P-0 *two distinct cells* of higher KE values exist, one to the south west of Africa, located at 45° S and 0° (500 m^2 s^{-2}), and the other one to the south east of Africa, located at 50° S and 80°E (600 m^2 s^{-2}).

Similar decreasing values of KE exist at P850 from P-1 to P-0. Figure 5-3c shows that at P-1 a single core area of high KE values (175 m^2 s^{-2}) is located at 45° S and 30° E and at P-0 (Figure 5-3d) is located at 15° E, but is somewhat weaker at 150 m^2 s^{-2}. Similar to the structure of the KE field at P_{200} at P-0, *two separate cells* of high KE values exist at P850 as well. The tropical Indian Ocean shows no activity, i.e. sluggish flow, whilst the tropical Atlantic shows more active flow (± 25 m^2 s^{-2}) in the area located between 20° S and 10° N and 30° W and 0°. Hence important structural differences from P-1 to P-0 are seen in a splitting from a single KE maximum to a double maximum pattern.

University of Cape Town

vertical winds

The most striking feature of the vertical wind fields at P500 is the dramatic increase in uplift over almost all of Africa south of 10° S at P-0. (Figure 5-4b). Figure 5-4a shows that at P-1 a core of vertical uplift is situated at 5° S 30° E where values of -6 x 10^{-2} Pa s^{-1} occur. A secondary core area of uplift exists at P-1 over the South Africa where values of -6 x 10^{-2} Pa s^{-1} exist. A dramatic increase in uplift occurs over South Africa at P-0 where values double to about -8 x 10^{-2} Pa s^{-1}. Also of interest is the increase in uplift at P-0 over Madagascar which extends into the Indian Ocean.

velocity potential

The dominant feature of the P200 χ-field at P-1 (Figure 5-5a) is the extensive divergent anomaly area (-250 x 10^4 m^2 s^{-2}) centered on 5° S 30° E over the tropics which extends into the central Indian Ocean at 80° E and southwards towards 45° S. There are two convergent areas, one over the eastern Atlantic (+50 x 10^4 m^2 s^{-2}) and the other over the south-eastern Indian Ocean at 30° S and 85° E (+100 x 10^4 m^2 s^{-2}). The core area of the south-east Atlantic convergence is at 20° S 5° W. The convergent areas are not as extensive as the divergent area over Africa and the western Indian Ocean. A strong χ gradient exists along the west coast of Africa and in the Indian Ocean at 25°S and 70° E.

At P-1 the A-field at P850 (Figure 5-5c) is opposite in sign to the upper-level χ-field, but similar in spatial structure, indicating that convergent areas (+125 x 10^4 m^2 s^{-2}) exist over eastern tropical Africa and a divergent centre (-125 x 10^4 m^2 s^{-2}) exists over the Atlantic Ocean. This field shows a dipole pattern. Unlike the upper level, the centres of divergence/convergence are equal in magnitude. The divergent area over the south-east Atlantic is more

University of Cape Town

extensive than the convergent area over eastern Africa which is centred on 5° S and 35° E.

At P-0 there is an increase in magnitude of the divergent area at P_{200} (-250 x 10^4 m^2 s^{-2}), (Figure 5-5b). The upper divergent area over Africa has enlarged in size and covers almost the entire western Indian Ocean. The main axis of divergence is zonally aligned from Africa along the 10° S latitude band towards the east Indian Ocean. The south-east Atlantic Ocean convergent area is displaced further eastwards and northwards and is aligned along the Greenwich meridian with values of +50 x 10^4 m^2 s^{-2}. Its spatial magnitude has also decreased. The other convergent area in the southern Indian Ocean has dissipated.

At P_{850} the south-east Atlantic divergent centre is displaced 15° polewards. The convergent area over eastern Africa is stronger than at P-1 (Figure 5-5d) where values have increased to +175 x 10^4 m^2 s^{-2}. Weakening of the divergent centre is evident at P-0. The χ_{850} dipole thus experiences a weakening over the south-east Atlantic and a strengthening over east Africa.

streamfunction

The dominant feature of all the mean composites at P-1 and P-0 at both the upper and lower levels is the extensive anticyclonic area (positive values in the Southern Hemisphere) covering the entire area of study. There are subtle differences in magnitude and spatial distribution of the core area between P-1 and P-0.

At P_{200} at P-1 the magnitude of the anticyclonic centre is +1750 x 10^4 m^2 s^{-2} and its core area lies over South Africa (Figure 5-6a). At P-0 the anticyclonic

University of Cape Town

centre has weakened and its core is located further north-eastwards over southern Madagascar (Figure 5-6b).

At P_{850} the spatial features are similar to those found at the upper levels. Figures 5-6c and 5-6d show that at the anticyclonic area decreases in magnitude from P-1 to P-0 and is located further polewards. At P-0 two individual core areas exist, one south-west of South Africa and the other south-east of Madagascar, as in the KE field.

5.1.2 MOISTURE AND THERMODYNAMIC RESULTS

temperature

The temperature field at P_{200} shows most changes in spatial structure in the mid-latitudes. Temperatures progressively decrease in the south-east Atlantic Ocean from P-1 (-56° C) to P-0 (-57° C). An interesting feature to note is that at P-1 (Figure 5-7a) there is a relatively cold pool of air at 55° S and 25° E, but this pool warms up rapidly at P-0 (Figure 5-7b), where the isotherms are strongly zonally aligned and are closely spaced, indicating a strong temperature gradient. Very slack temperature gradients exist south of Africa in the westerly wind belt prior to P-0.

University of Cape Town

The only noteworthy feature of the temperature field at P_{850} is the slacker temperature gradient south of the African continent at P-0 (Figure 5-7d), as well as a poleward shift of the 20° C and 10° C isotherms. The temperature gradient in the westerly wind belt strengthens after P-0, but not dramatically. At P-0 the area of temperatures > 20° C decreases over Africa, mainly in the tropical regions, but especially over the eastern regions of Africa where the 20° C isotherm moves westward from the Mozambique Channel (P-1) to over the land (Figure 5-7c). Temperatures drop significantly over the interior of

South Africa at P-0 owing to evaporative cooling in the wet phase (Figure 5-7d).

water vapour flux

The vertically integrated water vapour flux (WVF) fields observed from P-2 to P+2 illustrate subtle differences. The composites show similar circulatory features to that of the P_{850} WVF field. Both composites show dominant anticyclonic areas, one in the south-east Atlantic Ocean and the other in the south Indian Ocean, which are a result of the SAA and SIA, respectively. Figure 5-8b shows that at P-0 eastward transport is found polewards of 40° S, but prior at P-1 (Figure 5-8a), eastward transport occurs as far north as at 30° S in the Atlantic Ocean and 35° S in the Indian Ocean.

From 5° to 15° S over the Indian Ocean there is a significant zonal band of westward transport at P-1. This band drains moisture from about 30° S to 20° N, which is an area over 50° of latitude. At P-0, there is a definite coherence in the westward transport over the Indian Ocean, except north of Madagascar.

Figure 5-8b suggests that Madagascar tends to split the westward transport into two jets. The more important one moves northwards around the northernmost point of Madagascar causing a north easterly flow into southern Africa, whilst the southern branch of the flow, travels around the southernmost tip of Madagascar. At P-0, when the eastward transport is limited polewards of 40° S, a southerly branch is able to penetrate South Africa from the south-east, and together with the flow from the north, increases the convergence of water vapour over the southern African region. Lyons (1992) has shown that the OLR minimum penetrates southern Africa from the south-east as it moves north-westwards into southern Africa. There is a gradual increase in the south easterly flow from P-2 to P-0 as the easterly transport gradually retreats

University of Cape Town

polewards, and then a decrease after P-0 as the poleward retreat of the easterly transport reverses direction.

Another subtle difference in the direction of transport occurs at P-0 over equatorial Africa and areas to the south of the equator. WVF which is predominantly westward at P-1 over equatorial Africa acquires a greater meridional component and the WVF is more polewards into the southern African region.

precipitable water

The composite vertically integrated PW fields have some important features. Both composites show two maximum PW areas. The lessor one is at the equator over west Africa, and the major one is over the central Indian Ocean, also near the equator stretching from the east Indian Ocean. The west African maximum PW area increases from 40 mm at P-1 (Figure 5-8c) to 50 mm at P-0 (Figure 5-8d).

University of Cape Town

The most interesting and important feature of the PW field occurs over the Indian Ocean. At P-1, PW values increases from 40 mm to over 55 mm which is a substantial increase in only five days. The 50 mm isohyet stretches from the east Indian Ocean almost to the east coast of Africa at 15° S and 40° E.

It is important to observe that the PW available over the summer rainfall regions of South Africa increases from between 20 and 30 mm at P-1, to between 30 and 40 mm at P-0. Another feature is the apparent tongue of PW that forms from P-1 over the Mozambique Channel and encroaches south-westwards towards South Africa at P-0. This is of great significance for the southern African region. Lyons (1992) has shown that midlatitude upper levels troughs merge with the TUTT over the south-western Indian Ocean and

help propagate an OLR minimum north-westwards into the interior of southern Africa. Since OLR is a well known proxy for convection, the high PW area that moves south-westwards as shown in Figure 5-8d could be propagated north-westwards into the interior of southern Africa by the TUTT, as proposed by the results of Lyons (1992), although they are not confirmed in this analysis.

divergent water vapour flux

The potential function of water vapour flux ($\chi_{\mathbb{Q}}$) and the divergent water vapour flux vectors ($\mathbb{Q}_{DIV}$) show a definite dipole situation in both composites similar to χ_{850}. The divergent circulation is generally seen as moving from a divergent (negative) area to a convergent (positive) area.

Figure 5-9a shows that at P-1 an area of divergent WVF exists over the south-east Atlantic Ocean (-60 x 10^8 kg s^{-1}), centred on 25° S and 5° E. A convergent area of WVF exists over the Indian Ocean (+20 x 10^8 kg s^{-1}) between the equator and 5°S, stretching from 25° E to over the east Indian Ocean. At P-0, the convergent area over the Indian Ocean has intensified to +30 x 10^8 kg s^{-1} (Figure 5-9b).

Of more interest and importance is the convergent area of WVF in the Indian Ocean. At P-1 a large area of $\chi_{\mathbb{Q}}$ values > +10 x 10^8 kg s^{-1} exists over the Indian Ocean between the equator and 20° S, with two smaller core cells, one situated over the east coast of Africa between 0° and 20° S, and the other between the same latitudes, but centred at 85° E. The convergence of WVF is weak at P-1, but at P-0 it has increased substantially and is at its strongest. A large area of $\chi_{\mathbb{Q}}$ values > +30 x 10^8 kg s^{-1} exists over the Indian Ocean from 5° S and 25° S, 45° E and 80°E, indicating a polewards displacement of the convergent area.

University of Cape Town

$\mathbb{Q}_{DIV}$ values decrease over the south east Atlantic Ocean from P-1 to P-0 as $\chi_{\mathbb{Q}}$ decrease. There is a strong increase in ÄDIV values over the Indian Ocean the divergent area increases in size and magnitude at P-0. Also noticeable is the increased divergent flow from the southern Indian Ocean which is all but absent prior to P-0. The largest $\mathbb{Q}_{DIV}$ vectors occur over equatorial Africa in a direction from the divergent area over the Atlantic to the Indian Ocean convergent area. Hence a see-saw occurs, but the dipole is quasi-stationary.

non-divergent water vapour flux

The dominant feature of the WVF streamfunction, $\psi_{\mathbb{Q}}$ in the composites is the anticyclonic area in the south east Atlantic Ocean. This is to be expected seeing that the irrotational component is divergent in this same area. This anticyclonic area weakens substantially over South Africa from P-1 to P-0, where values decrease from +165 x 10^8 kg s^{-1} to +120 x 10^8 kg s^{-1}.

The core of the anticyclonic region centred at 25° S and 25° E over South Africa at P-1 (Figure 5-10a) weakens and decreases in size and is located further eastwards at 55° E at P-0 (Figure 5-10b). Another core area exists to the south-west of south Africa at P-0. It is interesting to note that the magnitude of anticyclonic centres are between 2 and 4 times greater than that of cyclonic centres, indicating that the anticyclonic rotational component of the total two-dimensional horizontal WVF circulation plays a larger role in modulating the meteorology of this region.

University of Cape Town

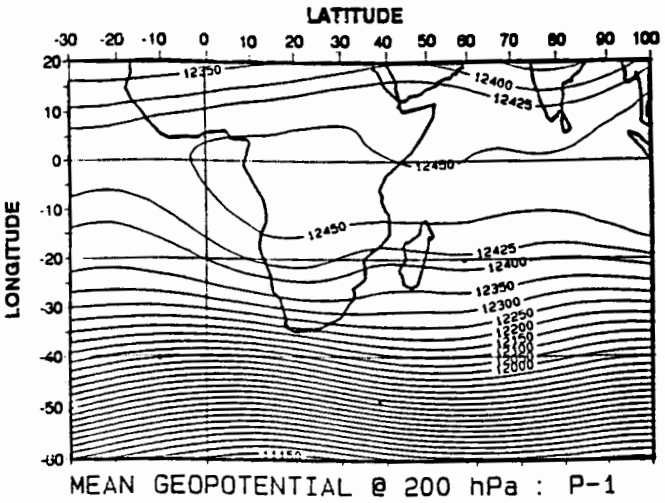

Figure 5-1a : Mean geopotential height @ 200 hPa for P-1. Contour interval below 12400 gpm = 50 gpm, and above 12400 gpm = 25 gpm.

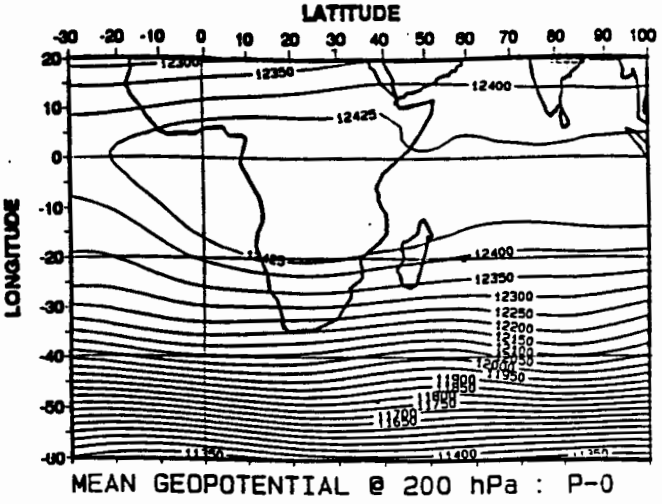

Figure 5-1b : Mean geopotential height @ 200 hPa for P-0. Contour interval below 12400 gpm = 50 gpm, and above 12400 gpm = 25 gpm.

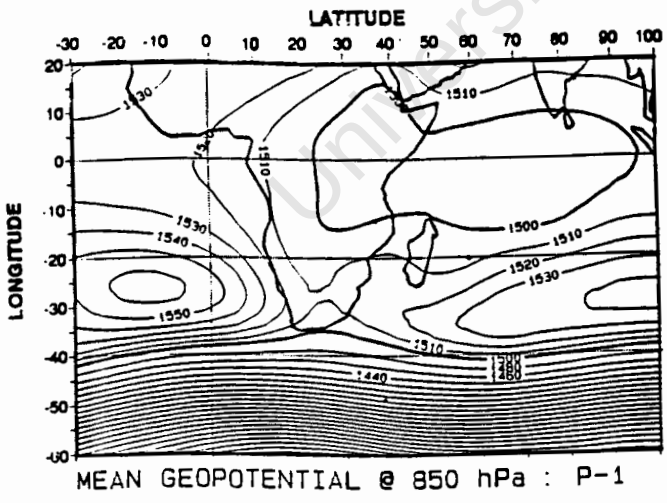

Figure 5-1c : Mean geopotential height @ 850 hPa for P-1. Contour interval below 1500 gpm = 25 gpm, and above 1500 gpm = 10 gpm.

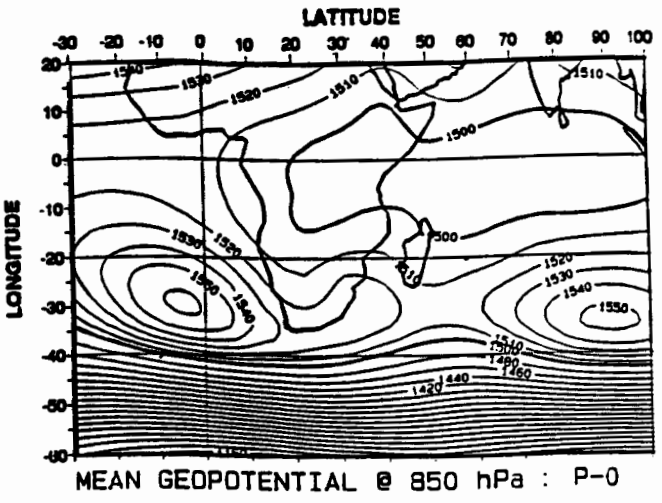

Figure 5-1d : Mean geopotential height @ 850 hPa for P-0. Contour interval below 1500 gpm = 25 gpm, and above 1500 gpm = 10 gpm.

University of Cape Town

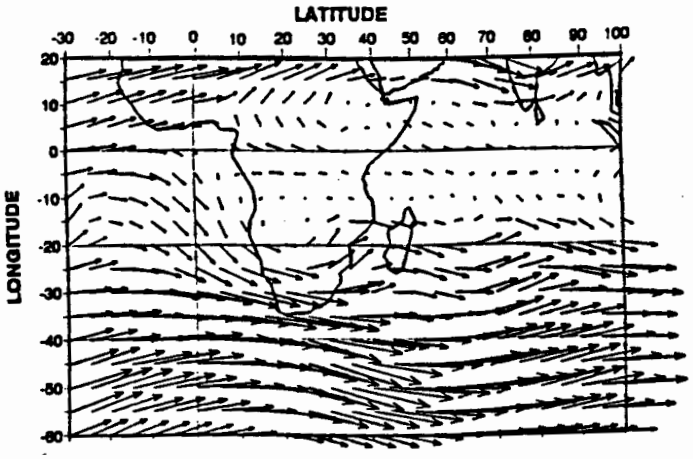

Figure 5-2a : Mean horizontal wind @ 200 hPa for **P-1**. Vector → = 20 m s^{-1}.

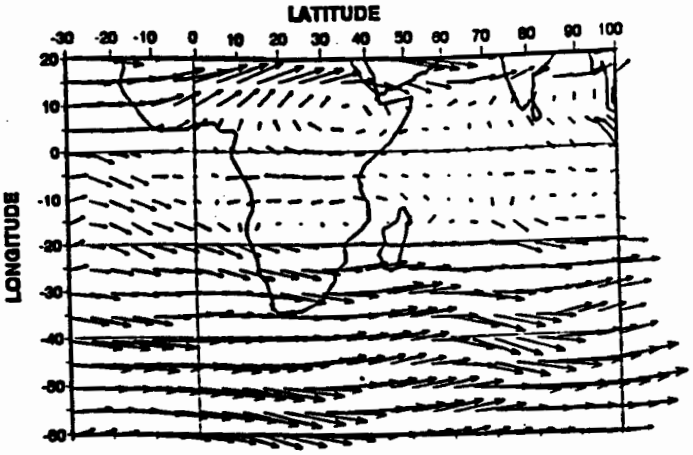

Figure 5-2b : Mean horizontal wind @ 200 hPa for **P-0**. Vector → = 20 m s^{-1}.

University of Cape Town

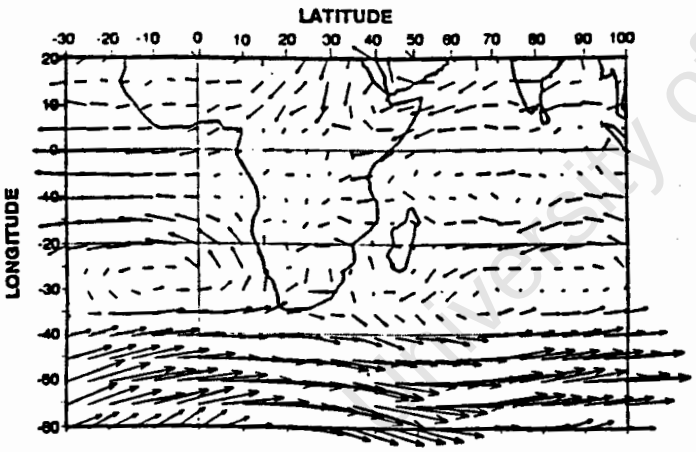

Figure 5-2c : Mean horizontal wind @ 850 hPa for **P-1**. Vector → = 10 m s^{-1}.

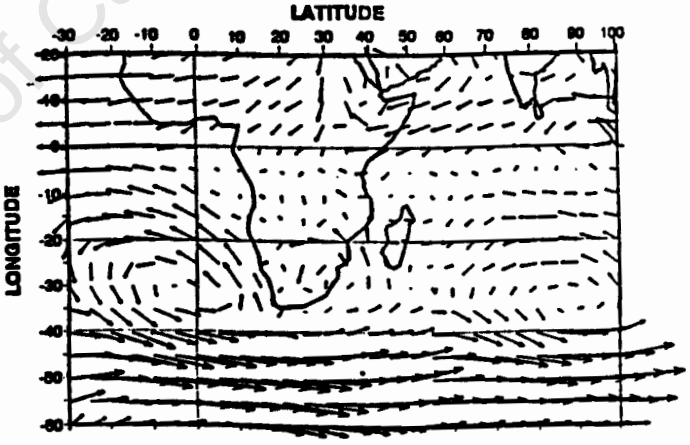

Figure 5-2d : Mean horizontal wind @ 850 hPa for **P-0**. Vector → = 10 m s^{-1}.

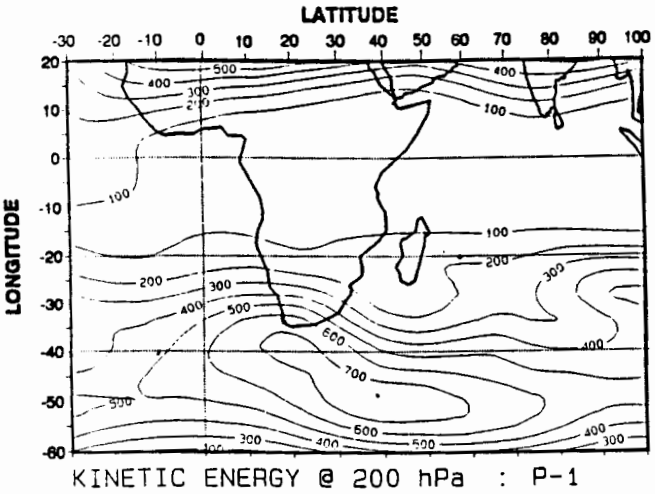

Figure 5-3a : Mean kinetic energy @ 200 hPa for **P-1**. Contour interval is 100 $m^2 s^{-2}$.

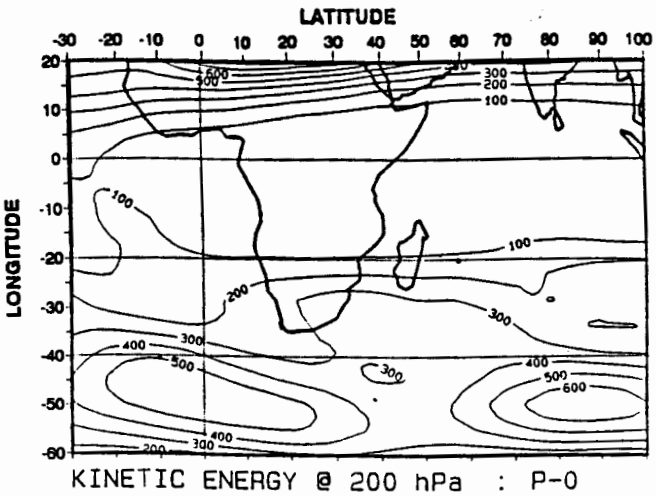

Figure 5-3b : Mean kinetic energy @ 200 hPa for **P-0**. Contour interval is 100 $m^2 s^{-2}$.

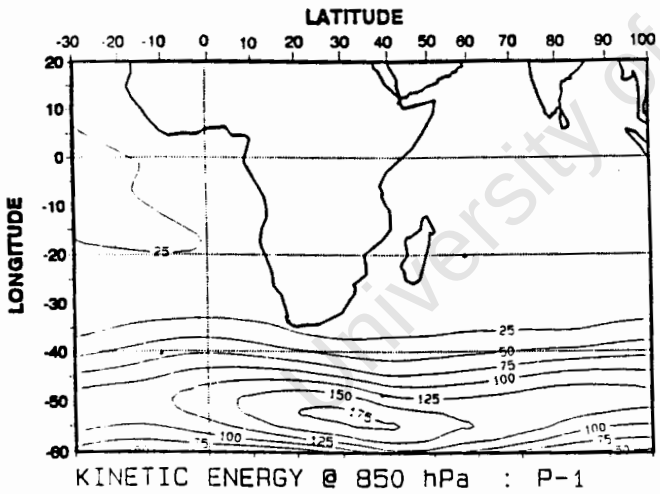

Figure 5-3c : Mean kinetic energy @ 850 hPa for **P-1**. Contour interval is 25 $m^2 s^{-2}$.

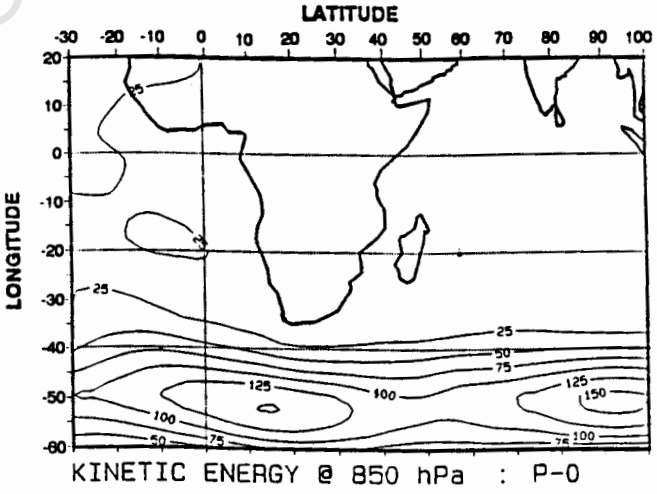

Figure 5-3d : Mean kinetic energy @ 850 hPa for **P-0**. Contour interval is 25 $m^2 s^{-2}$.

University of Cape Town

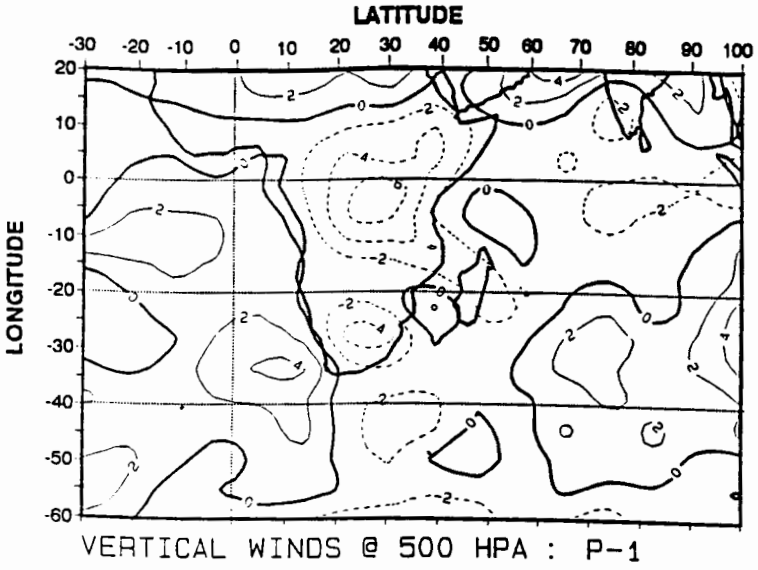

Figure 5-4a : Mean vertical wind @ 500 hPa for **P-1**.
Contour interval is 2 x 10^{-2} Pa s^{-1}.

University of Cape Town

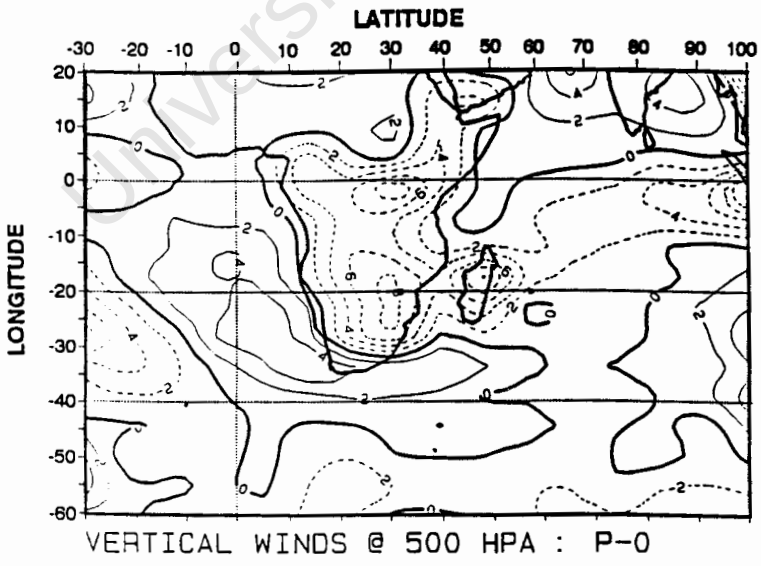

Figure 5-4b : Mean vertical wind @ 500 hPa for **P-0**.
Contour interval is 2 x 10^{-2} Pa s^{-1}.

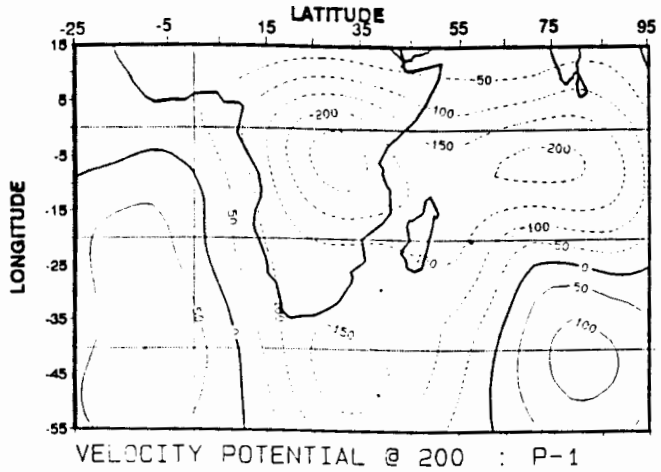

Figure 5-5a : Mean velocity potential (χ) @ 200 hPa for **P-1**. Contour interval is 50 x10^4 m^2 s^{-1}.

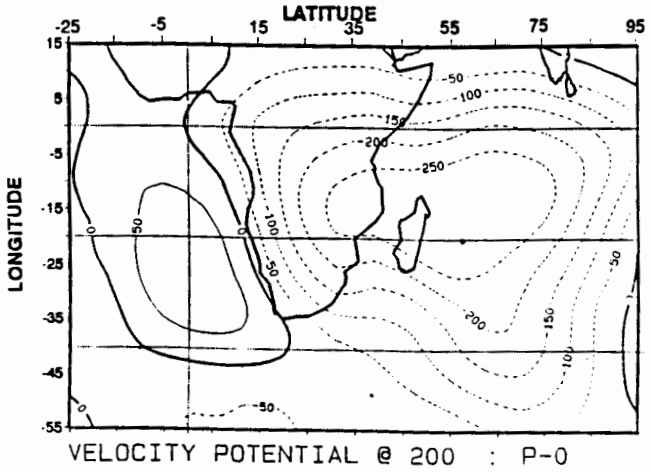

Figure 5-5b : Mean velocity potential (χ) @ 200 hPa for **P-0**. Contour interval is 50 x10^4 m^2 s^{-1}.

University of Cape Town

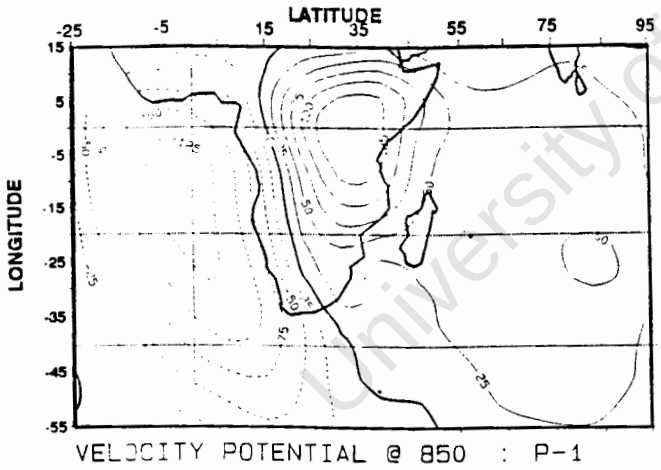

Figure 5-5c : Mean velocity potential (χ) @ 850 hPa for **P-1**. Contour interval is 25 x10^4 m^2 s^{-1}.

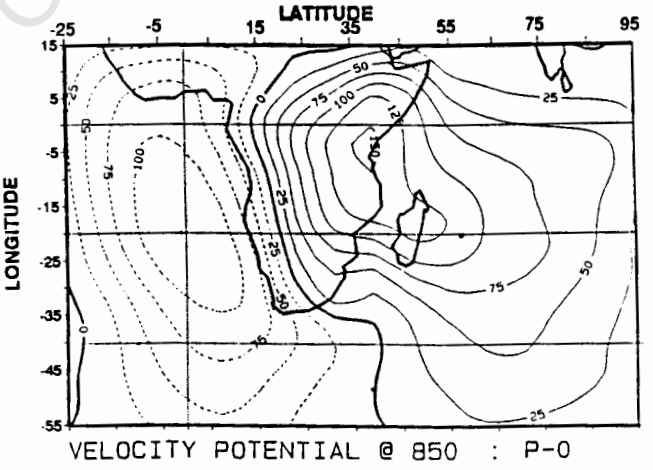

Figure 5-5d : Mean velocity potential (χ) @ 850 hPa for **P-0**. Contour interval is 25 x10^4 m^2 s^{-1}.

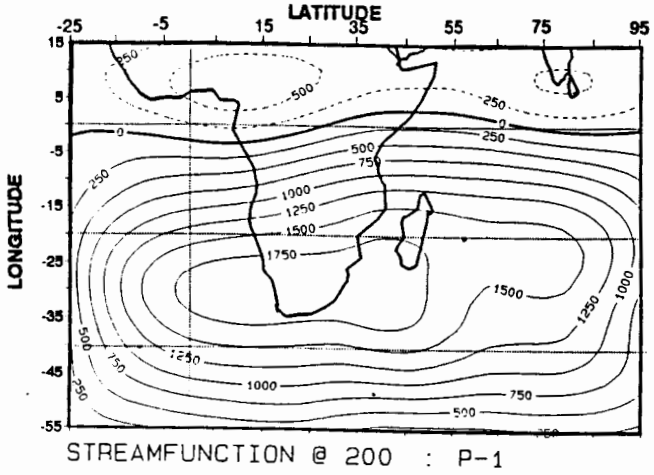

Figure 5-6a : Mean streamfunction (ψ) @ 200 hPa for **P-1**. Contour interval is 250 x10^4 m^2 s^{-1}.

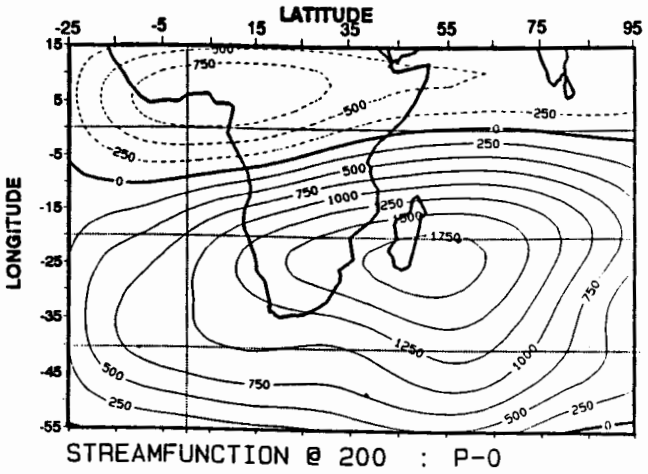

Figure 5-6b : Mean streamfunction (ψ) @ 200 hPa for **P-0**. Contour interval is 250 x10^4 m^2 s^{-1}.

University of Cape Town

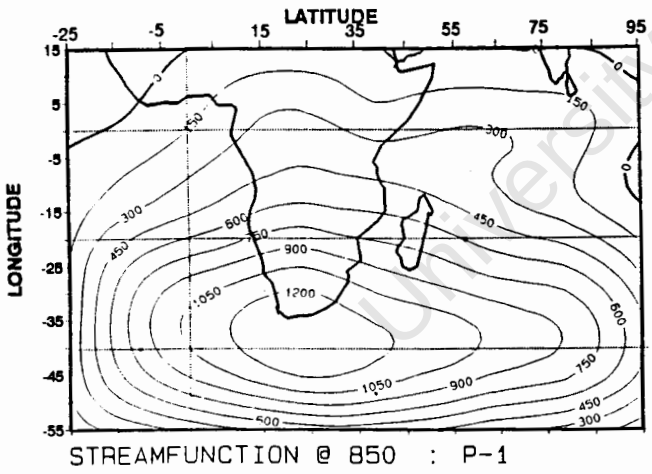

Figure 5-6c : Mean streamfunction (ψ) @ 850 hPa for **P-1**. Contour interval is 150 x10^4 m^2 s^{-1}.

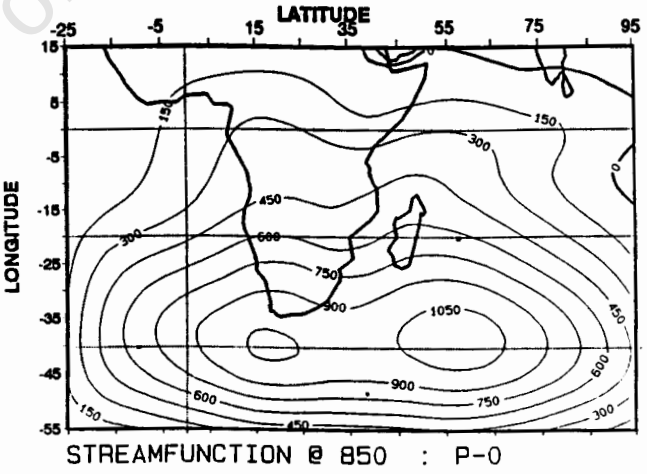

Figure 5-6d : Mean streamfunction (ψ) @ 850 hPa for **P-0**. Contour interval is 150 x10^4 m^2 s^{-1}.

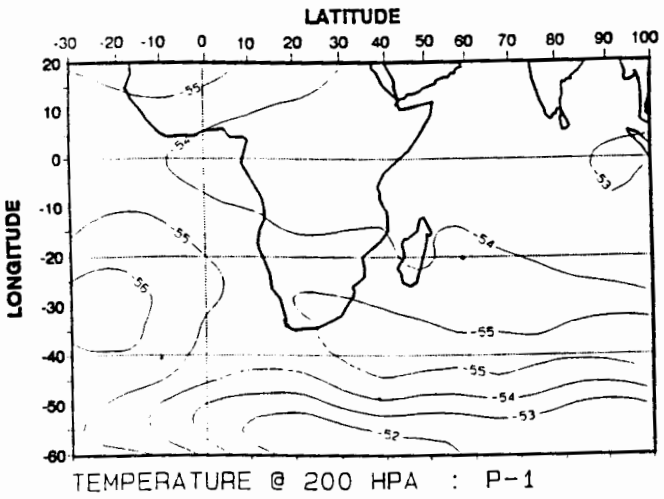

Figure 5-7a : Mean temperature @ 200 hPa for **P-1**. Contour interval is 1° C.

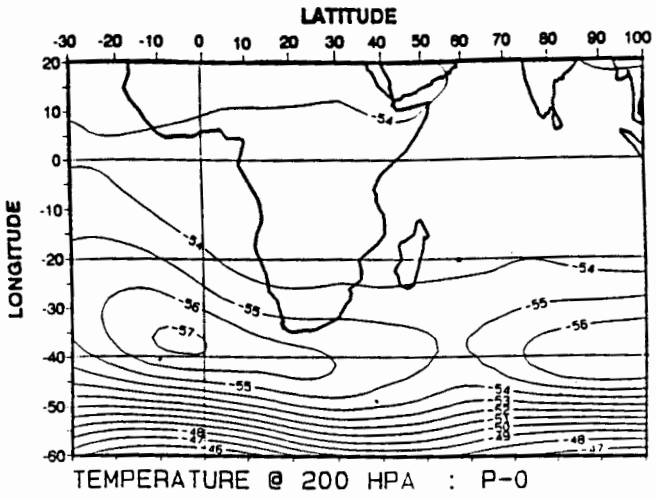

Figure 5-7b : Mean temperature @ 200 hPa for **P-0**. Contour interval is 1° C.

University of Cape Town

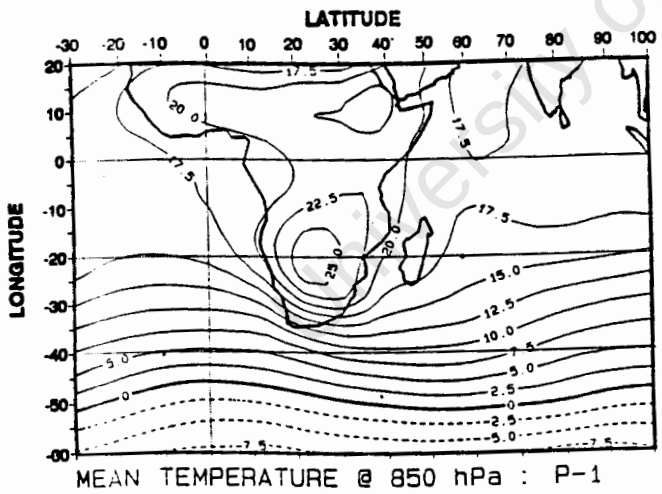

Figure 5-7c : Mean temperature @ 850 hPa for **P-1**. Contour interval is 2.5° C.

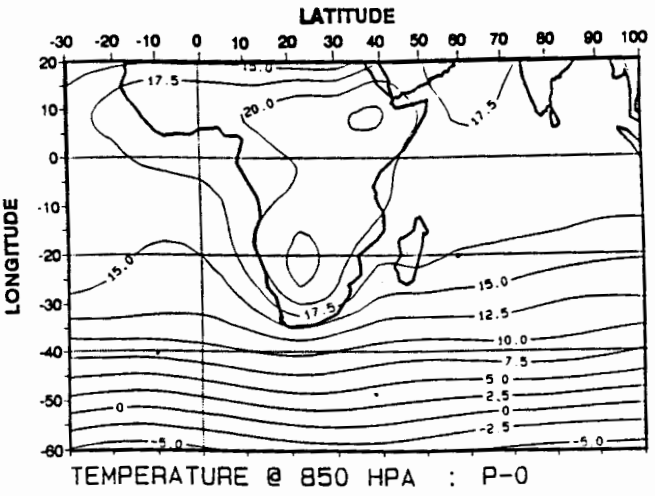

Figure 5-7d : Mean temperature @ 850 hPa for **P-0**. Contour interval is 2.5° C.

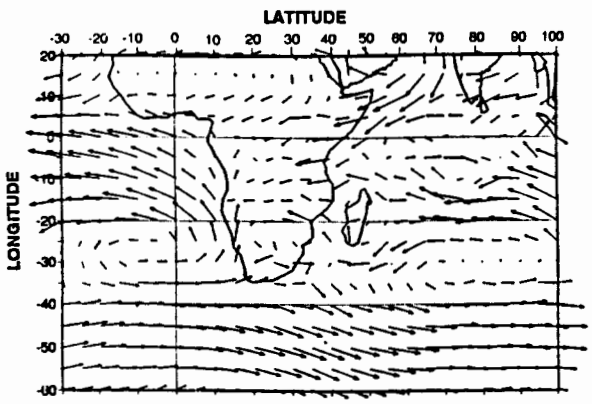

Figure 5-8a : Mean integrated water vapour flux between the surface and 500 hPa for **P-1**. Vector ⟶ = 150 g kg^{-1} m s^{-1}.

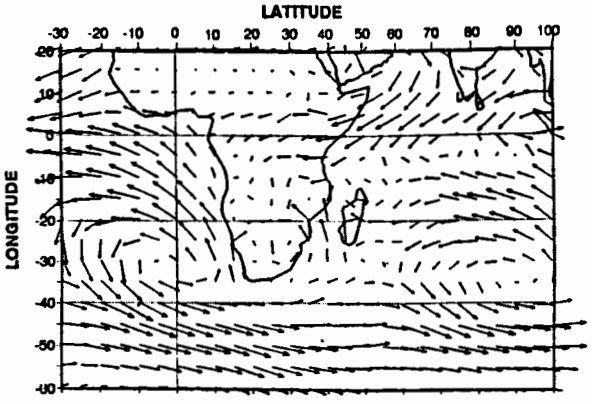

Figure 5-8b : Mean integrated water vapour flux between the surface and 500 hPa for **P-0**. Vector ⟶ = 150 g kg^{-1} m s^{-1}.

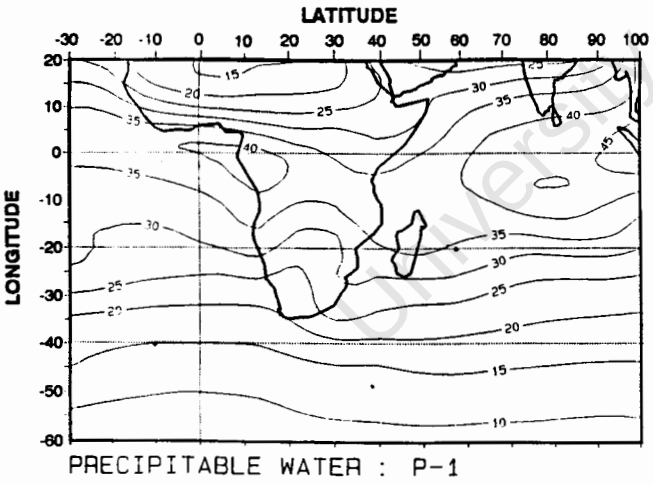

Figure 5-8c : Mean integrated precipitable water between the surface and 300 hPa for **P-1**. Contour interval is 5 mm.

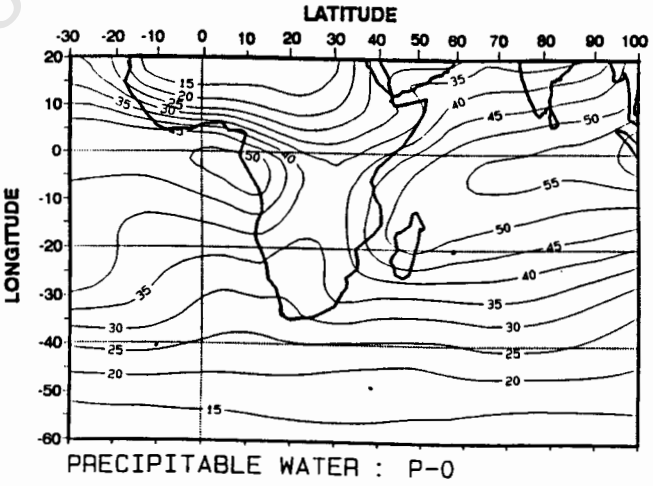

Figure 5-8d : Mean integrated precipitable water between the surface and 300 hPa for **P-0**. Contour interval is 5 mm.

University of Cape Town

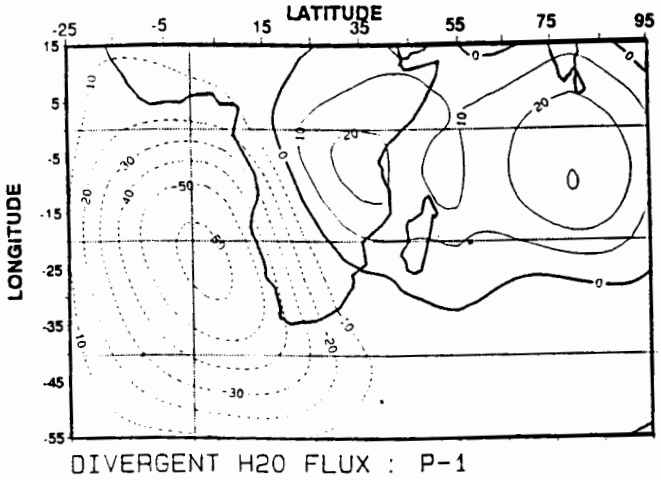

Figure 5-9a : Mean integrated divergent water vapour flux (χ_Q) between the surface and 500 hPa for **P-1**. Contour intrerval is 10 x 10^8 kg s^{-1}.

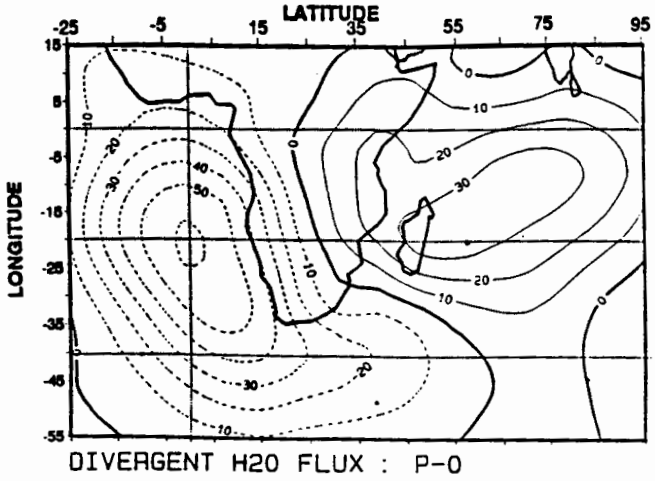

Figure 5-9b : Mean integrated divergent water vapour flux (χ_Q) between the surface and 500 hI for P-0. Contour intrerval is 10 x 10^8 kg

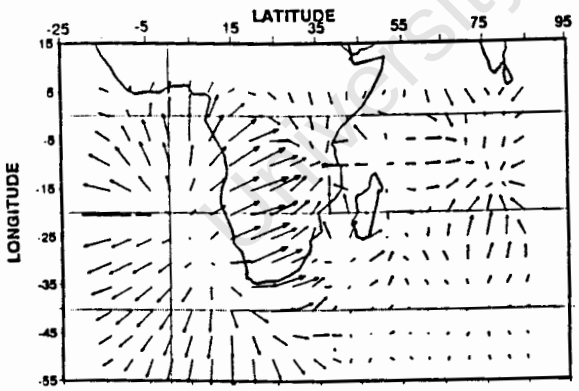

Figure 5-9c : Mean integrated divergent water vapour flux vectors ($\mathbb{Q}_{DIV}$) between the surface and 500 hPa for **P-1**.
Vector → = 10 kg m s^{-1}.

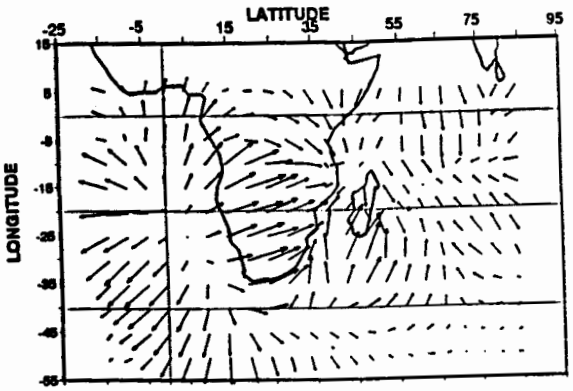

Figure 5-9d : Mean integrated divergent water vapou flux vectors ($\mathbb{Q}_{DIV}$) between the surfac and 500 hPa for P-0.
Vector → = 10 kg m s^{-1}.

University of Cape Town

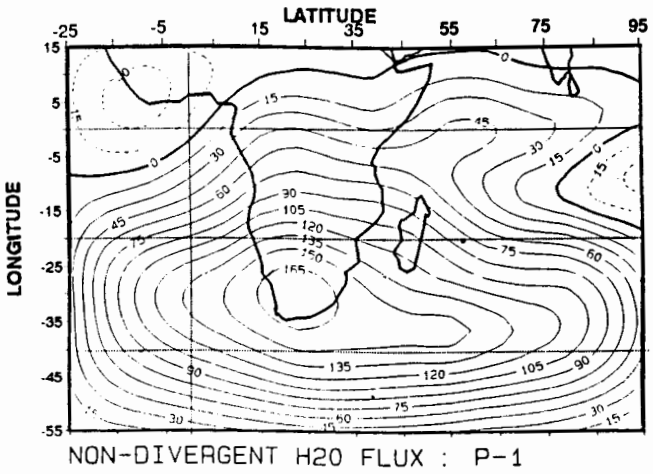

Figure 5-10a : Mean integrated non-divergent water vapour flux (ψ_Q) between the surface and 500 hPa for **P-1**.
Contour interval is 15 x 10^8 kg s^{-1}.

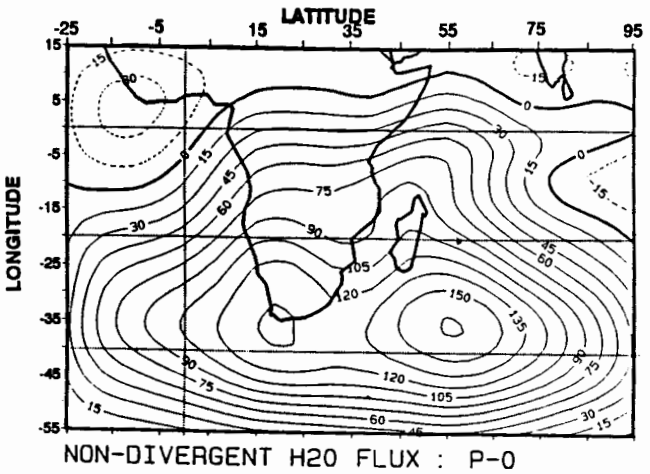

Figure 5-10b : Mean integrated non-divergent water vapour flux (ψ_Q) between the surface and 500 hPa for **P-0**.
Contour interval is 15 x 10^8 kg s^{-1}.

Looking at the total water budget, Figure 5-8a shows how during the precursor (P-1) stage the there is a pulse in the WVF field over the tropical Indian Ocean north of Madagascar. It takes at least five days (as seen in P-0, Figure 5-8d) to advect large quantities of PW south-westwards over Madagascar and south-eastern South Africa during the wet phase. The divergent component of the WVF field shows that convergence of PW in the lower atmosphere further aids the occurrence of large quantities of PW in the south-western Indian Ocean. The rotational component of the WVF field shows that the main core area of BÄ moves eastwards in the progression from the precursor stage to the wet phase over southern Africa, further enhancing westward flow of PW into southern Africa.

University of Cape Town

5.2 ANOMALY COMPOSITE ANALYSIS

Composite anomaly analysis has been used to highlight the differences in the various stages of the 25 day ISO operating over southern Africa. Often mean composite patterns do not show the changes taking place from one stage to another very clearly, but negative and positive anomalies occurring during the different stages of the temporal progression from P-2 to P+2 can be more easily seen.

5.2.1 KINEMATIC RESULTS

geopotential height

In the temporal progression from P-2 to P+2 (Figure 5-11a), there are alternate positive and negative geopotential height anomalies in the mid-latitudes at P_{200}. At P-2 there are two positive anomaly areas, one over the south Atlantic Ocean and one over the south Indian Ocean. However, both these anomalies are weak (+25 gpm). A weak negative anomaly (-25 gpm) exists at 25° S, 0° E. These two positive anomaly areas indicate weak ridging at P_{200}. At P-1 the two positive anomaly areas are replaced with two very negative areas, one at 50° S and 10° E (-125 gpm) and the other at 45° S and 90° E (-75 gpm). A weak positive anomaly (+25 gpm) exists between these two areas. At P-0 the positive anomaly that existed at P-1 has been replaced by a weak negative anomaly (-50 gpm) at 35° S, 55° E and the two strongly negative areas, by strong positive anomalies (+150 gpm) which also occur polewards to 60° S. Negative anomalies also occur over the southern African region. At P+1, negative anomalies once again dominate the Southern Ocean, with negative deviations of up to -50 gpm. At P-0 there is very little structure in the anomaly field other than weak positive anomalies that exist over the Southern Ocean. It can be seen that at P-1, a strong trough exists to the south

University of Cape Town

west of the sub-continent, whereas it is replaced by a strong ridge at P-0, and weak trough to the east of the continent. This change in sign of the anomalies from composite to composite is a result of the upper level Rossby waves affecting the area south of southern Africa.

The P_{850} geopotential anomaly field (Figure 5-11b) shows very similar structures at P-2 and P-1 where large negative anomalies exist to the south of South Africa south of 40° S. Two positive anomalies exist over the south-west Indian Ocean and south-east Atlantic Ocean at P-2 and P-1 indicating stronger sub-tropical anticyclones. However, at P-0 the anomaly field is reversed, with a strong positive anomaly to the south of the continent indicating SAA ridging. A weak negative anomaly exists to the south-east of Madagascar. At P+1 the anomaly field reverts back to the precursor stage where negative anomalies exist to the south of South Africa. By P+2 two separate negative anomaly cells occur in the south-east Atlantic and south-west Indian Ocean.

horizontal winds

At P-2 the horizontal wind anomaly field at P_{200} (Figure 5-12a) shows two positive anomalous areas in the westerly circulation. Stronger westerlies occur polewards of 40° S in both oceans, and in a band between the equator and 25° S, and the anomalies are more positive over the Atlantic than over the Indian Ocean. Weaker westerly flow (easterly anomalies) exists between 25° and 40° S in both the Atlantic and Indian Oceans, but over southern Africa the upper level westerlies are stronger (westerly anomalies). The easterly flow in the western tropical Indian Ocean is also weaker.

At P-1 the north westerly flow over the southern areas of South Africa and the area to the south of Africa is much stronger (strong north-westerly anomalies) than the mean condition of all composites. The spatial distribution of the

University of Cape Town

anomalies in the south Atlantic Ocean indicates a trough with its axis at 5° E. Easterly flow is also weaker over tropical Africa (westerly anomalies). The north westerly flow is much weaker over southern Africa (strong south east anomalies). A cyclonic anomaly exists at 20° S 40° E.

The cyclonic anomaly described above at P-1 is replaced by an anticyclonic anomaly as the easterly flow into Africa and over tropical Africa between the equator and 20° S is strengthened, while there is a dramatic reduction in the westerlies over the southern parts of South Africa and the area immediately to the south of South Africa (south easterly anomalies). The north westerly flow over the eastern tropical Atlantic is also weaker (south easterly anomalies). The anomaly wind field at P-0 is a virtual reversal of the patterns observed at P-1.

At P+1 the westerly circulation is stronger between 25° S and 40° S over the Atlantic Ocean and between 35° S and 45° S over the Indian Ocean. The westerlies are weaker over the tropical eastern Atlantic Ocean as well as over the interior of southern Africa. The easterlies have strengthened along the equator over the Indian Ocean, but are weaker over tropical Africa. Two strong anticyclonic anomalies appear in the anomaly wind field, one at 35° S 90° E in the Indian Ocean and the other at 20° S 5° W in the Atlantic Ocean.

Almost everywhere polewards of 15° S the westerly flow is weaker (easterly anomalies) at P+2. Little else of importance is observed at P-2 at P_{200}.

The anomaly wind fields (Figure 5-12b) observed at P_{850} are similar to the fields observed at P_{200}. At P-2 a very strong anticyclonic anomaly exists over the southern Indian Ocean indicating an intensified SIA. The westerlies are stronger polewards of 40° S . The easterly flow over the Indian Ocean is also

University of Cape Town

stronger south of the equator, but weaker to the north. The anomaly field at P-1 is similar in structure to P-2, but less intense, but the easterly flow into East Africa is weaker than at P-2.

At P-0 there is a strong anticyclonic anomaly to the south of the country with weaker westerlies over the southern areas of the continent as well as in the areas south and west of South Africa. Easterly flow over tropical Africa occurs as far south as 25° S is stronger.

The westerly flow is strengthened again at P+1 between 20° and 40° S over the Atlantic. A cyclonic anomaly exists at 35° S 70° E indicating a weaker SIA. A similar weaker cyclonic anomaly exists over the South Atlantic, indicating a weaker SAA. The easterlies over the tropical Atlantic ocean are weaker.

The most striking feature of the wind anomaly field at P+2 is the weaker westerly circulation polewards of 40° S. The easterly flow is also much weaker over the tropical Indian Ocean and the flow is actually westerly between the equator and 10° S.

University of Cape Town

kinetic energy

The KE anomaly fields (Figure 5-13a) reflect the changes in the upper level Rossby wave trains propagating eastwards over this region. The greatest anomalies occur in the mid-latitudes, which is to be expected.

At P_{200}, large positive KE anomalies (+250 m^2 s^{-2}) exist at P-2 over the southern Indian Ocean at 50° S. Positive anomalies exist everywhere polewards of 40° S indicating a strengthened westerly circulation. Between 20° and 40° S negative anomalies occur, with two negative centres, one south west of South Africa (-100 m^2 s^{-2}) and the other at 35° S over the Indian Ocean (-50 m^2 s^{-2}).

At P_{850}, (Figure 5-13b), a strong positive anomaly band occurs from the southern Atlantic Ocean between 35° S and 50° S to a core area (+50 m^2 s^{-2}) at 45° S 50° E in the Indian Ocean. Weak negative anomaly cells occur in a band between 20° S and 30° S.

Progressing to P-1, the negative anomaly that existed south west of South Africa at P-2 at the upper level, P200, has been replaced by a strong positive anomaly (+200 m^2 s^{-2}). This positive area stretches south eastwards to 60° S 60° E in a north-west south-east axis. A negative anomalous area also lying in a north-west south-east axis exists to the east of the positive anomaly axis, but is not as strong (-100 m^2 s^{-2}) as the positive area.

The spatial distribution of the KE anomaly field at P_{200} is reflected to a similar degree at P_{850}. However, the anomalies are located further polewards and are orientated more zonally with the positive core (50 m^2 s^{-2}) at 55° S 40° E, and the negative core (-20 m^2 s^{-2}) at 45° S 55° E.

The anomaly field at P-0 at P_{200} is almost a complete reversal to the field observed at P-1. The positive anomaly axis observed at P-1 has been replaced by a very strong negative anomaly axis (-300 m^2 s^{-2}) stretching from 30° S 15° W to 60° S 80° E. Positive KE anomalies occur on either side of this negative axis, with the strongest positive anomalies (+50 m^2 s^{-2}) occurring over the southern Mozambique Channel. The negative axis observed at P200 is also reflected at P_{850}. The negative KE anomaly band (-20 m^2 s^{-2}) occurs from Greenwich to 60° E between 40° and 50° S indicating a reduced westerly flow at P_{850} in this region.

University of Cape Town

The anomaly fields at P+1 and P+2 are similar at P_{850}. Weak positive anomalies occur between 20° and 45° S, with weak negative anomalies polewards of 45° S. This pattern is also reflected at P_{850}, although the negative anomalies become stronger (-40 m^2 s^{-2}) at P+2 in the southern Indian Ocean.

vertical winds

Care must be taken when interpreting the anomaly results where deviations from both positive and negative numbers occur. There are some interesting features in the anomalous vertical wind field patterns at P_{500} (Figure 5-14) from P-2 to P+2. Uplift weakens over southern Africa at 20° S from P-2 to P-1 where the vertical wind decreases in magnitude and at P-1 is 3 x 10^{-2} Pa s^{-1} weaker than the mean. The rate of uplift also increases over the southern areas of South African from P-2 to P-1. Over the subsident areas of the Indian Ocean, an increase in subsidence is noted over the south-eastern half of the Indian Ocean at P-2, but is weaker at P-1, although it is stronger in the south-eastern Atlantic Ocean. At P-2 a strong negative anomaly occurs adjacent to the stronger subsidence, which implies an eastward migration of the SIA.

A dramatic reversal occurs at P-0 over equatorial Africa where uplift is about 3 x 10^{-2} Pa s^{-1} weaker, although the uplift is stronger over the southern African region (+8 x 10^{-2} Pa s^{-1}). A dramatic intensification of uplift occurs at P-0 over Southern Africa over a large area centred on 22° S 30° E where negative anomalies of -5 x 10^{-2} Pa s^{-1} occur. Strong positive anomalies (+3 x 10^{-2} Pa s^{-1}) occur in a belt stretching from the south eastern Atlantic Ocean to south- east of South Africa. Most of the southern Indian Ocean display negative anomalies.

University of Cape Town

At P+1 the strong uplift area has weakened (positive anomaly) over almost all of Africa south of 15° S, but by P+2 it starts to strengthen again, except over South Africa where positive anomalies remain.

velocity potential

Evident in the P_{200} χ anomaly field (Figure 5-15a) is the obvious intensification of the divergent centre over Africa and over the Indian Ocean.

At P-2, there is a weak positive convergent anomaly (+50 x 10^4 m^2 s^{-2}) in the south east Atlantic. The strongest convergent anomaly (+175 x 10^4 m^2 s^{-2}) occurs in the Indian Ocean at 30° S 90° E. This indicates that convergent centres in both the Atlantic and especially in the southern Indian Ocean are more intense at P-2. Weak divergent anomalies (-25 x 10^4 m^2 s^{-2}) exist over the southern Africa and southwards.

The strong convergent anomaly in the Indian Ocean has dissipated somewhat (+100 x 10^4 m^2 s^{-2}) at P-1. The Atlantic convergent anomaly has shifted further polewards at 45° S, but is weaker close to the equator inferring that the convergent centre in the south-east Atlantic has been displaced polewards at P-1. The divergent anomaly over South Africa intensifies in magnitude and in space, but the strongest divergent anomaly (-100 x 10^4 m^2 s^{-2}) exists to the south east of South Africa at 42.5° S 30° E.

The χ_{200} anomaly field at P-0 is almost completely the opposite to P-1. The divergent centre over Africa has weakened considerably, especially over tropical Africa. This is shown by the positive anomalies (+50 x 10^4 m^2 s^{-2}) over this region. However, over southern Africa negative anomalies of -25 x 10^4 10^4 m^2 s^{-2} indicate enhanced divergence aloft. The convergent anomaly in the Indian Ocean has disappeared and has been replaced by a divergent one.

University of Cape Town

The negative anomalies (-150 x 10^4 m^2 s^{-2}) in this region indicate this change. The convergent area in the south-east Atlantic at 30° S shows signs of intensifying again with positive anomalies (+50 x 10^4 m^2 s^{-2}) being observed in this region.

The intensification of the convergent area in the south-east Atlantic seen at P-2 is short-lived since at P+1 it has weakened considerably (-125 x 10^4 m^2 s^{-2}). A positive anomaly exists over South Africa indicating weakened divergence, whereas over the eastern Indian Ocean divergence is intensifying (shown by negative anomalies).

The $\dot{P}_{850}$ χ anomaly field (figure 5-15b) from P-2 to P+2 is weak when compared to the upper level velocity potential, but similar to the divergent WVF field. Negative anomalies occur over almost the entire area at P-2 indicating enhanced divergence over the south East Atlantic Ocean and decreased convergence over Africa and the Indian Ocean. However, at P-1 convergence strengthens over much of Africa, except the eastern parts. At P-0 the convergence over the south-western Indian Ocean and over south-eastern Africa intensifies dramatically. This is shown by the strong positive anomalies of +50 x 10^4 m^2 s^{-2} centred at 20° S 55° E adjacent to Madagascar. At P+1 convergence weakens over South Africa as well as over the south-east Atlantic Ocean where positive anomalies +50 x 10^4 m^2 s^{-2} occur. At P+2 most of the Indian Ocean remains weakly convergent.

streamfunction

Negative anomalies are anticyclonic areas and positive anomalies denote cyclonic centres (Knutson and Weickmann, 1986; Weickmann and Khalsa, 1989). Figure 5-16a and 5-16b denote anticyclonic and cyclonic centres by the letter "A" or "C" respectively.

University of Cape Town

At P-2 the P_{200} ψ anomaly field (Figure 5-16a) shows positive (cyclonic) anomalies (+500 x 10^4 m^2 s^{-2}) south of 40° S, while a weak negative (anticyclonic) anomaly exists between 20° S and 40° S over the Indian and east Atlantic Ocean (-200 and -100 x 10^4 m^2 s^{-2} respectively). The positive anomaly intensifies over the south-east Atlantic between 20° and 40° S along the Greenwich Meridian. Southern Africa also shows and strengthening of the cyclonic area at P-1 where values of +200 x 10^4 m^2 s^{-2} are observed.

However, at P-0, the cyclonic area over the south east Atlantic in general has weakened considerably and this is shown by the strong negative (anticyclonic) anomalies over almost the entire area with a maximum negative anomaly core of -400 x 10^4 m^2 s^{-2} occurring at 40° S 40° E. At P+1 the circulation over the eastern half of southern Africa and western Indian Ocean becomes cyclonic (+200 x 10^4 m^2 s^{-2}). A strong anticyclonic anomaly -450 x 10^4 m^2 s^{-2} occurs to the south-west of South Africa at P+1. At P+2 the domain in general displays an anticyclonic anomalous circulation.

The P_{850} ψ anomaly field (Figure 5-16b) shows that the lower atmospheric circulation is most intensely cyclonic at P-1 with positive anomalies of +200 x 10^4 m^2 s^{-2} occurring over most of the south-east Atlantic Ocean. At P-2 this area is slightly less positive. At P-0, negative anomalies exist over all of Africa with the maximum negative anomaly core of -175 x 10^4 m^2 s^{-2} occurring over the south-eastern parts of South Africa. Strong negative anomalies -175 x 10^4 m^2 s^{-2} occur over the south-eastern Atlantic Ocean polewards of 25° S. Positive anomalies are +125 x 10^4 m^2 s^{-2} observed over the southern Indian Ocean. At P+2 almost the entire are shows maximum negative anomalies of -175 x 10^4 m^2 s^{-2} occurring south of South Africa.

University of Cape Town

An interesting feature to note is at P-0 where anticyclonic ridging to the south of the continent is very evident at both levels.

5.2.2 MOISTURE AND THERMODYNAMIC RESULTS

temperature

There is an eastward propagating weak positive temperature (+1° C) anomaly at P_{200} from P-2 to P-1 in the south Atlantic (Figure 5-17a). At P-0 it is replaced by a weak negative anomaly (-1° C) south of the sub-continent. Over southern Africa, the weak negative anomalies are replaced at P-0 by weak positive anomalies, but revert to negative anomalies from P+1 to P+2. The negative anomalies existing polewards of 50° S at P-2, P-1, P+1 and P+2 are replaced by positive anomalies.

Figure 5-17b shows that at P_{850} the most interesting features in the temperature anomaly field occur in the transition from P-1 to P-0. At P-1 there is a large negative anomaly (-3° C) south west of the continent at 45° S 0° E and over the southern African interior there is large weak positive anomaly (+1° C) centred at 20° S 35° E. At P-0, the anomalies reverse sign and a positive anomaly (+3° C) exists south of the continent, while a negative anomaly (-2° C) exists over the eastern interior of South Africa. At P+1 the anomalies have disappeared and a weak negative anomaly exists south of the African sub-continent at 50° S.

precipitable water

The precipitable water field at P-2 (Figure 5-18a) shows widespread negative anomalies. Almost the entire area south of the equator shows negative anomalies, except to the south west of South Africa where a weak positive deviation occurs at 45° S 10° E. The most negative anomaly (-5 mm) area

University of Cape Town

exists at 30° S 75° E. The anomalies in the Indian Ocean are much more negative than those in the Atlantic Ocean. Over the South African interior a negative anomaly of -3 mm exists.

At P-1 the entire area south of the equator is strongly negative, indicating that P-1 is the driest of the five composites. The strongest negative anomaly (-10 mm) in the Indian Ocean occurs in the tropical western Indian Ocean. A large strong negative anomalous area (-9 mm) exists at 30° S 15° W in the Atlantic Ocean. The negative anomaly area over the interior of South Africa has increased in magnitude to -5 mm.

Almost the entire area south of the equator becomes anomalously positive at P-0, with the exception of the equatorial Africa where a negative anomaly (-5 mm) exists, centred at 10° N 20° E. A strong positive anomaly (+5 mm) occurs over the northern areas of Madagascar. Another strong positive anomaly (+6 mm) area exists over the Atlantic at 25° S 30° W. The anomalies have become positive over southern Africa (+2 mm) which shows a change of +7 mm from P-1 to P-0.

P+1 shows positive anomalies everywhere, and strong positive anomalies in excess of +8 mm occur in the western tropical Indian Ocean and over the Atlantic Ocean at 25° S 5° E. Values over South Africa have increased to +6 mm.

At P+2, anomalies decreases rapidly, with only the Atlantic and Indian Oceans and the western interior of southern Africa showing weak positive anomalies of +3 mm and +1 mm respectively. The eastern half of South Africa shows a weak negative anomalously of -1 mm. Most of northern Africa also show weak negative anomalies (-3 mm).

University of Cape Town

water vapour flux

The water vapour flux (WVF) anomaly field at P-2 (Figure 5-18b) shows an intense anticyclonic anomaly in the southern Indian Ocean at 35° S 70°. Westward transport between the equator and 20° S is prominent especially at 10° S from 45° to 90° E. However, north of the equator the easterly transport is weaker (smaller WVF vectors). Enhanced eastward transport is observed in a zonal band between 40° S and 45° S south of the continent. Weak northerly WVF anomalies exist over South Africa.

The strong anticyclonic anomaly in the southern Indian Ocean has disappeared at P-1. Strong northward anomalies occur over the Atlantic between 20° S 30° W and 40° S 0° E. Most importantly, the strong westward WVF anomalies that persist over eastern Africa indicate enhanced moisture advection from the Indian Ocean region at 10° S to 15° S, 35° E to 65° E.

At P-0 there are three areas of strong WVF anomalies. The most important area is over the southern Mozambique Channel in terms of moisture advection into southern Africa. The north-westward transport of moisture onto the eastern plateau of South Africa is indicated by the south easterly WVF vectors in this region. A strong anticyclonic anomaly exists to the south of South Africa with enhanced westward transport into South Africa. Reduced eastward transport to the south and increased transport north-westwards from the south western parts of Africa to the central Atlantic Ocean complete the anticyclonic pattern. The strongest WVF anomalies occur in the Atlantic in the area, and represent moisture outflow. Over the south-west escarpment of South Africa and Namibia strong northerly anomalies indicate tropical inflow in conjunction with a west coast trough and intensified SAA.

University of Cape Town

The WVF anomaly field at P+1 shows an interesting "sub-tropical-jet" feature. A narrow meandering zonal band of strong westerly WVF anomalies stretches from 25° S 0° to 40° S 20° E in the Atlantic. It proceeds eastwards along the South African coast, then moves north-eastwards into the Mozambique Channel to over northern Madagascar and finally continues polewards in a south-easterly direction to 40° S where strong north-westerly WVF anomalies occur in the south Indian Ocean. This meandering anomaly band indicates enhanced eastward transport in the subtropics.

At P+2 the strongest anomalies occur over the monsoon region of the Indian Ocean between the equator and 20° S from 50° to 95° E where strong eastwards transport exists. This represents a complete reversal from P-2 and signifies a phase shift of the tropical ISO. The WVF transport south of 40° S is also weaker (weak easterly anomalies).

University of Cape Town

divergent water vapour flux

At P-2, the divergence of WVF anomaly field (Figure 5-19a) shows two negative anomaly areas, one in the southern Atlantic Ocean at 35° S 5° W (-8×10^8 kg s^{-1}) indicating stronger divergence of the WVF field in this region, and the other area is over the Indian Ocean at 35° S 85°E (-12×10^8 kg s^{-1}) which indicates weaker convergence of the WVF field over the Indian Ocean. A positive anomaly of $+6 \times 10^8$ kg s^{-1} exists to the south east of the sub-continent.

A very strong negative anomaly of -12×10^8 kg s^{-1} exists in the Indian Ocean north of Mauritius at 20° S 55° E indicating greatly reduced convergence in the WVF field at P-1. The divergent area over the Atlantic is stronger further south where weaker negative anomalies exist (-8×10^8 kg s^{-1}).

At P-0, the strongly negative anomalous area which existed in the Indian Ocean at P-1, has been replaced by a strong positive anomaly (+12 x 10^8 kg s^{-1}) showing that convergence in the WVF field has been greatly enhanced. This strong convergent anomaly stretches south-westwards towards South Africa in the same axis as the PW field (Figure 5-18b). Positive anomalies (+6 x 10^8 kg s^{-1}) in the south Atlantic west of Greenwich indicate that divergence in the WVF field has become somewhat weaker. Two negative anomaly areas are also present at P-0. One exists to the south east of South Africa (-10 x 10^8 kg s^{-1}) indicating that divergence has increased in this area. The negative area at 0° 20° E also indicates enhanced divergence of the WVF field. These patterns clearly show how convergence in the WVF field has been greatly increased over the tropical Indian Ocean and the southern Atlantic Ocean.

Weaker negative anomalies persist south-east of South Africa at P+1. Divergence of the WVF field in the south-east Atlantic is at its weakest with strong positive anomalies (+8 x 10^8 kg s^{-1}) observed in this region. The very strong convergent area over the Indian Ocean north of Mauritius has weakened considerably.

At P+2 most of area south of the equator shows positive anomalies, indicating that the Atlantic divergent area is still in a weakened state, whereas the Indian Ocean convergent area remains stronger, but weakly so. The positive anomaly over southern Africa indicates weaker divergence, therefore stronger convergence.

Figure 5-19b shows the progression from P-1 to P+2 of the Q_{DIV} anomaly wind. It can be seen that the greatest changes occur from P-1 to P-0 where the divergent anomaly reverses from P-1 to become strongly convergent at P-0, especially over northern Madagascar. A line of convergence of Q_{DIV} extending

University of Cape Town

along the PW axis through Madagascar at P-0 suggests the need for dynamical alignment of Indian and African convective systems during the wet phase of the ISO.

non-divergent water vapour flux

The non-divergent (streamfunction) WVF anomaly field has some very strong anomalies in the different composites (Figure 5-20) indicating that the rotational component of the WVF field is changing rapidly during various phases of the ISO.

At P-2, a very strong positive anomaly of +25 x 10^8 kg s^{-1} exists south of South Africa. This anomaly indicates an intensified cyclonic vortex which enhances convection. A negative anomaly of -25 x 10^8 kg s^{-1} exists over the southern Indian Ocean. The non-divergent WVF anomaly field at P-1 is similar in structure to that observed at P-2, except that the anomalies are less intense.

The anomaly field is almost completely reversed at P-0 where the strongest anomalies of the entire composite progression occurs. An intense negative (anticyclonic) anomaly exists with two core areas, one over the south-east Atlantic north of 40° S and the other over southern Africa (-25 x 10^8 kg s^{-1}). A positive (cyclonic) meridional axis of +10^8 kg s^{-1} exists over the Indian Ocean. At P+1 the anomalies are reversed with strong positive anomalies of +25 x 10^8 kg s^{-1} occurring over the Indian Ocean at 20° S, which extend westward over southern Africa. A negative anomaly exists to the south-west of South Africa. At P+2 almost the entire area is anomalously negative (anticyclonic) and in sharp contrast to the positive biased pattern at P-2, again highlighting the opposing ISO phase. Weak positive anomalies still exist over the Atlantic and a weak negative anomaly (-20x 10^8 kg s^{-1}) has appeared in the southern Indian Ocean where a positive anomaly previously existed at P+1.

University of Cape Town

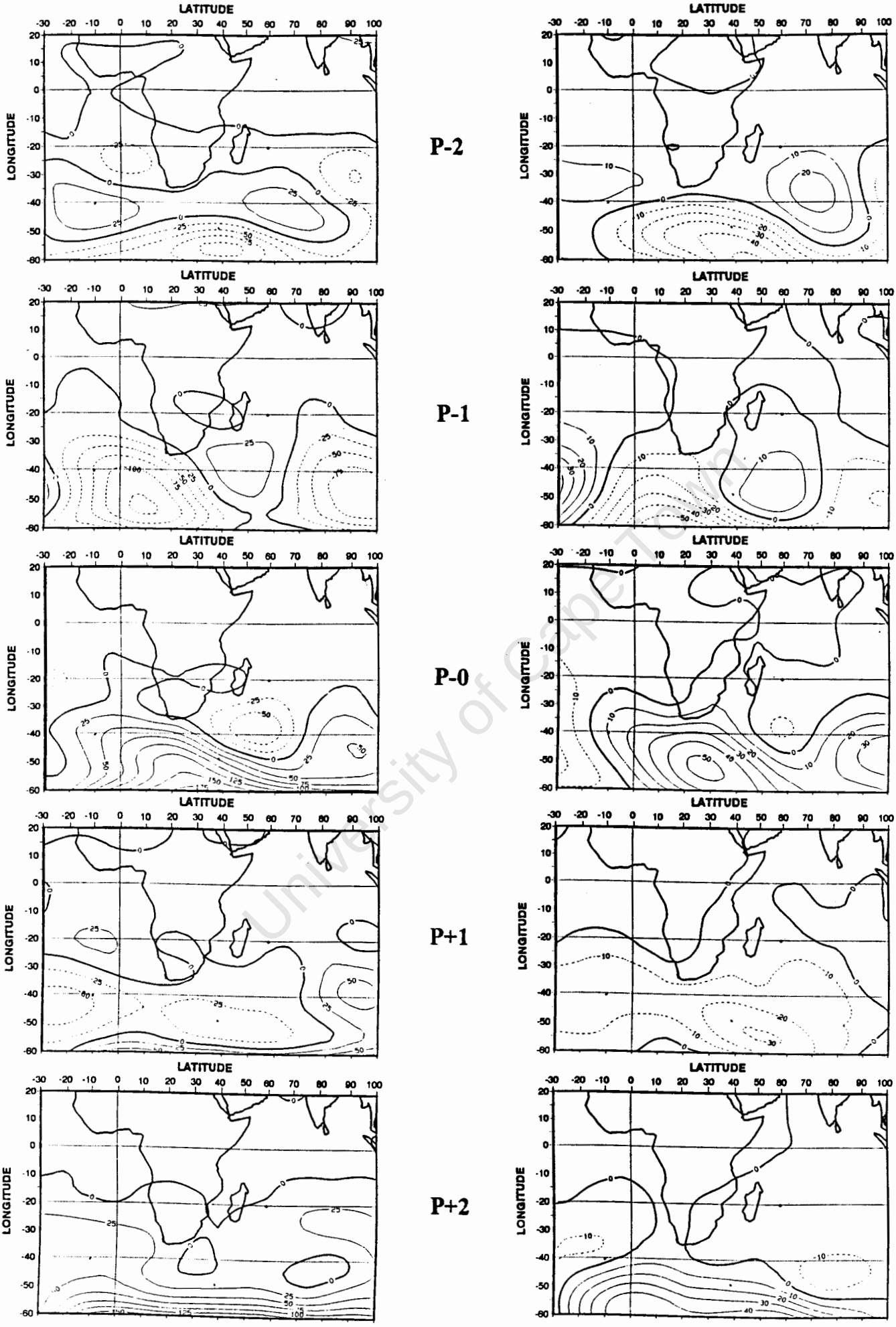

Figure 5-11a : Geopotential height anomaly @ 200 hPa for **P-2** to **P+2**. Contour interval is 25 gpm.

Figure 5-11b : Geopotential height anomalies @ 850 hPa for **P-2** to **P+2**. Contour interval is 10 gpm.

University of CapeTown

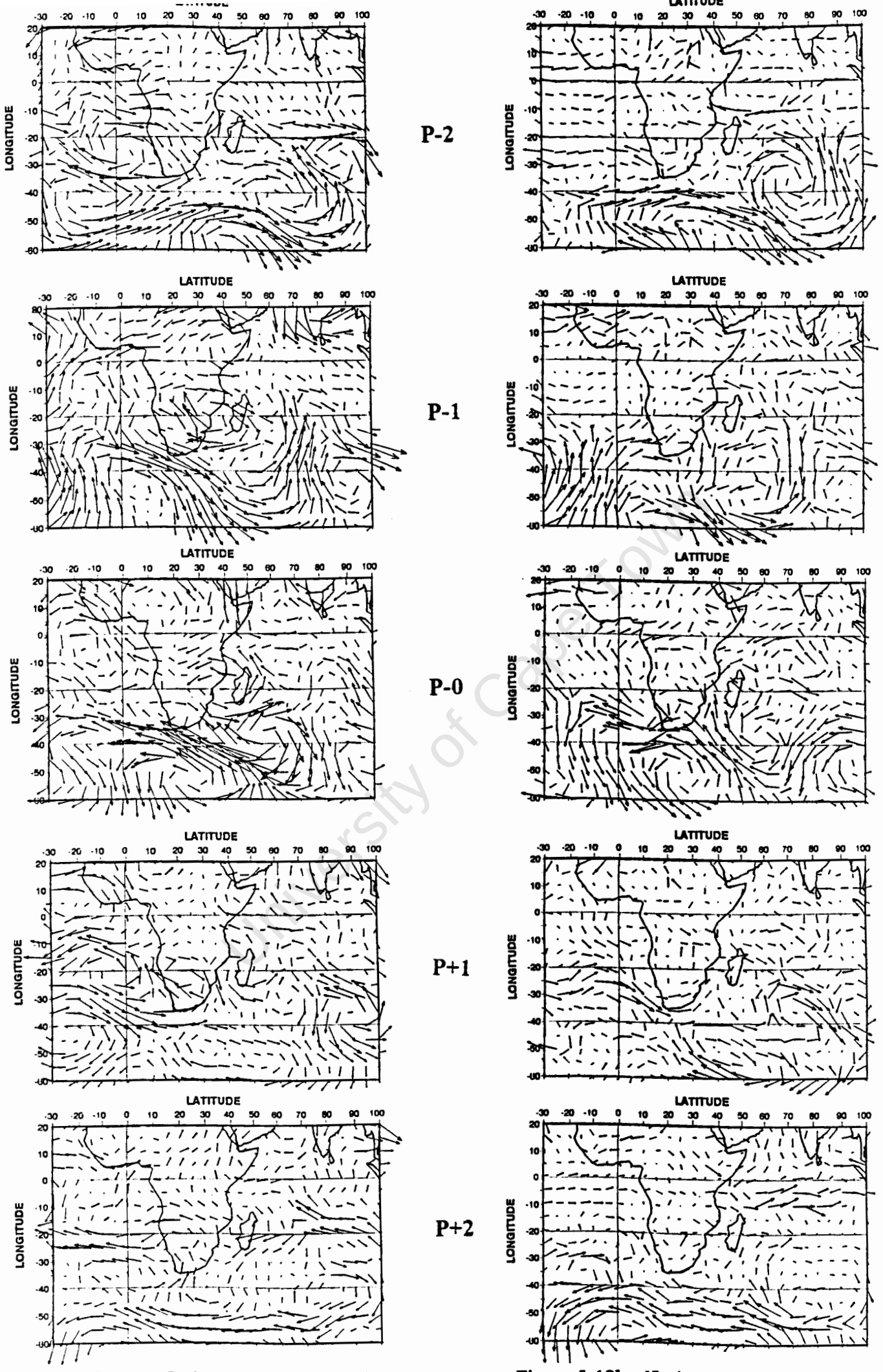

Figure 5-12a : Horizontal wind anomalies @ 200 hPa for P-2 to P+2. Vector → = 10 m s^{-1}.

Figure 5-12b : Horizontal wind anomalies @ 850 hPa for P-2 to P+2. Vector → = 5 m s^{-1}.

University of Cape Town

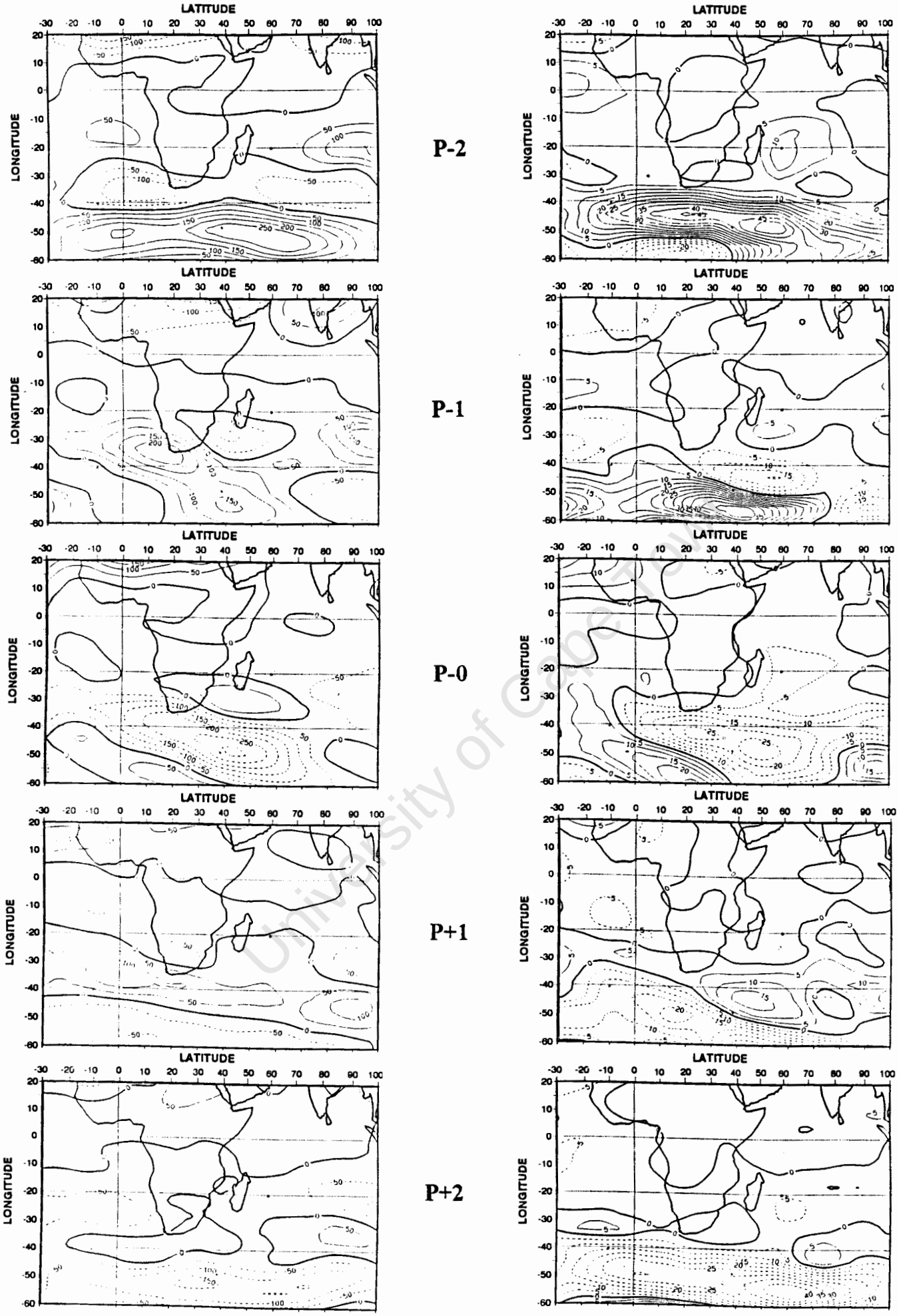

Figure 5-13a : Kinetic energy anomalies @ 200 hPa for **P-2** to **P+2.** Contour interval is 50 $m^2 s^{-2}$.

Figure 5-13a : Kinetic energy anomalies @ 850 hPa for **P-2** to **P+2.** Contour interval is 5 $m^2 s^{-2}$.

University of Cape Town

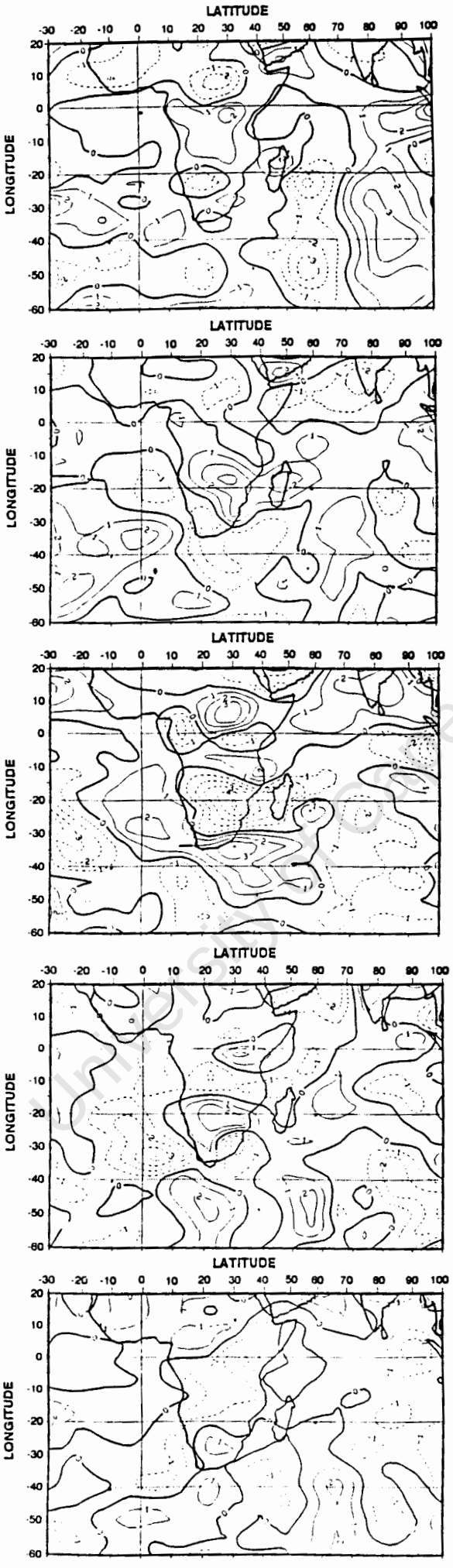

Figure 5-14 : Vertical wind anomalies @ 500 hPa for P-2 to P+2. Contour interval is 2 x 10^{-2} Pa s^{-1}.

University of Cape Town

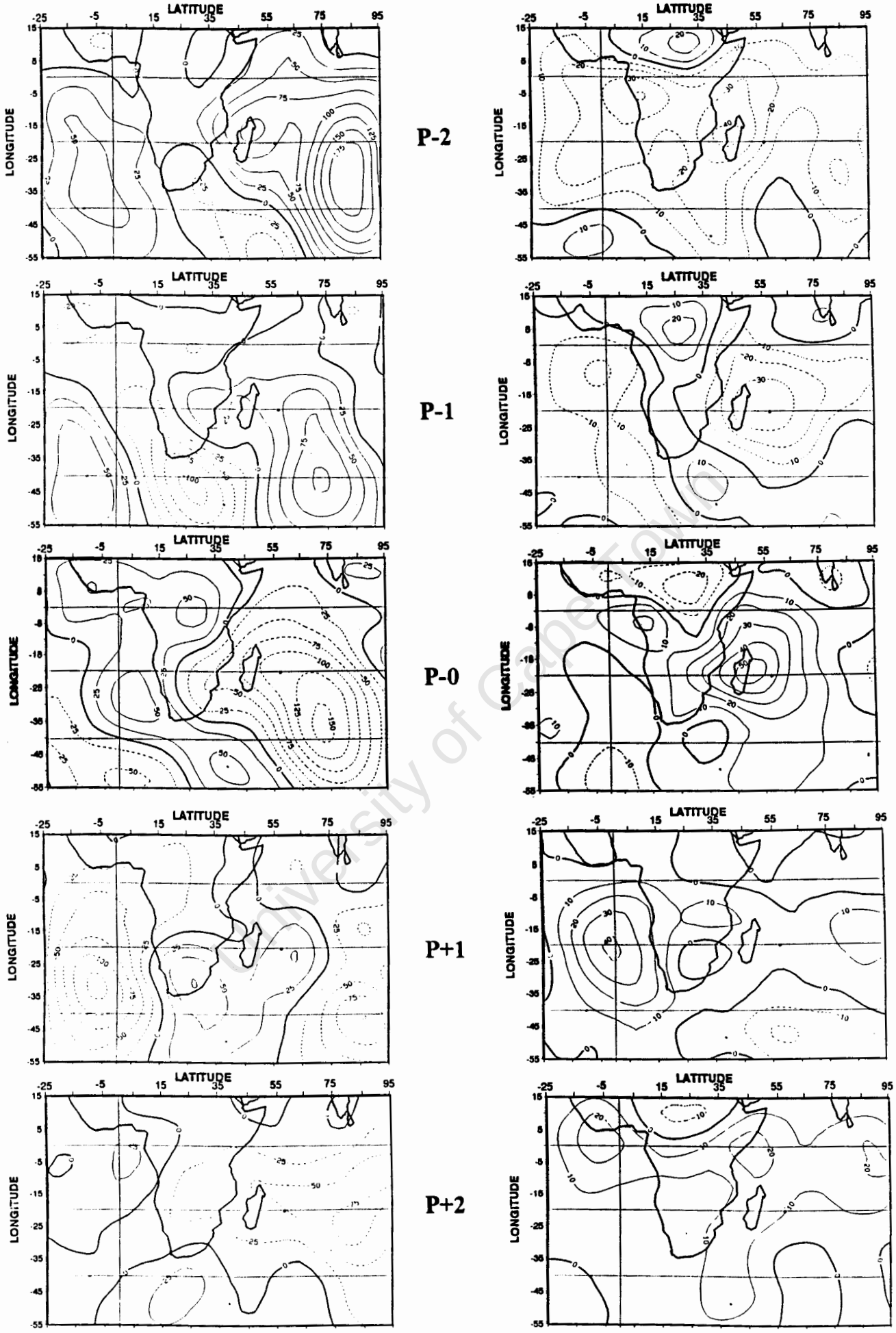

Figure 5-15a : Velocity potential (χ) anomalies @ 200 hPa for **P-2** to **P+2**. Contour interval is 25 x10^4 m^2 s^{-2}.

Figure 5-15b : Velocity potential (χ) anomalies @ 850 hPa for **P-2** to **P+2**. Contour interval is 10 x10^4 m^2 s^{-2}.

University of Cape Town

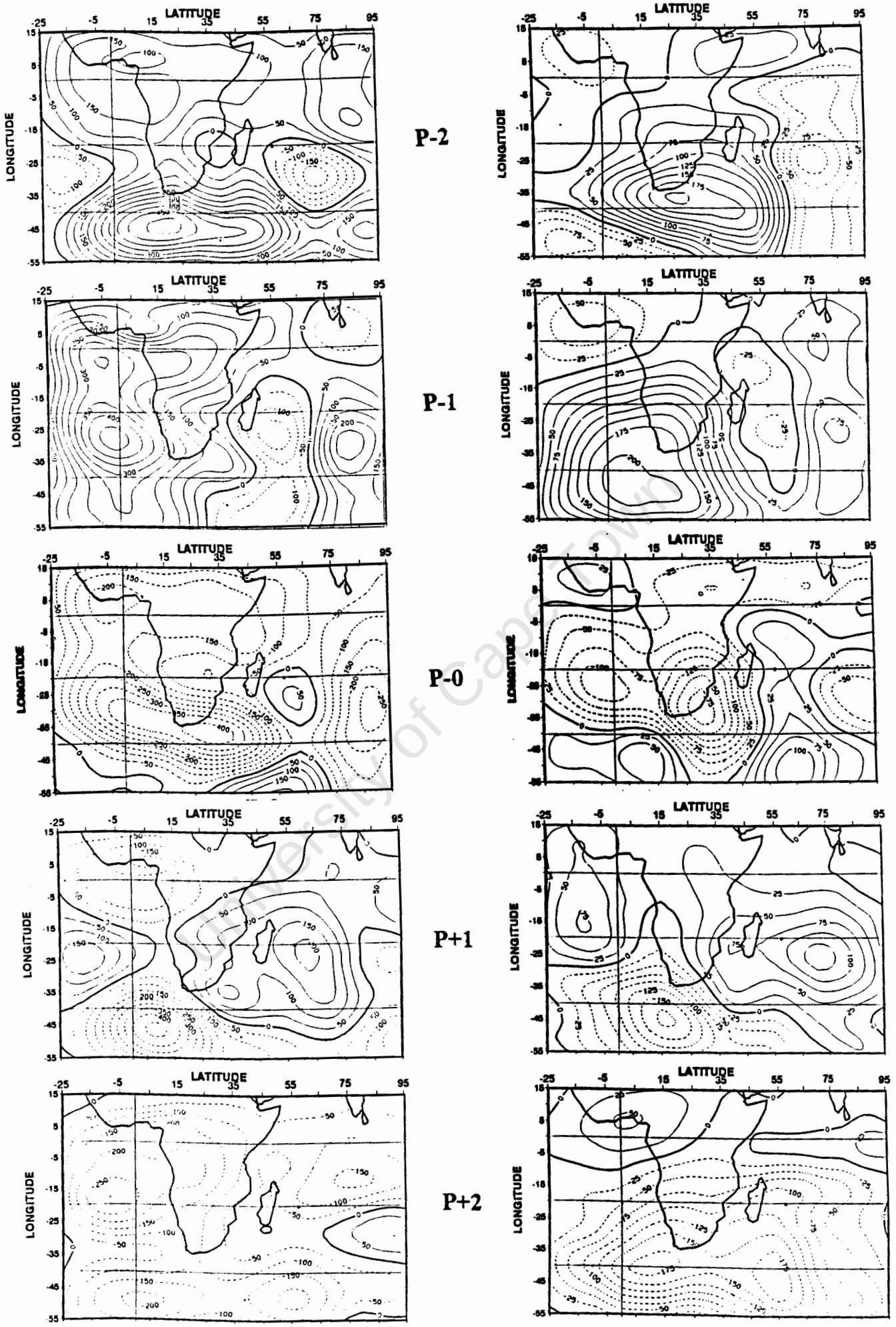

Figure 5-16a : Streamfunction (ψ) anomalies @ 200 hPa for **P-2** to **P+2**. Contour interval is 50 x10^4 m^2 s^{-2}.

Figure 5-16b : Streamfunction (ψ) anomalies @ 850 hPa for **P-2** to P+2. Contour interval is 25 x10^4 m^2 s^{-2}.

University of Cape Town

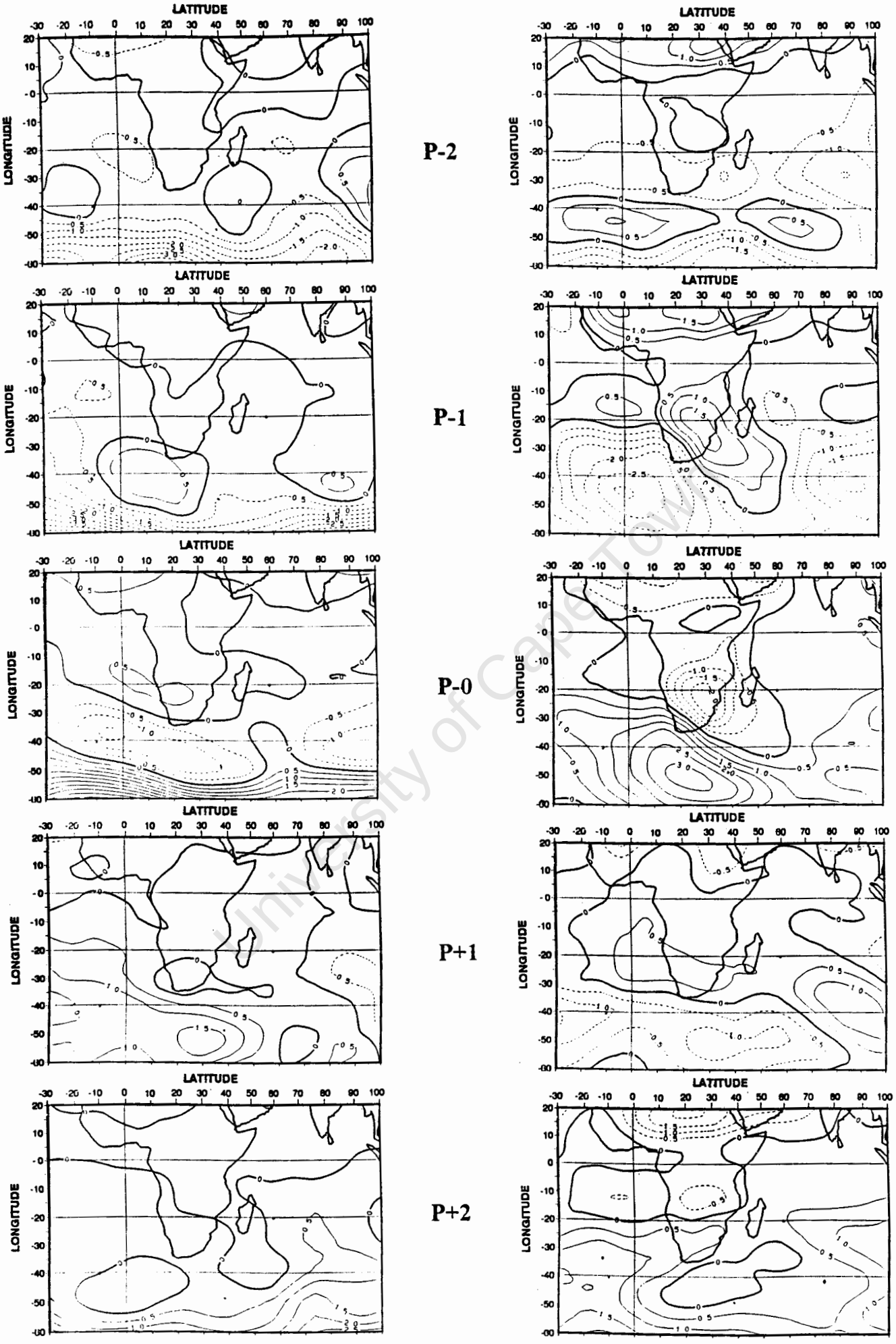

Figure 5-17a : Temperature anomalies @ 200 hPa for **P-2** to **P+2**. Contour interval is 1° C.

Figure 5-17b : Temperature anomalies @ 850 hPa for **P-2** to **P+2**. Contour interval is 1° C.

University of Cape Town

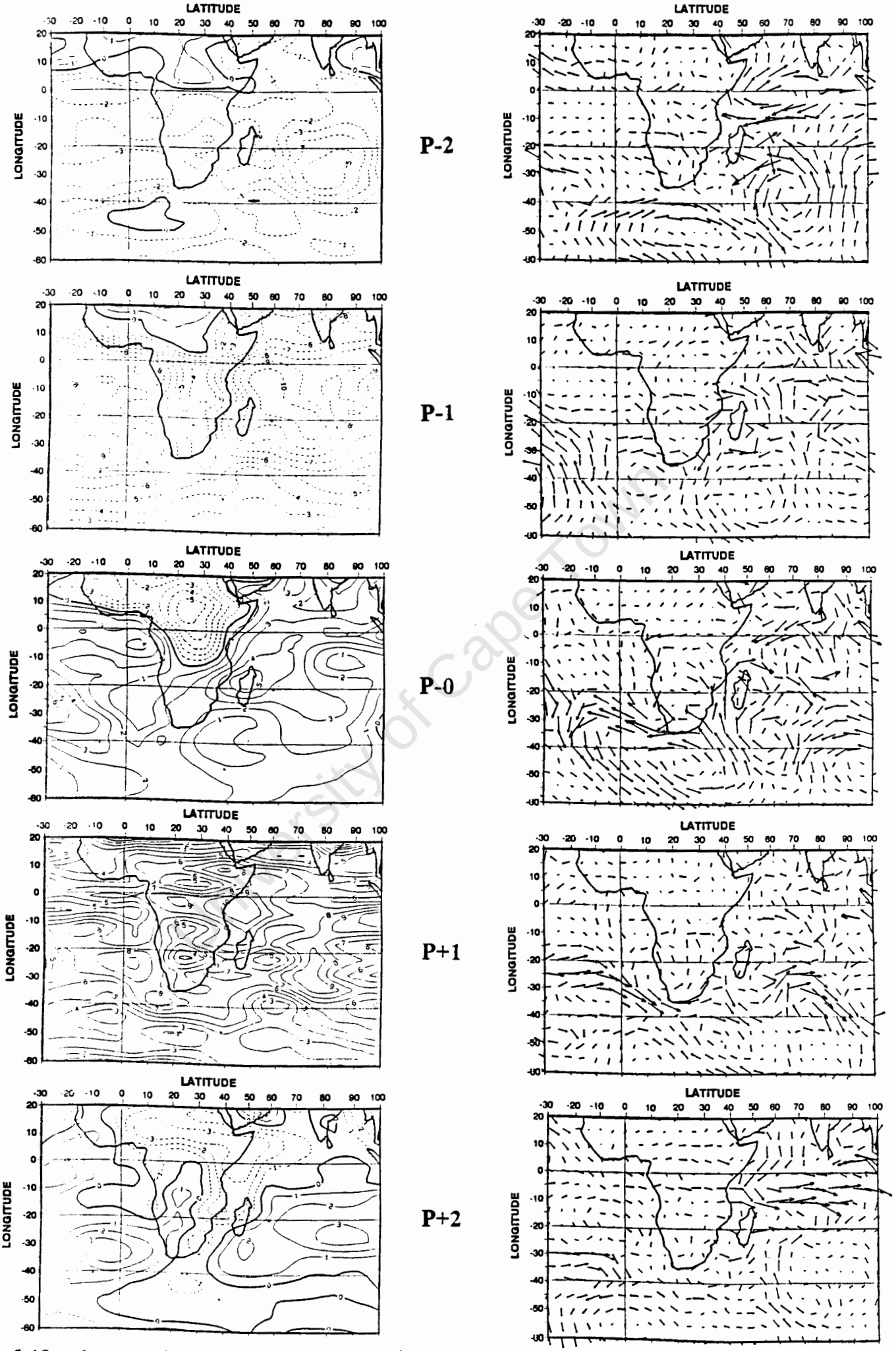

Figure 5-18a: Integrated precipitable water anomalies between the surface and 300 hPa for P-2 to P+2. Contour interval is 1 mm.

Figure 5-18b: Integrated water vapour flux anomali between the surface and 500 hPa for P-2 to P+2. Vector → = 100 g kg^{-1} m s

University of Cape Town

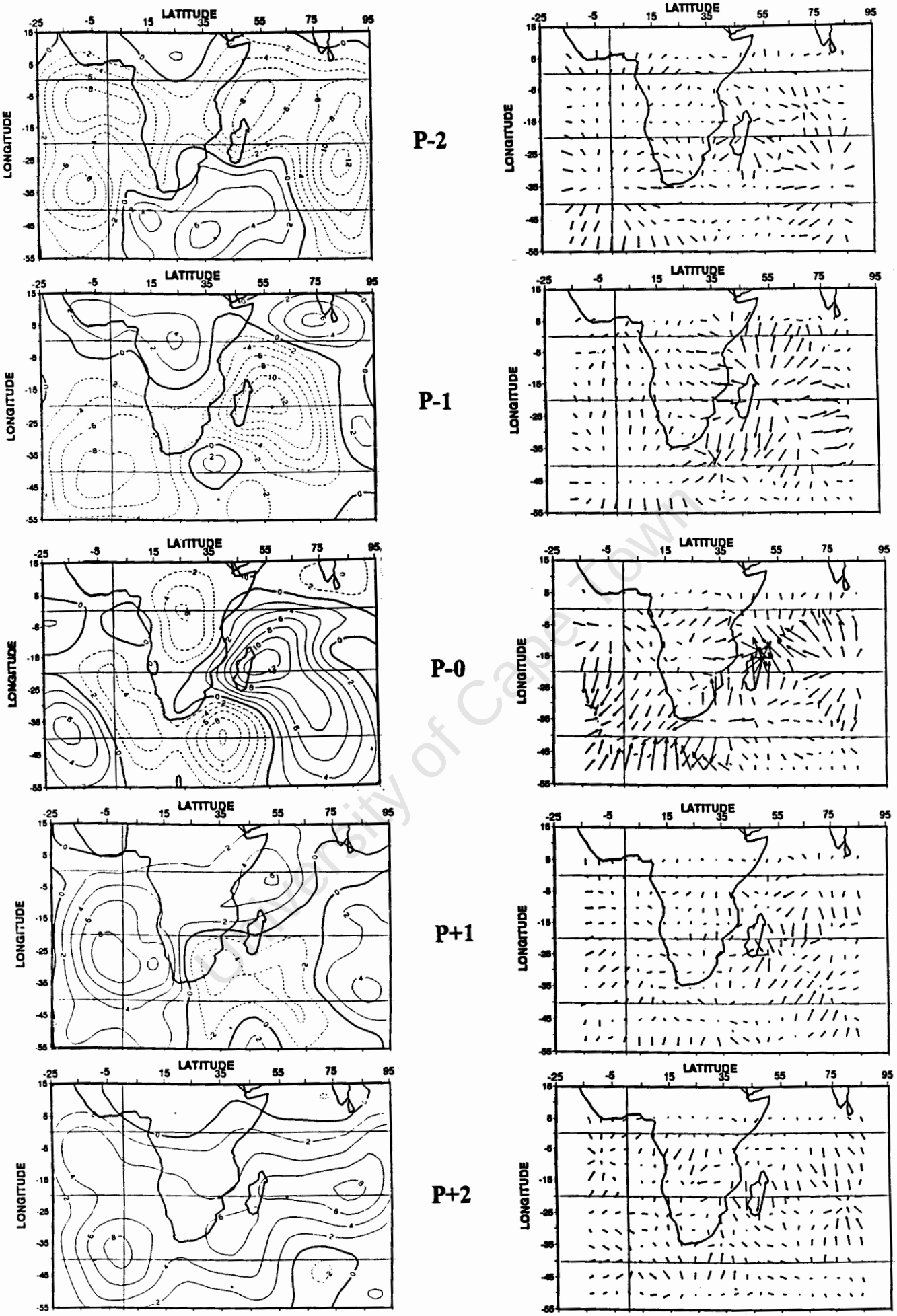

Figure 5-19a : Integrated divergent water vapour flux (χ_Q) anomalies between the surface and 500 hPa for **P-2** to **P+2**.
Contour interval is 2 x 10^8 kg s^{-1}.

Figure 5-19b : Integrated divergent water vapour flux vectors(Q_{DIV}) between the surface and 500 hPa for **P-2** to **P+2**.
Vector ⟶ = 10 kg m s^{-1}.

University of Cape Town

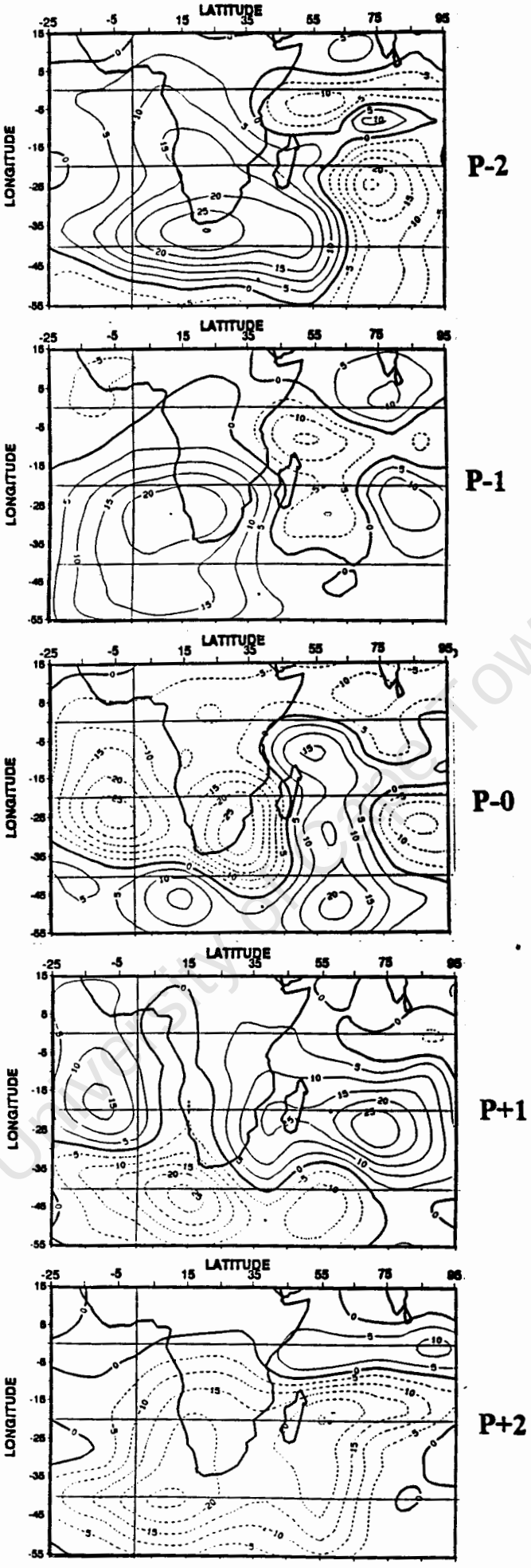

Figure 5-20 : Integrated non-divergent water vapour flux (ψ_Q) between the surface and 500 hPa for **P-2 to P+2.** Contour interval is 5 x 10^8 kg s^{-1}.

University of Cape Town

5.3 TEMPORAL TREND COMPOSITE ANALYSIS

By subtracting the mean composite field at P-2 from the mean composite field at P-1, it is possible to identify climatic indicators prior to the wet event at P-0. Should these indicators be present in a forecasting scenario at P-1, then the forecasting accuracy will be enhanced for P-0, especially the accuracy regarding the duration and intensity of wet events, since five-day forecasts have been well established in the context of South African weather forecasting. The (P-1)-(P-2) (referred to from here as P1-P2) anomaly field is therefore an excellent tool for identifying the major atmospheric processes taking place prior to a wet event over the southern African region, especially over the summer rainfall region of South Africa

5.3.1 KINEMATIC RESULTS

geopotential height

Figure 5-21a shows at P_{200} there are negative anomalies (-125 gpm) in the South Atlantic at 40° S 0° E. Another negative anomaly area exists over the southern Indian Ocean at 45° S 85° E. A positive anomaly (+75 gpm) occurs between these two negative anomaly areas at 55° S 47.5° E. Anomalies are weakly positive (+25 gpm) over southern Africa.

At P_{850} (figure 5-21b) there is similar anomaly pattern. A strong negative anomaly (-40 gpm) exists south-west of the continent, whereas a strong positive anomaly (+40 gpm) exists to the south-east. A weaker negative anomaly (-20 gpm) exists over the southern Indian Ocean at 40° S 80° E. Weak negative geopotential anomalies occur over the interior of South Africa. The distribution of the anomaly field indicates, in the progression from P-2 to P-1, the development of a westerly trough to the south west of the

University of Cape Town

continent at about Greenwich, with a ridge south-eastwards of Africa at about 47.5° E. Another trough exists further eastwards over the Indian Ocean. Geopotential heights decrease at P_{850} over South Africa, but increase at P_{200} from P-2 to P-1.

horizontal winds

The horizontal wind anomaly field is consistent with the geopotential anomalies. At P_{200} there are various cyclonic and anticyclonic anomaly centres associated with the negative and positive geopotential anomalies. Figure 5-22a shows greatly enhanced sub-tropical westerlies occur over the south-western areas of the sub-continent and adjacent ocean. Another weaker area of stronger sub-tropical westerlies occurs on the northern side of the cyclonic anomaly in the southern Indian Ocean between 20° S and 40° S. The mid-latitude westerlies are generally weaker south of 50° S. Therefore, from P-2 to P-1 the westerlies become much stronger over the southern areas of South Africa and areas to the south of the continent, especially between 30° S and 40°

The anomaly field at P850 is slightly different. The anomalies observed at P_{200} appear to be located further northwards at P850 as expected; cold lows tilt polewards, warm highs tilt equatorwards (Figure 5-22b). Westerlies are stronger over South Africa, but weaker between 40° and 50° S and between 10° W and 80° E. There is a strong cyclonic anomaly over the southern Indian Ocean at 40° S 80° E indicating that the anticyclone that was very intense at P-2, has weakened considerably by P-1. Most of the easterly trade winds in the tropical Indian Ocean south of the equator are also weaker (shown by westerly anomalies).

University of Cape Town

kinetic energy

The kinetic energy anomaly field (Figure 5-23a) confirms the strengthening of the sub-tropical westerlies at P_{200} over the southern areas of the continent as a pre-cursor ISO signal. A strong positive anomaly (+350 m^2 s^{-2}) exists south-west of Cape Town at 35° S 15° E. Another weaker positive anomaly exists over the southern Indian Ocean. The negative anomalies south of 40° S indicates that the winds in this region have weakened from P-2 to P-1. At P_{850} a band of negative anomalies exists between 30° S and 50° S over the Atlantic Ocean and the western parts of the Indian Ocean (Figure 5-23b). The core negative area (-60 m^2 s^{-2}) is centred at 45° S 50° E. The mid-latitude westerlies therefore weaken to the south of South Africa from P-2 to P-1, but are strengthened further southwards, indicating a possible polewards retreat of the westerlies near the surface, while a possible splitting of the jet-stream at the upper-levels may occur (Barclay et al, 1993), shown by the kinetic energy anomaly patterns at the upper-level.

vertical winds

Figure 5-24 shows that at P_{500} there are no great changes taking place from P-2 to P-1. Subsidence increases in the pre-cursor stage over southern Africa and this is evident from the positive anomalies (+2 x 10^{-2} Pa s^{-1}). The strongest positive anomalies occur over the south-eastern Atlantic Ocean (+4 x 10^{-2} Pa s^{-1}) at 30° W and significantly over the southern Indian Ocean in a meridional axis near 60° E. This may be a "dipole-building" phenomena. Similar axis occur in the velocity potential at P_{200}, the streamfunction field at P_{850} and the WVF field where strong northward transport exists. Negative anomalies exist over the southern parts of South Africa (-2 x 10^{-2} Pa s^{-1}) as well as over the central Indian Ocean at 80° E (-5 x 10^{-2} Pa s^{-1}).

University of Cape Town

velocity potential

Figure 5-25a shows at the upper-level, the circulation has become more convergent over the southern areas of South Africa (+25 x 10^4 m^2 s^{-2}) and to the south-east of the continent at 50° S 65° E (+75 x 10^4 m^2 s^{-2}). Strong negative anomalies (-175 x 10^4 m^2 s^{-2}) also occur over the eastern Indian Ocean indicating that divergence is increasing in this region from P-2 to P-1. Negative anomalies (divergent anomalies) of -75 x 10^4 m^2 s^{-2} also occur to the south-west of south Africa. This is the same area where increased westerly wind anomalies were observed.

The spatial distribution of velocity potential anomalies at P_{850} (Figure 5-25b) is much simpler. Divergence over the central Indian Ocean south of the equator has increased, whereas convergence has increased over Africa, especially to the south-east of South Africa (+30 x 10^4 m^2 s^{-2}) and the Atlantic Ocean (+10 x 10^4 m^2 s^{-2}). The African-Indian (meridional) dipole is obvious.

University of Cape Town

streamfunction

Figure 5-26a shows some very intense anomalies at P_{200}. Two strong cyclonic (+500 x 10^4 m^2 s^{-2}) anomalies exist, one at 27.5° S 10° W and the other at 27.5° S 82.5° E (+400 x 10^4 m^2 s^{-2}). These two anomalies indicate that the circulation in the area to the west of South Africa is becoming more cyclonic, as well as over the south-eastern Indian Ocean where sub-tropical highs reside at the surface. A strong negative (anticyclonic) anomaly exists to the south-east of South Africa (-400 x 10^4 m^2 s^{-2}).

The streamfunction anomalies at P_{850} are shown in Figure 5-26b. The circulation becomes more anticyclonic south of Madagascar, indicating a weakening cyclonic area at 40° S 55° E (-150 x 10^4 m^2 s^{-2}) from P-2 to P-1. Two positive anomaly areas exist, one over the south-eastern Atlantic

Ocean (+ 250 x 10^4 m^2 s^{-2}) at 50° S 5° E and the other over the central Indian Ocean (+175 x 10^4 m^2 s^{-2}). This indicates that in the lower atmosphere the SAA has weakened from P-2 to P-1 indicating a Rossby wave trough moving eastwards fro the Atlantic Ocean.

5.3.2 MOISTURE AND THERMODYNAMIC RESULTS

temperature

There is very little change in the temperature field at P_{200} from P-2 to P-1 (Figure 5-27a). A 1° C increase in temperature occurs south-west of South Africa as well as over the southern Indian Ocean at 45° S 80° E. Temperatures are slightly lower over southern Africa. The temperature anomaly field at P_{850} (Figure 5-27b) shows more structure. A strong negative anomaly (-4° C) occurs over the south-eastern Atlantic Ocean at 42.5° S 2.5° W. The whole Atlantic south of 25° S has become colder from P-2 to P-1, but has become warmer (+2° C) over southern Africa. Another weak negative anomaly exists over the southern Indian Ocean.

water vapour flux

The WVF anomalies over the tropical Indian Ocean are indicating a possible surge in the Indian Monsoon. This is a clear indication of the ISO being tropically initiated. Two strong cyclonic anomalies exist, one to the south-west of South Africa at 35° S 5° E and the other over the southern Indian Ocean at 40° S 80° E. Strong anomalous WVF occurs around the two cyclonic areas with anomaly values of up to 100 g kg^{-1} m s^{-1}.

precipitable water

The precipitable water field (figure 5-28b) shows that the atmosphere is drying out quite rapidly from P-2 to P-1. Very strong negative anomalies occur over

University of Cape Town

the western tropical Indian Ocean at 5° S 55° E (-9 mm) in a meridional axis. Another strong negative area lies to the south west of the continent at 40° S 0° (-6 mm). A negative anomaly area (-7 mm) exists over the west coast of Africa at 5° S. The entire area south of the equator shows a dramatic decrease in precipitable water from P-2 to P-1. The decreases in precipitable water over southern Africa are not that great (-2 mm).

divergence of water vapour flux

The WVF field over the eastern Indian Ocean has become much less convergent (Figure 5-29). Strong positive anomalies of +14 x 10^8 kg s^{-1} confirm this. The negative anomalies (-10 x 10^8 kg s^{-1}) over the western Indian Ocean, however, suggest that the WVF field has become more divergent. The tropical eastern Atlantic has also become very much more convergent (+8 x 10^9 kg s^{-1}), but further south, the opposite is true where divergence (-10 x 10^8 kg s^{-1}) has increased substantially from P-2 to P-1.

non-divergent water vapour flux

Two cyclonic (positive) anomalies exist, one in the Indian Ocean at 25° S 85°E (+9 x 10^8 kg s^{-1}), and the other to the west of South Africa at 25° S 5° W (+10 x 10^8 kg s^{-1}). These two positive anomaly regions indicate that from P-2 to P-1 the WVF field has become cyclonic in these two regions, especially over the Indian Ocean. A weak strong negative anomaly (-25 x 10^8 kg s^{-1}) region occurs between the two intense negative anomalies showing that over the south-western tropical Indian Ocean and at 37.5° S 50° E the WVF field has become more anti-cyclonic.

Chapter 6 will discuss the results of the composite analyses. Figures relating to the above results follow this section.

University of Cape Town

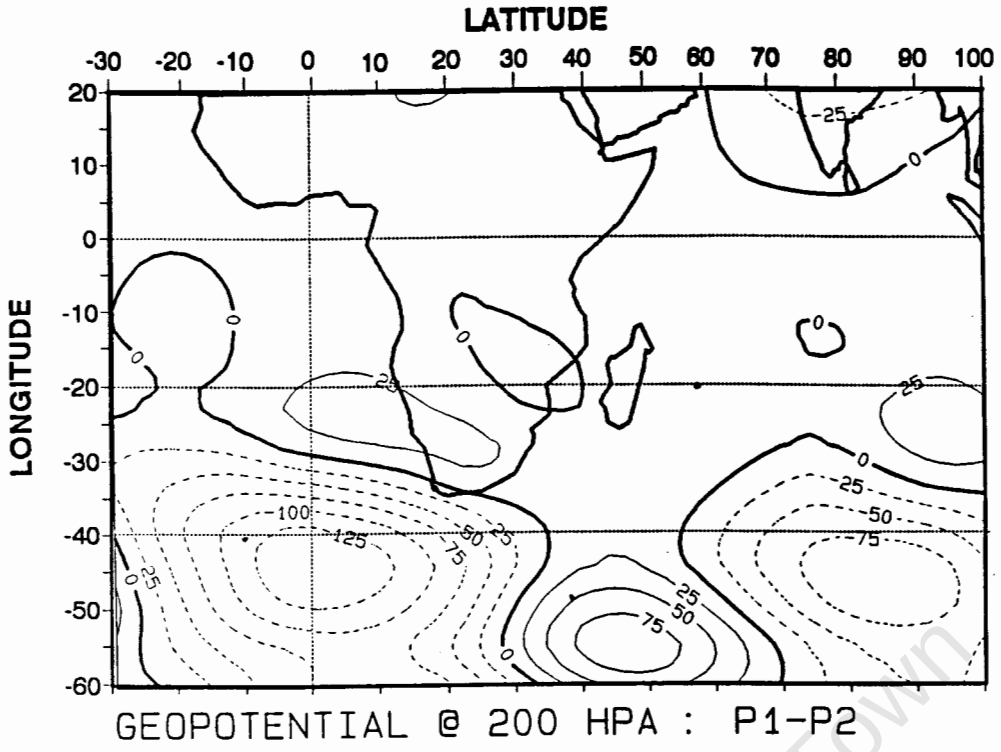

Figure 5-21a : Geopotential height anomaly @ 200 hPa for **P1-P2**.
Contour interval is 25 gpm.

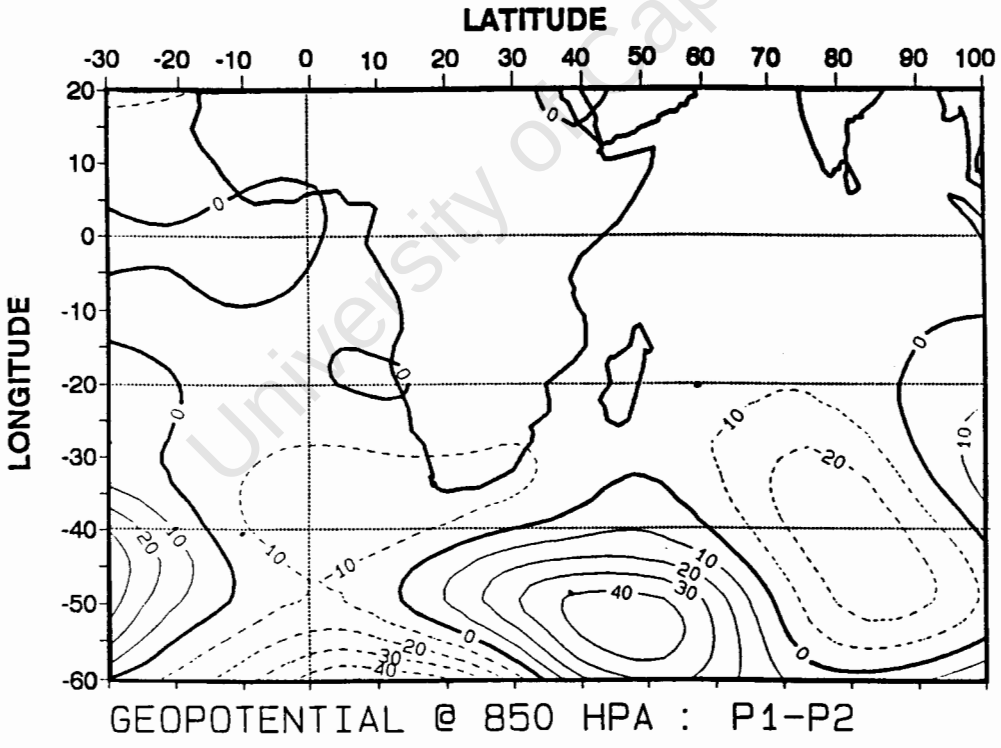

Figure 5-21b : Geopotential height anomalies @ 850 hPa for **P1-P2**.
Contour interval is 10 gpm.

University of Cape Town

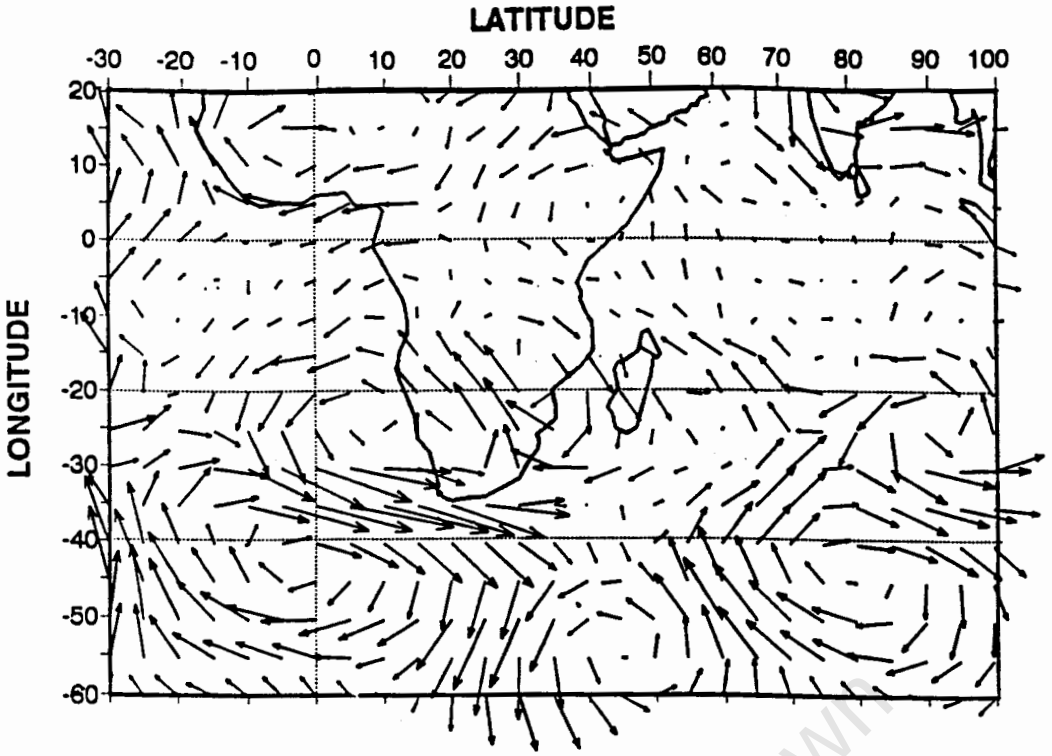

Figure 5-22a : Horizontal wind anomalies @ 200 hPa for **P1-P2**.
Vector ⟶ = 10 m s^{-1}.

University of Cape Town

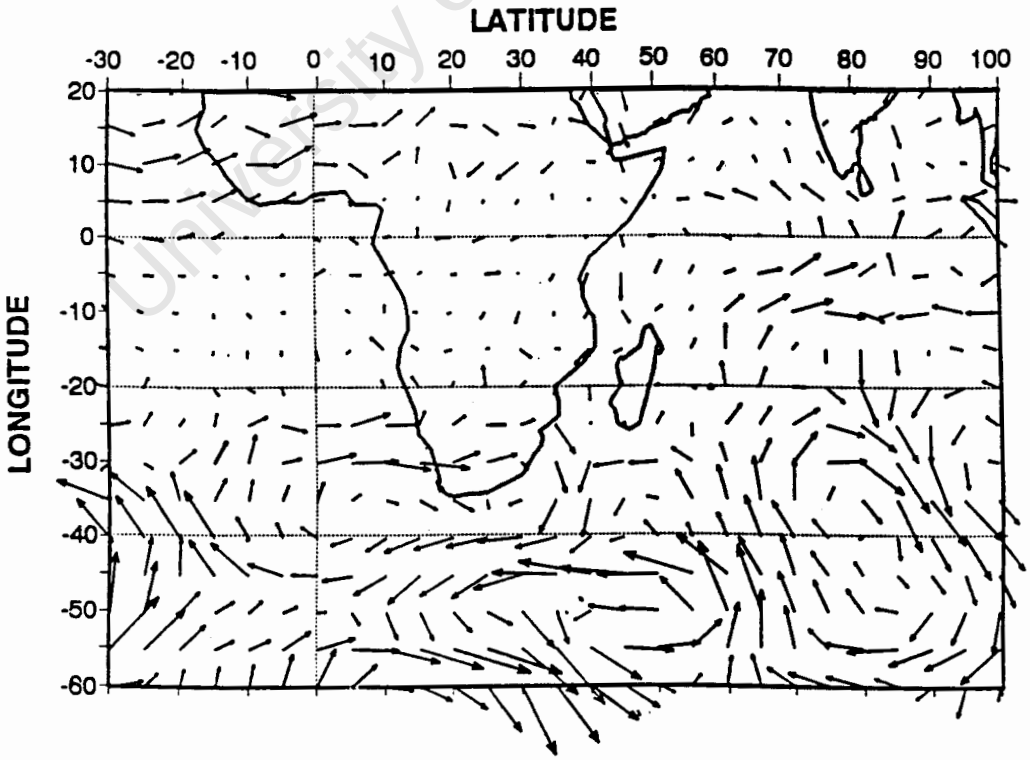

Figure 5-22b : Horizontal wind anomalies @ 850 hPa for **P1-P2**.
Vector ⟶ = 5 m s^{-1}.

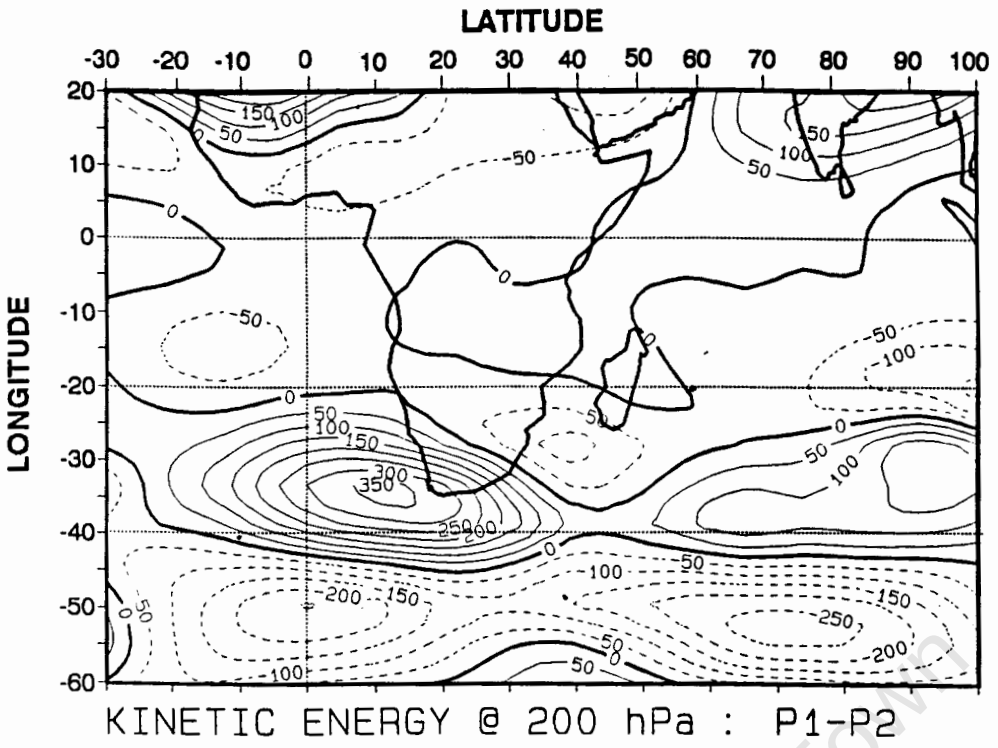

Figure 5-23a : Kinetic energy anomalies @ 200 hPa for **P1-P2.**
Contour interval is 50 $m^2 s^{-2}$.

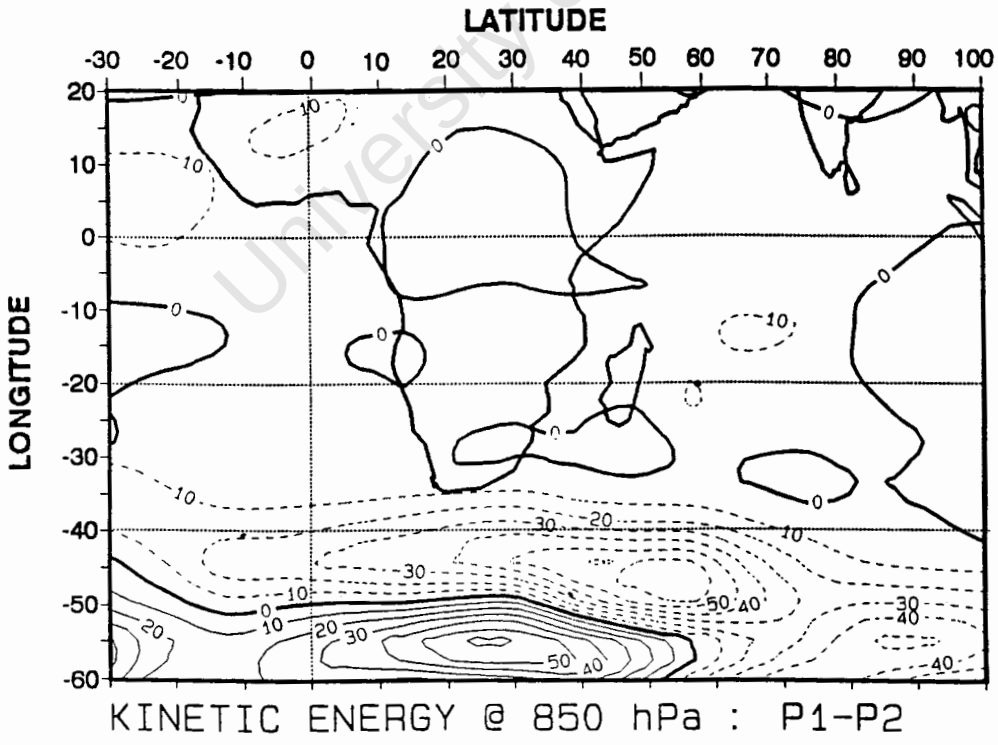

Figure 5-23b : Kinetic energy anomalies @ 850 hPa for **P1-P2.**
Contour interval is 10 $m^2 s^{-2}$.

University of Cape Town

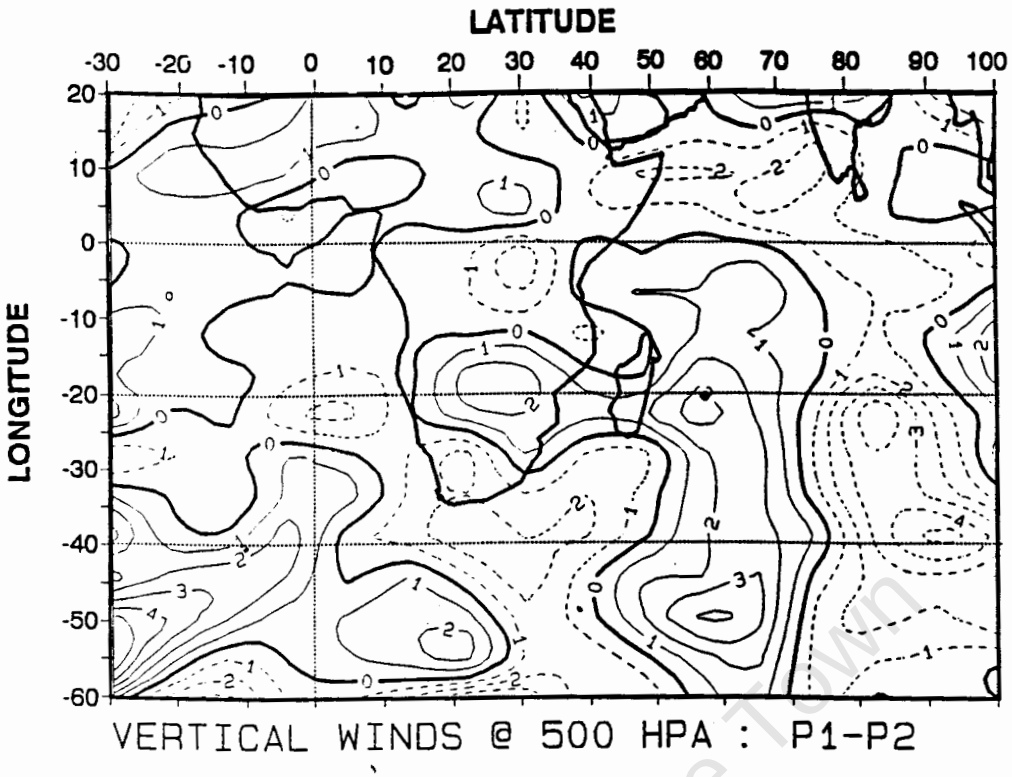

Figure 5-24 : Vertical wind anomalies @ 500 hPa for P1-P2.
Contour interval is 2 x 10^{-2} Pa s^{-1}.

University of Cape Town

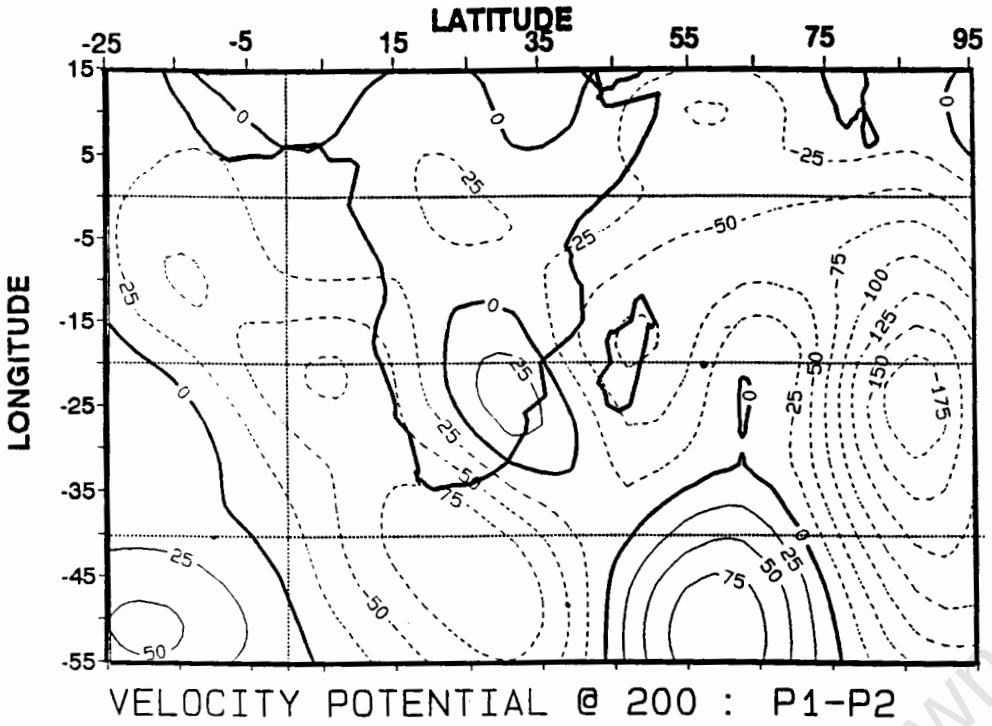

Figure 5-25a : Velocity potential (χ) anomalies @ 200 hPa for **P1-P2**.
Contour interval is 25 x10^4 m^2 s^{-1}.

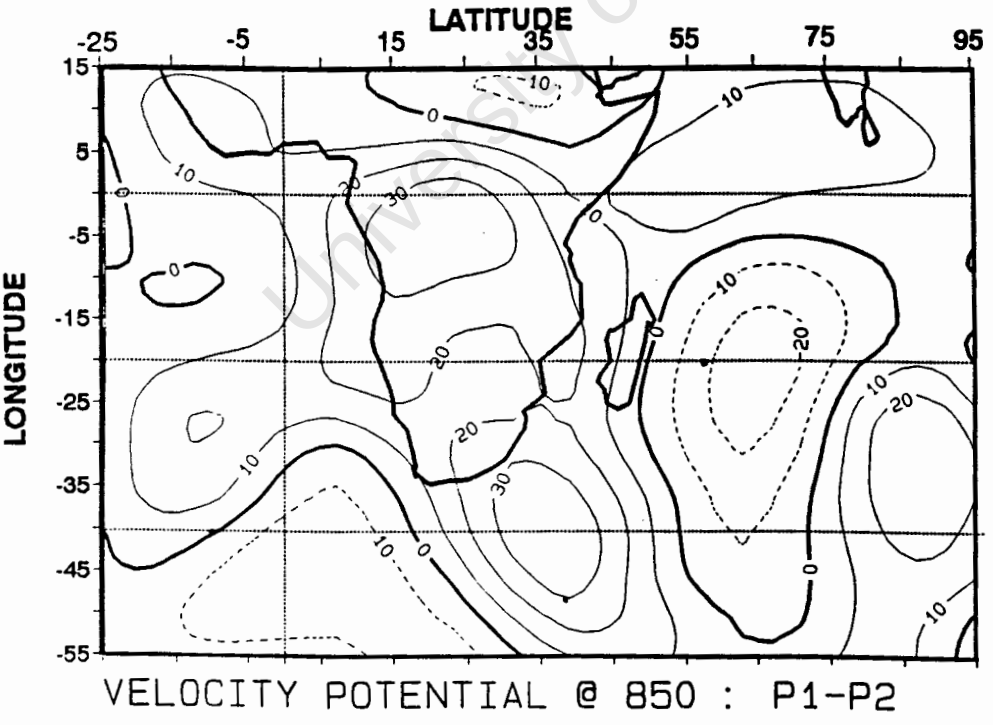

Figure 5-25b : Velocity potential (χ) anomalies @ 850 hPa for **P1-P2**.
Contour interval is 10 x10^4 m^2 s^{-1}.

University of Cape Town

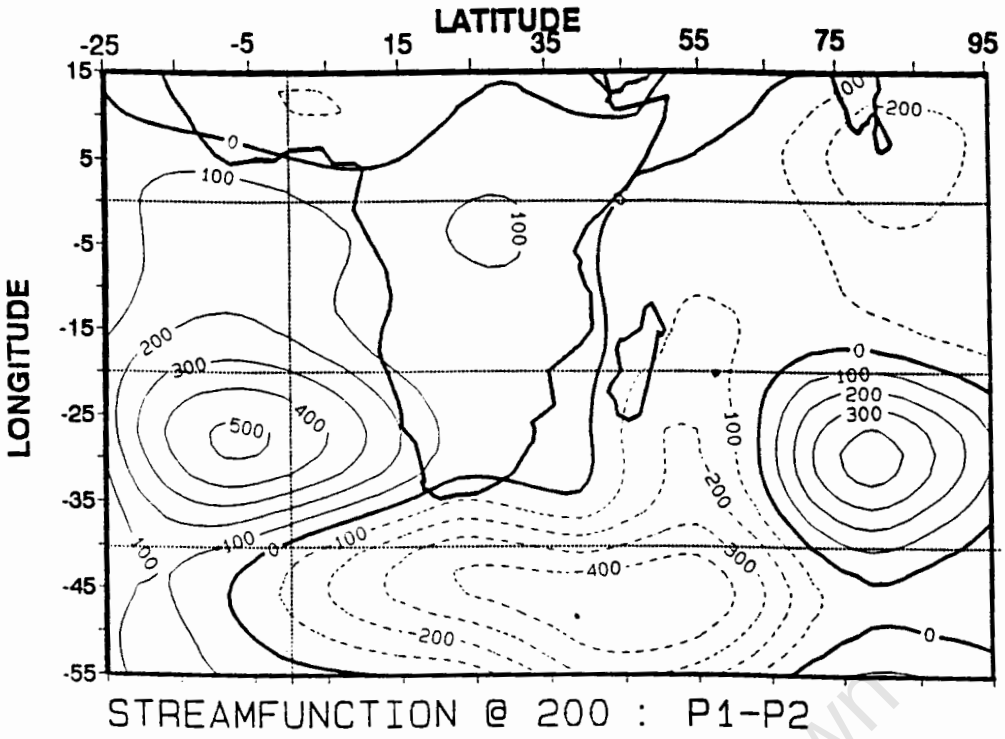

Figure 5-26a : Streamfunction (ψ) anomalies @ 200 hPa for **P1-P2**.
Contour interval is 100 x10^4 m^2 s^{-2}.

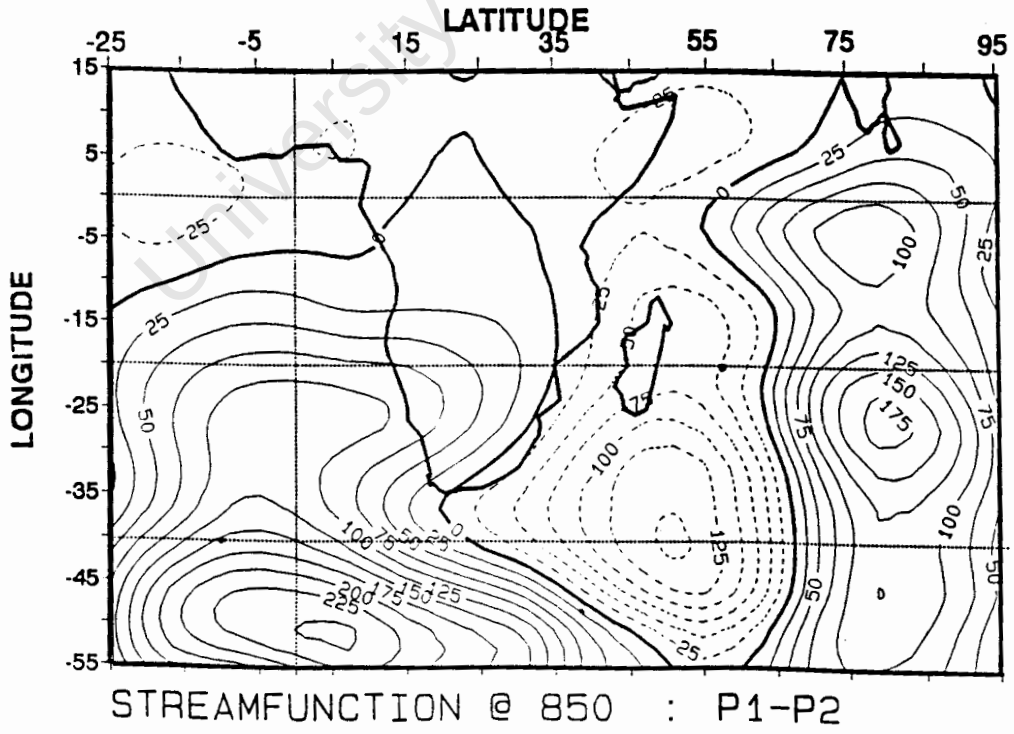

Figure 5-26b : Streamfunction (ψ) anomalies @ 850 hPa for **P1-P2**.
Contour interval is 25 x10^4 m^2 s^{-2}.

University of Cape Town

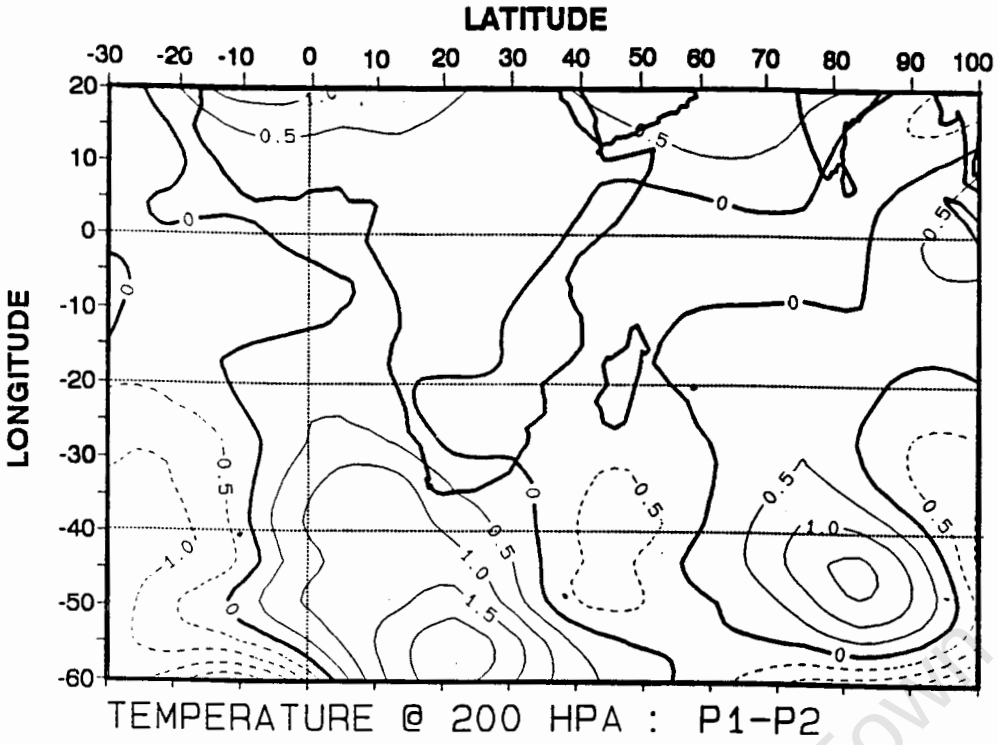

Figure 5-27a : Temperature anomalies @ 200 hPa for **P1-P2**.
Contour interval is 0.5° C.

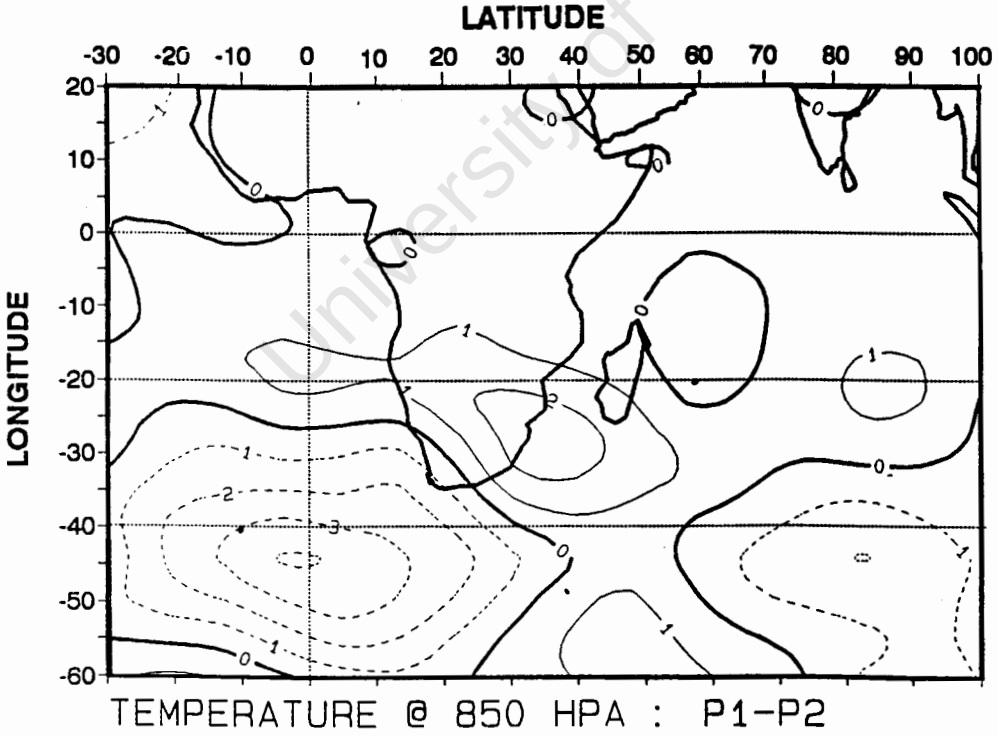

Figure 5-27b : Temperature anomalies @ 850 hPa for **P1-P2**.
Contour interval is 1° C.

University of Cape Town

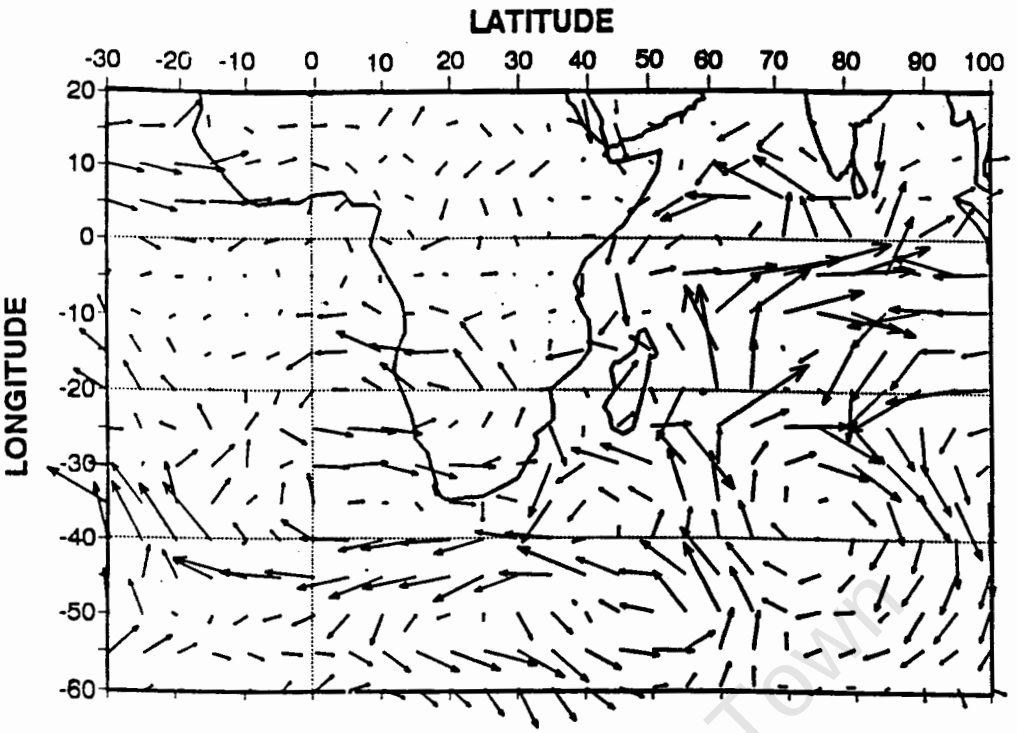

Figure 5-28a : Integrated water vapour flux anomalies between the surface and 500 hPa for **P1-P2**. Vector → = 50g kg^{-1} m s^{-1}.

University of Cape Town

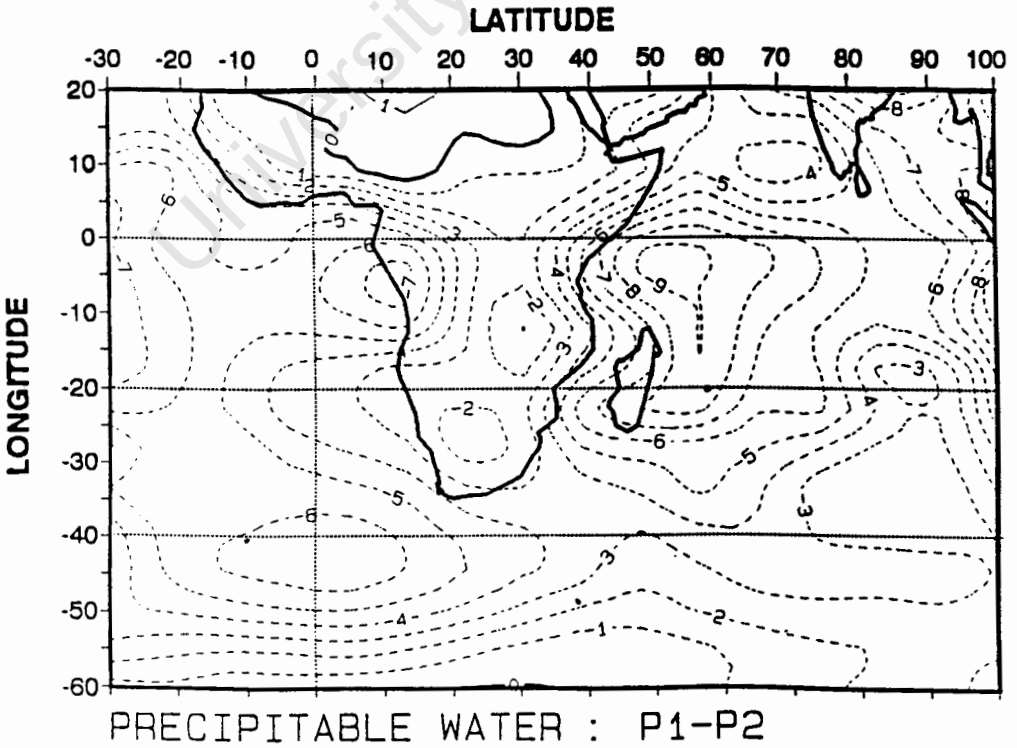

Figure 5-28b : Integrated precipitable water anomalies between the surface and 300 hPa for **P1-P2**. Contour interval is 1 mm.

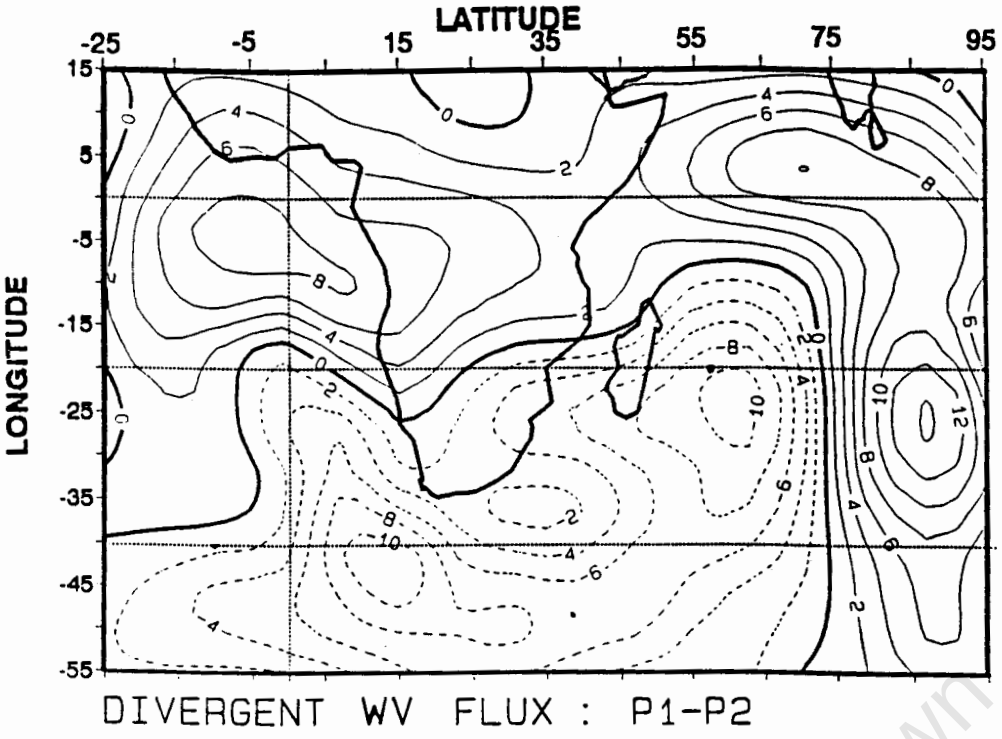

Figure 5-29 : Integrated divergent water vapour flux (χ_Q) anomalies between the surface and 500 hPa for **P1-P2.** Contour interval is 2 x 10^8 kg s^{-1}.

University of Cape Town

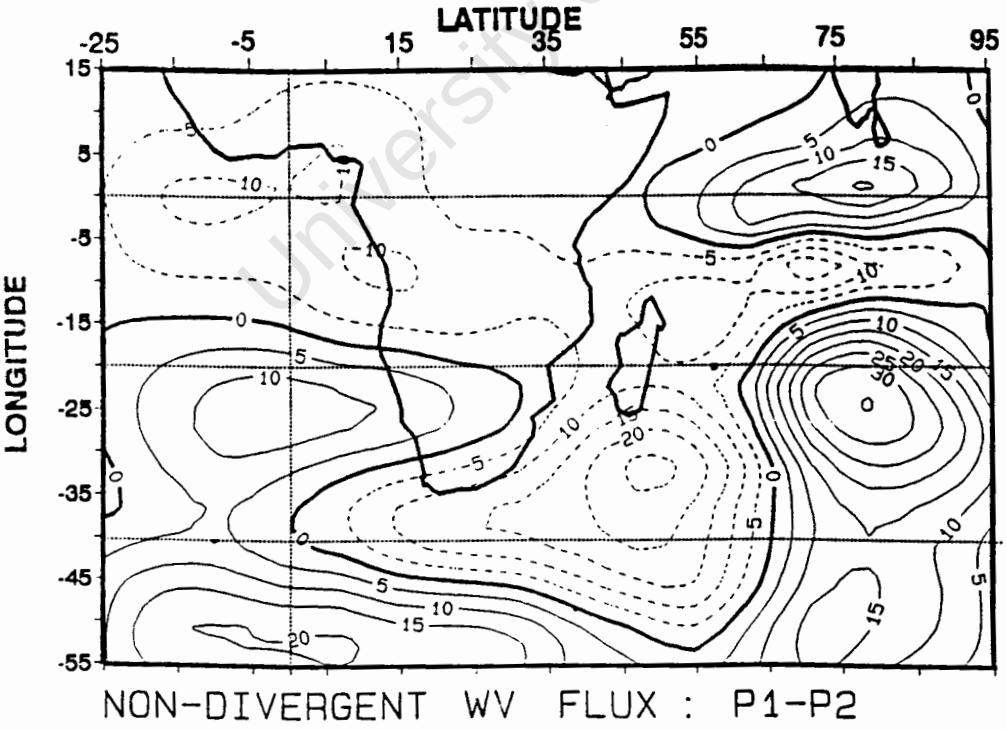

Figure 5-30 : Integrated non-divergent water vapour flux (ψ_Q) anomalies between the surface and 500 hPa for **P1-P2.** Contour interval is 5 x 10^8 kg s^{-1}.

CHAPTER 6

INTERPRETATION AND CONCLUSIONS

6.1 INTERPRETATION

A strong 20-30 day oscillation in the OLR and P-E indices is found over South Africa. This 20-30 day oscillation is also found in the other meteorological parameters as shown by the Hovmöller analysis. The 20-30 day ISO is evident in Figures 6-1a and 6-1b.

6.1.1 HÖVMOLLER ANALYSES

The Hovmöller plot analysis has shown that the period of most of the eastward propagating anomalies at 10° S is between 40-60 days, which can be attributed to the well-established MJO operating in the tropics at frequencies of between 40-60 days. However, at 40° S, the frequency of most of the eastward transiting anomalies is less than 30 days, although there are instances when they are longer. This result is also important since it has been shown that the 20-30 day ISO is most dominant over South Africa. This therefore implies that the extra-tropical influence is important in modulating the climate over South Africa. It can be inferred that the MJO is indirectly modulating the climate over South Africa through extra-tropical interaction which will be discussed later in section 6.1.2.

However, since the MJO is propagated along and equatorwards of the ITCZ, it is possible that the effects of the MJO will be felt more directly over the summer

University of Cape Town

rainfall region of South Africa when the ITCZ is particularly close to or over South Africa and when the westerly wind belt is displaced polewards.

It is important to note, that in the case histories investigated, *at least* 40% of the total systems accounted for at 10° S and 23% at 40° S in chapter 4 are *not* propagating features. This implies that the subtropical region of South Africa is influenced by a variety of different modes as described in chapter 4. Eastwards propagating systems play the most important role, hence the interaction of the tropical MJO and the Rossby wave trains of the extra-tropics play an important role in modulating the 20-30 ISO over south Africa. However, the effects of the standing wave and "flip-flop" patterns cannot be ignored.

It was shown in chapter 3 that the length of ISO operating during drier years was *longer* (45-60 days), whereas during the wet years the length of ISO's operating over the region were *shorter.*

Initially it was felt that the 20-30 day ISO may be the result of the extra-tropical westerly wind belt modulating the weather over southern Africa. The findings of Hayashi and Golder (1992) conclude that a 25 day ISO also exists in the tropics and is independent of the longer MJO. However, the longitude-time analysis has shown that the dominant period of oscillations operating in the extratropics is between 20-30 days. Section 6.1.2 will show the interactions between the tropics and extratropics in the composite anomaly analysis.

Wang and Rui (1990) have shown that in the temporal evolution of ISO's in the tropical regions, that east Africa is the initiation area of these ISO's. The Hövmoller plots confirm this in the u-wind component at 850 hPa, vertical wind

University of Cape Town

component at 500 hPa and the velocity potential at 200 hPa of five summers between 1987 and 1992.

6.1.2 COMPOSITES

The mean geopotential composite fields at both levels change very little in the progression from P-2 to P+2. However, there are subtle shifts in the positions in the circulation field. Geopotential heights drop at P-0 indicating the presence of a trough at P_{200} and the results show that at P-0 the ridge that was dominant at the upper-level at P-2 and P-1 over southern Africa has been replaced by a trough over the south-eastern parts of South Africa. At the lower-level, geopotential heights have increased at P-0 over southern Africa. During the ISO the SAA migrates polewards and eastwards closer to South Africa from P-2 to P-0 and then migrates northwards over the south-east Atlantic Ocean from P-0 to P+2. The SIA also shows a tendency to migrate eastwards during the pre-cursor stage (P-2 and P-1), but tends to decrease in intensity at P+1 and finally disappears at P+2 (not shown). The SIA is at its strongest at P-2.

University of Cape Town

It therefore appears that mid-latitude forcing causes the eastward and southward migration of the subtropical anticyclones during the dry pre-cursor stage with the accompanying eastward displacement of the surface trough over southern Africa. The upper-level trough is positioned over south-eastern Africa at P-0 favouring divergence to the east of the trough. At P-0, the SIA is located closer to the sub-continent, but this is temporary, since at P+1 it has shifted eastwards.

The geopotential anomaly fields at both levels have shown that strong SAA ridging takes place during P-0 and is preceded at P-1 by the eastward movement of a

Rossby wave trough from the Atlantic Ocean. This eastward ridging is evident in the horizontal wind field anomalies from P-1 to P-0. Lyons (1991) has shown this SAA ridging process to be important since the extra-tropical trough propagating eastwards interacts with the Tropical Upper Tropospheric Trough (TUTT) over the Mozambique Channel. The TUTT is strengthened by this interaction and it intensifies. A cyclonic anomaly exists in the horizontal wind anomalies and a negative anomaly in the geopotential height anomalies at P-1 over the Mozambique Channel and moves south eastwards during P-0. The main interaction between the TUTT and the Rossby wave trough occurs at P-0 with the cyclonic anomaly at 35° S 60° E.

The features discussed above are also seen in the mean horizontal wind field composites. A distinct feature of the upper-level wind fields was the jet at the upper-level emanating at the equator at 15° W flowing south-eastwards over southern Africa. It appears that the northern hemisphere subtropical jet stream splits southwards and weakens from P-2 to P-0, but then strengthens towards P+2. The upper-level flow over South Africa backs from north-westerly to westerly at P-0. This jet may be affecting the anticyclone over southern Africa in the midtroposphere at 500 hPa, although this has not been confirmed. At P-0, when the jet is virtually non-existent, the geopotential heights are lower over southern Africa. This north-westerly jet axis is strongest 5 days prior to the wet event which may be useful for forecasting purposes.

Low-level northerly flow over the interior of South Africa is enhanced at P-0 which has intensified advection of available moisture into this region. The Hövmoller analysis showed that during P-0 the v-component shows northerly anomalies in the tropics at 10° S and southerly anomalies at 40° S. The composites

University of Cape Town

also show that at P-0 stronger south-easterly flow from the southern Mozambique Channel occurs. This WVF signal is secondary to the one observed at P-2 in the central-west Indian Ocean. The anomaly field shows strong south-easterly anomalies into the southern African region from flow around the SIA. This easterly flow curves south-westwards to the south of Madagascar and then north-westwards over the eastern half of South Africa. The non-divergent (streamfunction) WVF field at P-0 confirms this south-east flow into South Africa. This flow is also shown as a strong anomaly in the non-divergent anomaly field at P-0.

Another feature in the precipitable water field is the large-scale negative anomalies in the pre-cursor stage, yet after the wet event (P-0) there are still large-scale positive anomalies. PW values are at their highest at P+1 indicating a surplus of precipitable water in the atmosphere after the wet-event. Individual analysis of the rainfall index shows that while very little rain falls during P-1, rainfall still occurs in the early stage of P+1. However, P+1 dries out quickly as the westerlies encroach northwards. The circulation is thus reverting back to the pre-cursor stage where drier conditions prevail.

University of Cape Town

Cheng and Tzeng (1989) have shown that positive (negative) precipitable water anomalies forced by the convergent (divergent) centre of the potential function of water vapour transport (χ_Q) anomalies couple with the divergent (convergent) centre in the upper-level divergent circulation anomalies.

Here the χ_Q field also shows a very strong convergent area to the north-east of Madagascar where the greatest positive PW anomaly occurs. This very strong convergent area extends south-westwards into southern Africa, where negative

divergent anomalies also occur. It appears that at P-0, conditions become very much more favourable for convection over South Africa because this WVF convergence is located further polewards over the Indian Ocean coupled with a poleward displacement of the westerly wind belt. The dramatic enhanced WVF convergence increases the precipitable water over South Africa by up to 8 mm from P-1 to P+1. The atmosphere remains anomalously moist at P+1, but divergence in the upper-levels over South Africa decreases, (shown by positive velocity potential anomalies), as does the WVF convergence. The convergent area in the χ_Q field migrates north-eastward towards the maritime continent.

Park and Schubert (1992) have found that OLR anomalies associated with zonal-wind fluctuations are characterised by eastward propagation of ISO's over the Indian Ocean and the western Pacific and *standing* oscillation over the tropical Atlantic. They found that the standing oscillation is the dominant component of the Atlantic OLR variability.

The mean velocity potential field at both upper and lower levels has shown the existence of a dipole between the Atlantic and East Africa. At the upper levels convergence exists over the south-east Atlantic Ocean while divergence exists over eastern Africa and the western Indian Ocean. This pattern is dominant throughout the composite progression from P-2 to P+2, but there is a definite see-saw effect as the velocity potential field over the south-east Atlantic Ocean *weakens* towards P-0 and at the same time the divergence over the western Indian Ocean and east Africa *intensifies*.

This pattern suggests a standing wave nature in the Atlantic Ocean, with initiation of ISO's propagating eastwards out of the Indian Ocean from P-0 and subsequent

University of Cape Town

- strong low level westerly vector anomalies between the equator and 10° S and 70° E to 90° E over the Indian Ocean which is a clear indication of tropical initiation;
- very negative PW anomalies north-east of Madagascar and over west Africa;

Figure 6-2a and 6-2b illustrates the last two signals mentioned above.

6.1.3 CONCEPTUAL MODELS

Before a conceptual model is proposed it is necessary to re-visit the most important dynamic processes taking place in the temporal progression from P-2 to P+2. Since the greatest changes in the temporal progression take place at P-1 (pre-cursor stage) and P-0 (wet event) dynamic processes associated with them will be discussed in more detail.

University of Cape Town

pre-cursor phase

Figure 6-3 shows the vertically integrated WVF field anomalies. At P-2 (pre-cursor stage, Figure 6-3 a) strong easterly vector anomalies are seen over the tropical Indian Ocean between the equator and 10° S between 40° and 80° E. This represents the monsoon "flip" stage. This is also seen in horizontal wind field anomalies at 850 hPa to a lesser degree (not shown).

During P-1 (Figure 6-4a) very strong negative PW anomalies (-10 mm) exist north-east of Madagascar with weaker negative anomalies over southern Africa. Tropical Africa north of the equator is the only region showing positive anomalies. Strong negative anomalies also exist over the south-east Atlantic Ocean (-9 mm). This is consistent with the divergent WVF field where strong divergence is noted east of

Madagascar and south-west of South Africa in the south-east Atlantic Ocean (Figure 6-5a).

Figure 6-6a shows the vertical wind anomaly field at P-1. Subsidence is evident over the western Indian Ocean, Madagascar and most of southern Africa except the south-western tip of Africa. This is consistent with the divergent WVF field (Figure 6-5a) and the velocity potential fields (not shown).

Figure 6-7a shows that P-1 strong cyclonic activity exists over the south-western half of the sub-continent in the non-divergent WVF field. The horizontal wind field at P-1 (Figure 6-8a) shows a Rossby wave trough to the south-west of South Africa which is consistent with the cyclonic anomaly noted in the non-divergent WVF field. P-1 signals the advent of strong SAA ridging at 850 hPa and this is evident over the south-east Atlantic between Greenwich and 30° W (Figure 6-9a).

To summarise the pre-cursor stage, a Rossby wave trough is situated to the south-west of South Africa with strong SAA ridging evident behind the trough at the lower levels. The non-divergent field shows strong cyclonic activity to the south-west of South Africa and anticyclonic activity over the western Indian Ocean at 55° E in a meridional axis. This same region shows strong divergence of the WVF field and very strong negative precipitable water anomalies exist there too.

University of Cape Town

wet event phase

At P-0 (wet event) a strong anticyclonic region exists to the south of South Africa (Figure 6-3 b, the "A" denotes anticyclonic activity and the "C" cyclonic activity). A cyclonic vortex exists at 35° S 60° E to the south east of Madagascar which is consistent with the findings of Lyons (1991). The WVF field also shows cyclonic

activity over southern Africa. Figure 6-4b illustrates how precipitable water has increased dramatically over most of the region, especially over Madagascar. A strong negative PW anomaly exists over tropical Africa. It has taken about 10 days from the time that the strong easterly jet noted at P-2 in the zone between the equator and 10° S over the central Indian Ocean for the high water vapour concentration (as seen by the high PW anomalies) to be advected around Madagascar and into southern Africa.

The divergent WVF anomaly field (Figure 6-5b) shows the convergence of this water vapour very clearly with a strong positive anomaly east of Madagascar stretching along a SW-NE axis into South Africa. Figure 6-6b shows how uplift has intensified dramatically over southern Africa with the greatest uplift taking place north of South Africa over Zimbabwe. Strong subsidence is evident to the south of South Africa where the SAA is ridging south of the country.

Figure 6-7 shows a strong anticyclonic (negative) anomaly over the southern parts of South Africa and the south-east Atlantic Ocean, indicating strong SAA ridging to the south of the country. A cyclonic anomaly exists in a meridional axis over the western Indian Ocean at 60° E where at P-1 an anticyclonic meridional anomaly axis was observed. The P-0 non-divergent anonaly field is almost the reversed pattern found at P-1.

Figures 6-8b and 6-9b show that P-0 a strong anticyclonic area exists to the south of South Africa indicating SAA ridging to the south of the sub-continent. A cyclonic vortex exists at 35° S 60° E at the upper level which is probably the TUTT (shown by Lyons, 1991) which has merged with the eastward moving extra-tropical Rossby wave seen distinctly at P-1. The lower level wind field anomalies

University of Cape Town

show a wide cyclonic area stretching from southern Africa polewards of 10° S to a centre at 30° S 60° E. This cyclonic area is the lower level expression of the TUTT. Strong anomalous south-easterly winds occur over the south-eastern half of South Africa.

To summarise the wet event over southern Africa it has been shown that a dominant feature at P-0 is the SAA ridging south of the South Africa advecting moist air from south of Madagascar where water vapour has been converged by the circulation. The convergence of water vapour over south-western Indian Ocean from P-2 to P-0 therefore acts as a source for moisture and instability over South Africa. Figure 6-3 b shows that P-0 water vapour is advected north-westwards into South Africa from the southern Mozambique Channel over the warm Agulhas Current.

post-wet phase

Figure 6-3 c shows a clear pulse signal in the monsoon which completes the seesaw phase with strong westerly WVF vectors between the equator and 10° S, 40° E and 90° E. Figures 6-10a and 6-10b illustrates the pre-cursor (P-1) and wet phases schematically. Anticyclonic areas are denoted by "**A**" and cyclonic areas by "**C**". The cross-hatched area is the zone of highest precipitable water and widespread convergence of the water vapour flux field.

University of Cape Town

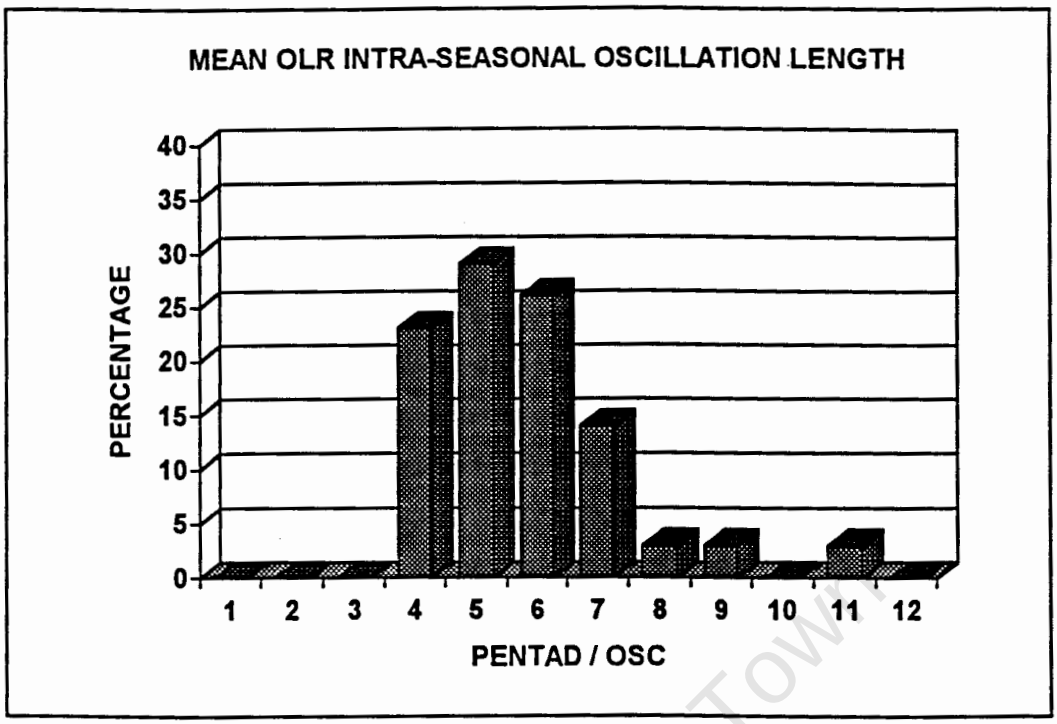

Figure 6-1a : Mean OLR ISO length shown as pentads per oscillation.

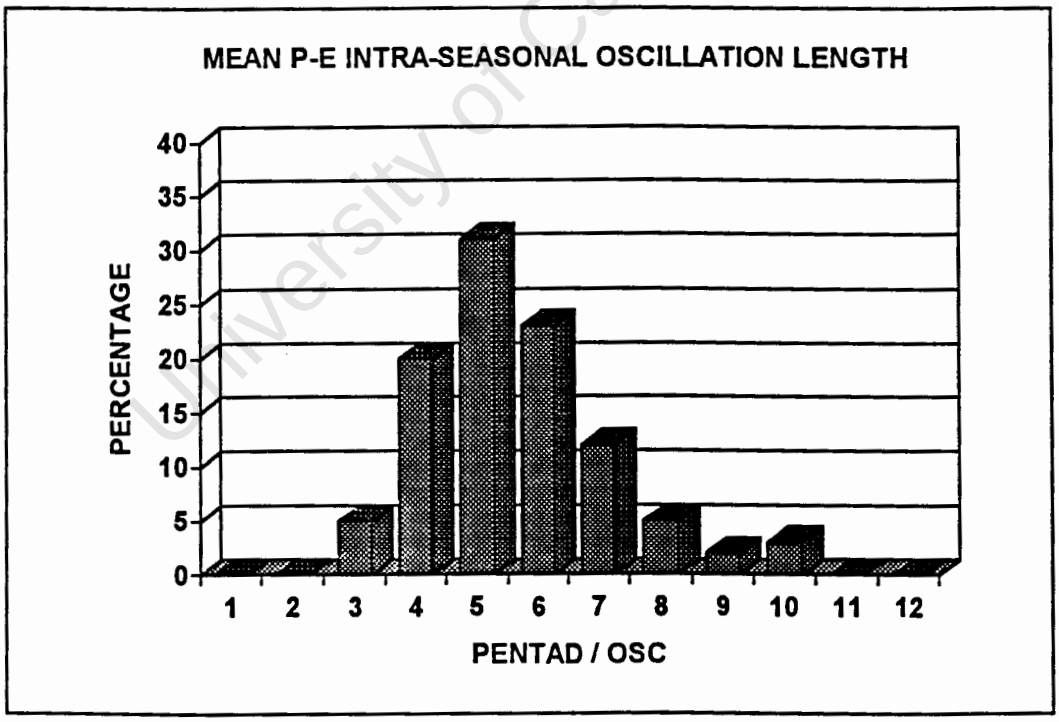

Figure 6-1b : Mean P-E ISO length shown as pentads per oscillation.

University of Cape Town

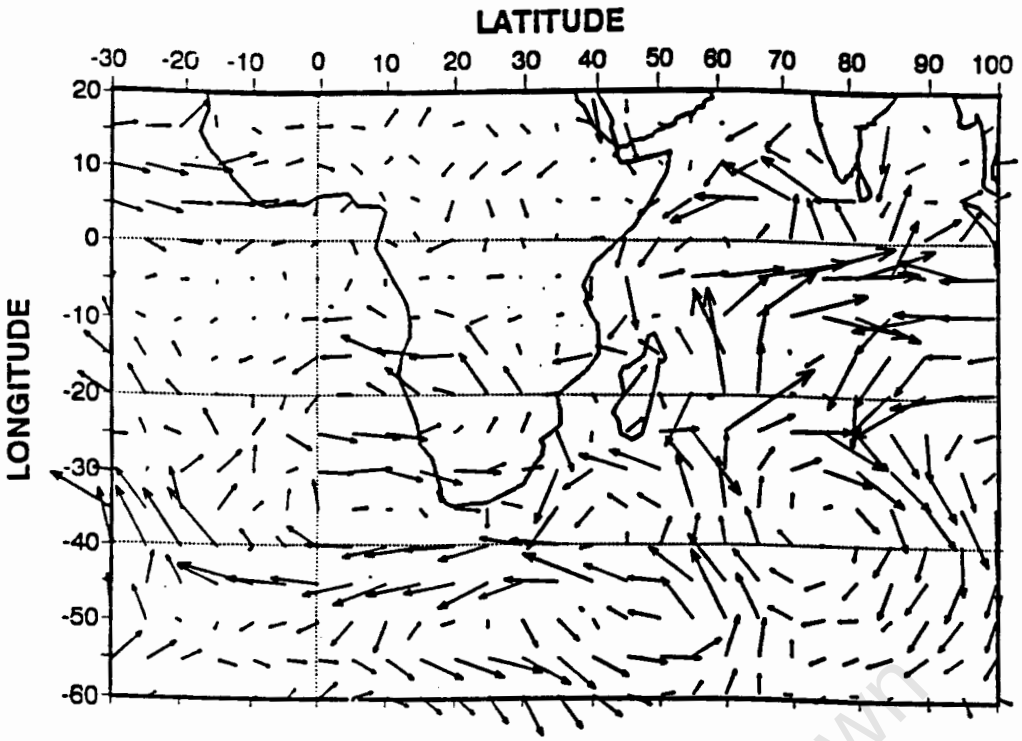

Figure 6-2a : Integrated water vapour flux anomalies between the surface and 500 hPa for **P1-P2** (as in Figure 5-28a). Vector ⟶ = 50 g kg^{-1} m s^{-1}.

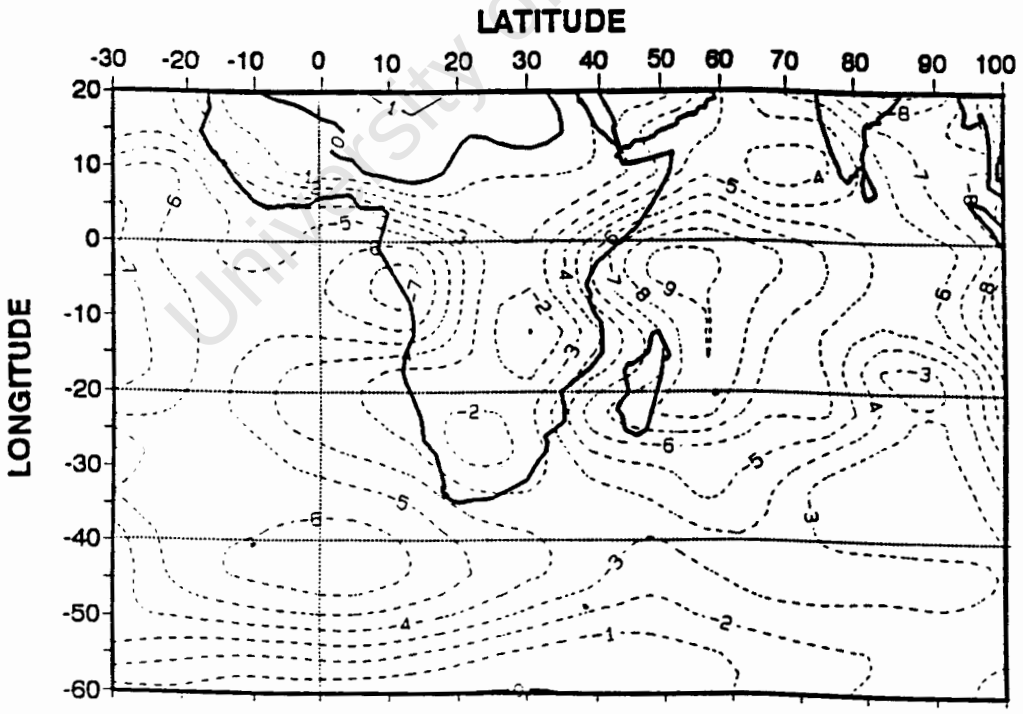

Figure 6-2b : Integrated precipitable water anomalies between the surface and 300 hPa for **P1-P2** (as in Figure 5-28b). Contour interval = 1 mm.

University of Cape Town

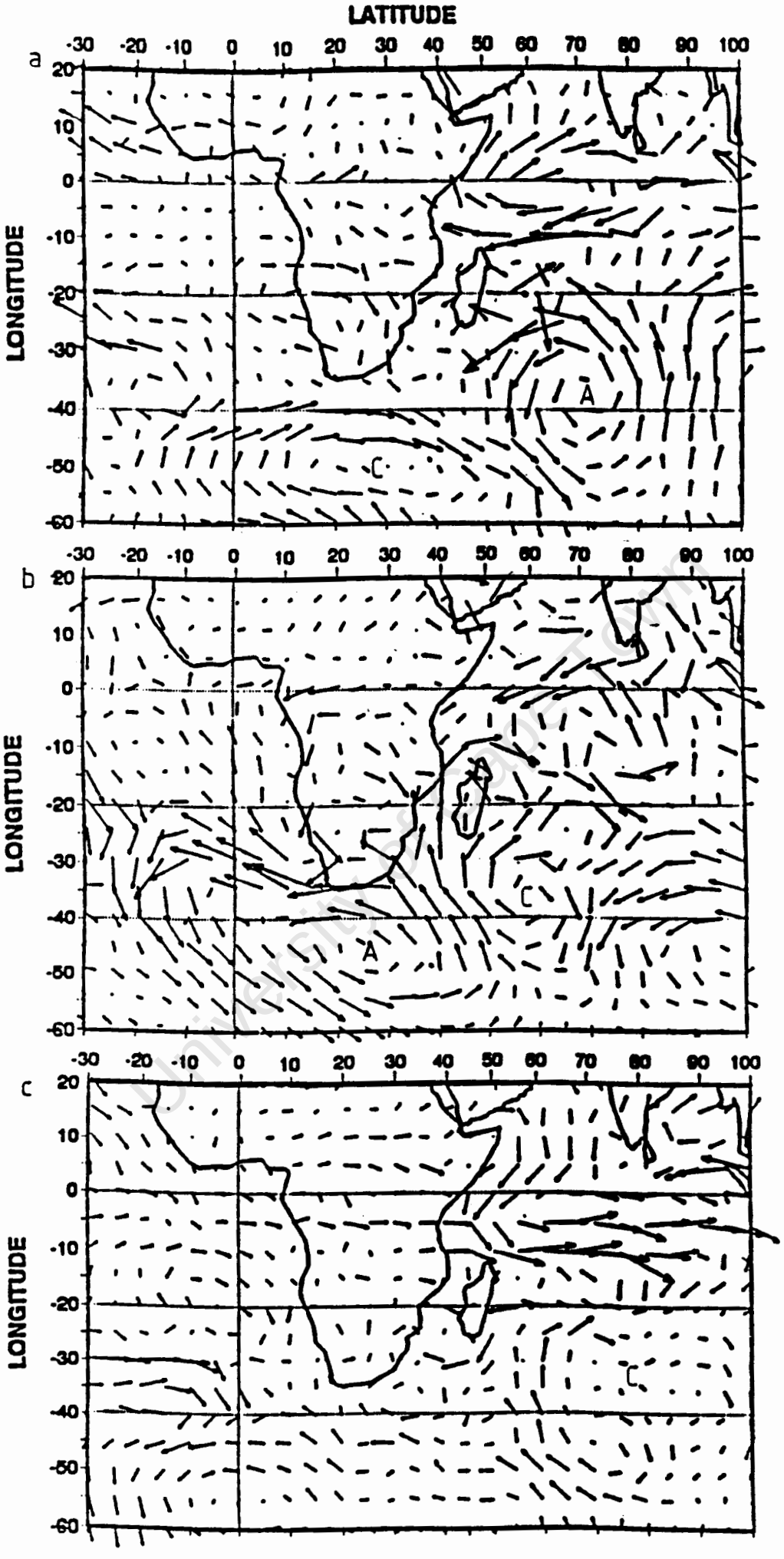

Figure 6-3 : Integrated water vapour flux anomalies between the surface and 500 hPa for **P-2 (a), P-0 (b)** and **P+2** (c) (as in Figure 5-18b). Vector ⟶ = **50 g kg^{-1} m s^{-1}**.

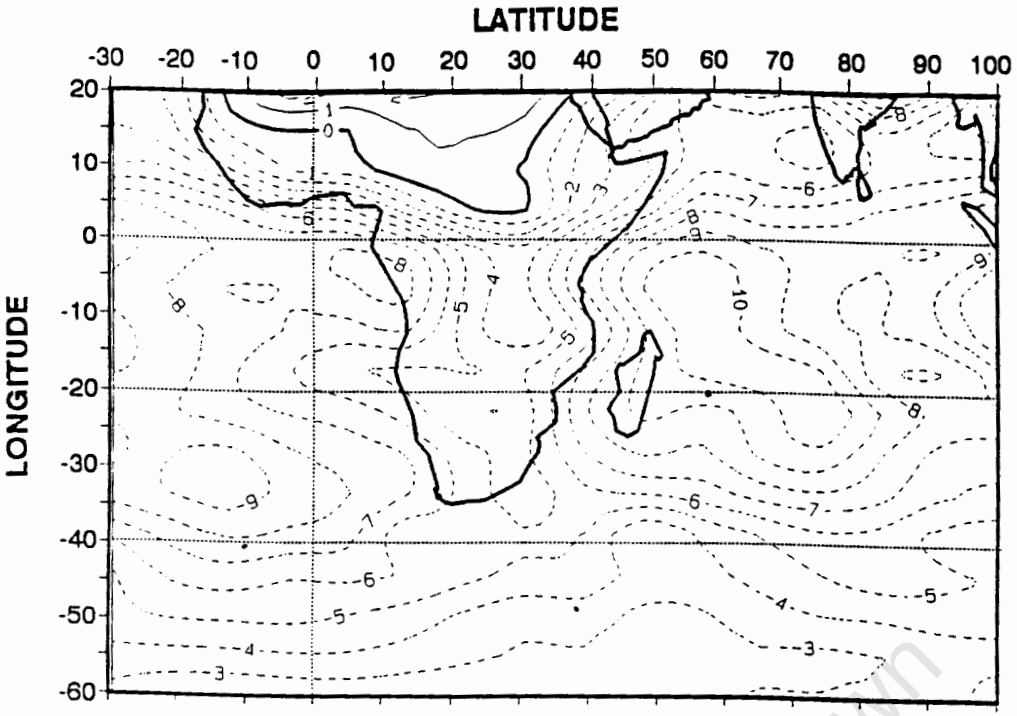

Figure 6-4a: Integrated precipitable water anomalies between the surface and 300 hPa for P-1(as in Figure 5-18a). Contour interval is 1mm.

University of Cape Town

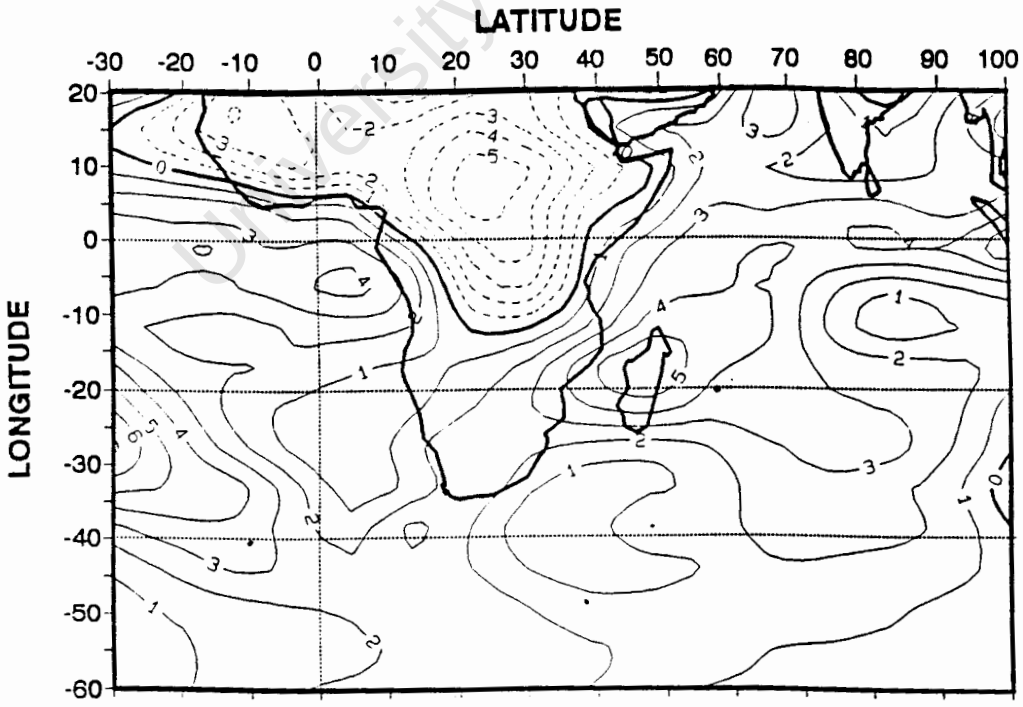

Figure 6-4b: Integrated precipitable water anomalies between the surface and 300 hPa for P-0.(as in Figure 5-18a). Contour interval is 1mm.

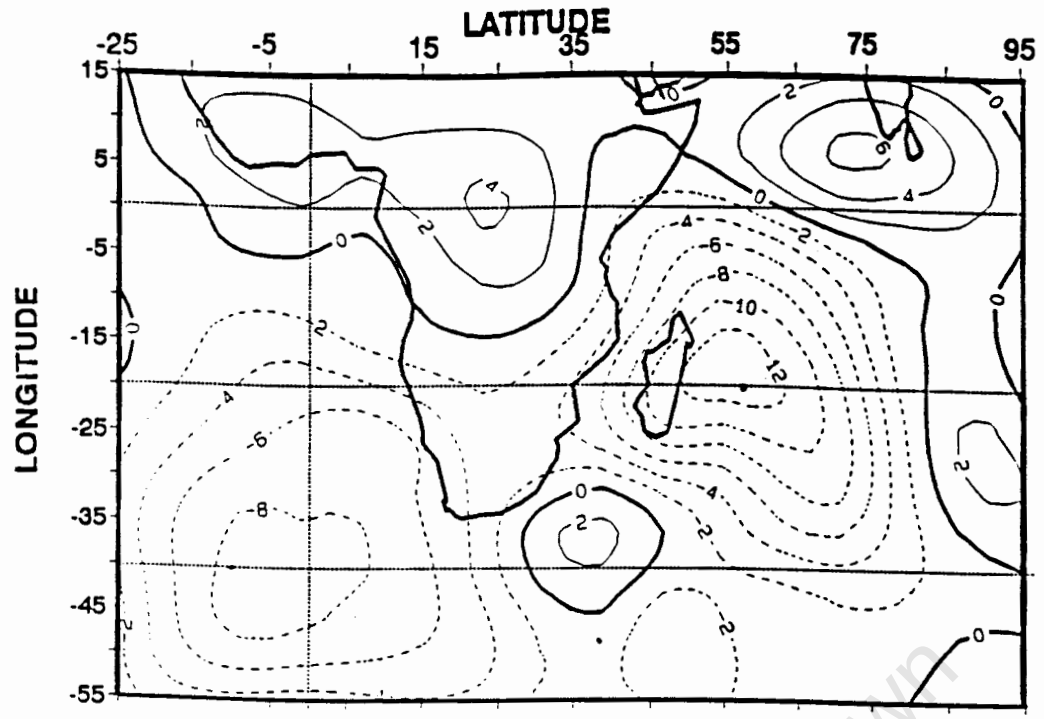

Figure 6-5a: Integrated divergent water vapour flux (χ_Q) anomalies between the surface and 500 hPa for P-1(as in Figure 5-19a).
Contour interval is 2 x 10^8 kg s^{-1}.

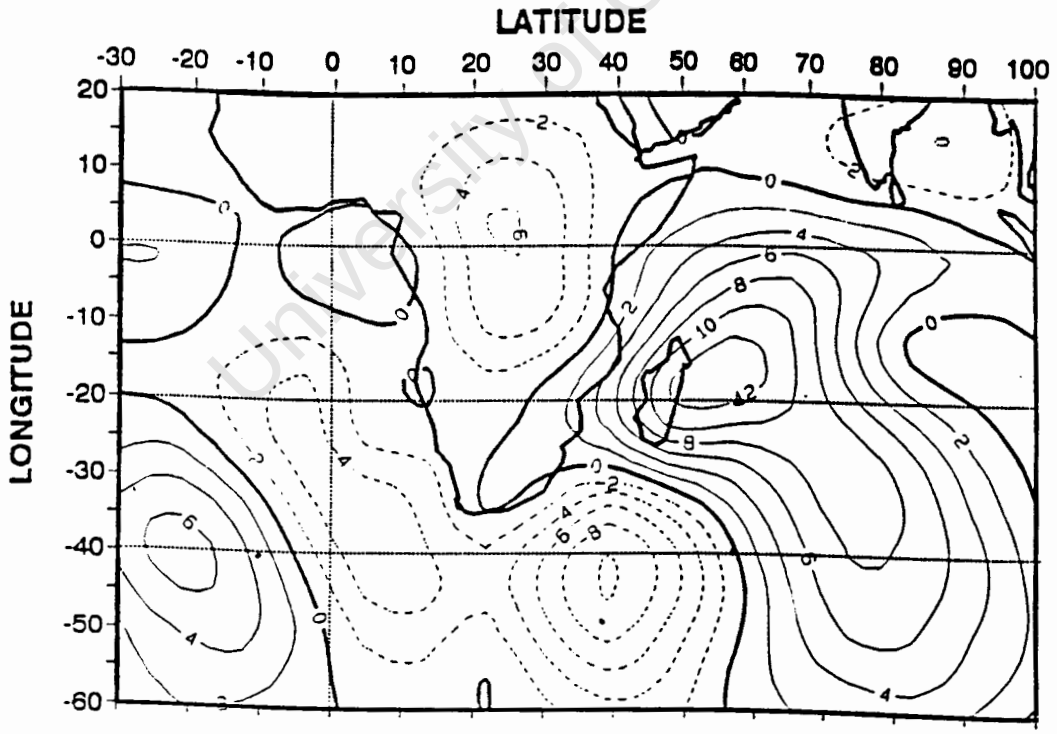

Figure 6-5b: Integrated divergent water vapour flux (χ_Q) anomalies between the surface and 500 hPa for P-0(as in Figure 5-19a).
Contour interval is 2 x 10^8 kg s^{-1}.

University of Cape Town

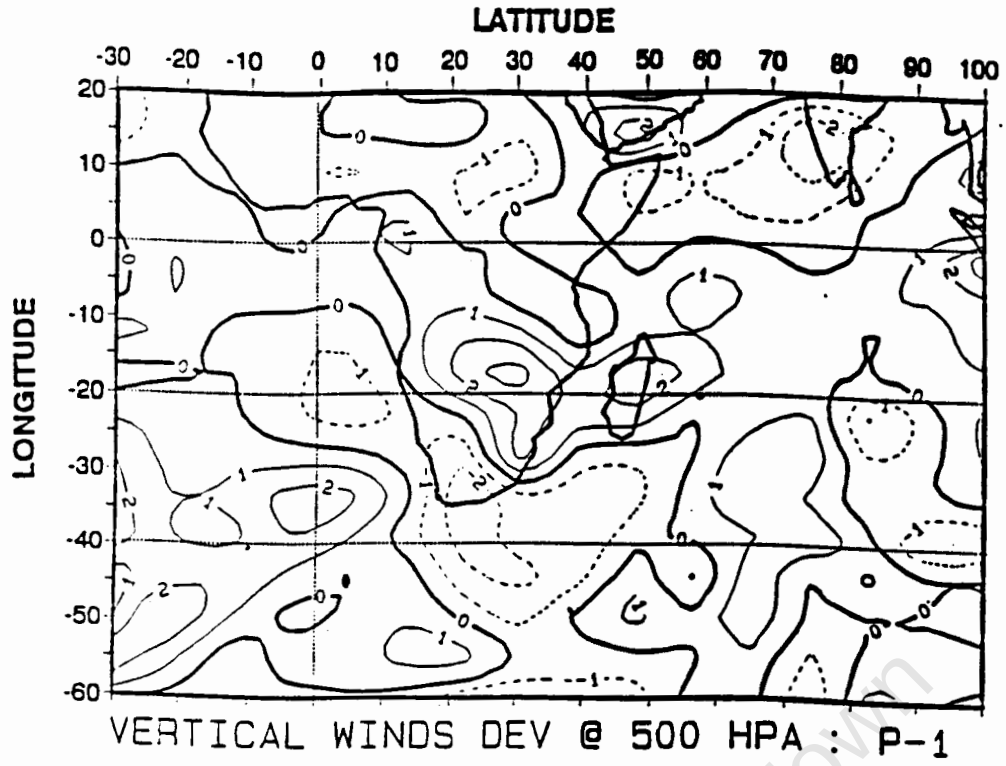

Figure 6-6a: Vertical wind anomalies at 500 hPa for **P-1** (as in Figure 5-14). Contour interval = 1 x 10^{-2} Pa s^{-1}.

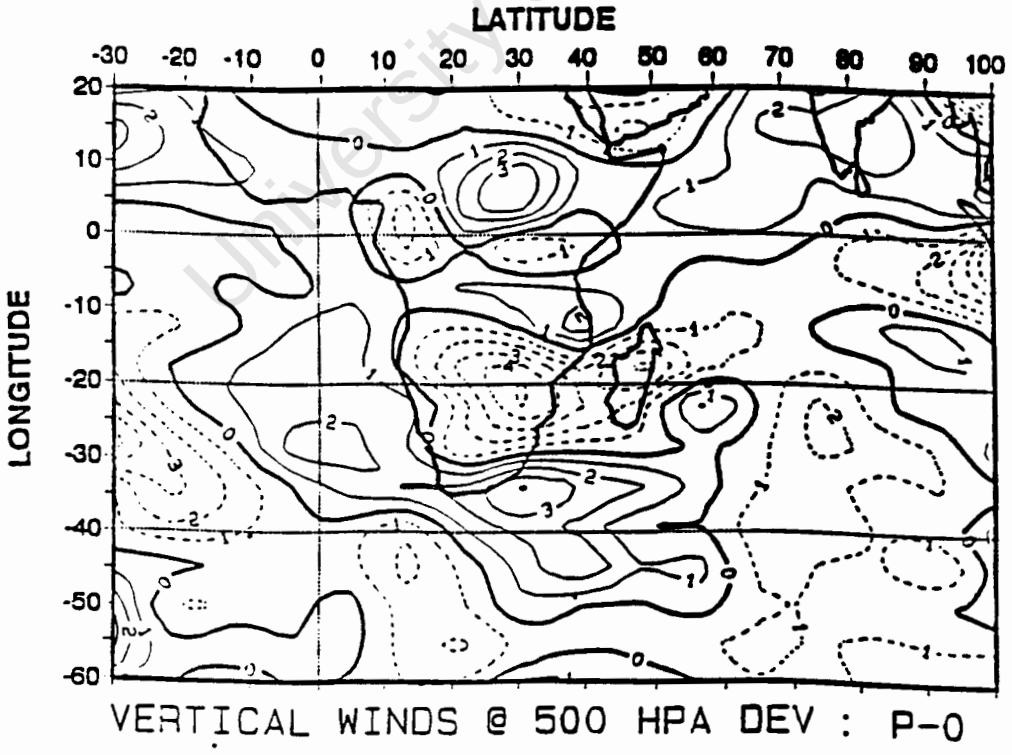

Figure 6-6b: Vertical wind anomalies at 500 hPa for **P-0** (as in Figure 5-14). Contour interval = 1 x 10^{-2} Pa s^{-1}.

University of Cape Town

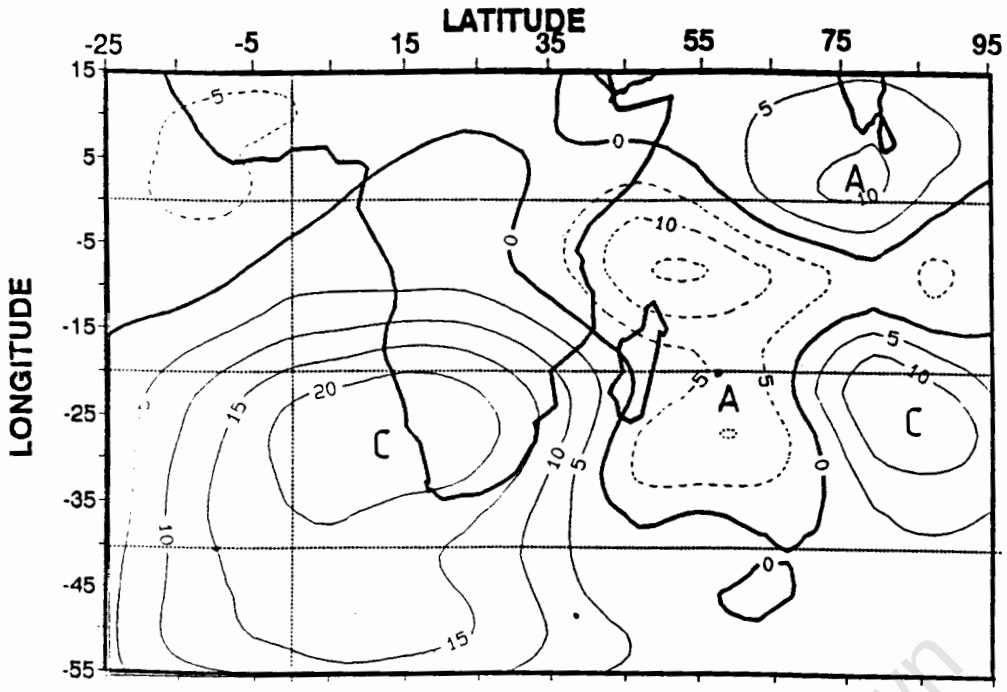

Figure 6-7a: Integrated non-divergent water vapour flux (ψ_Q) anomalies between the surface and 500 hPa for **P-1** (as in Figure 5-20). Contour interval is 5 x 10^8 kg s^{-1}.

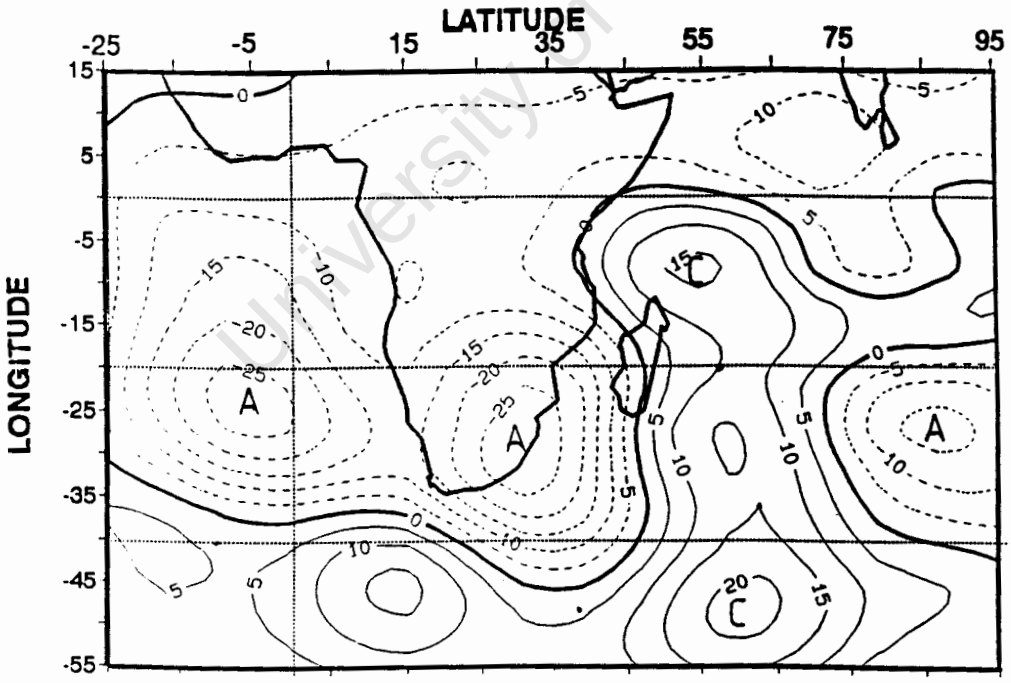

Figure 6-7b : Integrated non-divergent water vapour flux (ψ_Q) anomalies between the surface and 500 hPa for **P-0** (as in Figure 5-20). Contour interval is 5 x 10^8 kg s^{-1}.

University of Cape Town

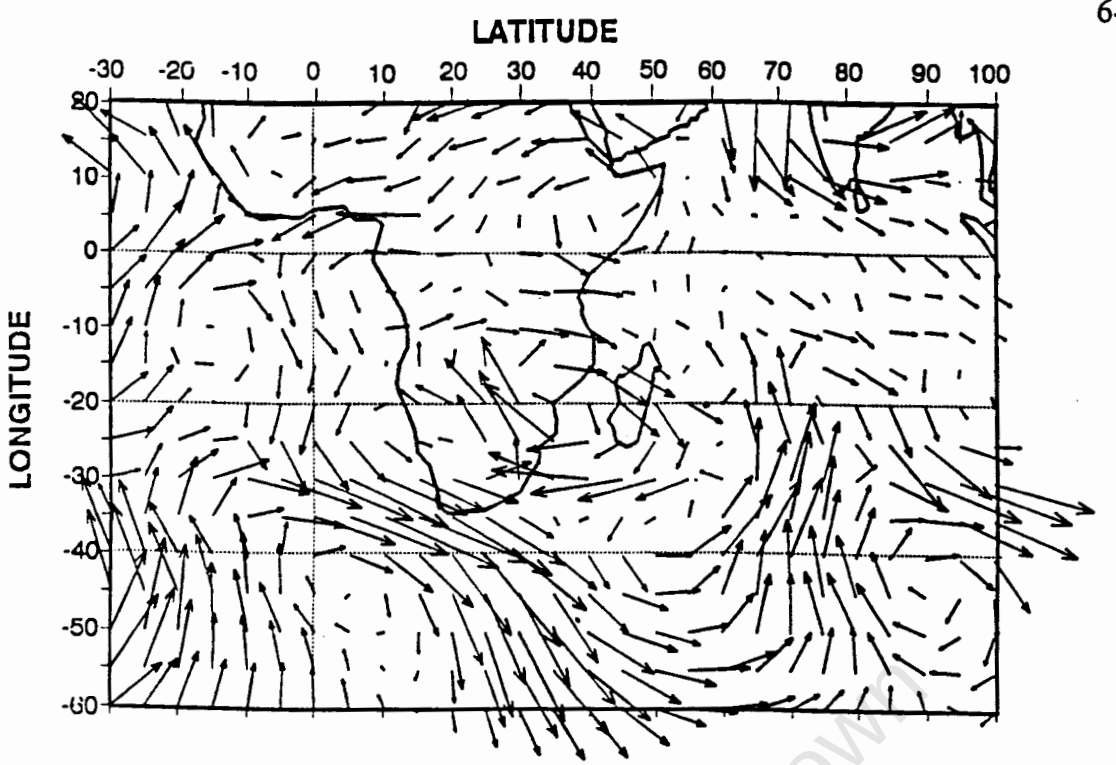

Figure 6-8a : Horizontal wind anomalies @ 200 hPa for **P-1** (as in Figure 5-12a). Vector ⟶ = 10 m s^{-1} .

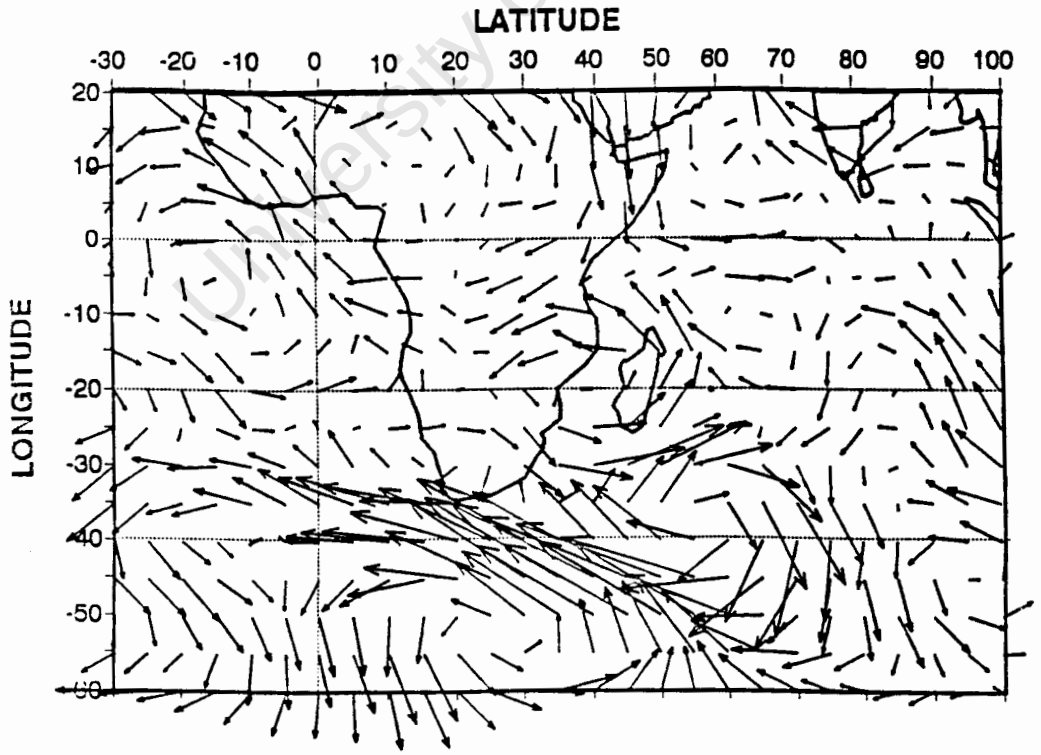

Figure 6-8b: Horizontal wind anomalies @ 200 hPa for **P-0** (as in Figure 5-12a). Vector ⟶ = 10 m s^{-1} .

University of Cape Town

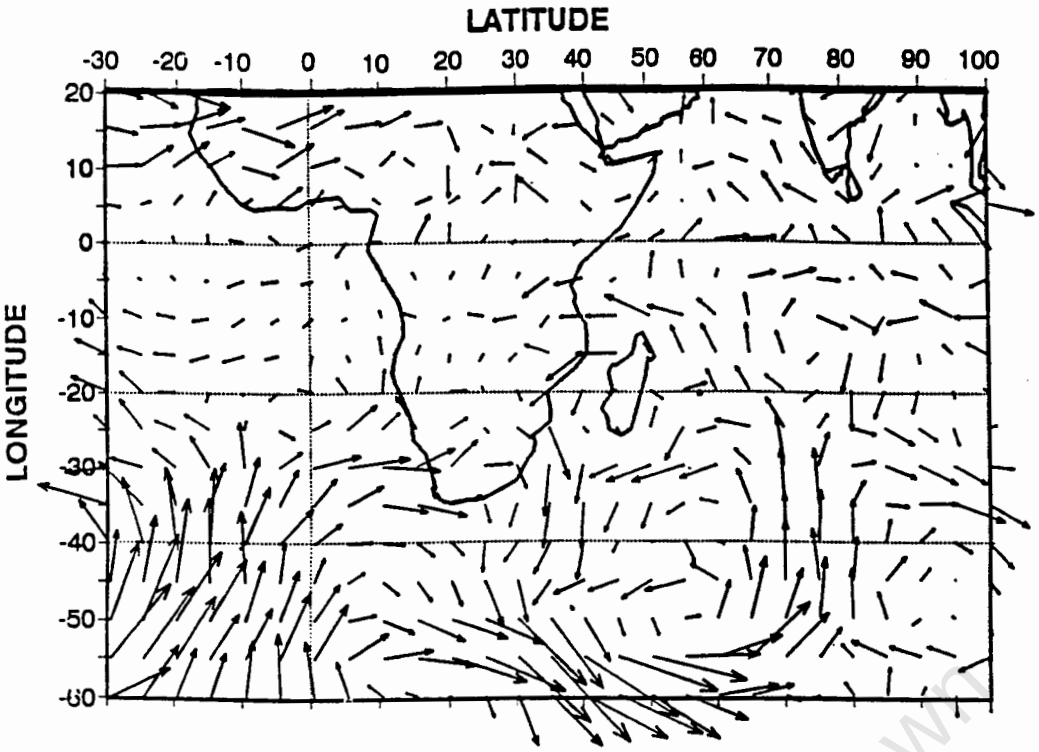

Figure 6-9a: Horizontal wind anomalies @ 850 hPa for **P-1** (as in Figure 5-12a). Vector ⟶ = 10 m s^{-1} .

University of Cape Town

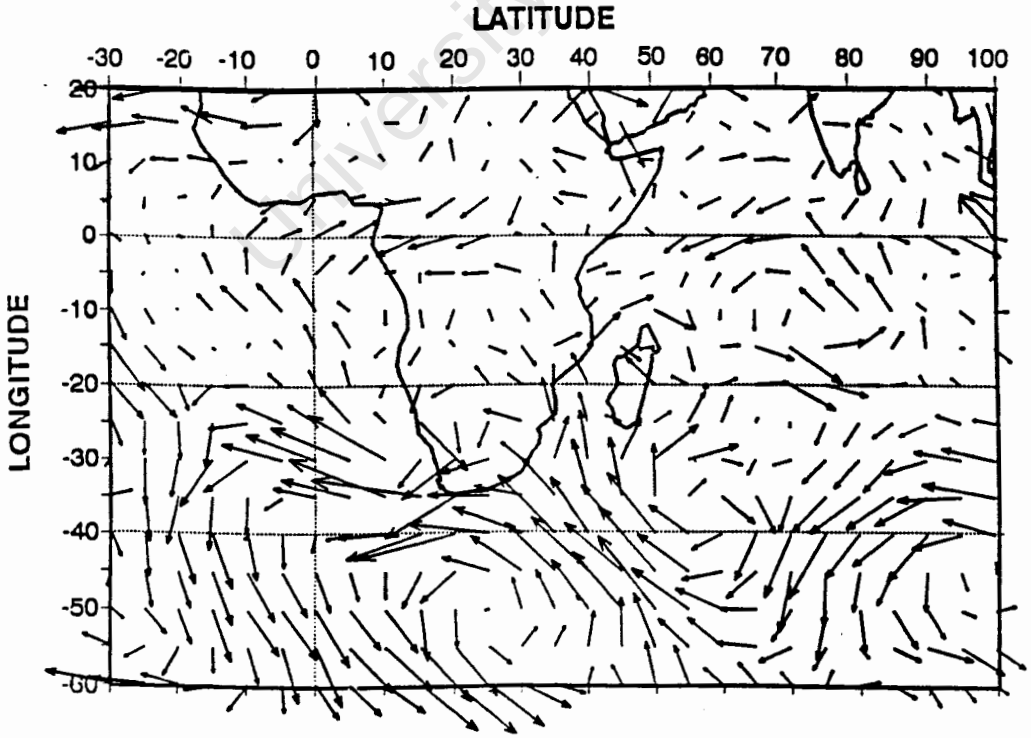

Figure 6-9b : Horizontal wind anomalies @ 850 hPa for **P-0** (as in Figure 5-12a). Vector ⟶ = 10 m s^{-1} .

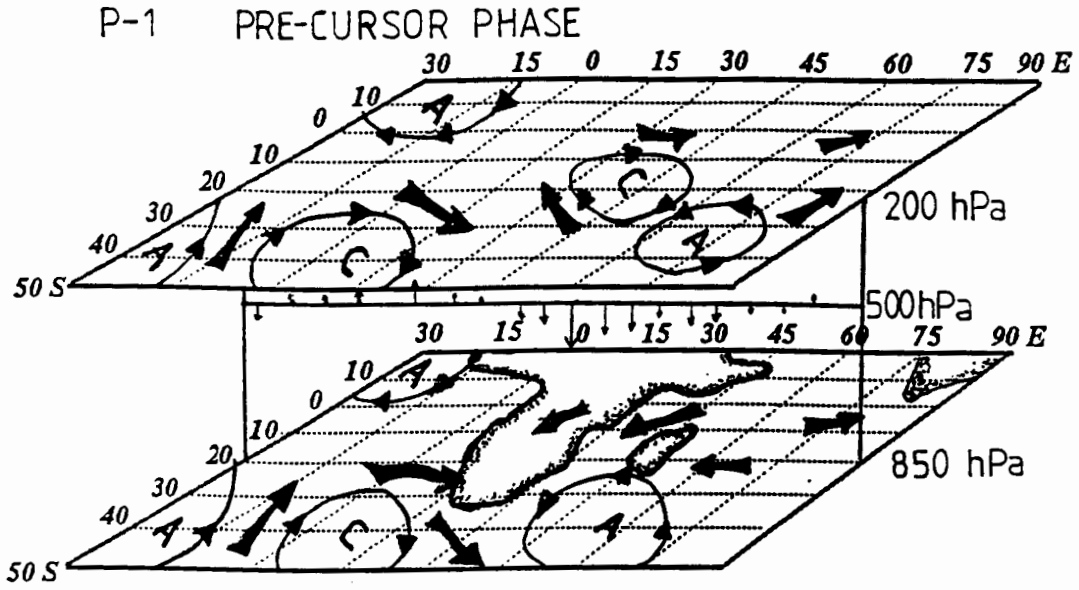

Figure 6-10a: Schematic representation of the circulation dynamics associated with **P-1** , the *pre-cursor phase*. Anticyclonic areas are denoted by "**A**" and cyclonic areas by "**C**".

University of Cape Town

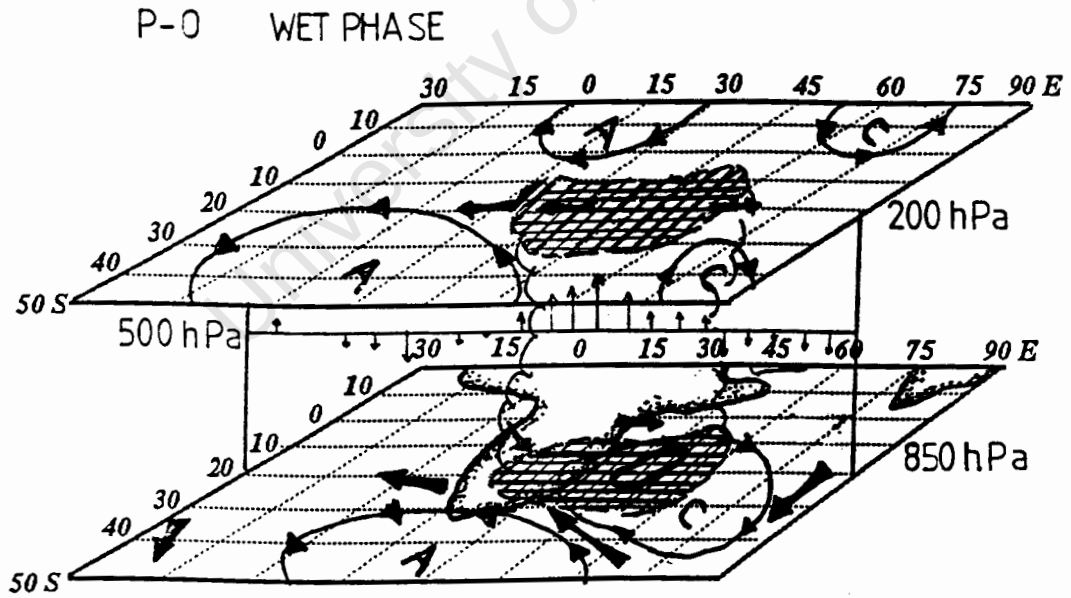

Figure 6-10b: Schematic representation of the circulation dynamics associated with **P-0** , the *wet phase*. Anticyclonic areas are denoted by "**A**" and cyclonic areas by "**C**".

6.1.4 ISO TEMPORAL ASPECTS

It is well-established that during the drier years over southern Africa, the circulation is more winter-like, i.e. the westerlies are located further northwards over South Africa and the ITCZ remains north of Zimbabwe. Therefore during the drier years when the MJO is operating further away from South Africa the tropical-extra-tropical interaction is diminished and shifted eastward. Results from chapter 3 have shown that during the wetter years the 20-30 day ISO is more dominant than during the drier years

Anyamba (1992) found that a 20-30 day ISO originates in the western Indian Ocean and propagates polewards, rather than eastwards along the equator, although zonal propagation is observed. This implies that this 20-30 day ISO is tropically sourced. It may be suggested that during wetter years over southern Africa when the westerlies are located further polewards, this 20-30 day ISO is able to penetrate into southern Africa more readily, than during drier years.

It is suggested that the 20-30 day ISO operating over southern Africa is a combination of the interaction of the extra-tropics with the MJO and possibly a shorter tropical 20-30 day ISO as proposed by Anyamba (1992) and Hayashi and Golder (1991).

Results from chapter 5 show some consistency with results obtained by Rui and Wang (1990). The wet event over South Africa (P-0) shows many similarities with their composite in phase 1 which are where strong negative OLR anomalies exist over much of Africa. However, their phase 7 also shows some similarities at 200 hPa in the anomaly horizontal wind field with P-0. This is at the same time when

University of Cape Town

the minimum OLR centre is at 160° W over the western Pacific. During their phase 7 an OLR minimum also exists over southern Africa, which is more consistent with P-0, where large precipitable water anomalies exist over tropical Africa.

The time between phase 1 and phase 7 is 30 days which is significant since spectral analysis has shown that the 20-30 day ISO is dominant in the P-E and the OLR indices over southern Africa. This implies a possible alternating weaker/ stronger 20-30 day ISO over South Africa depending on whether or not the MJO and subtropical ISO are in phase or not.

Chen and Tzeng (1989) have shown that positive precipitable water anomalies occur over southern Africa at the beginning of the MJO (category 1) for the austral summer. From their analysis, they follow the convergent centre (positive PW anomaly area) in the divergent WVF field emanating from the Indian Ocean across the maritime continent in to the Pacific and re-establishing itself over Africa. An interesting feature is that at category 8 smaller positive PW anomalies are evident over South Africa similar to the results shown by Wang and Rui (1990). Chen and Tzeng's (1989) category 8 is 35 days after category 1 indicating a longer period than observed in Wang and Rui's work. It is significant that both results show that when the MJO is strongest over the western Pacific Ocean conditions become favourable for another wet event to take place over South Africa, but with less intensity than when the MJO is being initiated over east Africa.

This has consequences for rainfall over South Africa. These results imply the following :

University of Cape Town

Every 40-60 days with some seasonal regularity the MJO will cause conditions to be more (less) favourable for convection over South Africa as the convergent (divergent) centre in the divergent WVF moves over or is initialised over the African continent. However, spectral analysis has shown that the 20-30 day ISO is also modulating the rainfall over South Africa. This implies that while the tropical MJO is operating, a shorter ISO is also operating. Anyamba (1992) and Hayashi and Golder (1992) have also shown that a shorter 20-30 day ISO is evident in the tropics. A combination of this shorter ISO, extra-tropical interaction with the MJO, standing wave and "flip-flop" patterns modulates the Walker Cell anomalies and climate over southern Africa at shorter time periods of between 20-30 days.

A possibility exists that the extra-tropics creates a harmonic of the MJO's period, hence a 20-30 day ISO of the main 40-60 day ISO. The interaction between the tropical MJO and extra-tropical Rossby wave trains, with a dominant wavenumber 4 pattern (20-30 day period as shown by the Hövmoller analysis), determines the sequence of wet and dry events over southern Africa. This infers more randomness of the 20-30 day ISO over southern Africa, since the Rossby waves are not seasonally dependent.

Another possibility exists that meridional propagation of the tropical sourced ISO as proposed by Anyamba (1992) is more dominant in the wetter years over South Africa when the westerlies have retreated polewards. This accounts for more 20-30 day ISO events over southern Africa in wetter years. However, extra-tropical interaction cannot be excluded since chapter 5 has shown that the extra-tropics are important in modulating the wet and dry events over southern Africa. The possibility exists that both the tropically sourced 20-30 day ISO and the extra-

University of Cape Town

tropics interact with the MJO causing different modes of propagation or standing wave and "flip-flop" systems to occur over southern Africa.

It can be inferred that when the wet-event of the 20-30 day cycle co-incides with the wet event of the tropical MJO, convection will be greatly enhanced, and the possibility exists for flooding. The converse is true. Should the dry-events of the shorter subtropical ISO co-incide with the divergent centre of the tropical MJO, then the possibility of extended drought is possible.

When viewing the pentad progression from P-2 to P+2, an attempt was made to establish the dynamic and thermodynamic mechanisms operating over South Africa and surrounding areas at the frequency of 20-30 days. However, these results may be influenced to some extent by the effect of the longer MJO. The choice of case studies for the composite analyses will have influenced the results.

An interesting feature of the P-E index analysis showed that the most likely time for the summer rainfall area of South Africa to receive good rainfall was towards the end of January at pentad 23 (21-25 January). Chapter 3 showed dominant spectral peaks in the P-E index at 20-30 days which may be the result of extra-tropical interaction as discussed earlier. The OLR index showed the same spectral peaks, but the 40-60 day oscillation was more dominant than the 20-30 day, inferring that OLR is modulated more by the MJO. This means that well-developed wide-scale convection over southern Africa seems to be more temporally (time) organised at frequencies closer to the MJO than the subtropical ISO. The dominant spectral peak in the P-E index is 20-30 days. This translates to there being 3 to 4 major wet/dry events per summer season modulated by the MJO

University of Cape Town

while the shorter 20-30 day cycle translates to 6 to 9 wet/dry events per summer season.

The time when the 20-30 day ISO actually starts at the beginning of summer is unknown, probably owing to its randomness. However, the fact that the end of January is on average the wettest period of summer, it may be implied that the subtropical ISO and MJO are in phase enhancing well-organised convection over southern Africa at this time. If this period is taken as being a "wet-event" of both the subtropical ISO and MJO it is possible to calculate other wet periods during the summer based on the fact that the subtropical ISO is 20-30 days (± 5 pentads) and the MJO is on average 40-60 days (±10 pentads).

6.2 CONCLUSIONS :

Chapter 3 has shown that one dominant ISO's operate in the southern Africa. The MJO operating between 40-60 days is more dominant in the OLR than in the P-E index. Wang and Rui (1990) results have shown that organised convection as shown by strong negative OLR anomalies are initialised over eastern Africa and propagated eastwards around the globe. A combination of the MJO and 20-30 day ISO operate over southern Africa resulting in various modes of propagation or standing wave and "flip-flop" patterns of meteorological parameters over South Africa.

Chapter 3 illustrated how during the drier 1980's, the 20-30 day ISO is less prominent than during the wetter 1970's. It was established that a longer-term ISO operates during wetter years, i.e. 40-60 days, whereas during wetter years the 20-30 day ISO is dominant, although the MJO is also operating. Hayashi and Golder

University of Cape Town

(1992) have shown that a 20-30 day ISO originates in the tropics and is independent of the MJO, although at times it does exhibit similar characteristics. Anyamba (1992) has shown that the zonal propagation of the 20-30 day ISO is weak, that the direction of propagation is polewards.

Extra-tropical interaction with the eastward propagating MJO appears to be the cause of the shorter 20-30 day subtropical ISO evident in the P-E and OLR indices, although the effect of the 20-30 day tropical ISO proposed by Anyamba (1992) and Hayashi and Golder (1992) on southern Africa is unclear at this stage. The south-eastward propagation of this tropical 20-30 day ISO into the south-west Indian Ocean could indirectly affect South Africa by "pulsing" the standing wave via the dipole that is seen clearly in the velocity potential and divergent water vapour flux fields.

Chapter 4 showed that the dominant direction of propagation of anomalies is eastward and they account for 50-60% of all propagating systems. At 10° S the eastward propagation is best seen in the geopotential height anomalies at 850 hPa, u-wind component at 850 hPa and v-wind component at 200 hPa. At 40° S the eastward movement is best seen in the geopotential height anomalies at both the 200 and 850 hPa levels, v-wind component at 200 hPa and the vertical wind anomaly field at 500 hPa. The region between 30° and 60° E appears to be the region where the MJO is initiated which is consistent with Wang and Rui's (1989) findings. Of significance is the high percentage (25%-40%) of *non-propagating* anomalies, which may be the result of the tropical-temperate interactions; variations in the Hadley Cell circulation between the tropics and the subtropics or both.

University of Cape Town

Chapter 5 has shown the dynamics associated with the various phases of the 20-30 day ISO. It has been shown that 10 days prior to the wet event a very distinct signal is observed in the tropical Indian Ocean where a "flip" monsoon signal in the form of strong easterly wind anomalies is witnessed. The temporal trend composite analysis also showed some distinctive signals in the transition from P-2 to P-1 during the precursor stage. An extra-tropical trough in the upper air is seen to the south-west of South Africa at P-1 and this is followed at both levels by strong SAA ridging. At the same time the circulation over the south-west Indian Ocean in the lower troposphere becomes strongly convergent and high values of PW are seen in this region. South-easterly flow around the ridging SAA into south Africa from the southern Mozambique Channel advects moist air into South Africa where strong uplift occurs during the wet phase.

It has been shown that WVF in the central Indian Ocean in the post wet phase composite anomaly at P+2 is 180° out of phase with the pre-cursor stage at P-2 indicating that a full-cycle is about 40-60 days. P+2 does show some similarities to the composite phase 7 found in Wang and Rui's (1989) work. This phase shows weaker negative OLR anomalies over South Africa indicating the advent of another (weaker) wet event, although the 20-30 day ISO is out of phase with the MJO. The strongest negative OLR anomalies occur in the western Pacific Ocean during P+2 (Chen and Tzeng, 1989; Wang and Rui, 1990). It therefore appears that the composite 25 day cycle proposed in this study is the dominant 20-30 day ISO and that *two* 20-30 day ISO's occur within the life time of the 40-60 day MJO and that they alternate in strength depending whether or not the 20-30 day ISO and the MJO are in phase with each other.

University of Cape Town

The summer rainfall region of South Africa is influenced by both the 40-60 day MJO and a shorter 20-30 day ISO. Together they modulate the succession of rainfall and drought events. When the two ISO's are in phase, they either produce good rains or severe drought. The intensities and duration of these wet and dry spells may be affected by whether the season as a whole is wet or dry. Very wet years tend to have shorter ISO's operating while longer ISO's operate in the drier years.

The water vapour flux field and the divergent water vapour flux field have shown themselves to be very useful prognostic tools for forecasting purposes. The potential function of the WVF field not only informs one about the divergent nature of the low level circulation, but also quantitatively shows the amount of water vapour convergence or divergence. Chen and Tzeng (1989) have shown that positive (negative) precipitable water anomalies couple with convergent (divergent) centres of the potential function of the WVF field and the divergent (convergent) centre of upper level velocity potential anomalies. This has been confirmed in chapter 5 during various phases of the 20-30 day ISO.

Further analysis needs to be undertaken to fully investigate the dynamics and relative importance of extra-tropical tropical interaction over the south-western Indian Ocean as proposed by Lyons (1991). This is important since it will confirm or refute evidence that shows that the extra-tropics are the cause of the shorter 20-30 day subtropical ISO operating over southern Africa.

The 20-30 day tropical ISO proposed by Anyamba (1992) also needs closer inspection to ascertain the role it may play in pulsing the standing wave operating over southern Africa.

University of Cape Town

Composites of strong events may also highlight some of the dynamical features more clearly. Wang and Rui (1990) showed by using stronger cases that certain features were more apparent than when using more moderate cases. The composite results of stronger or more extreme cases studies may then show better consistency with the work of Chen and Tzeng (1989) and Wang and Rui (1990).

Further investigation into the possibility of an alternating weak/strong 20-30 day ISO within the period of the 40-60 MJO is needed. Chapter 5 showed that the post wet phase anomaly composite patterns (P+2) are not the same as those encountered during the pre-cursor stages. Chen and Tzeng (1989) and Wang and Rui (1990) have shown that increased convective activity takes place over South Africa when the MJO is half way through its 60 day period. The convection appears weaker over South Africa as compared with the stage where the MJO and the 20-30 day ISO are in phase. The possibility exists therefore that *two* 20-30 day ISO's occur per *one* MJO and that the 25 day composite progression may be *one* such 20-30 day ISO operating during the MJO.

University of Cape Town

★ ★

ACKNOWLEDGEMENTS

I wish to thank my supervisor, Dr. Mark R. Jury, of the Oceanography Department, University of Cape Town, for his tireless support of this thesis. His great enthusiasm and interest in this work has given me the motivation to complete

this work. Under his guidance the final objectives of this work were achieved. I would also like to thank Professor Geoff Brundrit, also of the Oceanography Department, University of Cape Town, for his assistance as far as the statistical analysis is concerned. Duane Waliser of SUNY, USA is thanked for the OLR pentad data which was made available to me. Peter D' Abreton, formerly of the University of the Witwatersrand and R Allen from the CSIRO in Australia for the velocity potential and streamfunction algorithms as well as other useful algorithms. A final word of thanks also to Shaun Courtney for his computer assistance while writing all the programs needed to process the data and to Bhawoodien Parker for valuable data analysis cross-checking.

I wish to thank the Water Research Commission of South Africa for funding this project. The South African Weather Bureau and the CCWR (Computing Centre for Water Research) are thanked for making the rainfall and evaporation data used in this study available in a usable pre-processed format.

★ ★

University of Cape Town

REFERENCES :

Anyamba, E.K., 1992 : Some Properties of a 20-30 Day Oscillation in Tropical Convection, *Journal of the African Meteorological Society (SMA),* 1, 1992, 1 - 19.

Barclay, J.J., 1992 : Wet and Dry Troughs over Southern Africa during early Summer, *Unpublished MSc Thesis*, University of Cape Town, 178 pp.

Barclay, J.J et al, 1993 : Climatological and Structural Differences Between Wet and Dry Troughs over Southern Africa in the Early Summer, *Meteorology and Atmospheric Physics,* 51, 41-54.

Bengtsson, L. and Shukla, J., 1988 : Integration of Space and In Situ Observations to Study Global Climate Change, *Bulletin American Meteorological Society*, vol. 69, no. 10 , 1130-1143.

Bolton, D., 1980 : The computation of Equivalent Potential Temperature, *Monthly Weather Review,* vol. 108, 1046-1053.

Chen, T. and Yen, M., 1990 : Intraseasonal variations of the tropical easterly jet during the 1979 northern summer, *Tellus*, 43A, 213-225.

Chen, T. and Yen, M., 1991 : Interaction between Intraseasonal Oscillations of the Midlatitude Flow and tropical convection during 1979 Northern Summer : The Pacific Ocean, *Journal of Climate,* vol. 4, no. 7, 653-671.

Chen, T. and Yen, M. 1991a : A study for the maintenance of the 30-60 day oscillation of planetary-scale divergent circulation, *Journal of Geophysical Research,* in press.

Chen, T. and Tzeng, R. 1989 : Global-Scale Intra-seasonal and Annual Variation of Divergent-Water Vapour Flux, *Meteorology and Atmospheric Physics,* 44, 133-151.

University of Cape Town

D' Abreton, P.C., 1992 : The dynamics and Energetics of Tropical-Temperate Troughs over southern Africa, *Unpublished PhD Thesis*, University of the Witwatersrand, 231 pp.

Dyer, T.G.J., 1979 : Rainfall along the east coast of southern Africa, the Southern Oscillation and the latitude of the subtropical high pressure belt, *Quarterly Journal of the Royal Meteorological Society,* 105, 445-451.

Geiger, R., 1965 : *Climate near the Ground,* Harvard University Press, Cambridge, 611 pp.

Gillooly, J. F. and Dyer T.G. J., 1979 : Spatial variations in the rainfall during abnormally wet and dry years, *South African Journal of Science*, 75, 261-262.

Ghil, M. and Mo, K., 1990 : Intraseasonal Oscillation in the Global Atmosphere. Part II : Southern Hemisphere, *Journal of the Atmospheric Sciences*, vol. 48, no. 5, 780-790.

Harrison M.S.J., 1986 : A synoptic climatology of South African rainfall variations, *Unpublished PhD Thesis,* University of the Witwatersrand, 341 pp.

Hartmann, D.L et al, 1991 : Seasonal Variations of the Tropical Intraseasonal Oscillations: A 20-25-Day Oscillation in the Western Pacific, *Journal of the Atmospheric Sciences*, vol. 49, no. 14, 1277-1289.

Hayashi, Y. and Golder, D.G., 1992 : Tropical 40-50- and 25-30-Day Oscillations Appearing in Realistic and Idealized GFDL Climate Models and the ECMWF Dataset, *Journal of the Atmospheric Sciences*, Vol. 50, No. 3, pp 464-494.

Hirst, A.C. and Hastenrath.S., 1983 : Atmosphere-ocean mechanisms of climate anomalies in the Angola-tropical Atlantic sector, *Journal of Physical Oceanography*, 13, 1146-1157.

University of Cape Town

Holton, J.R., 1979 : *An Introduction to Dynamic Meteorology,* Academic Press, New York, 391 pp.

Hsu, H., Hoskins, B.J. and Jin, F., 1990 : The 1985 / 86 Intraseasonal Oscillation and the Role of the Extratropics, *Journal of the Atmospheric Sciences*, vol. 47, no. 7, 823-839.

Illari, L. 1986 : The quality of the ECMWF humidity-analysis, *Workshop on High Resolution Analysis*, 24-26 June, 1985, ECMWF, 41-68.

Illari, L. 1989 : The quality of satellite precipitable water content data and their impact on analysed moisture fields, *Tellus*, 41A, 319-337.

Jury, M.R, MacArthur, C.I., and Brundrit, G.B., 1991 : Pulsing of the Benguela Upwelling Region : Large-Scale Atmospheric Controls, *South African Journal of Marine Science,* 9, 27-41.

Jury, M.R., and Lyons, S.W., 1992 : Contrasting synoptic events over South Africa in the dry summer of 1983, *South African Geographical Journal*, in press.

Jury, M.R., and Lutjeharms, J.R.E, 1993 : Die Struktuur en Moontlike Aandrywingskragte van die 1991-1992-droogte in Suidelike Afrika, *Suid Afrikaanse Tydskrif vir Natuurwetenskap en Tegnologie*, 12, no.1, 8-15.

Kawamura, R., 1991 : Modification of the 30-60 Day Oscillation by Air-Sea Interaction in the Warm Pool Region of the Western Pacific during the Northern Summer, *Toga Notes*, October 1991, 4-8.

Knutson, T.R. and Weickmann, K.M., 1986 : 30-60 Day Atmospheric Oscillations : Composite Life Cycles of Convection and Circulation Anomalies, *Monthly Weather Review*, vol. 115, 1407-1437.

Krishnamurti et al 1973 : Tropical east-west circulations during the northern winter, *Journal of the Atmospheric Sciences*, 30, 780-787.

University of Cape Town

Lau, K.M. and Chan, P.H., 1986 : Aspects of the 40-50 day oscillation during the northern summer as inferred from outgoing longwave radiation, *Monthly Weather Review*, vol. 114, 1354-1367.

Lindesay, J.A., 1984 : Spatial and temporal rainfall variability over South Africa, 1963 to 1981, *South African Geographical Journal*, 66, 168-175.

Lindesay, J.A., 1988 : The Southern Oscillation and atmospheric circulation changes over southern Africa, *Unpublished PhD Thesis*, University of the Witwatersrand, 283 pp.

Lindesay, J.A. and Jury, M.R., 1991 : Atmospheric circulation controls and characteristics of a flood event in central South Africa, *International Journal of Climatology*, in press.

Lyons, S.W., 1991 : Origins of Convective Variability over Equatorial Southern Africa during the Austral Summer, *Journal of Climate*, vol. 4, 23-39.

Madden, R.A., and Julian, P.R., 1971 : Detection of a 40-50 day oscillation in the zonal wind in the tropical Pacific, *Journal of the Atmospheric Sciences*, vol. 28, 702-708.

Magaña, V. and Yanai, M., 1990 : Tropical-Midlatitude Interaction on the Time Scale of 30 to 60 Days during the Northern Summer of 1979, *Journal of Climate*, vol. 4, 180-201.

Matarira, C.H., and Jury, M.R., 1990 : Contrasting atmospheric structure during wet and dry spells in Zimbabwe, *International Journal of Climatology*, in press.

Miron, O. and Lindesay, J.A., 1983 : A note on changes in airflow patterns between wet and dry spells over South Africa, 1963-1979, *South African Geographical Journal*, 65, 141-147.

University of Cape Town

Miron, O. and Tyson, P.D., 1984 : Wet and dry conditions and pressure anomaly fields over South Africa and the adjacent oceans, 1963-1979, *Monthly Weather Review*, vol. 112, 2127-2132.

Norcliffe, G.B., 1985 : *Inferential Statistics for Geographers : An Introduction*, Hutchinson, 263 pp.

Park, C. and Schubert, S.D., 1992 : Remotely Forced Intraseasonal Oscillations over the Tropical Atlantic, *Journal of the Atmospheric Sciences*, vol. 50, no. 1, 89-103.

Preston-Whyte, R.A. and Tyson, P.D., 1988 : *The Atmosphere and Weather of Southern Africa,* Oxford University Press, Cape Town, pp 374.

Rasmusson, E.M. and Carpenter, T.H., 1982 : Variations in tropical sea surface temperature and surface wind fields associated with with the Southern Oscillation/ El Niño, *Monthly Weather Review*, 110, 354-384.

Rui, H. and Wang, B., 1990 : Development Characterstics and Dynamic Structure of Tropical Intraseasonal Convection Anomalies, *Journal of the Atmospheric Sciences*, vol. 47, 357-379.

Schubert, S.D. and Park, C., 1990 : Low-Frequency Intraseasonal Tropical-Extratropical Interactions, *Journal of the Atmospheric Sciences*, vol. 48, no. 4, 629-651.

Sutton, O.G., 1953 : *Micrometeorology*, McGraw-Hill, New York, 327 pp.

Taljaard, J.J. 1981 : The anomalous climate and weather systems of January to March 1974, *South African Weather Bureau Newsletter*, no. 397, 51-53.

Taljaard, J.J., 1985 : Cut-off lows in the South African region, *South African Weather Bureau*, Technical Paper No. 14, 154 pp.

University of Cape Town

Taljaard J.J., 1986a : Change of rainfall distribution and circulation patterns over southern Africa in summer, *Journal of Climatology*, 6, 579-592.

Taljaard J.J., 1986b : Contrasting atmospheric circulation during dry and wet summers in South Africa, *South African Weather Bureau Newsletter*, no. 445, 1-5.

Tsai, T.H, et al 1992 : The 26-Day Oscillation observed in the satellite Sea Surface temperature Measurements in the Equatorial Western Indian Ocean, *Journal of Geophysical Research*, vol. 97, no. C6, 9605-9618.

Tyson, P.D., 1980 : Temporal and spatial variation of rainfall anomalies in Africa south of longitude 22 during the period of meteorological record, *Climate Change*, 2, 363-371.

Tyson, P.D., 1981 : Atmospheric circulation variations and the occurrence of extended wet and dry spells over southern Africa, *Journal of Climatology*, 1, 115-130.

Tyson, P.D., 1984 : The atmospheric modulation of extended wet and dry spells over South Africa, 1958-1978, *Journal of Climatology*, 4, 621-635.

Tyson, P.D., 1986 : *Climatic Change and Variability in southern Africa*, Oxford University Press, Cape Town, 220 pp.

Tyson, P.D. and Dyer, T.G.J., 1975 : Mean annual fluctuations of precipitation in the summer rainfall region of South Africa, *South African Geographical Journal*, 57, 104-110.

Vincent, D., Sperling, T., Fink, A., Zube, S. and Speth,P., 1990 : Intraseasonal Oscillation of Convective Activity in the Tropical Southern Hemisphere : May 1984-April 1986, *Journal of Climate*, vol. 4, 40-53.

University of Cape Town

Wang, B. and Rui, H. 1990 : Synoptic Climatology of Transient Tropical Intraseasonal Convection Anomalies : 1975-1985, *Meteorology and Atmospheric Physics*, 44, 43-61.

Weickmann, K.M. and Khalsa, S. J. S., 1989 : The Shift of Convection from the Indian Ocean to the Western Pacific Ocean during the 30-60 Day Oscillation, *Monthly Weather Review,* vol. 118, 964-978.

Wiesner, C.J., 1970 : *Hydrometeorology*, Upman and Hall, London, 227 pp.

Yasunari, T., 1980 : A quasi-stationary appearance of 30-40 day period in cloudiness fluctuations during the summer monsoon over India, *J. Met. Soc. Japan*, 58, 225-229.

Zhu, B. and Wang, B., 1993 : The 30-60 Day Convection Seesaw between the Tropical Indian and Western Pacific Oceans, *Journal of the Atmospheric Sciences,* vol. 50, no. 2, 184-199.

University of Cape Town

APPENDIX A

CALCULATION OF :

A] VAPOUR PRESSURE :

1] Calculate absolute temperature T_K

$$T_K = T + 273.15 \qquad \text{Eq. A-1}$$

where : T = temperature

2] Calculate condensation level temperature T_L

$$T_L = \{1 / [1/ (T_K - 55) - (\ln(RH/100) / 2840)]\} + 55 \qquad \text{Eq. A-2}$$

where : RH = relative humidity (%)

3] vapour pressure (e)

$$e = \exp(3.5 \times \ln T_K - (2840/(T_L - 55)) - 4.805 \qquad \text{Eq. A-3}$$

B] MIXING RATIO :

The mixing ratio (x) is the ratio of the mass of water vapour to the mass of dry air. It is dependent on vapour pressure and total atmospheric pressure and can be derived using temperature and relative humidity (Bolton, 1980) .

University of Cape Town

Using e from Eq. A-3

$$x = (0.622 \times e) / (P - e) \qquad \text{Eq. A-4}$$

where : P = set-level pressure (hPa)

e = vapour pressure

C] SPECIFIC HUMIDITY :

Specific humidity (q) is defined as the mass of water vapour which is a proportion of the total mass of moist air of which it forms part (Preston-Whyte and Tyson, 1988) and is measured in g kg^{-1}. Specific humidity is calculated as follows :

$$q = (0.622 \times e) / (p - [0.378 \times e]) \qquad \text{Eq. A-5}$$

Specific humidity is calculated for purposes of deriving water vapour flux.

University of Cape Town

APPENDIX B

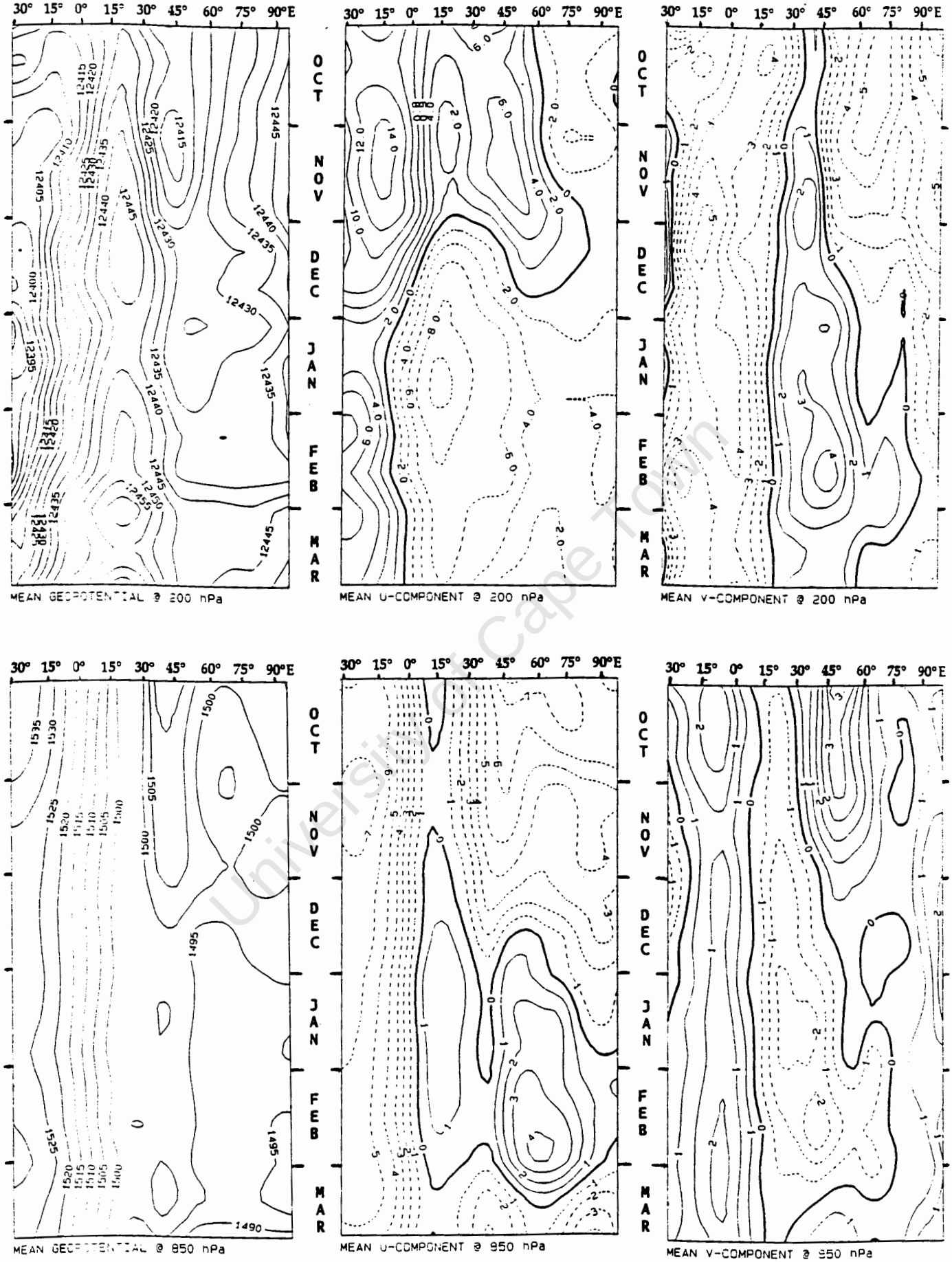

Figure B-1: Hovmöller plots of mean geopotential heights, u and v wind components @ 200 hPa and 850 hPa at 10° S. 1987 - 1992.

University of Cape Town

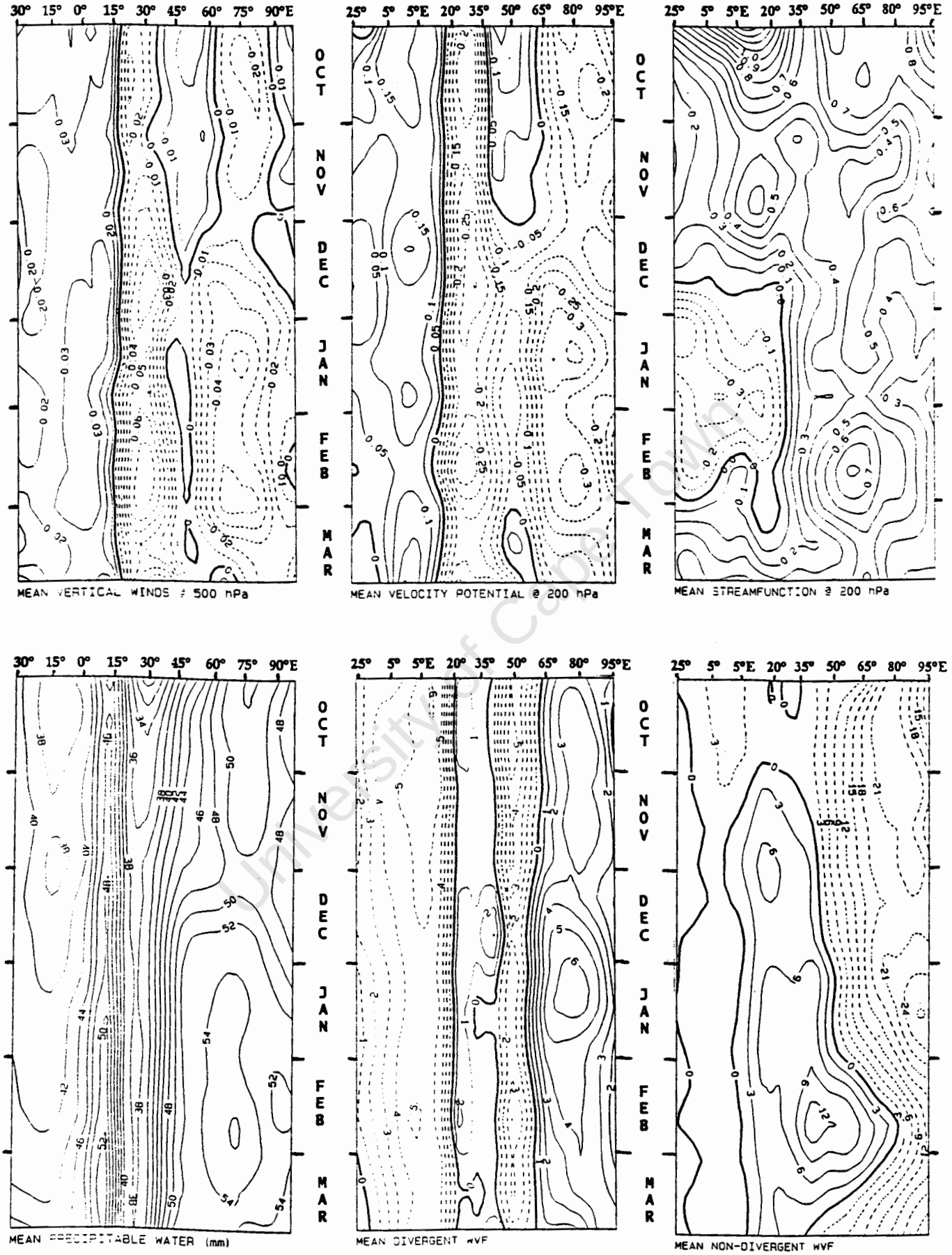

Figure 3-2: Hovmöller plots of mean vertical winds @ 500hPa, velocity potential and streamfunction @ 200 hPa, precipitable water, divergent and non-divergent water vapour flux at 10 ° S. (χ and $\psi = 10^6\ m^2\ s^{-1}$)

University of Cape Town

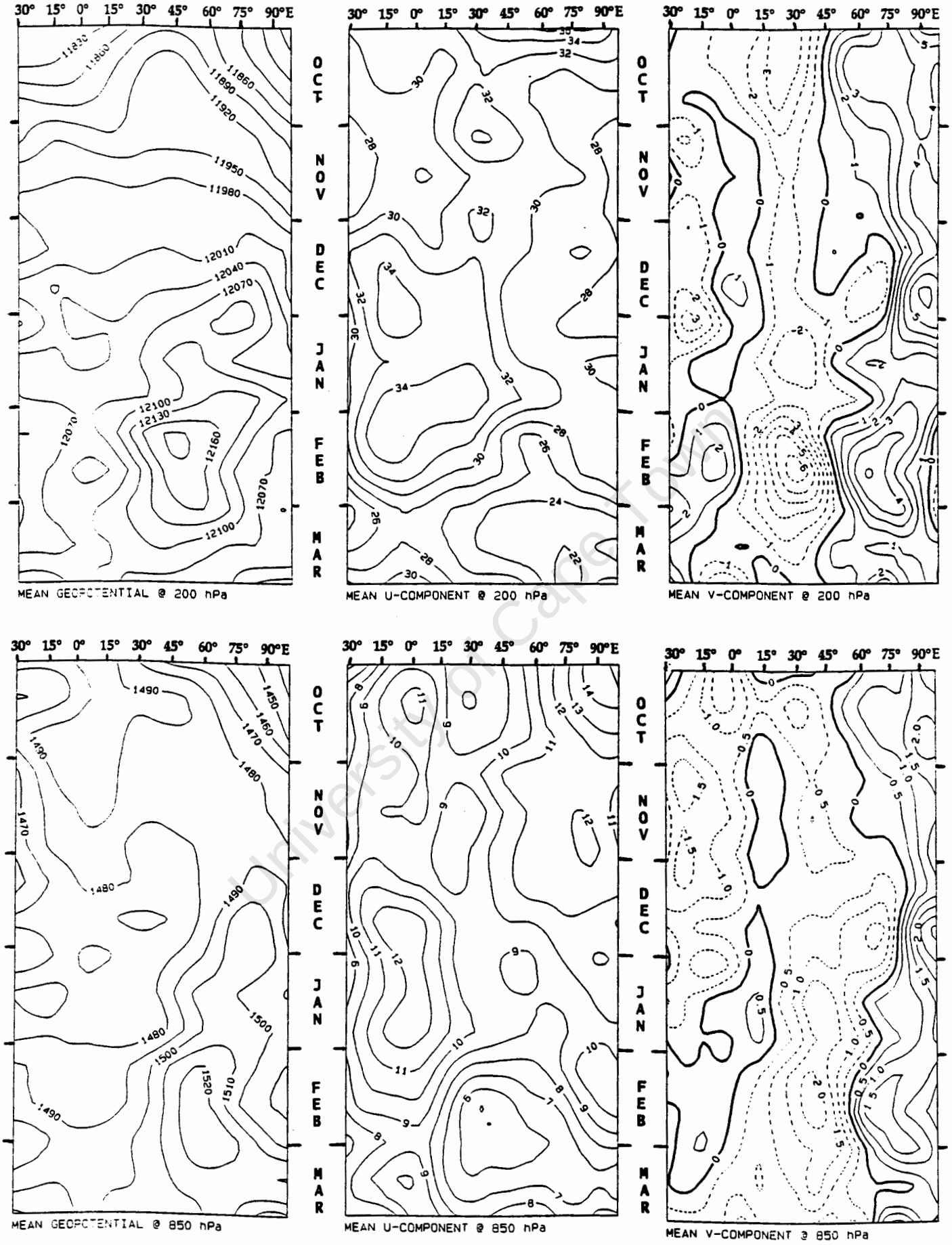

Figure B-3: Hovmöller plots of mean geopotential heights, u and v wind components @ 200 hPa and 850 hPa at 40° S.

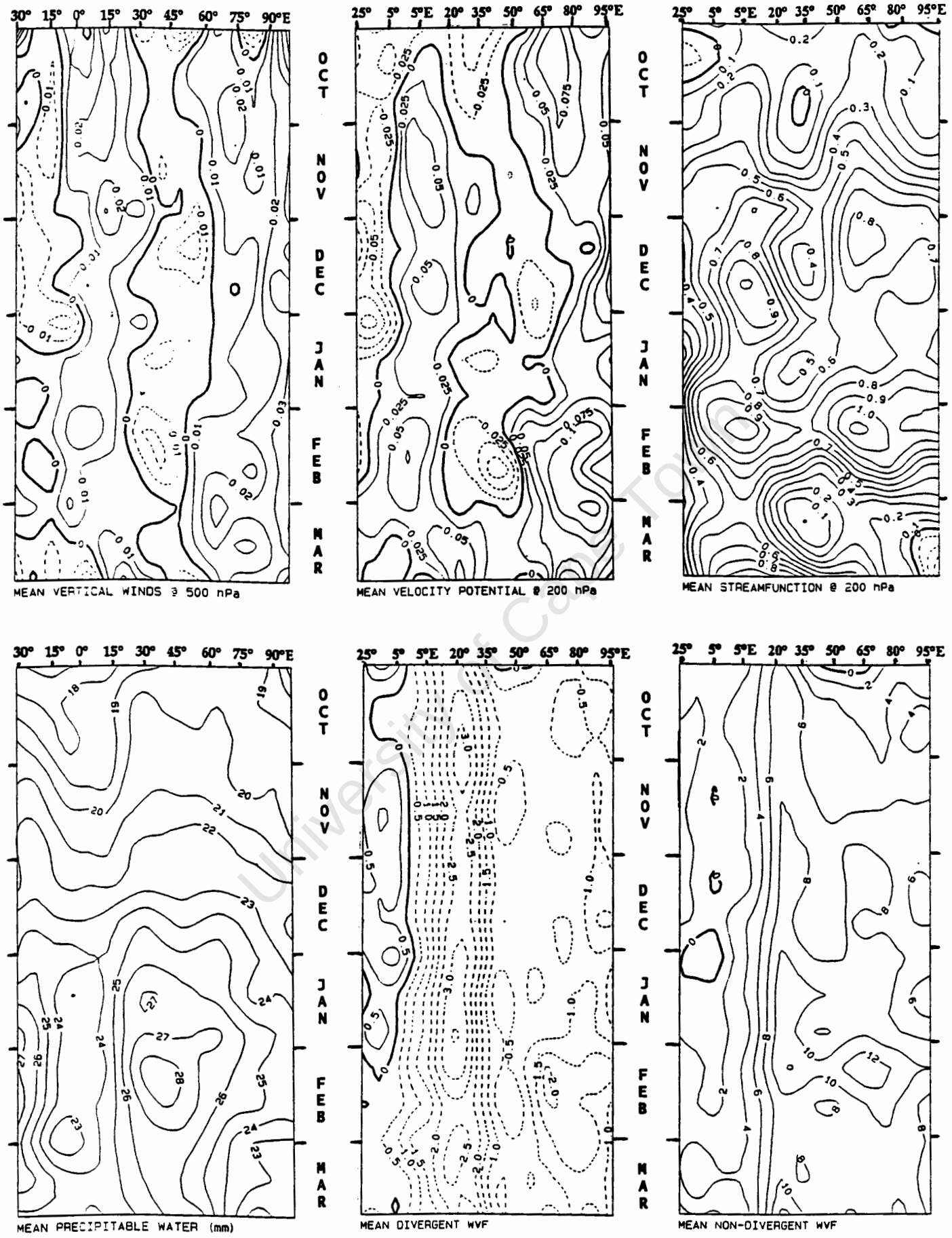

Figure B-4: Hovmöller plots of mean vertical winds @ 500hPa, velocity potential and streamfunction @ 200 hPa, precipitable water, divergent and non-divergent water vapour flux at 40 ° S. (χ and $\psi = 10^6$ m^2 s^{-1})

University of Cape Town